Modulated Microwave Retro-reflectors and Their Applications

Thesis

UNRESTRICTED

Modulated Microwave Retro-reflectors and their Applications.

by John Thornton BSc. MSc.

A Thesis Submitted to The Open University for the Degree of Doctor of Philosophy.

Discipline: Department of Materials Engineering

Submitted: 15th May 2002

DATE OF SUBMISSION: 20 MAY 2002
DATE OF AWARD: 5 SEPTEMBER 2002

Modulated Microwave Retro-reflectors and their Applications.

Abstract:

This work seeks to investigate the viability of establishing communications links using modulated microwave reflectors, and explores potential application areas. A primary and underlying objective has been to combine modulation of radar cross section (RCS) with the wide-angle RCS response of a microwave retro-reflector so as to yield a transponder which imparts information content on the reflected spectrum. Since the RCS is electrically large, the communications link is directive and yet the transponder is not a transmitter of microwave energy and hence has modest power needs.

The microwave retro-array was quickly identified as the most promising structure to achieve these aims, and hence the further objectives of the work have been to investigate this structure and fabricate working prototypes so as to:

- achieve a manufacturable structure.
- perform measurements to compare with theoretical models of behaviour.
- explore the limits of performance, and seek to expand them.
- identify applications and markets.
- explore and pursue such related discoveries that may occur.

All the above aims have been explored to some extent, and the findings have been reported in the body of the thesis. The background and historical context is discussed in chapter 1, while chapter 2 reports on the construction and characterisation of 16-element modulated retro-array prototypes operating at a 2.5 GHz carrier frequency. The applied nature of this work is extended in chapters 3 and 4 to printed integrated circuits for passive transponders, and the scaling of these methods to frequencies around 9.2 GHz. Theoretical models for the properties of much larger arrays are presented in chapter 5, and range finding applications and results presented in chapter 6. Two applications are then discussed for which the required array dimensions are estimated, before closing with conclusions and suggestions for future work.

List of publications and patents directly arising from the work.

1) "Modulating Retroreflector as a Passive Radar Transponder"
J. Thornton, D. J. Edwards. *Electronics Letters* Vol 34 No. 19 September 1998 p.1880

2)"Range measurement using modulated retro-reflectors in FM radar system."
J. Thornton and D. J. Edwards. *IEEE Microwave and Guided Wave Letters.* vol.10, no.9; Sept. 2000; p.380-2.

3) "Dimensioning a Retro-directive Array for Communications via a Stratospheric Platform", J. Thornton, *Journal of the Electronics and Telecommunications Research Institute (ETRI)* (Korea). Vol. 24, No.2. April 2002.

4) UK Patent Application Nos. 9907117.7 and 9912840.7. and International Application no. PCT/GB00/01136. "Transponder", J. Thornton and D. J. Edwards.

This suite of patent applications relate to a novel microwave transponder and its use in communications systems and also range finding systems for vehicle guidance and collision avoidance.

5) UK Patent Application No 0207550.5 filed 02.04.02 by J. Thornton "Telecommunications System using Aerial Platforms and Self-phasing Antennas."

This patent application relates to the application of retro-directive and other classes of self-phasing arrays to address the problem of platform orientation and movement for Aerial Platform communications.

Acknowledgements.

This thesis covers a research project in microwave communications which has survived a change of job, city, and the turn of a millennium. Acknowledgement must first be made to Prof. David Edwards at the University of Oxford, for whom I worked during 1997 - 2000 and whom won the EPSRC research grant which initiated my joining the Department of Engineering Science to develop modulated microwave reflectors. My activities at the Communications Research Group soon expanded, and I must also acknowledge the support and enthusiasm of Dr. Alan Jenkins and Dr. Andrew Street who made such an enormous contribution to the group's vibrancy and activity.

Enrolment with the Open University did not occur to me until early 1999, and I must acknowledge the immediate support of my O.U. supervisor Prof. Nick Braithwate and his continued guidance, particularly when circumstances led to a change of location - mid-way through the registration period - to my current research position at the University of York. Despite my move, Prof. Edwards continued to act as my external supervisor, which is a measure of his interest in this work - indeed, we still aspire to finding further applications and commercial niches for its exploitation.

Thanks also to Cyril Band and Steve Mellors at Oxford's Department of Physics for their rather excellent production of the printed circuits. Thanks also to Yurij Zakharov and David Grace at York for their interest and encouragement.

I would also like to thank the following people for the opportunities they have provided over the years: Dr. Sean Paling, Dr David Nixon (University of Portsmouth), Dr. Chris Mann (Rutherford Appleton Laboratory) and Tim Tozer (University of York.)

JT
May 2002

Modulated Microwave Retro-reflectors and their Applications.

Thesis Contents

Chapter 1. Introduction to Modulated Retro-reflectors.

Chapter 2. Prototyping at 2.5 GHz

Chapter 3. Printed Circuits for Modulated Retro-arrays.

Chapter 4. Planar Modulated Retro-arrays at X-band.

Chapter 5. Modelling the Characteristics of Large Retro-Arrays.

Chapter 6. Range Measurements to Modulated Retro-reflectors.

Chapter 1

Introduction to Modulated Retro-reflectors.

1.1 Introduction.

This work seeks to investigate the viability of establishing communications links using modulated microwave reflectors, and explores potential application areas. The technique of modulating the radar cross section (RCS) of a microwave retro-reflector (a structure which maintains its RCS over a wide range of look-angles), so as to impart information content on the reflected spectrum, was first suggested at least as long ago as 1961 by Bauer [1]. Surprisingly, the technique appears to have been almost entirely over-looked by the modern communications arena. This is most likely because technological difficulties encountered by the pioneers of three or four decades ago, combined with the lack of any real marketing drives, stifled any serious development. However, considering the over-crowding of today's radio spectrum and traffic management systems, many niche applications for transponder technology are being suggested. In this light, the ability to realise a *passive* transponder based on a microwave reflector, which may be realised as a cheap and mass-producible structure, becomes an elegant and attractive solution to a number of these application areas.

At the inception of the project at the University of Oxford, the remarkable utility of such a device had been suggested by Professor D. J. Edwards, particularly as a means to enhancing the effective radar cross section (RCS) of small vessels in adverse sea conditions. In this case, a filter matched to the modulation signal of the transponder would effectively reject high levels of clutter (unwanted radar returns). Many additional application areas were soon suggested, including long range tagging, vehicle tracking, telemetry, or indeed any situation where it is advantageous to establish a communications link with a *passive* transponder. In essence, such a link is established by illuminating a

structure which has a RCS which is modulated with the information signal to be conveyed. The reflected spectrum contains frequency components which include this modulation signal and which may be recovered at a receiver, in most cases co-located at the transmitter. If a phase-conjugating (retro-reflecting) structure is employed, the signal strength in the direction of the transmitter is greatly enhanced, while reflected power in other directions is suppressed. Thus the power link budget is improved and the technique is "clean" in terms of radio pollution. Many transponders may be interrogated by a single transmit/receive station. The power consumption of each transponder is extremely low since they require neither radio frequency (RF) power sources nor amplifiers in the simplest case, merely a low power modulation circuit and hence the term *passive* may be used.

1.2 Historical Summary.

The field of radio communications is vast and the following overview of radar techniques is necessarily brief. Long range identification transponders have been in use for many years [2] in a number of areas and basically follow the IFF ("Identify Friend or Foe") approach of actively transmitting a response to an interrogating radar. Such a class of transponder might be called "responder". These approaches suffer the disadvantages that the target requires signal processing equipment to generate a response, and generally transmits omni-directionally so that other listeners on the same frequency are likely to receive the broadcast. This also means that the power transmitted by the responder is unnecessarily larger than that required to establish the link. The retro-reflecting transponder is an alternative approach which is highly under-exploited at the present time and is the subject of this work. A small number of prior works alluding to this technique, mostly confined to the realm of suggestions rather than demonstrable hardware, have been published and will be reviewed here. It appears that no actual devices or systems are commercially available.

In the early stages of the investigation, reflective structures based on optical principles, such as trihedral reflectors, were considered the most likely starting point. However, the concept of the modulated retro-reflecting antenna array was adopted as the most promising structure even before prior work in the area came to light. The retro-array [3,4] is an antenna array where antenna pairs are joined by transmission lines to achieve approximate phase-conjugation. Modulation of the array may be readily achieved by employment of switches in the transmission lines. This technique presents many advantages compared to optical corner reflectors:

- Ideal for the microwave spectrum where commercial radar operates.
- Polarisation, bandwidth and angular response can be tailored by the characteristics of the antenna element chosen.
- There is the potential to develop structures which are planar.
- Efficient solid state switches allow for high index of modulation and low power consumption.
- It will be shown that they may be fabricated as cost effective printed circuits, ideal for commercial applications.

Historically, applications for the retro-array were being suggested in the early 1960s, mostly in the context of communications satellites. At that time, purely passive, unmodulated satellite reflectors [5] were being postulated as a means of facilitating over-horizon communications. The concept of an active (i.e. amplified) Van Atta reflector was also advanced in this context [6]. References to reflective communications links to satellites may be found in textbooks of this era, such as [19] which has a section entitled "Passive space communication systems" and which reviews such diverse concepts as balloon reflectors, retro-reflectors and "distributed reflectors", the latter including, possibly, a belt of orbiting chaff. Interestingly this reference concludes that an active "repeater" is approximately 51 dB better than a passive repeater for a low orbit (at a height

of around 1000 km). However, satellite communications evolved in a very different direction, based on separate uplink and downlink frequencies transmitted via active travelling wave tube amplifiers and high gain antennas mounted on a stabilised space vehicle. It is suggested that the pioneers in retro-arrays were largely overlooked in light of such developments.

The concept of a passive transponder for terrestrial applications still appeared to be sound, but the relative under-development of semiconductors and printed microwave circuits in the 1960s are likely to have precluded their general adoption since they could not be realised as cheap, mass-producible structures. For example, Bauer [1] in 1961 suggested using ferrite phase shifters as a modulation mechanism, each of which would consume 100 mW of power and allow modulation rates up to 10 kHz. This approach is highly unwieldy and performance is poor compared to the printed circuits & semiconductor switched arrays the development of which forms a large part of the content of this work.

1.3 Coherent Transponding Systems:

A number of transponding systems based on coherent detection of modulated scatterers, suggested up to the mid 1970s, are summarised by King [7]. They are based on homodyne detection of the spectrum of a co-operative scatterer and illustrate some of the advantages of the employment of such scatterers. None, surprisingly, suggest the employment of retro-reflecting transponders even though the advantages in terms of range and power budget must have been known (at least in theory) at that time. The lack of modulating retro-reflecting *hardware* may explain why the inclusion of this technique appears to have been again overlooked during this period.

1.4. Statistical Aspects of Radar.

This section will review the important statistical aspects of radar systems.

1.4.1 Clutter

The term *clutter* refers to unwanted echoes in the returned signal at a radar receiver. Its source is the environment which is illuminated by the outgoing signal, and its effect is to mask out the returns from the targets of interest which may produce a weaker echo than the clutter. Clutter tends to increase the number of "false" echoes on a radar display, and is usually very dependent on siting factors for the transmit and receive antennas which in turn are usually co-located. For terrestrial applications, clutter effects are dominated by unwanted returns from the surface near the transceiver, typically from buildings, vegetation and uneven terrain. In maritime applications, clutter is highly dependent on the condition of the sea's surface (the "sea state") and in all cases the weather and precipitation in particular are a major source of clutter.

The Earth's curvature tends to limit surface clutter to echoes from short range, whereas long range radar sensitivity is limited by signal-to-noise ratio. Therefore, in pulsed radar systems, it is often advantageous to reduce receiver sensitivity (gain) in the earlier detection period between pulses, and ramp up the gain to its maximum for the latter part of the detection period. This common technique is known as *swept gain* or *sensitivity time control* (STC).

The suppression of clutter is a major concern to the radar systems designer. Weather clutter may be minimised by adoption of circularly polarized radiation, since rain droplet RCS is much reduced in this case. Ground clutter is best minimised by careful sighting of antennas. Moving targets are more easily distinguished from clutter than stationary ones, either by direct observation of the doppler shift on the RF carrier, or by detection of the doppler shift applied to the pulse repetition frequency (PRF) of the returned pulse train. In

these cases, only a radial velocity, i.e. towards or away from the transceiver, will give rise to a doppler shift. Non-radial movement may be detected by comparing successive pulses and cancelling common components. Until the 1970s quartz ultrasonic delay lines were widely used for this purpose, but the modern approach is to compare successive video frames by digital signal processing techniques.

1.4.2 Matched Filtering

In pulsed, and in particular pulse compression systems, matched filtering is usually employed to maximise signal-to-noise ratio. The matched filter is a type of correlator, whose output is found by convolving the input signal with the filter's impulse response. This is equivalent to multiplication of their respective frequency spectra. Since the filter is matched to the transmitted waveform, typically a CW pulse or FM pulse, its frequency spectrum is the complex conjugate of that transmitted, so that multiplication of the spectra performs autocorrelation. Use of matched filters optimises the decision making process at the receiver, since the random fluctuations which can lead to "false alarm" signals are minimised. It should be added that real hardware can produce only approximate matched filtering.

1.4.3 Target Fluctuations.

It is very difficult to derive analytical solutions for RCS since a mathematical description for boundary conditions, necessary for the exact solution of Maxwell's equations, cannot generally be derived for arbitrary surfaces in free space. An analytical solution for the sphere does exist [13] since in this case the surface of the target conforms to the natural co-ordinate system used to describe its surrounding space. For other surfaces, such as a plane reflector or corner reflector, approximations based on geometrical optics are useful if the object is large compared to the wavelength of the illuminating radiation. In such cases, diffraction effects at surfaces edges may be neglected without a large loss in accuracy. To

include such effects, more physically accurate methods based on numerical techniques may be employed such as the moment method (or Boundary Element Method) [14] which has been successfully applied to, for example, wire antennas.

A typical radar target (e.g. ship or aircraft) has many reflecting surfaces each of which contributes to the overall reflectivity of the object. Wave interference effects lead to a complicated response for target RCS as a function of look angle in either monostatic or bistatic radar installations. Hence, in practical cases, RCS is always strongly dependent on angle of illumination and angle of observation. In addition, wave polarization, frequency, and the electrical properties of the materials comprising the target have a strong effect. For these reasons, average values are often used to compare different targets. Table 1.1 gives typical values for a variety of targets at X-band [16, 17].

Target	RCS (m^2)
bird	0.01
missile	0.5
person	1
small aircraft	1-2
bicycle	2
small boat	2
fighter aircraft	3-8
bomber	30-40
large airliner	100
truck	200

Table 1.1 Typical RCS for common targets.

Further, similar examples are given by [18] which also states that the RCS for an "advanced tactical fighter" would be as low as –60 dBsm (decibel square meters) – some 10 dB less than that of an insect. Corroboration of this impressive claim for stealth technology has not been pursued by this work.

1.4.4 Ultra Wideband Radar

The term Ultra Wideband (UWB) radar has recently come to encompass impulse, time domain, non-sinusoidal, carrier free and large-relative-bandwidth signals. A good, two-part review article may be found in [20]. In the context of this work, UWB would be best considered to be synonymous with *ultra short pulse length*, and would represent the logical extension of the short pulse length and pulse compression techniques which have evolved to extract increasingly detailed information about a target under examination. Interestingly, [20] draws a clear distinction between a UWB *radar* and a UWB *sensor*. The former is intended to *detect* a target, while the latter is intended to *identify* the target and is therefore more closely related to our theme. In a UWB sensor, the pulse length in space is much shorter than the target's length, and information may be extracted from the target in the time domain. The ultra shortness of the pulse leads to individual scattering components of the target's structure becoming distinguishable rather than forming a composite RCS term. This process is sometimes called time domain decomposition of RCS. The information extracted may thence be analysed in the frequency domain, or shown as time-frequency plots which effectively express a target's spectral signature. For this technique to be useful, it would seem that prior knowledge of the target's signature is required so that a comparison with a look-up table can be carried out for purposes of identification.

Alternatively, matched pulse or matched adaptive time-frequency packet (MAP) techniques [20] have been suggested, whereby a target is interrogated by a (non-sinusoidal) test pulse which is intended to be the complex conjugate of the target's impulse response. If the test pulse has been correctly chosen, the return from the target is maximised in what is effectively a matched filtering process, while that from other targets is minimised. Again, a database of test-pulse shapes, and hence prior knowledge of target characteristics, is implied by this technique.

1.4.5 Cooperative and Non-cooperative Targets.

The identification of non-cooperative targets has become increasingly important in civil as well as military applications. By "identification" we mean the discrimination of different types of target and also of similar targets within a class of targets. This clearly implies the extraction of more information content from the radar measurement than just range, bearing and RCS. The process consists of firstly establishing a database of the properties of the backscattered waves from known targets. The actual measured properties for the unknown target under scrutiny are then compared with the database (as discussed above), and decisions based on the degree of correlation are made. The properties which contribute to radar signature that are studied in this context include polarisation, time domain response and frequency domain response [15]. For example, the natural resonance of a target may be examined by illuminating with a range of frequencies. Also, moving components such as aircraft propellers or compressor blades produce doppler shifts which may help identify the target if those properties are listed in the database. A difficulty of this method is the initial study of the targets of interest to generate the database of radar signatures. The signal processing required is clearly not trivial.

1.4.6 Summary

When we consider the likely information content which may be extracted from such a statistical approach to target identification, and the confidence of its accuracy, we may feel that the investment in effort in gaining this data is disproportionately large. In military situations non-cooperative target identification will remain an ongoing and competitive study, but there is less need for civil radar system development to evolve along similar principles. When a target is co-operating with its traffic managers, a small investment in hardware and power consumption can yield an effective, high data-rate communications link, and hence we return to the theme of generating a cooperative radar signature by RCS modulation.

1.5. Optical Retro-reflectors and Retro-directive Arrays.

This section will discuss optical retro-reflectors and then introduce microwave retro-arrays.

1.5.1 Rationale.

Retro-reflectors have found use in many application areas from road signing to satellite and space applications. These devices are essentially passive in that the retro-reflecting structures have fixed radar cross section and the reflected signal is effectively the same signal as that transmitted.

In the field of terrestrial and marine traffic control there is an increasing need to detect, track and identify craft within the surveillance area. This is of particular relevance to harbour and airport traffic management, particularly considering small vehicles with inherently low radar cross sections (RCS). At present, simple retro-reflectors comprising corner structures are sometimes employed on small craft to increase their RCS. These are passive devices, designed along physical optics principles – some variants are illustrated in Figure 1.1. They are relatively simple and inexpensive to produce. Clearly, a requirement of future transponders employed in these fields are simplicity, light weight, low cost, low power consumption and furthermore not polluting the electromagnetic environment.

Long range identification is traditionally achieved by actively transmitting a response to an interrogating radar. Such a method is employed by the military "Interrogate Friend or Foe" (IFF) system. (We have discussed the disadvantages of transmitter and signal processing equipment on board the target and the omnidirectionality of the response, which requires a transmitted power which is excessively large and pollutes the local radio environment.) The rationale behind the development of the retro-reflecting transponder is the establishment of the communication link by redirecting the interrogating signal back toward its source, thus eliminating the need for a transmitter and associated equipment on the target. Many types of structure exist, based mainly on physical optics principles [8] and

much literature exists reporting work undertaken to investigate and model their performance.

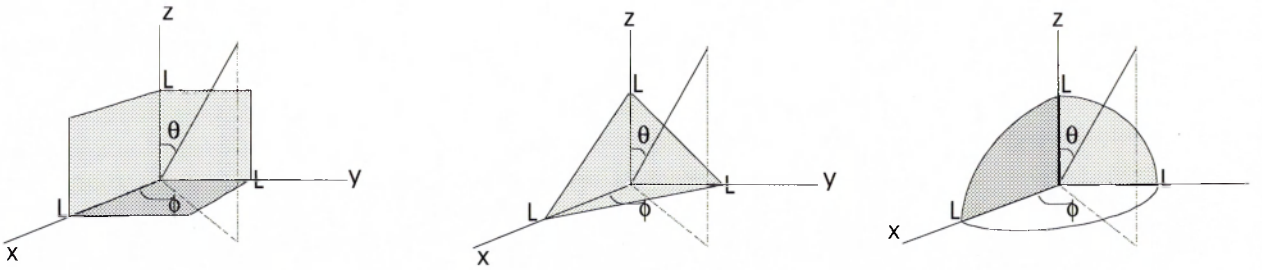

Square Trihedral Triangular Trihedral Circular Trihedral

Figure 1.1. Variants of trihedral corner reflector.

1.5.2 Corner Reflector.

As part of the initial investigation, literature on conventional dihedral and trihedral corner reflectors was reviewed [10,11,12]. The former are retro-reflective in a single plane only, whereas the latter retro-reflect in three dimensions. As mentioned above, simple corner reflectors have been employed as a means of increasing RCS in the maritime environment. A comparison of variants of the trihedral reflector are shown in Table 1.2 below.

Type	Maximum RCS	Average RCS	Angular coverage (3 dB points)
square	$\frac{12\pi L^4}{\lambda^2}$	$\frac{0.7\pi L^4}{\lambda^2}$	23° cone about symmetry axis
triangular	$\frac{4\pi L^4}{\lambda^2}$	$\frac{0.17\pi L^4}{\lambda^2}$	40° cone about symmetry axis
circular	$\frac{15.6\pi L^4}{\lambda^2}$	$\frac{0.47\pi L^4}{\lambda^2}$	32° cone about symmetry axis

Table 1.2. Comparison of Trihedral Corner Reflectors.

The theoretical angular response for these devices is reported in [8], along with some experimental data. In summary, Figure 1.2 illustrates the trend in angular response for these device types, by showing theoretical plots for the triangular trihedral corner reflector for various angles away from boresight. The axis system is shown in Figure 1.1.

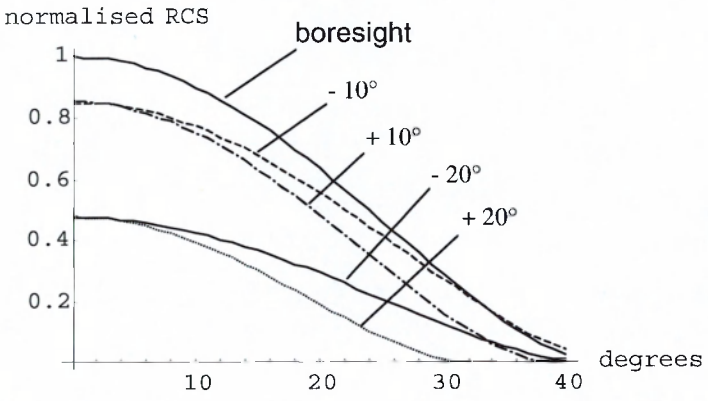

Figure 1.2 Normalised RCS for triangular corner reflector ($\lambda = L^2$) as a function of α (where $\alpha = \phi - 45°$) for various values of theta away from boresight. The maximum RCS occurs along the boresight, defined as $\theta = 54.7°$, $\phi = 45°$

Apart from the physical volume occupied by these devices, they present other disadvantages. The corner reflector is a device based on simple geometric optics considerations and is in reality only functional when the wavelength is small compared to the reflector's dimensions [12]. At typical maritime radar frequencies, this may require bulky 3-dimensional structures, which may reduce the practicality of this approach, particularly for small craft. To establish a unique radar signature/communications link, modulation of the reflector's RCS is required, but this is non-trivial and may for example require the employment of frequency selective surfaces in the aperture of the device.

If an effective means of RCS modulation can be developed, the retro-reflected signal may be modulated with a code unique to the target, hence the target may identify itself to the interrogator without the need to supply power for a transmitted RF signal. A pre-requisite for any modulation mechanism is therefore that of low power consumption, to capitalise on the energetic advantages of this approach. Furthermore such a device primarily returns the signal to the interrogator and little or no power is re-radiated elsewhere, thus reducing the

probability of detection by other receivers and hence limiting the pollution to the electromagnetic environment.

1.5.3 Modulated Corner Reflector.

A modulated dielectric corner reflector was suggested by Lewis and Pietch [9] in 1968, in which the means of modulation is a gaseous discharge tube on one of the reflecting walls. The gas may be ionised by a suitable electric field. The incident electromagnetic wave suffers a phase shift at the dielectric-gas interface. If the gas is ionised, this phase shift is always close to π, but in the absence of ionisation the incident wave must arrive at an angle greater than θ_c (the critical angle) to undergo total internal reflection. This reflection suffers a phase change between 0 and π which is dependent on angle of arrival. The phase modulation thus produced has a modulation index which is dependent on arrival angle, which is a disadvantage of this approach. A variation of this method achieves amplitude modulation by placing the gas tube up to 0.175 λ behind the dielectric wall to reflect the evanescent field in this region, which would interfere destructively with the internally reflected wave. King [7,9] does not comment favourably on the modulation index which might be possible using this scheme. Other disadvantages of corner reflectors in the microwave spectrum include the physical size of the reflecting surfaces. A trihedral reflector is by definition a three dimensional structure, whereas the antenna retro-array may be a planar structure which still functions over the three spatial dimensions and is better suited to the microwave region.

1.5.4 The Retro-Array

This comprises an antenna array where antenna pairs are joined by transmission lines to achieve (an approximate) phase conjugation, as illustrated in Figure 1.3 below. This structure lends itself to the modulation of the properties of the transmission line and hence the RCS of the array.

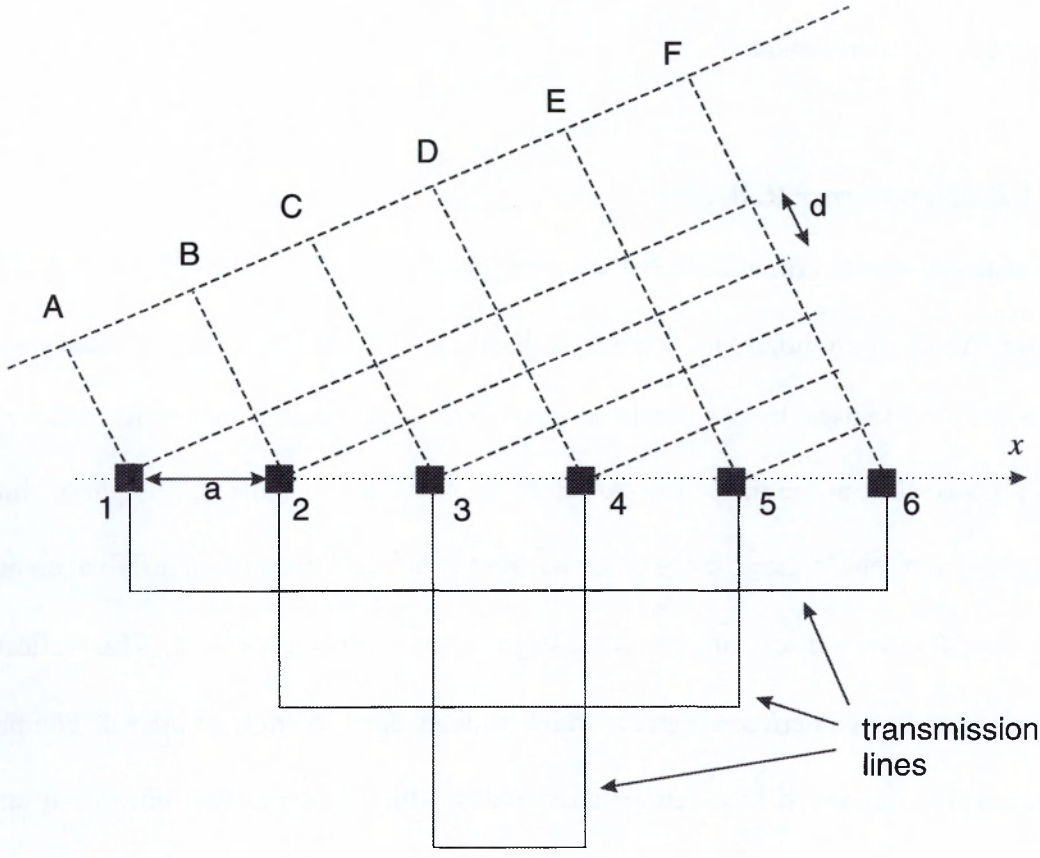

Figure 1.3. Geometry of retro-array.

Figure 1.3 shows a six element linear array of like antennas (1 - 6) aligned along the x-axis. The elements may be considered to be omnidirectional with regard to radiation pattern and well matched to both free space and the connecting transmission lines. The antennas are joined in pairs, by transmission lines of equal length L_{TL}. Thus antenna pairs 1 and 6, 2 and 5, and 3 and 4 are linked bidirectionally. Consider a plane wave incident at an angle θ to the x-axis. If we take points A to F in the incident wave front, energy from point A is received by antenna 1 and re-radiated by antenna 6, energy from point F is received by antenna 6 and re-radiated by antenna 1, and so on for the other antenna pairs. The path lengths AF, BE and CD are all equal and given by:

$$L_{AF} = L_{TL} + 5d + \text{constant} \tag{1.1}$$

where $$d = k\,a \cos\theta \tag{1.2}$$

and $$k = \frac{2\pi}{\lambda} \tag{1.3}$$

Therefore the radiated power from each antenna adds constructively in the direction θ i.e. the reflected wave is in the same direction as the incident wave.

Another way of visualising the array's characteristics is a consideration of the array factor of a phased array antenna, where the gain pattern of the array $G(\theta,\phi)$ is given by the product of antenna element gain $g(\theta,\phi)$ and the array factor F:

$$G(\theta,\phi) = F\, g(\theta,\phi) \tag{1.4}$$

For a uniform, linear array:

$$F = \frac{\mathrm{Sin}\frac{Nu}{2}}{\mathrm{Sin}\frac{u}{2}} \tag{1.5}$$

where $u = k\, a \cos\theta + \delta$, N is the number of elements and δ is the phase shift between elements.

For the retro-array, the phase delay between each element's radiation is given by

$$\delta = -\, k\, a \cos\theta \tag{1.6}$$

so $u = 0$ and the array factor converges and is simply given by

$$F = N \tag{1.7}$$

Therefore, to a first order (since we will not consider here the mutual coupling between elements, the finite size of the ground plane and mismatches between free space and the antennas and the antennas and the transmission lines) the gain of the retro-array is given by:

$$G(\theta,\phi) = N\, g(\theta,\phi) \tag{1.8}$$

The RCS is given by the square of the gain, since the transmit gain is the same as the receive gain in this case. It is worth noting that the RCS of the array may be tailored by selection of an appropriate $g(\theta,\phi)$ - this will then define the angular variation of the RCS of the array. The choice of array element is therefore of fundamental importance in defining

the performance of the retro-reflector in both its angular response and the magnitude of its reflectivity.

In this class of structure, modulation of the RCS may be achieved by means of suitable switching circuitry on the transmission lines. Additionally, antenna elements may be chosen which have a selected polarisation response and radiation resistance. We observe that an advantage of this approach is that the array may readily be tuned or tailored for a specific application, be it broad or narrow band. It was observed at an early stage in the research that photolithographic techniques could facilitate economic production of planar antenna arrays for this application and be easily integrated with solid state modulation circuits. These techniques are explored in the following chapters.

1.6 The Radar Equation.

The essential form of the radar equation is often given by:

$$P_r = \frac{Pt.Gr.Gt.\sigma.\lambda^2}{(4\pi)^3 r^4} \tag{1.9}$$

in the monostatic case i.e. the receiver and transmitter are co-located. P_r is the power received by a target of radar cross section σ which is at a distance r from the transceiver which transmits power P_t . G_r and G_t are the gains of the transmit and receive antennas respectively. If a single antenna performs the same task, or the antennas are identical, the terms may be replaced simply by G^2. The received power is clearly dominated by its inverse relationship to the fourth power of distance, so signal to noise ratio and receiver sensitivity are limiting factors at large distances.

References.

[1] "Technique for amplitude modulating a Van Atta radar reflector", L. H. Bauer. *Proc. IRE,* 1961, Vol 49 no. 3 pp 634 – 635.

[2] "Radar Systems", P.Lynn, *MacMillan.* 1987

[3] "Antennas", John D. Kraus (2nd ed.) *McGraw-Hill* 1988 pp. 496 - 497.

[4] "Van Atta Reflector Array", E. D. Sharp and M. A. Diab, *IRE Transactions On Antennas And Propagation* VOL AP-8 July 1960. pp 436 - 438.

[5] "Passive Satellite Communication", J. L. Ryerson, *Proc. IRE,* 1960, Vol 48 no. 6 pp. 613 – 619

[6] "Communications Satellites Using Arrays", R. C. Hansen, *Proc. IRE,* 1961, Vol 49 no. 6 pp. 1066 – 1074 (also correction pp. 1340 – 1341)

[7] "Microwave Homodyne Systems", R. J. King, 1978, *Peter Peregrinus Ltd. on behalf of IEE.*

[8] "Radar Cross Section Handbook" Vol 2, Edited by Ruck, *Plenum Press* 1970. pp 588 - 599

[9] "Modulated Retrodirective Corner Reflector", B. L. Lewis and L. Pietch. US Patent 3,417,398 Dec.1968. (See also [7] pp. 264 – 266.)

[10] "Simple Model of Corner Reflector Phenomena". H. D. Eckhardt. *Applied Optics* Vol.10 No.7 July 1971

[11] "Efficient Solution for Backscattered Field of a Corner Reflector". C. G. Park, N. H. Myung, S. D. Choi, *Electromics Letters* Vol 31. No.9 April 1995

[12] Ref [3] pp. 560 – 561

[13] "Beitrage zur Optik trüber Medien, Speziell Kolloidal Metaläsungen", G. Mie, *Ann Phys.* 25, 1908, pp 377 – 466.

[14] "Field Computation by Moment Methods", R. F. Harrington, *MacMillan.* 1968.

[15] "Advanced Radar Techniques and Systems", Edited by G.Galati, . *Peter Peregrinus Ltd. on behalf of the IEE,* 1993. pp 542 - 591

[16] "Microwave Engineering." p 687. David M. Pozar. *Addison Wesley* 1993

[17] "How to Design an 'invisible' Aircraft", J. A. Adam, *IEEE Spectrum* pp.26-31, April 1988

[18] "Antenna Theory, Analysis and Design" (2nd Ed.) C. A. Balanis, *Wiley* 1997. p. 91

[19] "Introduction to Space Communication Systems" G. N. Krassner, J. V. Michaels, *McGraw-Hill* 1964. pp. 25 - 28, 149 - 150, and 239

[20] "History of Ultra Wideband Communications and Radar", part I, Microwave Journal, January 2001, Vol. 44 no. 1 and part II, Microwave Journal, February 2001, Vol. 44 no. 2.

Chapter 2

Prototyping at 2.5 GHz

2.1 Unmodulated Retro-array Prototypes.

The retro-array, described in chapter 1, was first conceived by Van Atta. Refs [1-3] report on the performance of such a device at 2.85 GHz, where the array consisted of a 4 x 4 rectangular matrix of half-wavelength dipoles, horizontally aligned a quarter wavelength above a ground plane and spaced at intervals of 0.61 wavelengths. As a convenient starting point, and to aid direct comparison, this design was replicated but scaled to an operating frequency in the 2.5 GHz band.

Prototype dipoles were built by feeding RG/316/U flexible co-axial line through an axial drilling in a PTFE rod of 8 mm diameter. The radiating elements were formed by stiff copper wire soldered to the inner and outer conductors. The properties of dipole antennas are well documented [4]. To summarise their characteristics, the optimum match (hence radiation efficiency) occurs for a wire length of slightly less than a half wavelength. The conductor thickness has a secondary effect on the resonant frequency, as does the proximity of a ground plane, so this type of antenna is often empirically tuned [5]. The resonant frequencies of dipoles of various lengths were measured using an HP 8753 vector network analyser - a tool much used throughout the project. The dipoles were placed horizontally 30 mm above a ground plane, thus meeting the quarter wavelength condition at the 2.5 GHz design centre frequency. The results are shown in Figure 2.1. The optimum length thus derived was 52.5 mm.

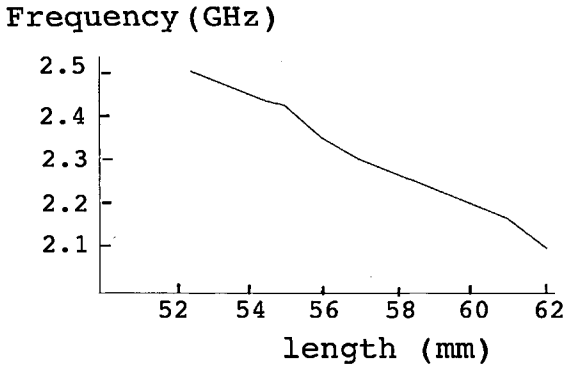

Figure 2.1. Dipole resonant frequency versus length.

The first prototype retro-array was fabricated by fixing a 4 x 4 array of such dipoles above an aluminium ground plane measuring 32 cm along the axis parallel to the dipoles and 28 cm along the orthogonal axis. The PTFE supports were press fitted into circular drillings in the aluminium plate. The antennas were joined in pairs in the ordering given by [2], which is the two dimensional equivalent of the coupling order shown in chapter 1. The coax lengths were chosen to be 500 mm – the length is not important but all lengths should be the same to preserve the phase relationships which produce phase-conjugation. Excessive cable lengths result in greater RF losses, and should be avoided. The maximum cable span required was 500 mm so this value was used for all 8 cables. A photograph of the fabricated 16 element dipole array is shown in Figure 2.15. (This dipole array layout was common to the various unmodulated and modulated arrays which are described in this chapter, and hence several were constructed)

2.2 Unmodulated Array Radar Cross Section

Neglecting the angular response, a uniform antenna array has maximum gain $G = N\, g_{el}$, where N = number of elements and g_{el} is the maximum gain of each element. For the dipole array prototype, $N = 16$ and $g_{el} = 2.8$, or 4.5 dBi [4].

the maximum RCS is then given by: $\sigma = \frac{\lambda^2}{4\pi} G^2$ (2.1)

and since $\lambda = 0.12$ m we have $\sigma = 2.3$ m^2

It is instructive to compare this with the maximum RCS of the ground plane, given by [6]:

$$\sigma_{max} = \frac{4\pi A^2}{\lambda^2} = 7 \text{ m}^2 \quad (2.2)$$

and consider why the maximum plate RCS is significantly bigger than that of the retro-reflector. The reason lies in the spacing of the retro-reflector antenna elements. To avoid the effects of mutual coupling between elements, they are spaced sufficiently apart that the effective areas of the elements do not overlap. Since the effective area of an antenna is:

$$A_{eff} = \frac{\lambda^2 G}{4\pi} \quad (2.3)$$

the effective area of the dipole has a diameter 0.54 λ, while the spacing of elements in the array is 0.61 λ. Therefore, the dipole effective areas are distributed over the ground plane, with effective gaps between the elements. Since the ratio of the effective area to physical area is 1.7, the associated RCS ratio would be the square of this, or 2.8, which is almost exactly the ratio (i.e. 3.0) between the retro-reflector RCS - which is due to dipole effective area - and the ground plane RCS - which is due only to a physical area. (The apparent error is due to the extra ground plane area at its edges). The consideration of antenna effective areas has thus given some insight into the relationship between the different types of target, and the way the retro-reflector utilises the physical space in which it is constructed.

To further study these effects, measurements of the monostatic RCS were performed using a network analyser as source and receiver. In the absence of a fully anechoic test facility, a semi-anechoic environment was facilitated by the use of radar absorbent foam lining a screened room, as illustrated in Figure 2.2. While this approach is unconventional, it did require the least number of components. The absolute magnitude of the RCS was not determined, but the measurement of relative RCS compared to a metal plate reflector was useful in demonstrating changes in RCS and the angular response of the retro-reflector during the earliest stages of the investigation.

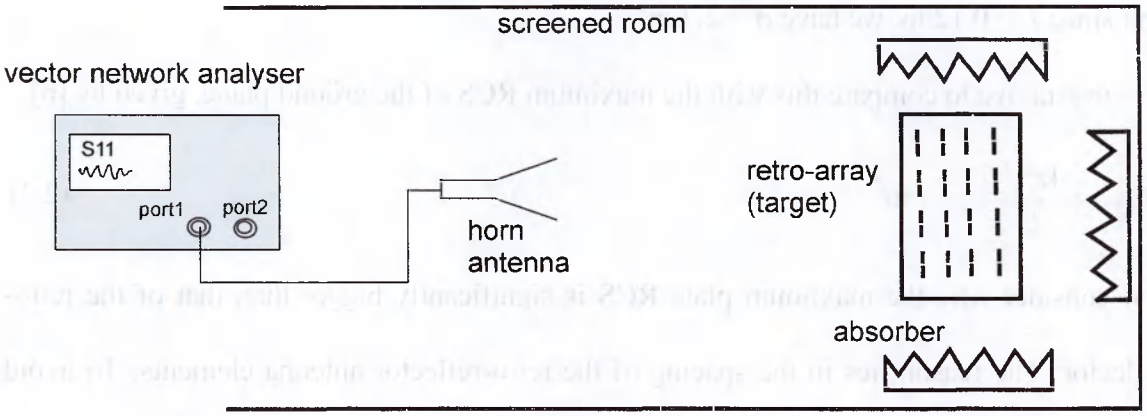

(a) Test method

feedhorn →

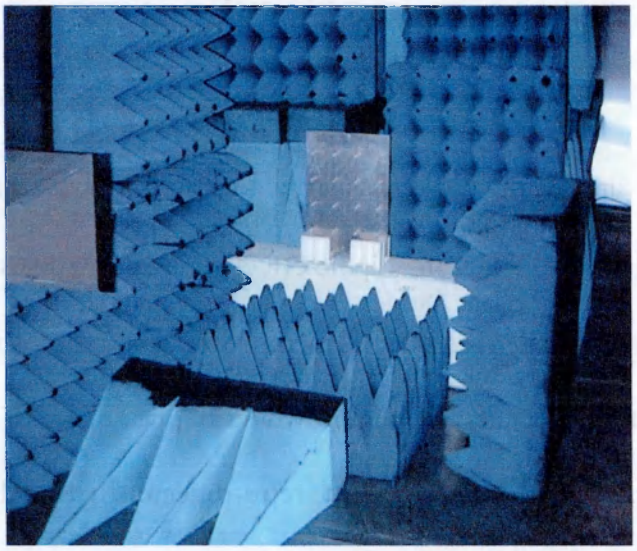

(b) Photograph of retro-array in measurement chamber

Figure 2.2. Method for approximate RCS measurement.

In this method, the reflection coefficient (S_{11}) of the horn antenna may be measured at a given frequency. The measurement is calibrated by storing the data in the absence of the target i.e. the data for the environmental reflections. The target is then put in place. Selecting "data/memory" at the HP8753 network analyser gives a relative signal the magnitude of which is dependent on both the magnitude and phase of the power reflected from the target, since a standing wave exists between the antenna and the target at a given frequency. It is then necessary to adjust this distance to obtain a maximum (or minimum) in the measurement. Alternatively, the measurement is more easily visualised by using a frequency sweep close to the frequency of interest (for example 2.2 – 2.8 GHz). The measurement then shows an oscillatory waveform in the frequency domain, and relative

RCS may be estimated by looking at the interference peaks adjacent to the frequency of interest. A further target, in this case a plane reflecting sheet of the same outer dimensions as the array, is used as a standard for obtaining a value of the array RCS.

Measurement errors: Clearly the signal strength returned in such a measurement is dependent on the magnitude of the target's RCS compared to the background reflections, thus a truly anechoic environment is needed for high signal-to-noise ratio measurements. The environment available was rather worse than this ideal. The plate's peak RCS corresponded to a reflection coefficient difference of just 0.65 dB, or 16% above background, while measurement accuracy, estimated from repeatability, was around 0.1 dB which is 2.3 % above background and therefore 0.14 of the plate peak RCS. From this figure, the error bars in Figure 2.3 are derived. Since the error is large compared to the measurement, not too much information about the structure of the targets' RCS versus angle should be inferred. However, the measurement has sufficient resolution to identify a difference in RCS response between the target types.

With the intention of building an amplitude modulated array at a later stage, a second prototype array was built where the coaxial transmission lines were terminated by absorptive loads, instead of being routed to the counterpart antenna. Here the intention was to achieve a low RCS so that a demonstration of different RCS magnitudes might be established. Again, the RCS was measured and compared with the retro-array. To achieve a high modulation index, a large change in RCS was sought between the two prototypes. Measurement results are shown in Figure 2.3.

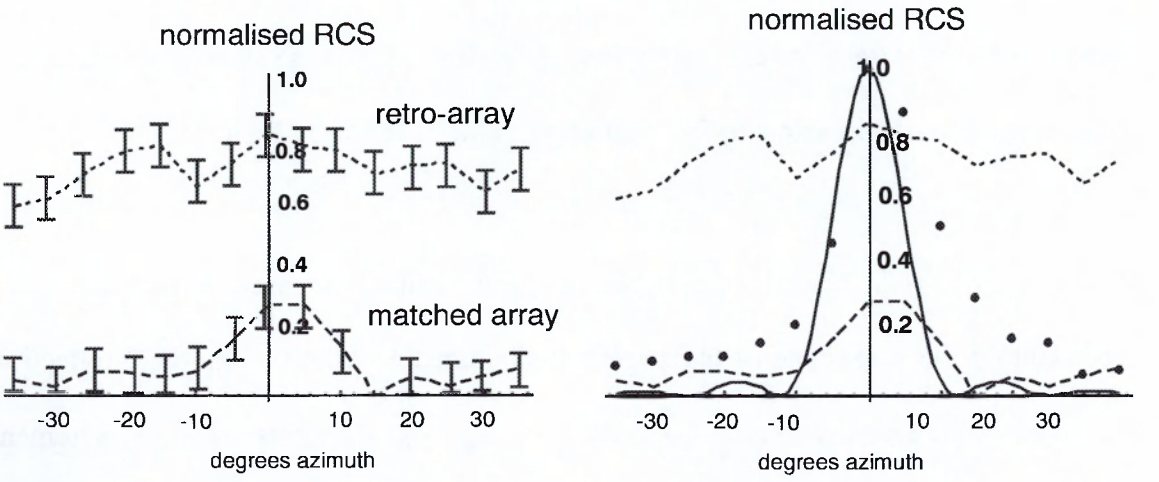

(i) measured data with error bars (ii) comparison with plate (— theory • measurement)

(a) measured at 0° elevation tilt.

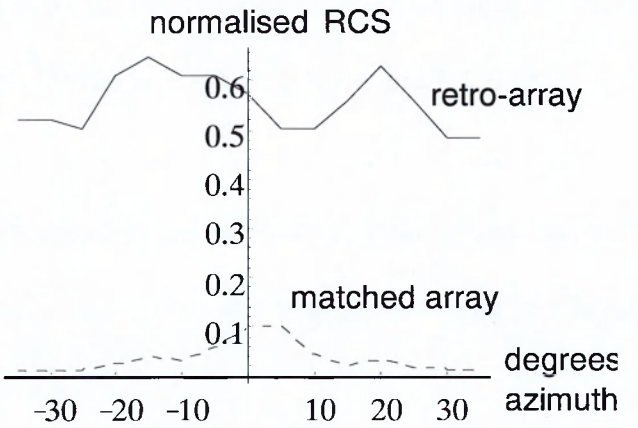

(b) measured at 20° elevation tilt

Figure 2.3. Array RCS variation with look-angle, relative to plane conducting plate.

In Figure 2.3 (a), the theoretical monostatic RCS of the plate is also shown, where, after [6]:

$$\sigma_{plate} = 4\pi\left(\frac{ab}{\lambda}\right)^2 \cos^2\theta\left[\frac{\sin(\beta b\sin\theta)}{\beta b\sin\theta}\right]^2 \qquad (2.4)$$

for a rectangular conducting plate of sides a and b rotated through incidence angle θ about the a axis.

The measurements demonstrated the required characteristic of the retro-array, namely, a strong RCS which varied weakly with the look angle. RCS is displayed as a function of azimuth rotation of the array for two cases of elevation rotation: a) 0° elevation rotation (i.e. vertical) and b) 20° elevation rotation, with respect to the incident RF wave. RCS is shown relative to the maximum measured RCS of the metallic plate of the same shape as the array ground plate.

In addition, it is apparent that the measured RCS ratio between the retro-reflector and the plane plate is rather greater than the theoretical case discussed above. This is because the retro-reflector is in reality a composite structure, consisting of two RCS components: (i) the retro-reflecting component and (ii) the specular reflecting component of the ground plane. The latter is due to the area of the ground plane which falls beyond the effective area of the dipoles, which, as was discussed above, is less than the physical spacing area. We thus expect some energy to "escape capture" by the antenna element, and be reflected by the plate - this is most apparent in the measured on-boresight reflectivity of the matched array. For the retro-reflector, while the phase relationship between the two components has not been determined, it would appear that constructive interference is contributing to an increase in the RCS. This effect contributes to the structure of the measurement, and could be determined theoretically from the phase and amplitude response of the plate's RCS. (We might also identify this composite nature of the retro-reflector RCS as a fundamental disadvantage compared to the optical corner reflector approaches discussed in chapter 1.) However, these concerns only apply to the un-modulated characteristics of the retro-array. The composite RCS nature disappears when the RCS is modulated, since the spectra of the retro-array component becomes decorrelated from the parasitic RCS due to energy which is not coupled into the antenna and modulation circuitry. As the work now focuses on modulated structures, the un-modulated RCS will not be further considered.

2.3 Modulated Retro-array Prototype.

Having demonstrated that a strong change in RCS could be achieved, a third prototype array was built where switching circuitry was added to the coaxial lines behind the ground plane. Thus, a double-pole, double-throw switch for each dipole pair was required. Purpose built switches based on microstrip circuit and PIN diodes were fabricated, with the aim of achieving the lowest possible insertion loss in the "on" state and low reflection coefficient in the "matched" (low-reflectivity) state. A schematic of such a switch is shown below in Figure 2.4.

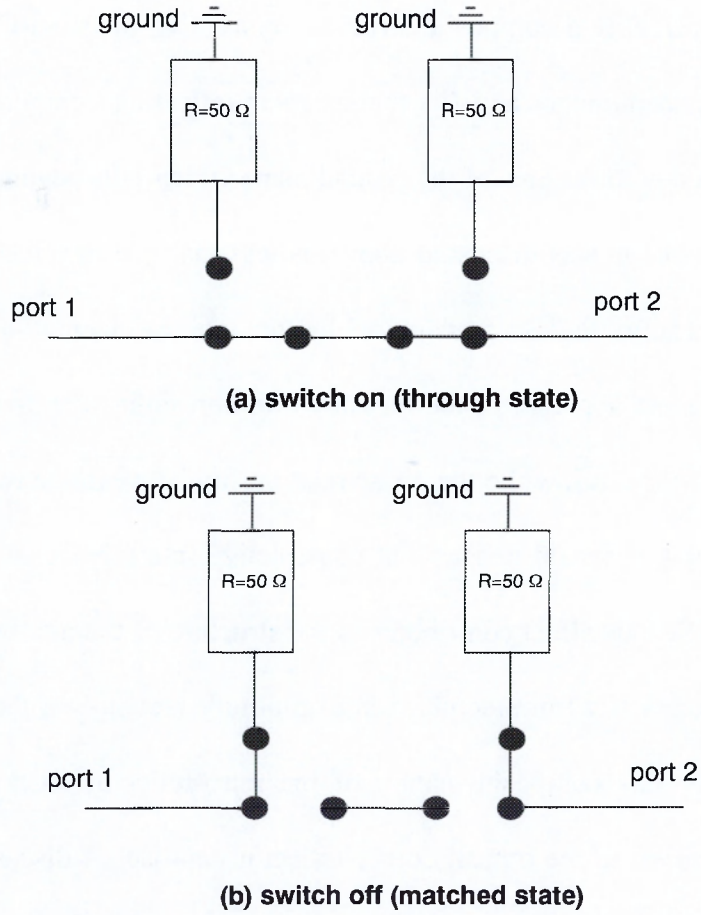

Figure 2.4. Schematic of double-throw, double pole RF switch

2.3.1 Microstrip Design Techniques.

To design microstrip circuits successfully it is vital to accurately model the characteristic impedance of the line (Z_0), and the wavelength in the line λ_{TL}. Both are a function of the

microstrip dimensions illustrated in Figure 2.5, and the dielectric constant of the substrate ε_r. There is much literature discussing microstrip design techniques [7-10] - it is nevertheless valuable to summarise the basic properties of this medium.

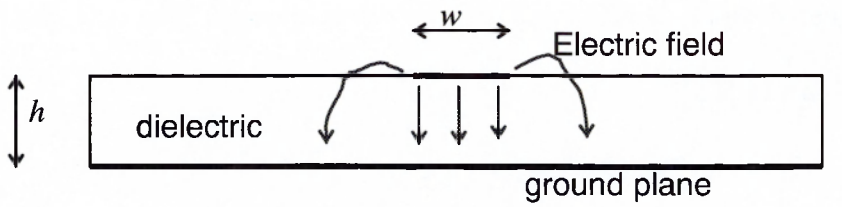

Figure 2.5. Microstrip Geometry

If the dimensions *w* and *h* are small compared to a wavelength, the mode of propagation in the transmission line is transverse electromagnetic (TEM) to a good approximation. That is, the electric and magnetic fields are orthogonal to the direction of wave propagation, and to each other. In any medium, the propagation constant β is a function of the dielectric constant. For microstrip we introduce a parameter called the *effective dielectric constant* (ε_{reff}) which is a measure of the distribution of electric field between the dielectric and the air above it. Hence:

$$\beta = \frac{2\pi}{\lambda_0}\sqrt{\varepsilon_{reff}} \tag{2.5}$$

And $$\lambda_{TL} = \frac{\lambda_0}{\sqrt{\varepsilon_{reff}}} \tag{2.6}$$

Wider microstrip tracks and thinner substrates lead to a greater confinement of the electric field within the substrate and hence larger values of ε_{reff}, which is always within the range

$1 < \varepsilon_{reff} < \varepsilon_r$

A common approximation [11] is:

$$\varepsilon_{reff} = \frac{\varepsilon_r + 1}{2} + \frac{\varepsilon_r - 1}{2}\frac{1}{\sqrt{1 + \frac{12h}{w}}} \tag{2.7}$$

but numerical methods lead to greater accuracy [12]. The characteristic impedance of the line is given by [11].

$$Z_0 = \frac{\sqrt{\varepsilon_{reff}}}{C.c} \tag{2.8}$$

where c = speed of light and C = capacitance per unit length. The latter is often computed by numerical means [13].

At this stage it became useful to use HP's *EESOF* microwave design CAD package, which includes the routine *Linecalc* for analysing microstrip - deriving ε_{reff} and Z_0 when given w for a given substrate - or conversely, synthesising a microstrip – deriving w for a required value of Z_0.

2.3.2 Microstrip Switch Design

Commercial laminates of the PTFE/ceramic composite based type typically have ε_r within the range 2.2 to about 11. The photo-etching facilities available at the time were not well suited to fabrication of circuits above 50 x 50 mm in size. To minimise the circuit dimensions, a high dielectric constant laminate – Roger's Duroid 6010 – was selected, with $\varepsilon_r = 10.8$ and $h = 0.64$ mm.

A double pole, double throw matched switch was designed using 3 PIN diodes, each with a DC bias supply fed by RF chokes of the classic principle requiring high and low impedance sections of line. The range of impedances practically possible was investigated using *Linecalc* and summarised in Table 2.1. The design techniques used are well established – the data is included to illustrate some of the trade-offs inherent in microstrip design which often lead to compromises in performance. For example, thinner substrates exhibit better field confinement, particularly at high frequencies, but require very narrow lines to achieve the high impedances required for filters. The photo-etching resolution is a factor which

must not be overlooked at the design stage. Similar issues became more critical to the project in later stages where the entire retro-reflector would be fabricated from printed circuits.

w (mm)	Z_0 (Ω)	$\varepsilon_{r\,eff}$	λ_{TL} (mm)
0.10	88.4	6.241	48.0
0.15	79.5	6.400	47.4
0.20	73.0	6.514	47.0
0.55	50.0	7.040	45.2
3.70	15.0	8.832	40.4
6.08	10.0	9.351	39.2

Table 2.1. Microstrip properties at 2.5 GHz. (Rogers Duroid 6010 laminate, ε_r = 10.8 and h = 0.64mm)

The bias filters were designed to present an open circuit to the RF signal at 2.5 GHz. The circuit was verified using EESOF/*Libra* (microstrip and transmission line analysis). The results are shown in Figure 2.6. The switch microstrip circuit is illustrated in Figure 2.7, with symbols for the lumped elements.

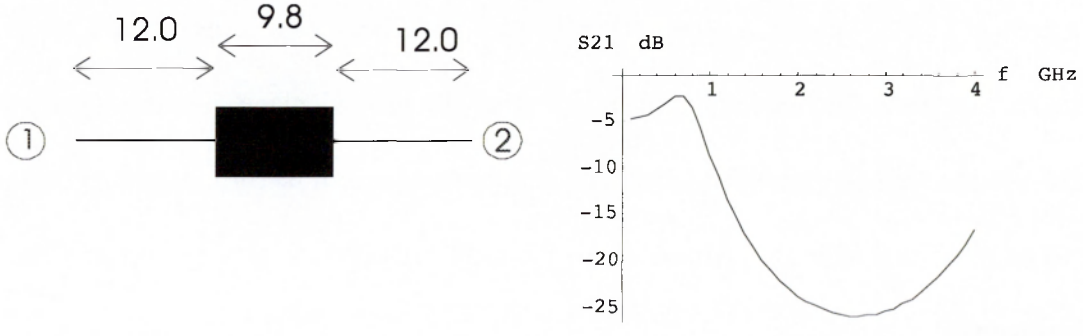

(i) Layout dimensions (mm). (ii) Simulated filter characteristic.

Figure 2.6. Bias Filter Circuit. (Rogers Duroid 6010 laminate, ε_r = 10.8 and h = 0.64mm)

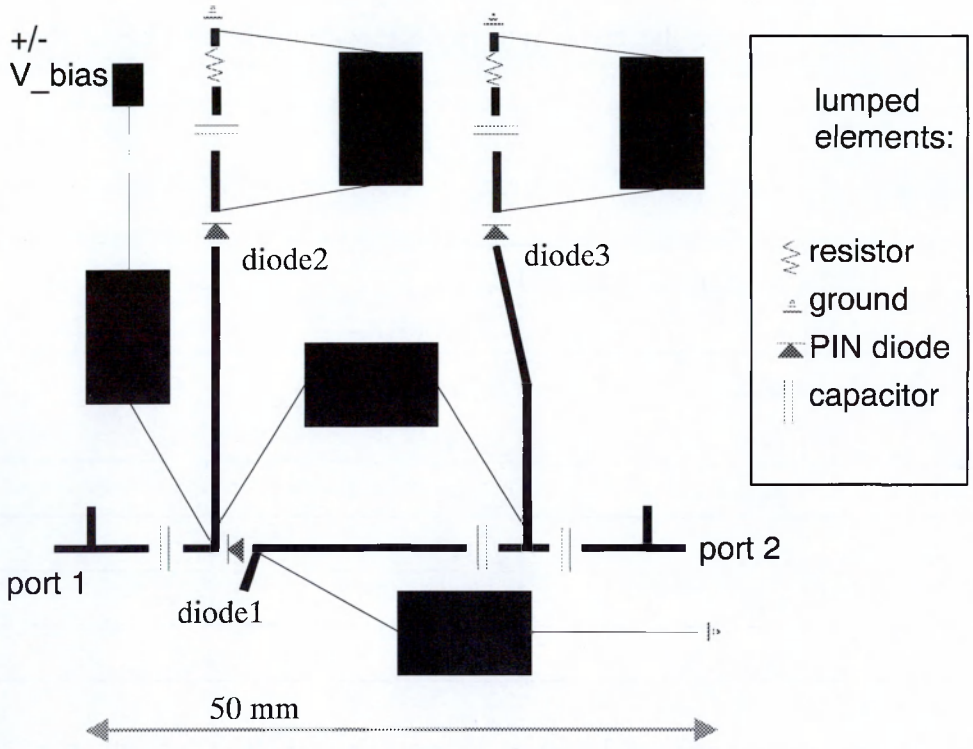

Figure 2.7. Double pole double throw microstrip switch layout.

Notes: (i) The dark pattern is the microstrip layout. (ii) The lumped element symbols have their usual meaning. (iii). RF ports 1 and 2 and the control voltage contact are labelled .

The ½ λ separation between the diodes and the microstrip branch points are required so that the open or short circuit presented by each diode (depending on its bias condition) is transformed to the same state at the branch point. Thus when the switch is "on" (biased for through transmission), the diodes 2 and 3 are open circuit, which remain open circuit at the branch points and the RF path between the ports is not perturbed. The earths, at the edge of the circuit board, were provided by short contacts to the ground plane. The line lengths introduced by this type of grounding introduce small impedance transformations, and thin wires tend to introduce inductive parasitics, so the circuit must be kept very compact and tidy in these areas.

Switch performance was measured using the HP 8753 network analyser. The results are shown in Figure 2.8. Optimum switching performance was achieved with a diode current

of 20 mA. (The silicon PIN diodes used were packaged for surface mount applications, being easy to handle and solder and costing around £1.50 from RS.)

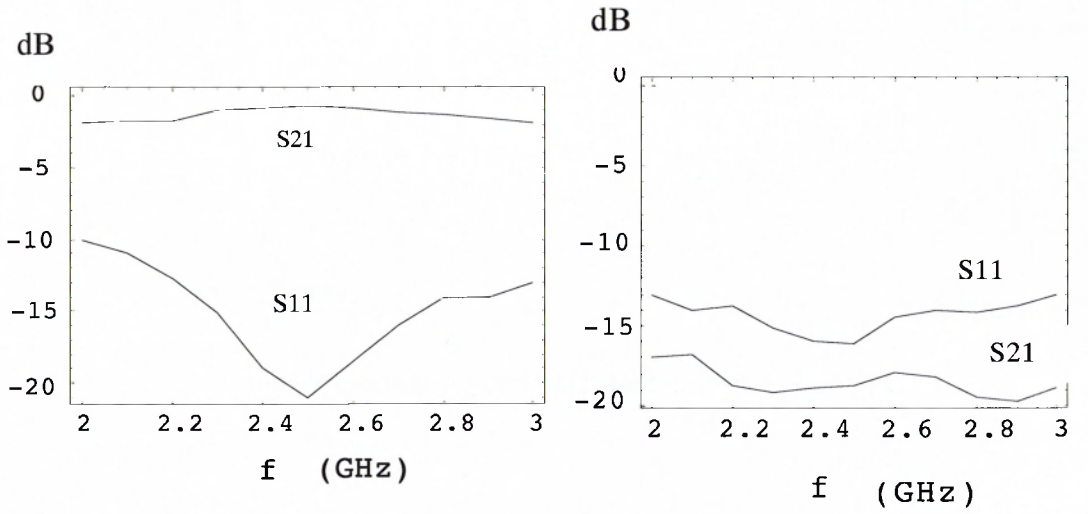

(i) switch on (through) (ii) switch off (matched to 50 Ω)

Figure 2.8.Measured switch performance: S_{11} and S_{21} for on and off states.

Eight such switches were fabricated. A further dipole antenna retro-array was fabricated, with one of the matched switches joined between antenna pairs by coaxial line. Again, line lengths were kept equal to about 1 mm accuracy. Having fabricated the amplitude modulating prototype, monostatic RCS measurements were repeated to confirm that the device could be electrically switched between the retro-reflectivity and low-reflectivity states.

2.4 Modulation Performance.

The switching circuitry on the array was modulated with a low frequency (typically 25 kHz) signal and the radiating array illuminated with an RF carrier at a frequency close to 2.5 GHz. For each switch, an op-amp circuit was used to provide the necessary current gain following the signal generator. The nature of the reflected signal was examined using the test arrangement shown in Figure 2.9.

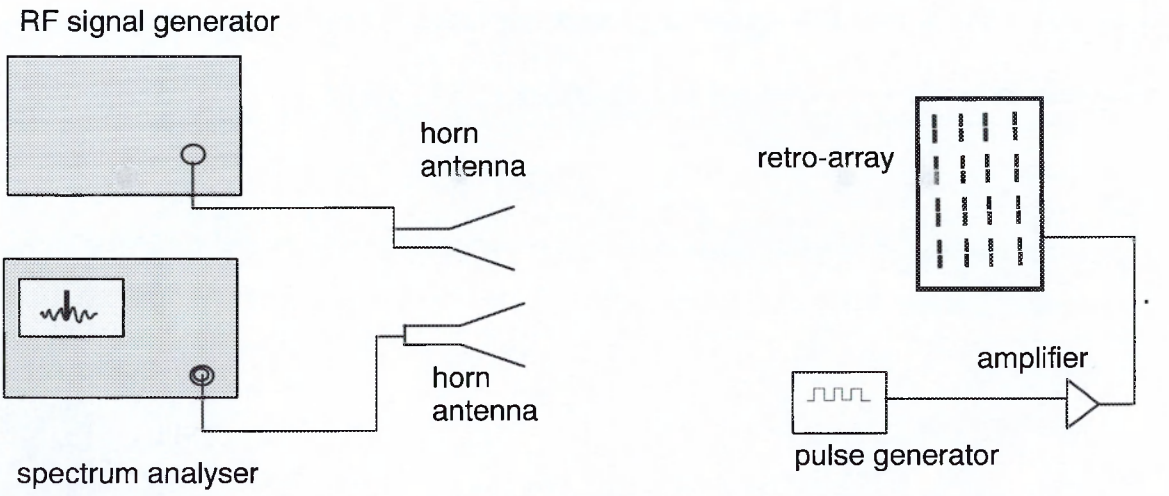

Figure 2.9. Modulated retro-array test arrangement.

The modulation waveform used was a square wave, resulting in digital amplitude modulation of the array RCS. Analogue modulation was considered, but the highly non-linear current-voltage (I-V) characteristics of the diode switches would make linear analogue modulation inconvenient.

The spectrum of the reflected signal was displayed on a spectrum analyser. The sidebands produced by the digital amplitude modulation of the reflected RF were clearly visible, as shown in Figure 2.10 below, where the modulation frequency is 25 kHz.

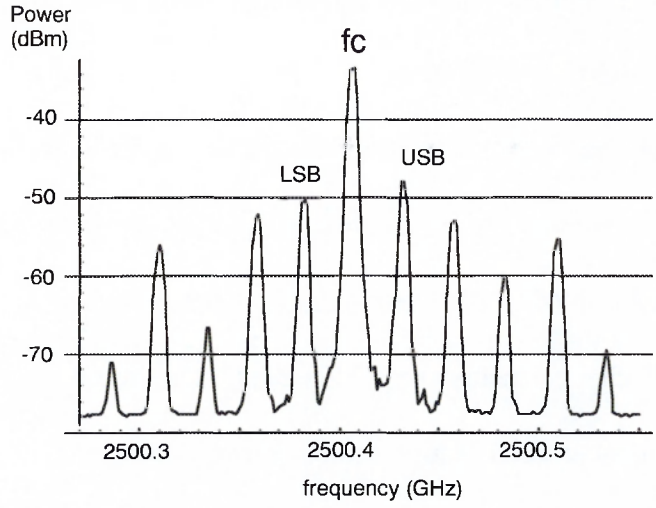

a) location for maximum carrier power

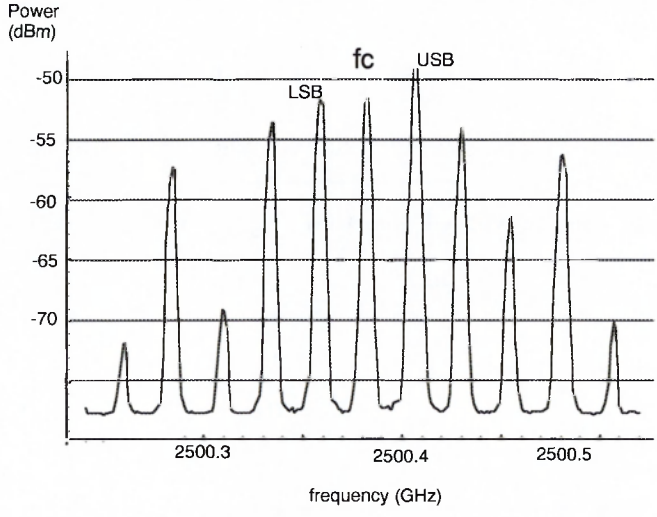

b) location for minimum carrier power

Figure 2.10. Amplitude modulation products for the reflected RF at 0° to the array boresight.
(Labels: fc - carrier, USB - first upper sideband, LSB - first lower sideband)

2.4.1 Discussion of Modulation Spectrum.

From Figure 2.10 we can see that the sidebands produced by square wave AM are strongly visible. It is also apparent that the power returned at the carrier frequency is strongly dependent on the location of the array with respect to its environment, but the power in the first upper sidebands is not. This is because the power available to the modulation products is primarily dependent on the RCS of the array, whereas the power returned at the carrier

frequency is strongly dependent on both the environment and the targets' relative locations since standing waves exist between them.

In case (a) the array was at a local maximum for received carrier power, whereas in case (b) the array was moved by just 30 mm (a quarter wavelength) and a minimum in carrier power - a reduction of 19 dB - resulted. The sideband powers are affected only very weakly by the small change in distance. This illustrates the enhanced detectability of a modulated scatterer in a cluttered or high-multi-path environment.

The modulation products were also studied as the orientation between the array and the incident signal was varied by rotating the array in azimuth (H-plane). As expected for a retro-array, the power reflected varied slowly with orientation angle. Figure 12 shows that the modulation products remain strongly visible when the array is at 35 degrees to the incident illumination - the power of the first upper sideband has diminished by 4 dB compared to the on boresight case of Figure 2.10.

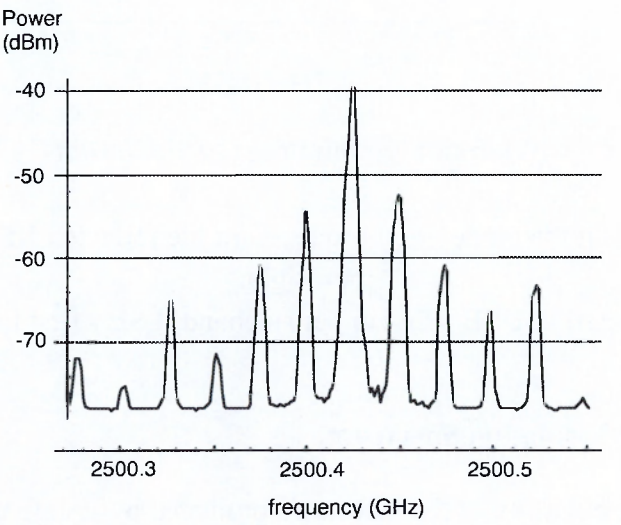

Figure 2.11. Amplitude modulation products for incident illumination at 35° azimuth to the array boresight.

To confirm that a communications link could be established by RCS modulation, the received signal was mixed with the RF source to recover the modulation signal applied to the array switching circuit. The modulation waveforms are shown in Figure 2.12 below. At

this stage the receiver was crude, being a direct homodyne downconversion (i.e. without IF stage) and the received waveform is distorted, but the 40 μs period is clearly visible.

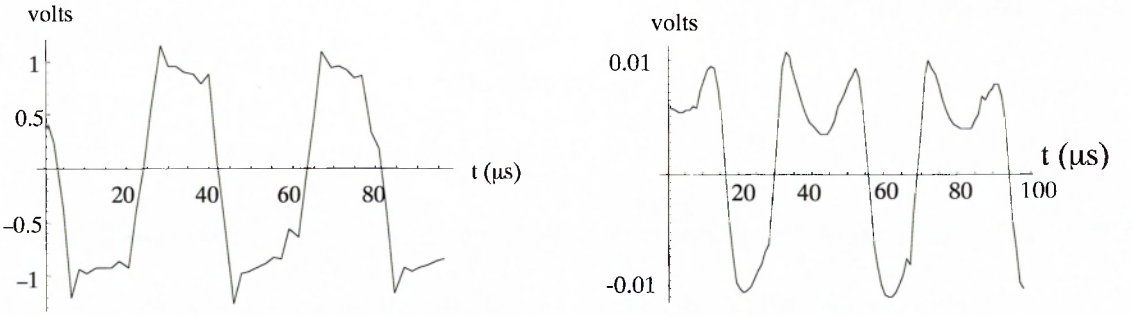

a) waveform across switch b) received waveform

Figure 2.12 Typical measured modulation waveforms.

2.4.2 Conclusions from Amplitude Modulated Prototype.

It is worth summarising the work described thus far, which covers the earliest investigative stages and experiments into modulated retro-reflectors:

- Study of optics-based microwave retro-reflectors; trihedral reflectors etc.
- Adoption of antenna retro-array as basic structure and suggestion to modulate array with switches.
- Fabrication of unmodulated prototype dipole arrays at 2.5 GHz
- Demonstration of amplitude modulated dipole array at 2.5 GHz including simple digital communications link.

At this stage confidence in the direction of the work was well established, since the concept had by now been demonstrated with working hardware. The work could now take many possible directions, a few of which are summarised below:

- refine 2.5 GHz communications link by design of receiver, optimisation of modulation scheme etc.
- develop more detailed theoretical models for RCS, link budget, coupling, losses etc.

- refine angular coverage by selection of other antennas, study of beam patterns, polarisation, and study interference effects in a multi-array structure.
- select another working frequency.
- investigate more convenient fabrication techniques.

While pursuing these areas, the author concentrated on improving the modulation circuitry whilst retaining the dipole array in the first instance. In particular, phase modulation was felt to be a more elegant and energetically efficient approach, and it will be shown how phase switches were developed which reduced the number of components and also assembly time. In the following chapters, it will be shown how the development of increasingly integrated microwave structures proved to be very beneficial, and how the methods developed were then scaled to higher carrier frequencies.

2.5 Phase Modulated Retro-Array

A further array was built, with the same dipole antenna geometry as described above, but using phase shifting switches in place of the double-pole double-throw matched switches. The combined feed line and switching circuit is shown photographed in Figure 2.16. The phase shifters were based on PIN diode circuits which switched between two different lengths of microstrip transmission line. The theoretical phase difference between the two lengths of line was 180° at 2.5 GHz, to achieve that maximum attainable modulation index, i.e. unity. The phase switch circuit layout is shown in Figure 2.13, where the overall circuit dimensions are 50 mm x 50 mm.

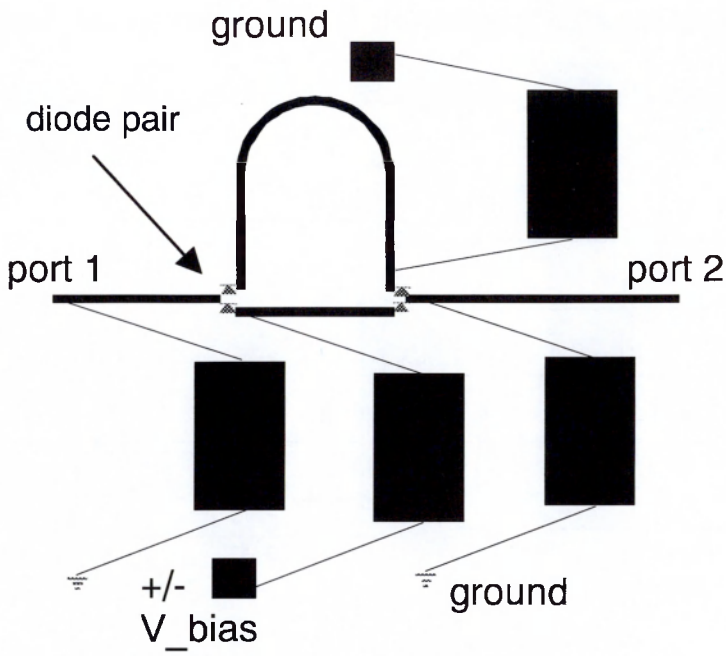

Figure 2.13. Microstrip phase switch layout.

Switching was achieved by using packaged in-series diode pairs, of a similar type to the single diodes used in the amplitude modulated array. Eight switches were fabricated (one for each dipole pair). Care had to be taken to ensure the packaged diode pairs were soldered in place with the correct polarity – in Figure 2.13 above it can be seen that the diode configurations requires one package to be placed upside-down with respect to the other. This also necessitated a mechanical adjustment of the solder pad heights for the upside-down package. A practical advantage of the adoption of phase switching was the reduction in the number of RF components – the resistors and capacitors used in the earlier amplitude switch are not required. A photograph of one such switch is shown in Figure 2.17.

Again, the current requirement was close to 20 mA for each diode. The typical measured phase shift was 164° ± 2° at 2.5 GHz. Digital phase shift modulation was achievable by applying a square wave of ± 1 V amplitude to each switch. Another dipole array was

fabricated, with a phase switch in series with each transmission line. Figure 2.14 shows the modulation products in this case, where the modulation frequency is again 25 kHz.

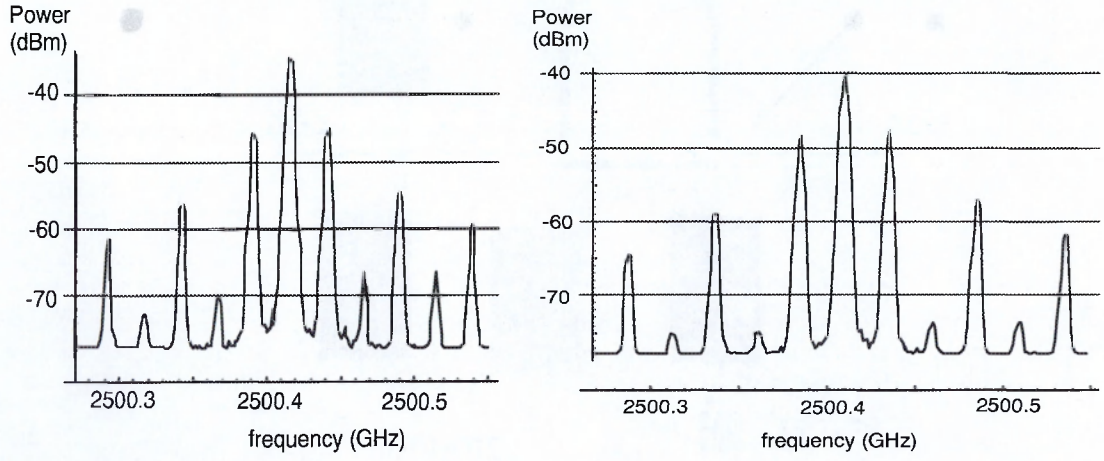

(a) array at 0° rotation (b) array at 35° rotation

Figure 2.14 . Phase modulation products for the reflected RF at 0° azimuth and at 35° azimuth to the array boresight.

Like the amplitude modulated array, the phase modulated array demonstrated that sideband power varied slowly with the orientation of the array to the illuminating signal. The first upper sideband power diminished by 3 dB when the array was rotated from 0° to 35° azimuth. The first upper sideband power was also 3 to 5 dB greater than that produced by AM, for any orientation angle from -35° to 35°. The greater sideband power produced is consistent with PM compared to AM, the latter being less energy efficient since energy is dumped into resistive loads on alternate cycles of the modulation signal. Hence the results demonstrate that phase modulation is energetically advantageous in this application.

Reflector bandwidth: The behaviour of both (AM and PM) arrays was also observed at other frequencies between 2.4 GHz and 2.9 GHz. The essential characteristic of the retro-reflector i.e. strongly visible modulation products over a wide range of orientation angles, was observed over this frequency range. However, it has not been possible to present results comparing the absolute performance at these frequencies, since the overall power

budget in the measurement system was not calibrated. Factors affecting the bandwidth of the device include the antenna bandwidth and the switch bandwidth. In both AM and PM switches, resonant ($\lambda/2$) line lengths were employed, which clearly imposes a bandwidth limitation.

The maximum usable modulation frequency is governed by the maximum rate at which the switches may be operated. In the devices described above, this is partly dependent on the switching speed of the PIN diodes. In the PM array, the PIN diodes used allowed higher switching speeds – it was possible to drive the switches at 250 kHz and retain an approximately square waveform. A trade-off between switching speed (i.e. data rate) and modulation efficiency became clearly apparent -a reduction of 2dB in first upper sideband power was evident at 250 kHz, compared to 25 kHz. Beyond 250 kHz, sideband power diminished more sharply. Part of the roll-off in switching efficiency is due to the bias circuit filter characteristic. The RF frequency range of the individual PIN diodes was also explored, and it was found that reasonable performance could be expected to about 3.5 GHz. Beyond this, the transmission characteristics become increasingly dominated by the parasitic impedance of the device package.

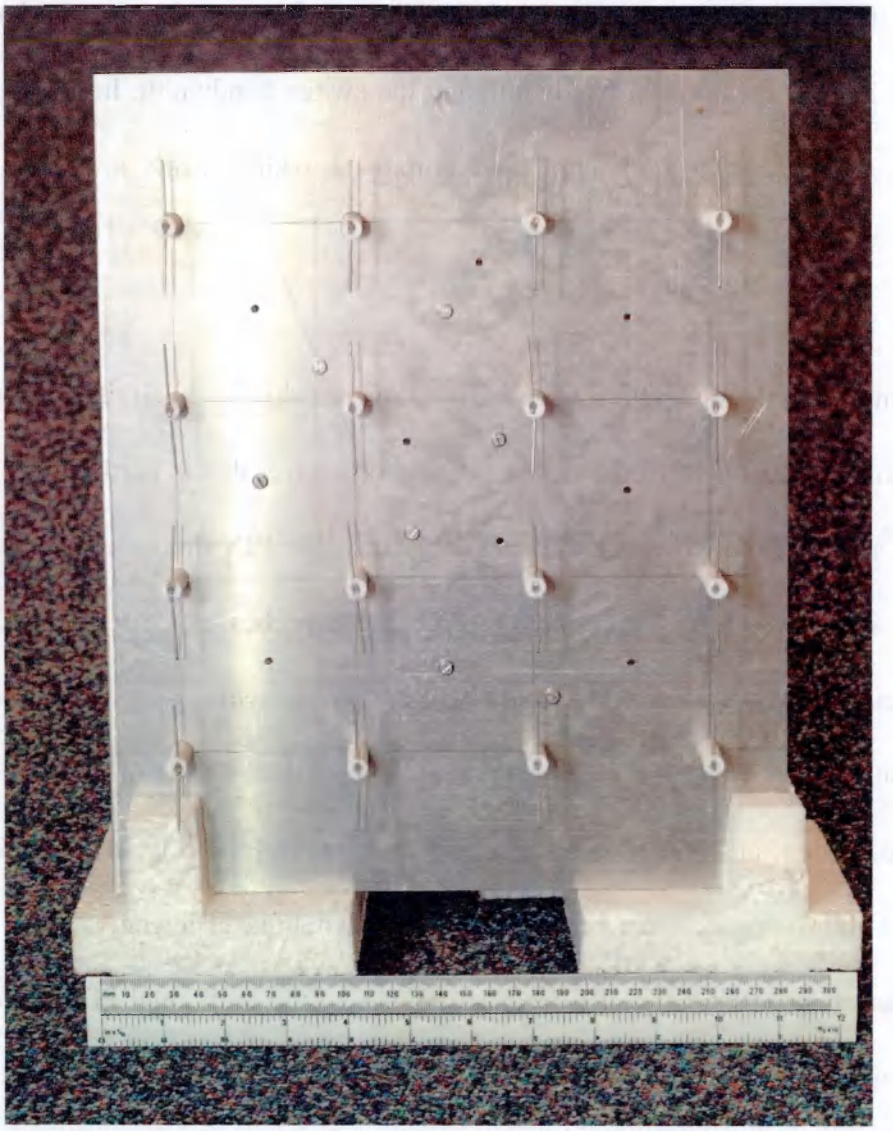

Figure 2.15 2.5 GHz retro-array antenna matrix. (The 16 dipole array common to the unmodulated and modulated versions)

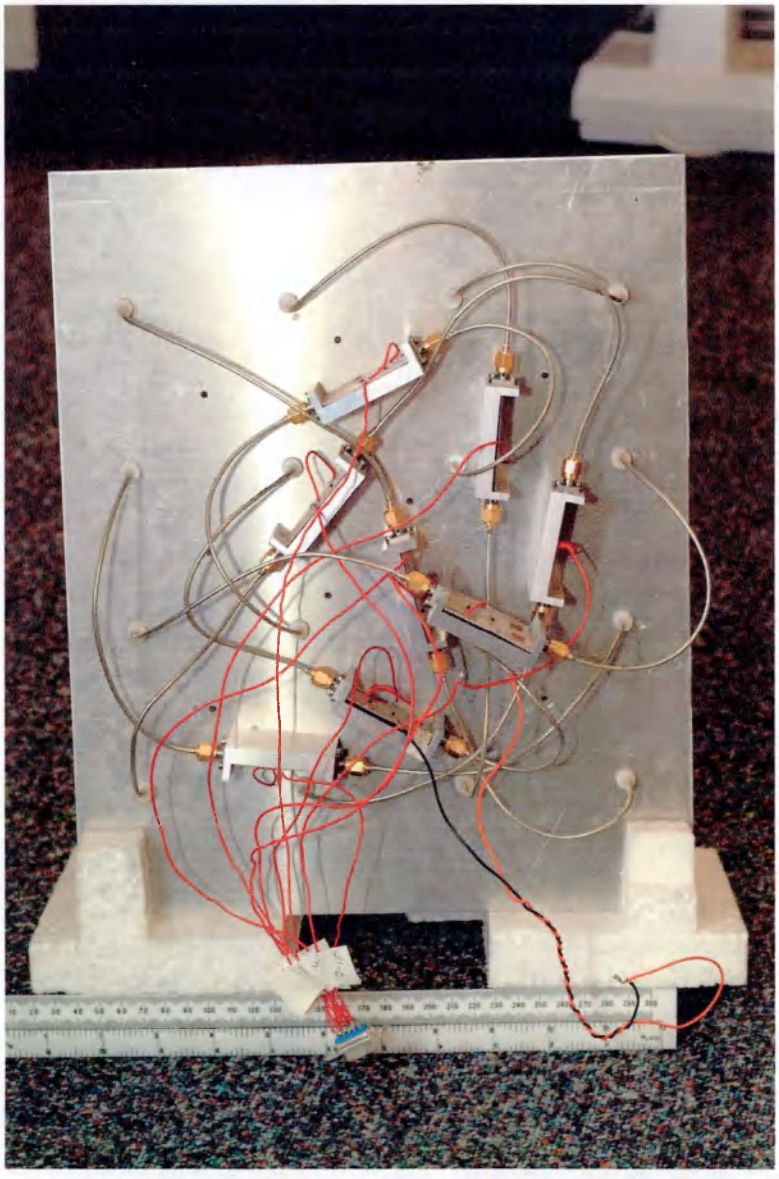

Figure 2.16. The 2.5 GHz phase modulated retro-array: transmission lines and switches.
(The red cables are the switch bias supplies, which plugged in to a current amplifier buffer.)

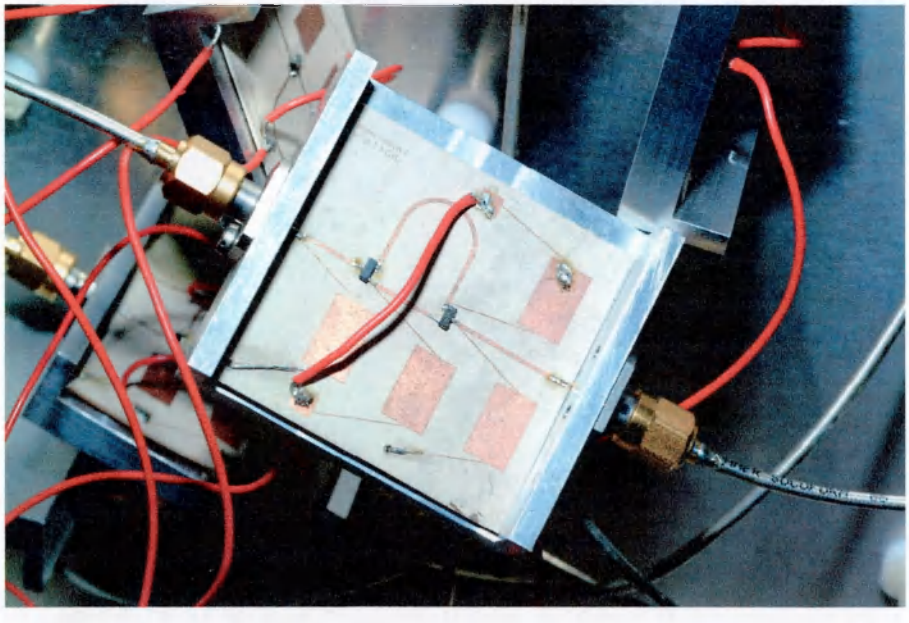

Figure 2.17. 2.5 GHz microstrip phase switch, shown in-situ.

2.6 Conclusions from Modulated Dipole Retro-Array Prototypes.

Having designed, built and partly characterised both an amplitude modulated and phase modulated array, it was again necessary to consider the future direction for the work from the many possibilities which have already been suggested. Since the mechanical fabrication of the arrays had been rather labour intensive, and they are also physically quite bulky, it was thought most advantageous to investigate the possibility of using printed circuits to fabricate the entire device. Microstrip switches had already been demonstrated as printed circuits, and to extend the use of planar circuits it would be necessary to develop printed antennas and also devise a planar transmission line layout that would facilitate integration of all the components. Thus, the aim would be to minimise the use of coaxial line and associated connectors, and minimise the number of fabrication stages. This would facilitate the construction of a larger number of modulated retro-arrays and lead to more experimental measurements examining and comparing their properties. If fully planar circuits could be realised this would also represent a step towards a mass-producible solution and hence marketability. The development of planar and integrated circuits for modulated microwave retro-arrays is presented in the next chapter.

References.

[1] "Radar Cross Section Handbook Vol 2", Edited by Ruck, *Plenum Press* 1970. pp 588 - 599

[2] "Van Atta Reflector Array", Sharp and Diab, *IRE Transactions On Antennas And Propagation* VOL AP-8 July 1960.

[3] Ref [1] pp. 509 - 602.

[4] "Antennas", John D. Kraus (second ed.) *McGraw-Hill* pp. 496 - 497.

[5] "The A.R.R.L. Antenna Handbook", The American Radio Relay League 1968, pp. 31 - 34.

[6] "Advanced Engineering Electromagnetics", C. A. Balanis, *Wiley*, 1989, p.594.

[7] "Foundations for Microstrip Circuit Design", T. Edwards, *Wiley* 1991

[8] "Microwave Engineering". David M. Pozar. *Addison Wesley* 1993

[9] "Microstrip Lines and Slotlines", K. Gupta, R. Garg, I. Bahl, P. Bhartia, *Artech House,* Boston, 1996

[10] "Foundations of Interconnect and Microstrip Design", T. C. Edwards, M. B. Steer, *Wiley*, 2000

[11] "Measurement and Modelling of the Apparent Characteristic Impedance of Microstrip", W. J. Getsinger, *IEEE-Transactions on Microwave Theory and Techniques* Vol 31, August 1983

[12] "Accurate Models for Microstrip Computer-Aided Design", E. Hammerstad and O. Jensen *IEEE MTT Symposium Digest*, 1980

[13] Ref [8] pp. 164 - 167.

this page intentionally blank

Chapter 3

Printed Circuits for Modulated Retro-Arrays.

3.1 Printed Antennas.

Also commonly known as patch antennas, printed antennas are popular in a wide range of applications. Much literature exists examining the properties of this class of antenna, refs. [1 – 4] make a good starting point for the designer. Since they may be fabricated using standard photolithographic techniques, they may be easily integrated with other printed circuit components - indeed this was their main attraction for the application described herein. Also, printed antennas are by nature planar, lightweight and mechanically robust structures. They lend themselves to array applications in that many antennas and their associated microstrip feed lines may be combined in configurations to give a required gain and beam pattern. They are also effective and compact radiators - the mechanism of radiation is illustrated in Figure 3.1 below.

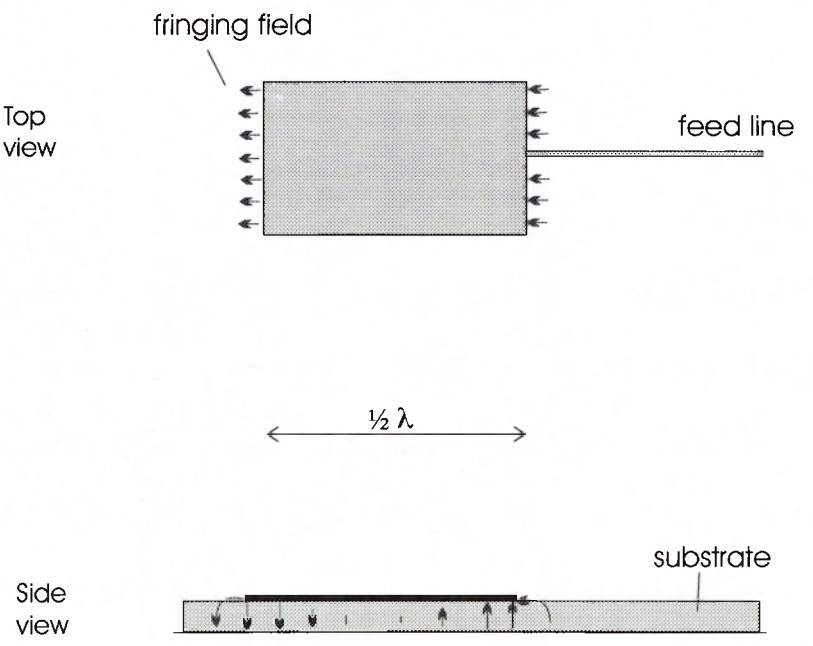

Figure 3.1 Patch antenna radiation mechanism.

A primary disadvantage of printed antennas is their inherent narrow bandwidth, 1.5 % being a typical figure, although this does not necessarily present a problem for retro-array

applications. However, the bandwidth limitation leads to a great sensitivity to the exact value of substrate dielectric constant, which is typically specified to a 1.5 % tolerance by manufacturers, and so it is usually necessary to prototype the antenna for any given batch of substrate, and tune the antenna dimensions to achieve the required resonant frequency. Also, the radiation efficiency and pattern is easily corrupted by stray radiation from discontinuities in other microstrip components such as the feed lines. A further problem is encountered if large values of array gain are required, since the large number of elements required can lead to difficulties in designing the feed line network, and requires larger physical areas of material. This in turn leads to greater losses in the feed lines which begins to negate the sought after increase in array gain.

3.2 Initial Design Considerations.

Firstly, the relationship between patch dimensions and resonant frequency had to be determined, so that the dimensions required for the 2.5 GHz design frequency could be established. An estimate can be found by calculating the wavelength using the microstrip design equations for ε_{reff} from chapter 2. Then:

$$L = \frac{1}{2}\frac{\lambda_0}{\sqrt{\varepsilon_{reff}}} \tag{3.1}$$

where L is approximately the length required to produce a resonance at a free space wavelength of λ_0 (0.12 m. in this case). This approximation does not account for the effective extra transmission line length introduced by the fringing fields which are the radiating mechanism, but would suffice to estimate overall dimensions so that a laminate could be procured. The photographic group at the University of Oxford Department of Physics were consulted about their photo-etching facilities, and in particular the range of circuit dimensions which could conveniently be handled, which was about 300 mm square for a non-flexible substrate (also a commercially available laminate sample size). The mask generating plotter could handle patterns up to 296 mm in width (A3 size).

Since ε_{reff} is a function of track width w, substrate height h and dielectric constant ε_r assumptions for these values must be made. Commonly used substrates have h = 0.76 mm so this value was assumed for initial design calculations. Since antenna gain diminishes with increasing ε_r a value of 3.0 was initially assumed, being toward the lower end of the commercially available constants. Using a nominal track width of 2 mm gives $\varepsilon_{reff} \approx$ 2.456 and L = 38.3 mm. A wider track yields more efficient radiation, so a width of 38.3 mm was then used to derive new values of ε_{reff} = 2.913 and L = 35.2 mm. It can be seen that a square patch antenna can be derived after a few iterations - this was later necessary. At this stage it became apparent that a 4 x 4 array of patches close to 36 mm square in dimension could lie within a total area of 300 mm square allowing a patch separation of about 70 mm, which was estimated to be sufficient separation to obviate mutual coupling. The preferred feed method was to aperture-couple the patches to a separate printed circuit which would contain the interconnections and switches with associated diode bias circuits. This printed circuit would also be subject to the 300 mm square size restriction, and some sketches showed that this would be possible. The design of the circuit for the interconnecting feeds is discussed in more detail in section 3.6.

3.3 Antenna Prototyping.

The laminate procured was Rogers RO3000, with ε_r = 3.0 ± 0.04 and h = 0.76 mm. This is a high performance PTFE/ceramic composite based laminate, with loss factor Tan δ = 0.0013. It was next necessary to model the resonant frequency/length relationship for the patch antenna more accurately. From [5] the extra length contributed by the fringing fields is approximated by:

$$\Delta l = 0.412h\frac{\varepsilon reff + 0.300}{\varepsilon reff - 0.258}\left[\frac{\frac{w}{h} + 0.262}{\frac{w}{h} + 0.813}\right] \tag{3.2}$$

The total length is then the sum of the conductor length and the two fringing field lengths:

$$L_{tot} = L + 2\,\Delta l \tag{3.3}$$

and resonance occurs at a wavelength:

$$\lambda res = 2L_{tot}\sqrt{\varepsilon reff} \tag{3.4}$$

A *Mathematica* program was written to examine the relationship between resonant frequency and dimensions for a square patch ($w = L$) in the frequency region of interest, as shown below in Figure 3.2.

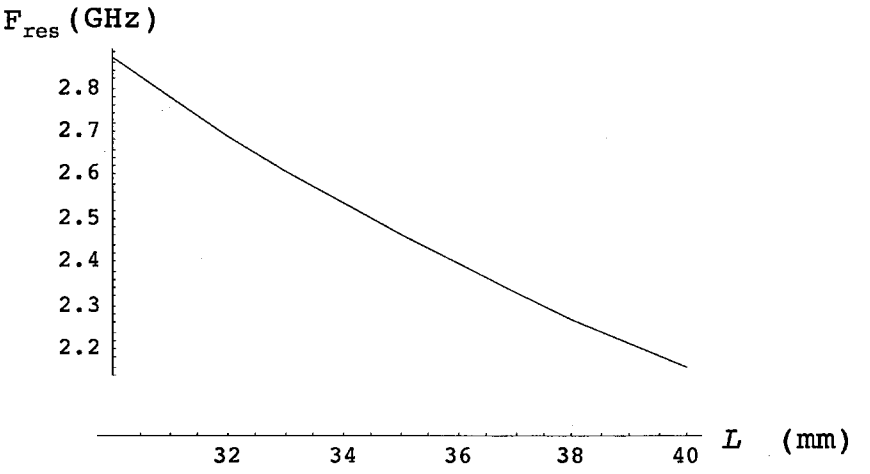

Figure 3.2. Resonant frequency versus length for a square patch.

Using the program, a value of 34.5 mm was derived for a resonant frequency of 2.50 GHz. Also using the design equations from [5], the *Mathematica* program was extended to calculate radiation resistance at the centre of one side of the patch. The value of 259 Ω which was derived represents the load impedance seen by the microstrip feed line.

3.4 Antenna Feeds.

To match the relatively high impedance of the patch antenna (R_{rad}) to a 50 Ω feed line, there is clearly a necessity for an impedance transformer between the feed and antenna.

The most convenient way of realising this is a quarter wave transmission line length of the classic type where $Z_t = \sqrt{Z_0.Z_L}$ where Zt is the required characteristic impedance of the transformer section which is λ/4 in length, Z_0 is the feed line characteristic impedance and Z_L the load impedance. At this stage, Z_0 has not been assumed. An arbitrary value may be selected since each line is to provide a connection to the counterpart antenna, rather than interface to the standard 50 Ω test environment. Here, another design trade off becomes apparent – lower impedance microstrip lines tend to exhibit lower loss than higher impedance lines, but are correspondingly wider, thus consuming more "real estate" on the printed circuit and reducing the spacing between the tracks. If the spacing is too close, parasitic electromagnetic coupling between the lines will corrupt the phase relationships between the antenna pairs, and degrade the array performance. The critical region is where, in a 4 x 4 array, 5 transmission lines need to pass between adjacent antennas. This can be seen in Figure 3.10 which shows the feed layout which was later derived.

Discussion: it will be apparent that at this stage, even before any circuit elements have been designed in detail, it has been necessary to consider the inter-relation of a large number of parameters which include for example, dependence of antenna dimensions hence total circuit dimensions on dielectric constant, total surface area available for the printed circuits, microstrip feed line impedance and inter-dependence on width, spacing, parasitic coupling, losses and required impedance of quarter-wave transformers.

Polarisation: As a further variation on the radiation characteristics of the preceding dipole array, it was thought useful to design an array with circular polarisation properties. This would respond to illuminating radiation of arbitrary linear polarisation, or the correct sense (right or left hand) circular polarisation. A circularly polarised patch antenna can be realised by feeding two edges of a square patch in phase quadrature [10], as suggested by the layout shown in Figure 3.3. The load presented by such an antenna was modelled as

two parallel loads each of R_{rad}, since the radiation modes are orthogonal and therefore the presence of one does not modify the radiation mechanism of the other.

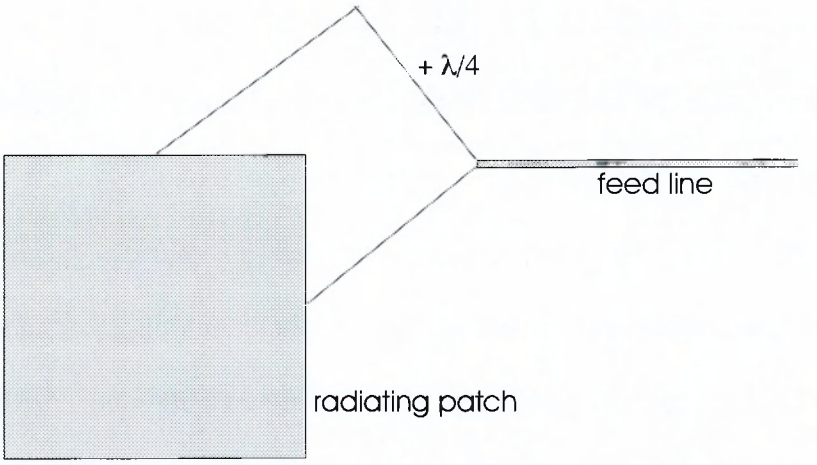

Figure 3.3 Circularly polarised patch antenna.

For the circularly polarised patch, the quarter-wave impedance transformers are required to present an impedance 2 Z_0 so that the parallel combination is Z_0 (the feedline characteristic impedance). The circuit dimensions at 2.5 GHz allowed the use of 50 Ω feeds (w = 1.89 mm) which, although not vital (as discussed above), was a convenient value for simulation purposes. In Figure 3.3 above, it can be seen that an additional quarter wavelength line is required to produce the necessary phase shift for circular polarisation. The characteristic impedance of the this line is 2 Z_0 . Using EESOF *Linecalc*, the required dimensions for these lines were derived, as shown in Table 3.1 below. The 161 Ω line transforms the 259 Ω patch radiation resistance to a load impedance of 100 Ω.

Z_0 (Ω)	w (mm)	¼ λ_{TL} (mm)
50	1.89	19.27
100	0.48	20.18
161	0.10	20.85

Table 3.1. Microstrip dimensions for circular polarised patch feeds.

The layout was modelled using EESOF's *Momentum* planar circuit simulator. This is a method of moments electromagnetic simulator which produces a two-dimensional mesh of

the planar circuit. Substrate and conductor losses may be accounted for and an arbitrary number of ports may be used. The package also derives far-field radiation patterns. The tool was used extensively from this part of the work onwards. Figure 3.4 below shows the physical layout modelled, and the simulated return loss (S_{11}) for the prototype antenna.

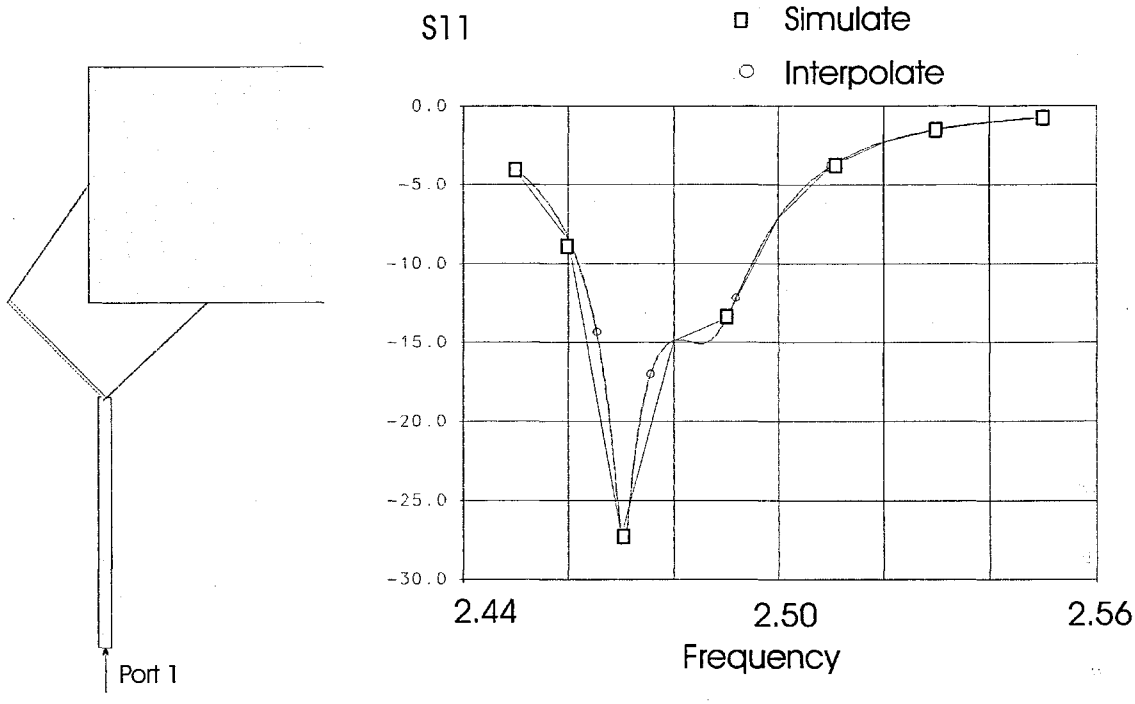

(i) Layout (ii) simulation results: return loss (S_{11})

Figure 3.4. Simulated antenna match from EESOF *Momentum*.

The simulation predicted a resonant frequency of 2.47 GHz which represented a discrepancy of 30 MHz compared to the design frequency of 2.50 GHz, or a 1.2 % error. The *Momentum* simulation was thought to be the more accurate indication of predicted frequency, since the approximate boundary conditions used in [5] do not apply, so the patch dimensions were scaled by the 1.2 % factor to yield a new square patch length of 34.09 mm.

3.5 Radiation Patterns.

The far field electric fields [5] for a linearly polarised rectangular patch antenna are given by:

$$E\theta = \mathrm{Cos}(k.h.\mathrm{Cos}\theta)\frac{\mathrm{Sin}\left(k_0\frac{a}{2}\mathrm{Sin}\theta.\mathrm{Sin}\phi\right)}{k_0\frac{a}{2}\mathrm{Sin}\theta.\mathrm{Sin}\phi}\mathrm{Cos}\left(k_0\frac{b}{2}\mathrm{Sin}\theta.\mathrm{Sin}\phi\right).\mathrm{Cos}\phi \qquad (3.5)$$

$$E\phi = \mathrm{Cos}(k.h.\mathrm{Cos}\theta)\frac{\mathrm{Sin}\left(k_0\frac{a}{2}\mathrm{Sin}\theta.\mathrm{Sin}\phi\right)}{k_0\frac{a}{2}\mathrm{Sin}\theta.\mathrm{Sin}\phi}\mathrm{Cos}\left(k_0\frac{b}{2}\mathrm{Sin}\theta.\mathrm{Sin}\phi\right).\mathrm{Cos}\theta.\mathrm{Sin}\phi \qquad (3.6)$$

where $k_0 = \frac{2\pi}{\lambda_0}$ and $k = k_0\sqrt{\varepsilon_r}$, a is the patch length, b is the patch width and h is the substrate height. The co-ordinate system is shown in Figure 3.5 below.

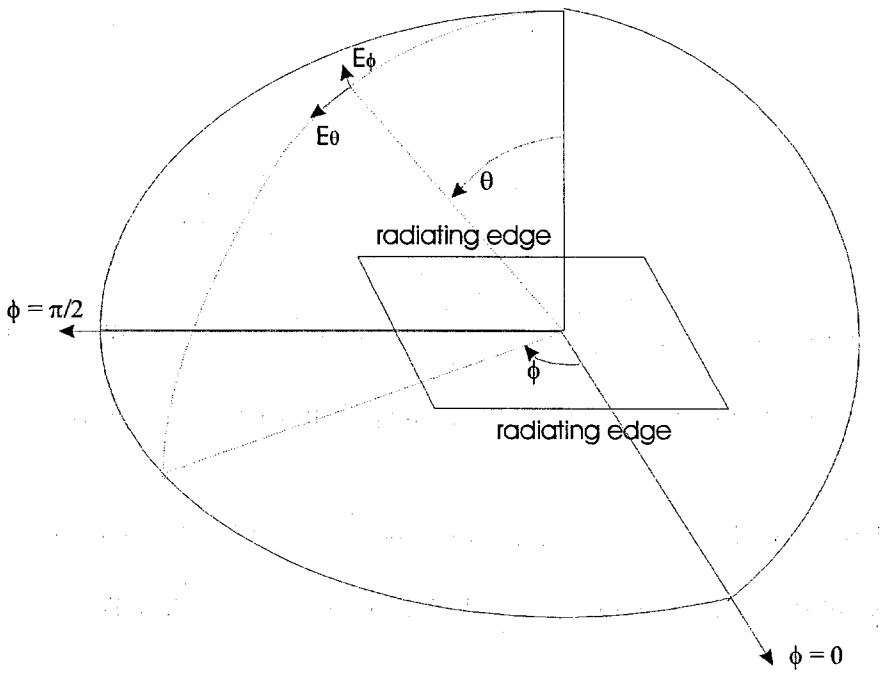

Figure 3.5 Patch antenna fields: coordinate system

Special cases of interest are the E-plane (plot E_θ as function of θ theta for $\phi = 0$) and H-plane (plot E_ϕ as function of θ theta when $\phi = \pi/2$). The E-plane may be visualised by remembering that the plane in which the electric field is linearly polarised is in the direction of the feed line, i.e. where $\phi = 0$. The H-plane is the orthogonal plane. The theoretical E-plane and H-plane radiation (power) patterns for one linear mode of the prototype patch are shown in Figure 3.6 below.

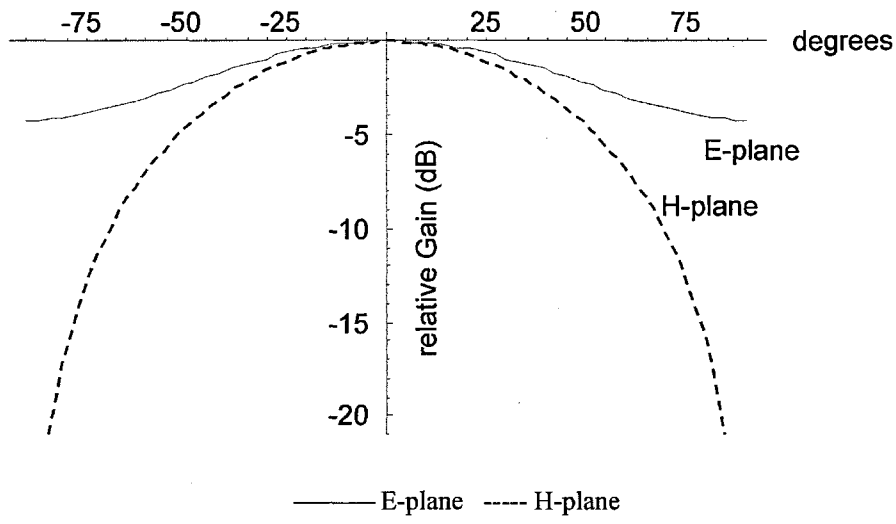

Figure 3.6 Linearly polarised patch antenna, theoretical radiation patterns.

The resultant field from the superposition of the two linear modes, which are fed in phase quadrature, may be assumed to be the time average of the E- and H-plane contributions, which is shown in Figure 3.7 below.

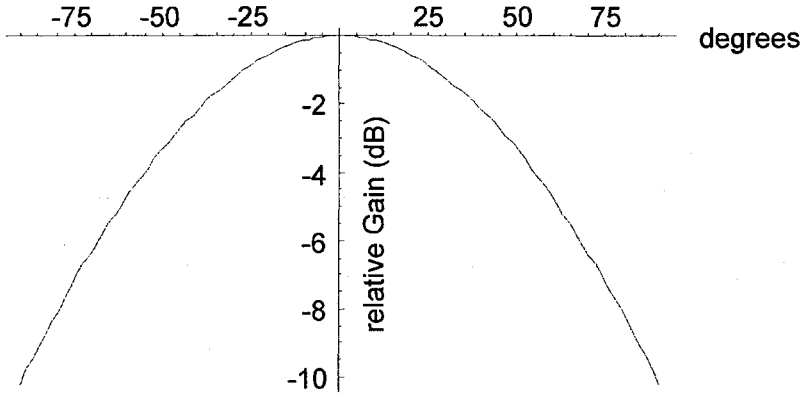

Figure 3.7 Circular polarisation radiation pattern.

The *Momentum* simulation showed that a slightly modified patch dimension of 34.09 mm (c.f. 34.50 mm) was necessary in this case to achieve the design frequency of 2.50 GHz. It was seen that the presence of the feeds and aperture slightly perturb the operating frequency of the patch radiator in the simulation. The simulated radiation patterns are shown in Figure 3.8 below.

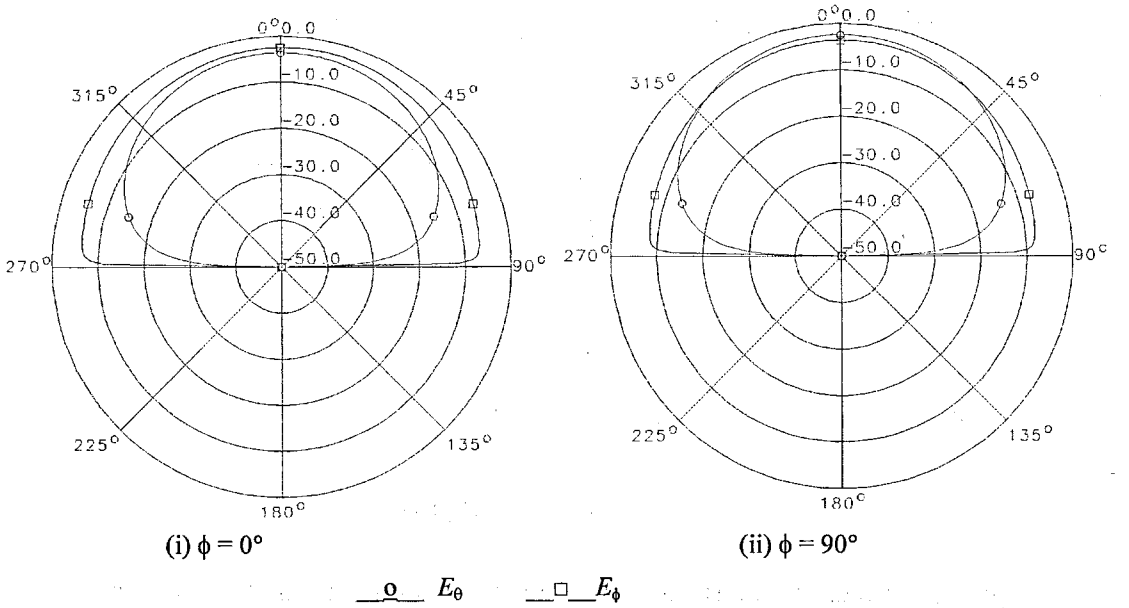

Figure 3.8 Simulated radiation patterns for circularly polarised patch antenna.

In Figure 3.8 the two components of electric field are shown (E_θ and E_ϕ) and a slight asymmetry in their powers is visible. For circular polarisation, both components should have the same peak magnitude. In case (i) it can be seen that E_ϕ has a slightly greater magnitude than E_θ by about 1 dB. That is, one of the orthogonal radiating modes is stronger than its counterpart. The same phenomena is visible in case (ii), but viewed at a different azimuth angle ϕ. The asymmetry is caused by parasitic radiation from the microstrip feeds, and results in slight ellipticity of the radiation pattern.

Aperture coupling. To separate the antennas from the interconnecting transmission lines and switching circuitry, a means of aperture coupling through the circuits' ground planes was sought. It was preferred to devise a means of coupling which would allow the circuits to be separated so that a different antenna matrix could be changed should this prove necessary, for example, to change the polarisation or centre frequency. For this reason, direct coupling to the antenna patches was not used, and a short transmission line stub was used as an interface. In this configuration the functions of the antenna, aperture and interconnecting lines are separated. Various aperture configurations were modelled using

Momentum, the best proved to be a long narrow slot perpendicular to the feed lines as shown in Figure 3.9. This configuration was derived by the author to meet the needs of the design as it developed.

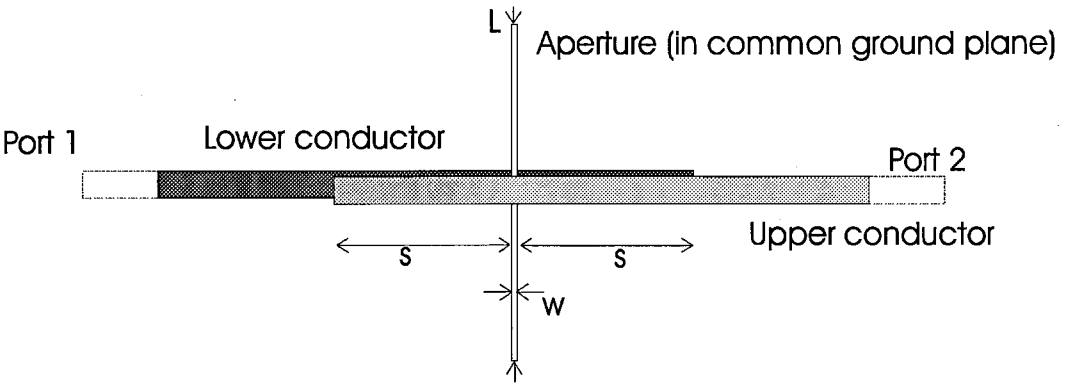

Figure 3.9 Microstrip aperture coupling.

Figure 3.9 shows the metalisation pattern of two "back-to-back" microstrip feed lines which share a common ground plane. The feedlines are shown slightly offset for clarity of illustration – in practice there is no lateral offset. The insertion loss was found to be very sensitive to the dimensions shown. The best results were obtained with a slot width w of 0.1 mm, a slot length L of 30.0 mm and a stub length s of 14.9 mm. This configuration gave a modelled insertion loss better than - 0.15 dB over a 500 MHz bandwidth. It is worth observing that the slots give rise to further restrictions on transmission line routing, since the interconnecting microstrip lines should not be routed over the apertures which "belong" to a neighbouring line.

3.6 Transmission Line Routing and the Unequal-line-length Retro-array.

At this stage the antenna matrix and aperture feeds were finalised, and it was necessary to devise the routings for the interconnecting microstrip lines which would populate a separate circuit board "behind" the antenna matrix. The classic retro-array requires that all transmission lines are of equal length, although that length may take any value. To realise a planar circuit which would perform this function, an important conceptual step was made.

Rather than attempting to map routes for equal lengths of line, lines may vary in length from one another by an integer multiple of wavelengths. Such a geometry preserves the phase relationship between antenna pairs that leads to phase-conjugation, albeit at a single frequency of operation. Approximate phase conjugation will occur at other frequencies close to this centre frequency. Thus the unequal-line-length retro-array is a narrow band variant of the Van Atta array. The unequal-line-length array is ideally suited to planar configurations, where the bandwidth limitation imposed by the unequal lengths is expected to be less than the typical 1.5 % bandwidth of the radiating patch elements. A further advantage of the unequal-line-length array is a reduction in transmission line losses since the total length of line used may be much reduced compared to the Van Atta array.

To determine the geometry for the interconnecting lines for the 8 antenna pairs, the longest interconnection was sketched out and its length determined. Earlier, the wavelength in the line λ_{TL} was accurately modelled at 77.1 mm. A set of allowed lengths could now be established i.e.

$$L_{\text{allowed}} = L_1 - n\,\lambda_{TL} \tag{3.7}$$

where L_1 is the first and longest line length. A schematic of a circuit layout realised using this principle is shown in Figure 3.10, where the antenna array spacing is 68 mm.

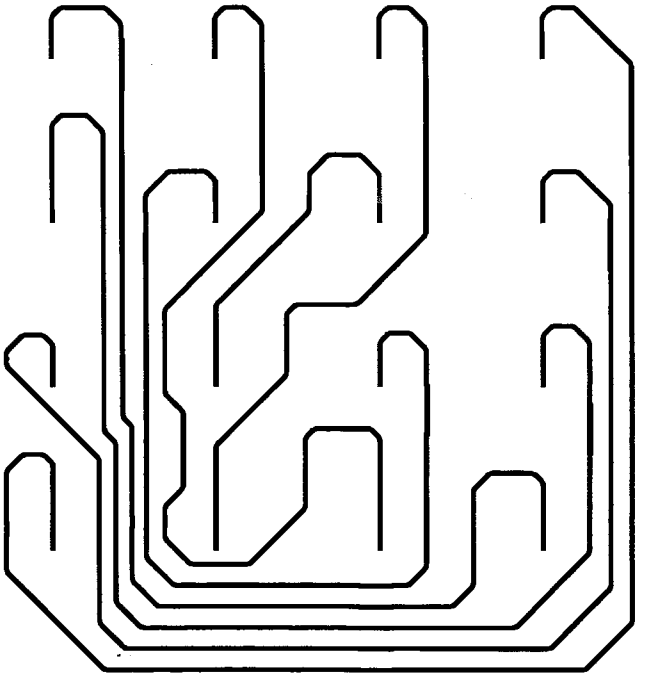

Figure 3.10 . Schematic for unequal-line-length retro-array feed configuration.

Switches: phase switches of a similar design to that described in chapter 2 were added to the circuit layout. Again, to maximise the modulation index a phase shift of π was sought by switching between two lengths of line differing by ½ λ_{TL} which is 38.5 mm. Packaged surface mount silicon PIN diodes were to be used as before.

Mask generation: The circuit geometry could now be written in the EESOF *Layout* editor, prior to generation of the mask sets. Great care had to be taken to ensure the feedlines overlay each other correctly via the apertures. Oversize apertures were used for one of the two circuit boards - although it would have been viable to remove the entire ground plane , this was thought to put an excessive loading on the chemical etching stage. Two pairs of masks were printed: the antenna patterns with aperture slots in ground plane, and the feed and switching circuits with oversize slots in ground plane. Two additional software translation stages were necessary between the EESOF *Layout* file and the printing of the mask to transparent film. The photographic process at by the Department of Physics used solid film negative resist, and so negative masks were required. For each circuit, the mask

pairs were pre-aligned, and the laminate placed in between them for double-sided UV exposure.

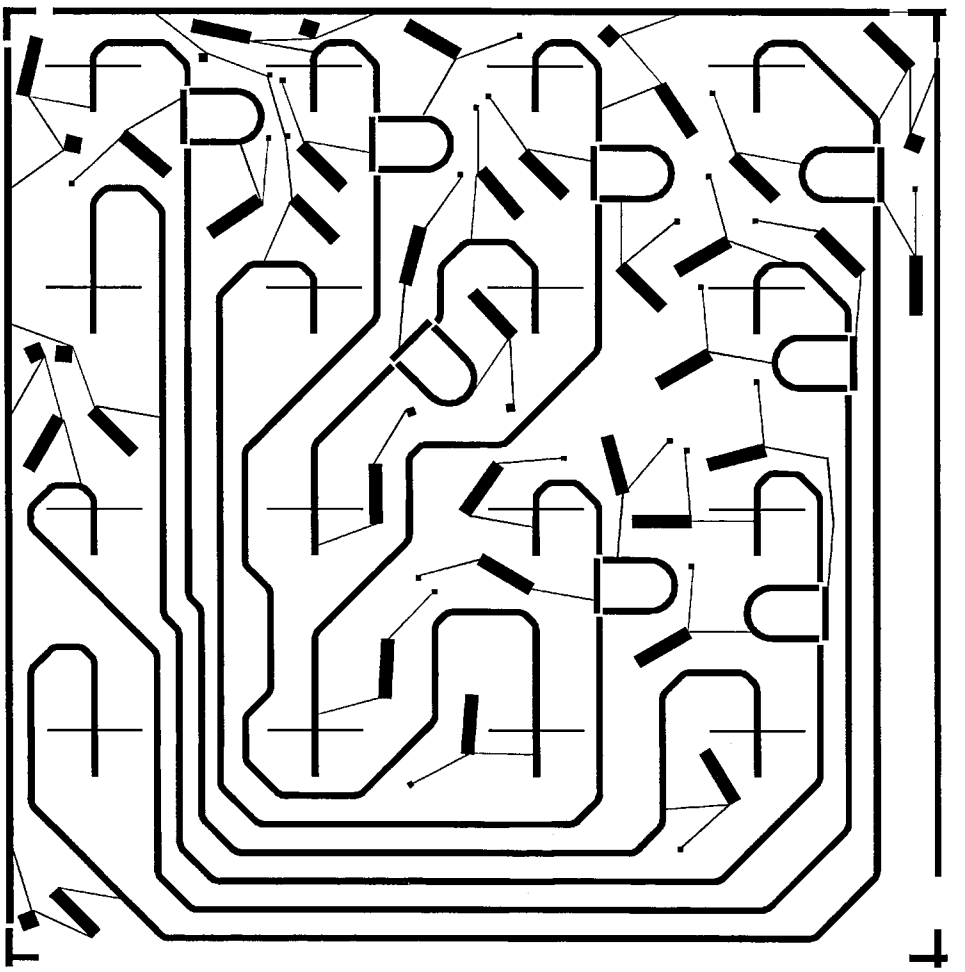

Figure 3.11. Combined graphic showing mask for 2.5 GHz retro array feed circuit, including apertures.

In Figure 3.11 the layout of the feed circuit is shown, including phase switches and bias filters. The Figure also shows the apertures – horizontal slots placed 14.9 mm from the transmission line ends – which were printed on a separate mask in practice. Attention is drawn to the region (lower left) where the transmission lines are close together to avoid crossing the apertures. The square border markers were used to aid mask alignment.

Fabrication: The etched boards were placed back-to-back and secured with adhesive tape. Permanent bonding of the boards was avoided so that they could be separated easily in the

future if necessary, for example to change the antenna matrix. The build of the switching and bias circuits was mostly straightforward, involving conventional soldering of the components.

3.7 Measurements.

The measurement method has been discussed in chapter 2, where a spectrum analyser was used to study the modulation products in the reflected signal. Of particular interest was:

- magnitude of reflected signal, being proportional to RCS magnitude
- angular response
- frequency response
- polarisation response.

The first three cases of measurements are straightforward to present. The centre frequency was established as 2.52 ± 0.01 GHz, where the peak reflected power (in the first upper sideband for a 25 kHz modulation signal) was found to be approximately 2dB lower than for the phase modulated dipole array. Since the gain of the individual radiators (dipole and patch) are similar in both cases, being approximately 4 dBi, the reduced peak directivity of the printed array is consistent with the expected increase in loss in the microstrip feed lines compared to the shorter co-axial lines used in the dipole array. Feed line losses are considered in more detail in chapter 5, which examines the implications for different construction methods and materials, particularly for larger arrays. Figure 3.12 shows the theoretical and measured angular response of the printed array, where linear polarisation was used for the illuminating signal and the array was oriented so that only one patch mode was excited. In this case, the reflected signal is also linearly polarised and the E and H-plane responses may be studied independently.

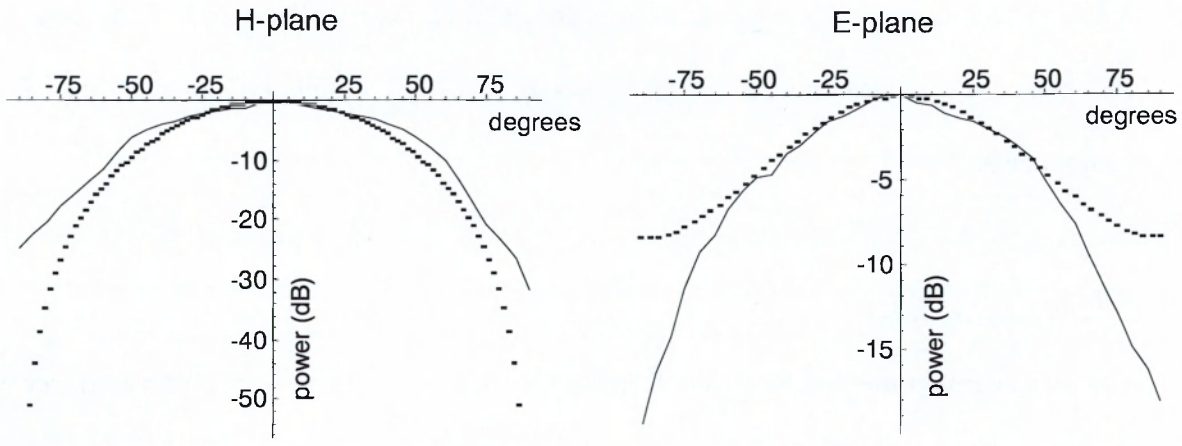

Fig 3.12. Reflected sideband power versus angle — measured • • • theoretical. (Plots are normalised)

For incidence angles between approximately ± 60°, both E and H-plane measured patterns are in good agreement with the theoretical cases. The trend that the H-plane measurement is slightly higher than the theoretical case while the E-plane is slightly below, is consistent with the simulated polarisation asymmetry of the individual patch antenna of Figure 3.8.

The polarisation response of the printed array proved much more problematic to interpret. While the above results relate to a single (and optimum) polarisation angle ϕ, the reflected power was seen to drop off sharply for other polarisation angles. The geometry is illustrated in Figure 3.13. The magnitude of this effect was not expected, because the radiating elements had been simulated and an almost circular polarisation demonstrated.

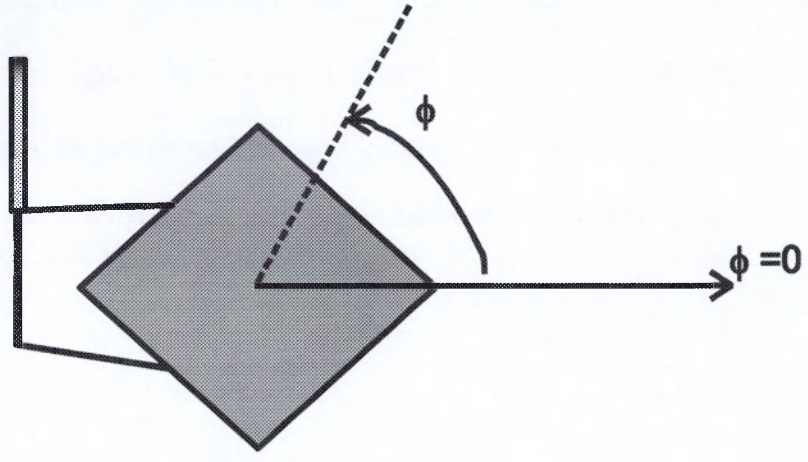

Figure 3.13 polarisation geometry

The polarisation response was studied by varying the incident polarisation angle with respect to the array, which was achieved by rotating the array about its boresight. To summarise the results, the peak reflected power was observed for $\phi = 45°$ and $\phi = 225°$, (in which case the incident polarisation is coincident with the patch mode fed by the "long" feed). The minimum reflected power was some 22 dB lower, and occurred for $\phi = 135°$ and $\phi = 315°$, (in which case the incident polarisation is coincident with the patch mode fed by the "short" feed). Thus the polarisation response of the array was so highly elliptic as to be linear for practical purposes, and the intended insensitivity to polarisation had not been achieved. A number of possible explanations were investigated. Firstly, it appeared that one of the orthogonal patch modes was being exited much less than the other. However, the simulated results shown in Figure 3.8 show an asymmetry of just 1 dB, which would be manifested as 2 dB in the combined transmit and received operations of the reflection measurement, so the mechanism causing the strong asymmetry has not been included in the simulation. A consideration of the manufacturing tolerances quickly rejected mask or etching tolerance as a likely mechanism.

It is important to recall that the simulation of the individual radiating element is not necessarily representative of the entire array of elements, since the effect of parasitic radiation from the microstrip stub feeds may be constructive or destructive in different planes depending on the array spacing. To further investigate the array, rather than the individual radiating element, a larger simulation was constructed which comprised 4 of the 16 elements in a square array. A corporate microstrip feed, with associated power dividers and impedance transformers, was included to simulate the behaviour of the array as an antenna, with all elements fed in phase. Processor and memory constraints precluded simulation of all 16 elements, (which in any case ought not have been necessary from a consideration of the array symmetry). The layout constructed for the *Momentum* simulation is shown in Figure 3.14.

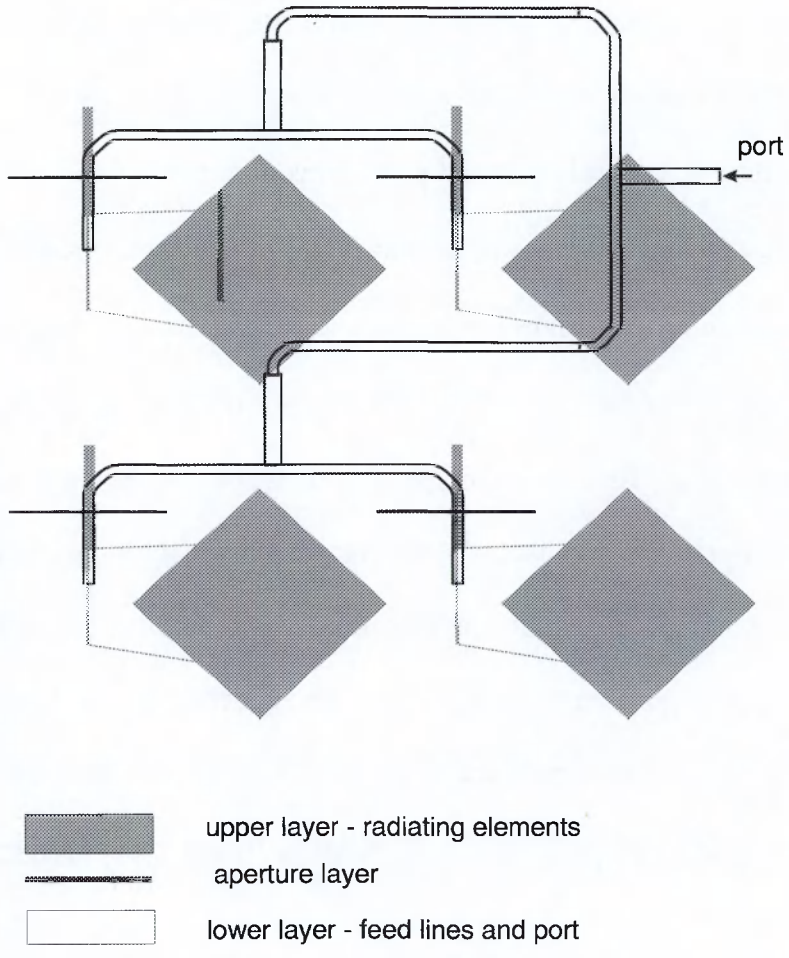

Figure 3.14 EESOF layout for diagnostic simulation of array extract.

3.8 Diagnostic simulation results.

Figure 3.15 shows the simulated fields E_θ and E_ϕ as a function of theta. In this case, the asymmetry between the field magnitudes is much greater than was observed for the simulation of a single element shown in Figure 3.8. The simulation reproduces the measured result, namely that the co-polar field E_θ is stronger than the cross-polar field E_ϕ when $\phi = 45°$. Had all 16 elements been included in the simulation, the 8 dB difference may have been expected to be greater. The plot for $\phi = 135°$ has been included to confirm that in this case it is the cross-polar field which is stronger. We also recall that for the reflection measurement, the polarisation loss will occur twice, and a figure of 16 dB would be expected.

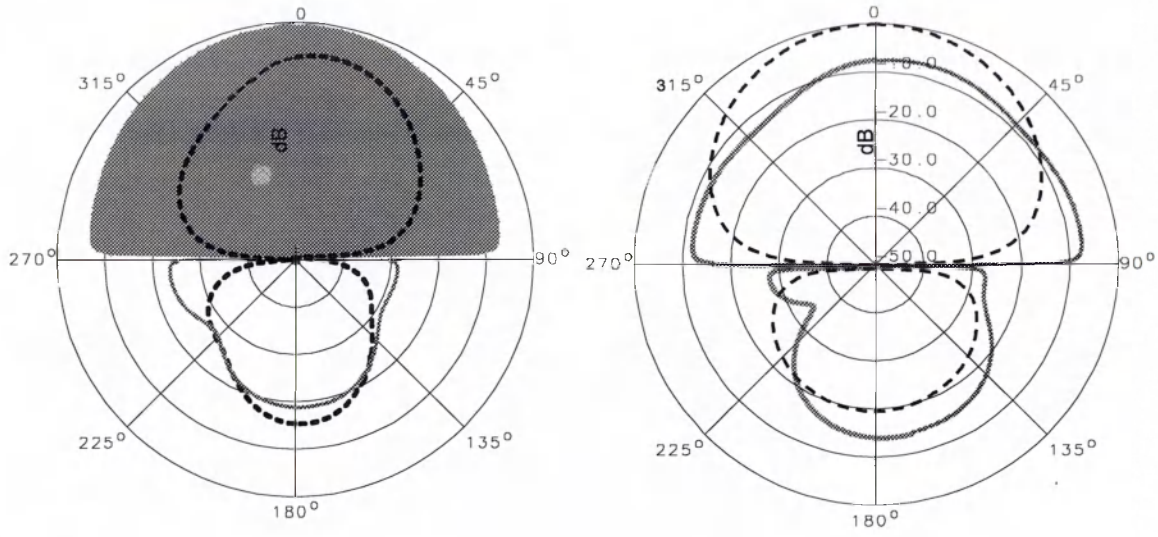

(i) $\phi = 45°$ (ii) $\phi = 135°$

—— E_θ --- E_ϕ

Figure 3.15. Orthogonal fields: relative magnitudes

It is postulated that the mechanism which has given rise to the polarisation asymmetry is the interference effect of the parasitic radiation from the microstrip feeds, since all the above investigation points towards this being the case. To re-iterate, while a single radiating element exhibits almost circular polarisation, when the simulation is extended to include 4 elements in a rectangular array, the ellipticity is much more severe. Means of obviating this difficulty are explored in the following section.

3.9 Alternative patch antenna configurations.

To overcome the adverse interaction between the antennas' radiation and that of the feeds, the stub feeds may be removed in favour of placing the apertures directly behind the patch antennas [6,7]. Circular polarisation may be achieved by feeding a pair of such apertures in phase quadrature [8] as illustrated in Figure 3.16, where the power dividers are fabricated on the same circuit as the feed lines.

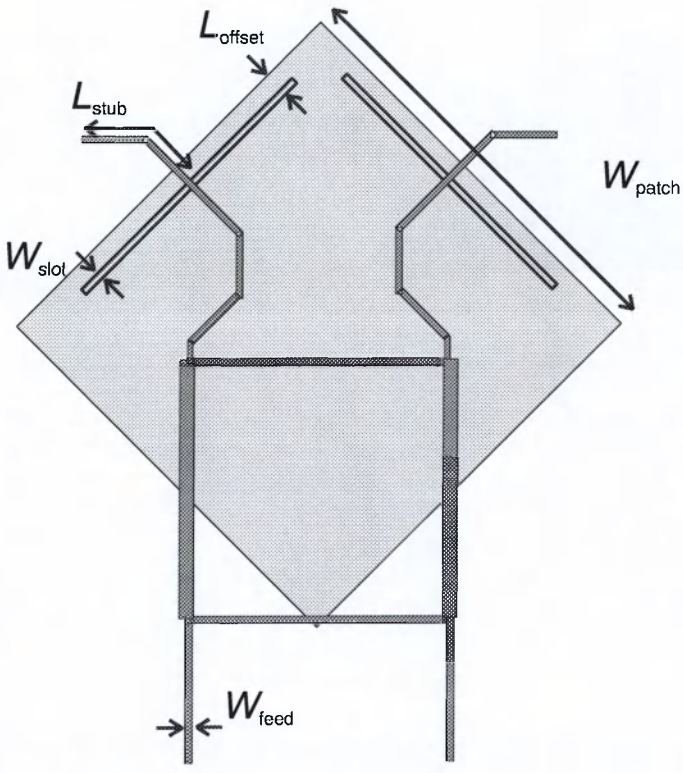

Figure 3.16 Dual aperture coupled circular polarised patch antenna.

A circular polarised patch antenna is described in [8] where a design frequency of 2.4 GHz was used and where: W_{feed} = 1.56 mm, W_{slot} = 0.6 mm, L_{patch}= 37.0 mm, L_{stub} = 14.0 mm and L_{offset} = 3.2 mm. In the example of [8], ε_r = 2.33 for the patch substrate and 2.22 for the feed substrate. The retention of both feed lines at the branch-line coupler allows for the sense of polarisation to be switched. While this approach is more robust from an electromagnetic point of view, it is less tractable for experimentation purposes, since feed circuits and antenna circuits cannot be so easily interchanged.

3.9.1 Omnidirectional Coverage.

To complete the study of printed antennas for retro-arrays, consideration was given to means of tailoring the antenna radiation pattern, so that a number of different applications (with differing requirements for spatial coverage) might be addressed. The angular coverage of the reflector has been shown to be equivalent to that of the individual antenna element chosen. For the patch antennas considered thus far, the radiation is inherently into

half-space, with a well defined power roll-off with increasing incidence angle which, for linear polarisation, is more rapid for the H-plane than for the E-plane. In a practical application, this radiation mechanism is useful to cover the majority of a hemisphere, such as might be applicable to a vehicle control or docking system. However, in applications where a transponder may be interrogated from any angle, a number of transponders (at least 2) would be required to prevent blind spots in coverage. The consequence of this approach is interference patterns between the two transponders' radiation patterns, unless the complexity of orthogonal access channels for each transponder is adopted (e.g. addressing each transponder with a different carrier frequency).

However, if we consider that there are few applications which require truly omnidirectional coverage, a radiator may be chosen to provide coverage in the region where it is most required. For example, a small marine vessel or ground-based vehicle may carry a transponder to enhance its detectability is a busy environment. Indeed, this was one of the original themes of the work which it is interesting to now re-visit. In this context, a transponder may be interrogated from any angle in azimuth i.e. from a ground based radar, and we may assume that interrogation "from above" will not occur. For this geometry, a vertical monopole or dipole would be an ideal candidate, such as are used in terrestrial broadcasting. Since fabrication and feed constraints render this type of antenna inconvenient for retro-array applications a printed equivalent has been sought. A promising solution is the over-moded rectangular patch, where radiation at a harmonic frequency of the fundamental mode is exploited. In this case, the components of the fringing fields which are parallel to the ground plane and make up the aperture fields are in anti-phase and constructive interference occurs in the plane of the substrate, with a null along the normal to the substrate, as illustrated in Figure 3.17 below.

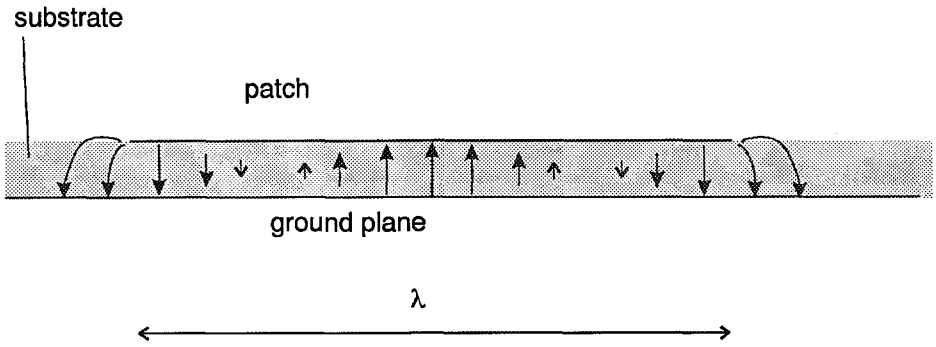

Figure 3.17 Over-moded patch radiation mechanism.

3.9.2 Circular Patch Antennas.

To examine the radiation pattern of a symmetrical radiator, a circular patch was simulated using *Momentum*. A nominal 33.3 mm diameter was chosen. From [5], an estimate for the fundamental resonant frequency is:

$$f = \frac{ck'_{10}}{2\pi a\sqrt{\varepsilon r}} \tag{3.8}$$

where a is the radius and $k'_{10} = 1.8412$. This yields $f = 3.05$ GHz for the test patch when a dielectric constant of 3.0 is used. Since the estimate is based on a model assuming a non-radiating zero-admittance wall around the cavity formed by the patch (the added length of the fringing field is not included and there is no dependence on substrate height), we may expect the actual resonance to occur at a slightly lower frequency. For a higher order resonance, we use:

$$f = \frac{ck'_{mn}}{2\pi a\sqrt{\varepsilon r}} \tag{3.9}$$

where k'_{mn} is the m^{th} zero of the derivative of the Bessel function of the first kind $J_n(x)$. The second resonance is derived using $k'_{20} = 3.05$, yielding $f = 5.06$ GHz, where we expect the over-moding to produce a boresight null and wide angle coverage in the plane of the substrate. A frequency sweep of 2.0 – 6.0 GHz was used in the simulation so as to be confident of capturing both the fundamental and second harmonic resonances. A substrate height of 0.76 mm was used. The reflection coefficient is shown in Figure 3.18, where the

first and second resonances at 3.0 and 4.95 GHz respectively are encouragingly close to the predicted values.

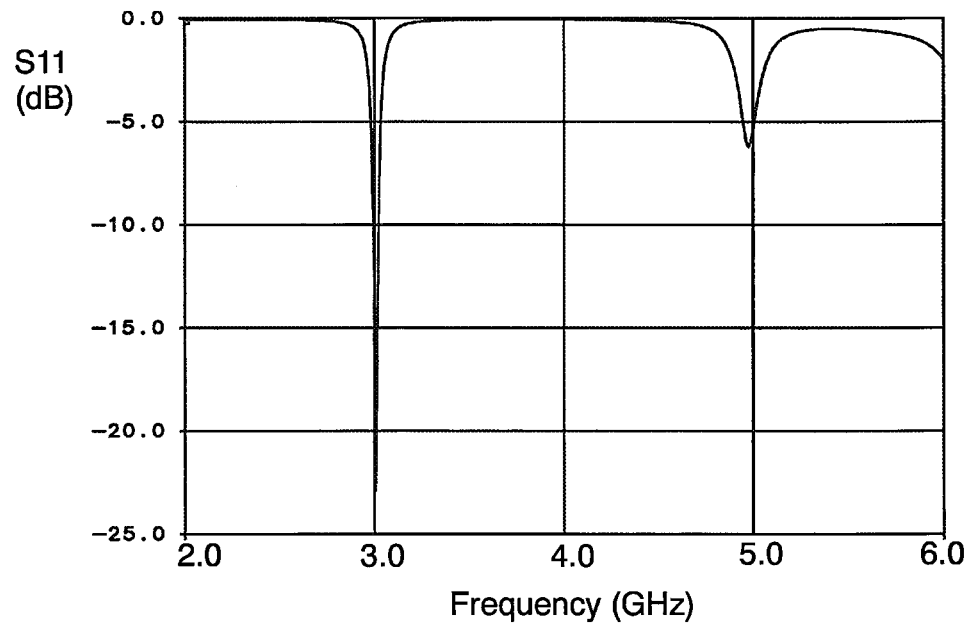

Figure 3.18. Return loss for circular patch, from wideband *Momentum* simulation. (d = 33.3 mm, ε_r = 3.0)

The radiation pattern for the fundamental mode will not be presented, being very similar to the rectangular patches presented earlier. The radiation pattern for the 2nd resonance is shown in Figure 3.19, where the characteristic on-boresight null is evident.

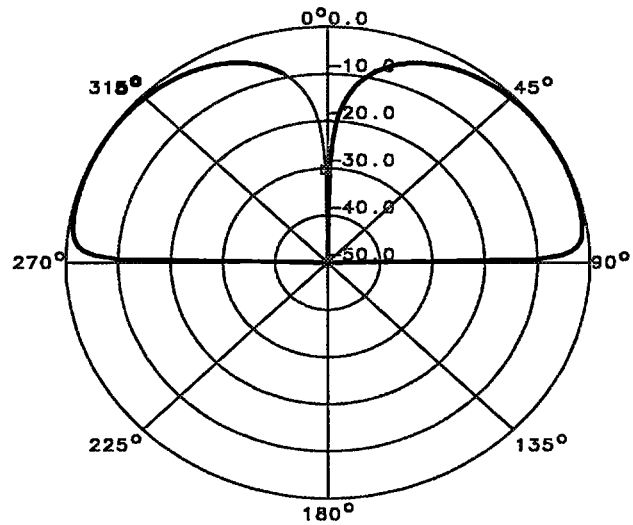

Figure 3.19. Circular patch antenna E-plane radiation pattern for 2nd resonance

To consider this approach in the context of the prototype retro-array described which was built and characterised, the over-moded circular patch could be scaled to an operating frequency of 2.5 GHz. From (6) above, the diameter required would be 67.4 mm. A patch of this diameter would preclude the adoption of the same array architecture since there would be insufficient space between the elements which were spaced at 68 mm intervals. The implications are that the bigger (over-moded) antenna element would require a bigger circuit board to accommodate an array of equivalent RCS. While use of a higher dielectric constant would allow for a smaller antenna element (using ε_r = 10.0 yields d = 36.7 mm.), the peak RCS would suffer from the reduction in antenna gain. A further observation is that while a circular patch is larger than a rectangular patch for a given fundamental operating frequency, the dimensions become comparable when the 2nd harmonic is exploited. This is because, for the rectangle, the length is approximately doubled to produce over-moding, while for the circular patch the ratio which applies to the scaling factor for diameter is:

$$\frac{k'_{10}}{k'_{20}} = \frac{3.05}{1.84} = 1.66 \qquad (3.10)$$

3.10 Conclusions.

In this chapter, a number of microwave design techniques have been brought together in the realisation of a modulated retro-reflector constructed from a pair of aperture-coupled printed circuits. The rationale for this development is to some extent economic, in that the dipole arrays discussed in chapter 2 are unattractive from a manufacturing point of view, are physically more bulky, heavy, and require more components. The constraints on the designer have been discussed in some detail, which are chiefly constraints of available space on the printed circuits. An important discovery arising from the solution which was adopted was the unequal-line-length retro-array, which is a narrow-band variant of the more general Van Atta array, and is an excellent solution for planar transmission line

routing. A useful corollary of this method is the reduction in total line length and hence attenuation. Polarisation has been studied in some detail. The intention was to develop a polarisation-insensitive response by adopting circularly polarised radiating elements, which would respond to any linear polarised interrogating signal. When the intended characteristic was not achieved, the underlying reasons were studied in some detail by recourse to CAD simulation of a representative structure. Parasitic radiation from the antenna feeds was identified as the underlying mechanism, and alternative feed configurations have been presented as a solution. In addition, alternative radiation patterns have been put forward so as to tailor the angular response for 360° azimuthal coverage from a single array. Alternative printed antenna geometries studied in this context have included circular and over-moded patches.

The work was successful in a number of aspects, not least of which was the confidence afforded by demonstration of working hardware in a field that appears to have been previously over-looked. Also, important lessons were learnt relating to the scaling of the parameters which define the performance which can be expected from a given aperture dimension and dielectric material. A number of interesting possible developments for the future could be identified at this stage. The array could be scaled in size to yield higher RCS values, and the fundamental limit explored - being mindful of the increasing effect of transmission line loss – which is discussed in chapter 5. Also, faster modulation circuitry could be developed to explore the limits of information transmission in a wireless link, or the design could be scaled to a higher operating frequency. The latter goals (bit rate and carrier frequency) were identified as the most important to pursue in the next stage of the work.

References

[1] "Antennas", John D. Kraus (2nd ed.) *McGraw-Hill* 1988 pp. 745 - 749.

[2] "The handbook of Antenna Design" Rudge, Milne, Olver, Knight. IEE Electromagnetics Waves Series 15 *Peter Peregrinus Ltd.* 1982. pp 526 - 543.

[3] "Antenna Design Using Personal Computers" D. Pozar, *Artech House* 1985 pp. 121 - 133.

[4] "Microstrip Antenna Design Handbook" R. Garg, P. Bhartia, I. Bahl, *Artech House,* 2001.

[5] "Microstrip Antenna Technology" K. R. Carver and J. W. Mink, *IEEE Trans. Antennas and Propagation.* Vol AP-29 no.1 Jan 1981. pp2 - 22.

[6] "Analysis of an aperture coupled microstrip antenna" Sullivan, Schaubert, *IEEE Trans. Antennas and Propagation.* Vol AP-34 No.8 Aug 1986 pp 977 - 984

[7] "A Reciprocity Method of Analysis for Printed Slot and Slot-Coupled Microstrip Antennas", D. Pozar, *IEEE Trans. Antennas and Propagation.* Vol AP-34 No.12 Dec 1986 pp. 1439 - 1446.

[8] "Circularly Polarized, Aperture-Coupled Patch Antennas for a 2.4 GHz RFID System", *Microwave Journal,* November 1999, Vol 42 No. 11, pp.20-44

[9] "Advanced Radar Techniques and Systems", Edited by G. Galati, pub. *Peter Peregrinus Ltd.* on behalf of the Institute of Electrical Engineers, 1993.

[10] Ref. [2], p. 534.

Chapter 4

Planar Modulated Retro-Arrays at X-band

4.1 Maritime Radar Applications

With the dual aims of developing the work toward commercial applications, and extending the performance envelope of the techniques discussed in the preceding chapters, a move in carrier frequency was sought. X-band (nominally 8-12 GHz) was identified as one of the most common bands used in mass-market applications, typically such as maritime radar. Pulsed radar sets in common use by sea-farers, from smaller amateur pleasure craft to larger commercial cargo vessels typically operate between 9.2 and 9.5 GHz [1]. (The more basic, mass-market sets [2] may cost as little as $ 2000). In a return toward the roots of the project, this frequency band was chosen for the development of transponder prototypes which might address the problem of target detectability for the smallest vessels not otherwise equipped. An increase in transponder modulation rates would also be sought so as to address other application areas and extend the use of spectrum as far as possible. Should the need arise, availability of components in this band was not expected to present a severe restriction on build of hardware.

A survey of regulatory issues was conducted with the aim of selecting the specific frequency and bandwidth of operation.

MHz

8850 - 9000	RADIOLOCATION	Government.
9000 - 9200	AERONAUTICAL RADIONAVIGATION	(1) Approach radar. (2) Government.
9200 - 9300	RADIOLOCATION (1) MARITIME RADIOLOCATION (2)	(1) Government. (2) The maritime radionavigation service is for shipborne radar and racons, with harbour radar by special agreement with other users of this band. Low Power Radiolocation Equipment for Detecting Movement and for Alert.
9300 - 9500	AERONAUTICAL RADIONAVIGATION (1) MARITIME RADIONAVIGATION (2)	(1) Ground and airborne radar. (2) The maritime radionavigation service is for shipborne radar and racons, with harbour radar by special agreement with other users of this band. The Motorwarn system operates on 9410 MHz. MDM equipment may use 9325 MHz and 9480 MHz on a non-interference basis to other users. The development of new airborne weather and new shipborne radars in this band will be limited in accordance with the aim of Rec. 600, WARC, 1979.
9500- 10000	RADIOLOCATION	Government. Existing harbour radars at Gravesend, Southampton and Crayfordness may operate up to 9530 MHz, on a temporary basis until withdrawn.
10000- 10125	MOBILE RADIOLOCATION AMATEUR	Government. 3cm survey equipment may use this band on a non-interference basis to other services.
10125- 10225	RADIOLOCATION (1) MOBILE (1) FIXED (2)	(1) Government (2) Civil Radio Fixed Access in the bands 10125-10225 MHz, paired with 10475-10575 MHz. 3cm survey equipment may use this band on a non-interference basis to other services.
10225- 10450	MOBILE (1) RADIOLOCATION (1) AMATEUR (2)	(1) Government. Shared with secondary service: 10300-10360 MHz - PMSE. Home Office/Scottish Office for the Emergency Services in the bands 10250-10270 MHz and 10360-10400 MHz. (2) Amateur service in the band 10225-10475 MHz. 3cm survey equipment may use this band on a non-interference basis to other services.

Table 4.1 UK frequency allocations, 8.85 - 10.45 GHz

Table 4.1 shows an extract of the UK Radiocommunication Agency's (RCA) published frequency allocations [3] within X-band known to be utilised by maritime radar applications. With the exception of the headings, the data is reproduced in its published state, and has not been otherwise edited or interpreted. A cursory inspection of the (in places vague) contents illustrates the difficulty in extracting specific information from these regulations. However, the bands 9.0-9.2 GHz, 9.2-9.3 GHz and 9.3-9.5 GHz would appear those most commonly used for maritime radar. Typical carrier frequencies for commercial pulsed radar sets include 9.375 and 9.410 GHz with an IF bandwidth between 20 and 60 MHz [2]. The centre frequency selected for design purposes was thus 9.39 GHz, being the mean of the aforementioned carrier frequencies.

4.2 Transponder Design.

In chapter 3 the difficulty in achieving circular polarisation was investigated in some detail. In particular, the aperture coupled microstrip feeds were found to suffer parasitic radiation which corrupted the polarisation purity. With the emphasis now on operation at 9-9.5 GHz, a new set of challenges would be encountered. In particular, prototyping of antenna arrays would be necessary to achieve the desired frequency of operation. Separation of the feed, aperture coupling and radiating functions of the microstrip elements was therefore still sought. For these reasons, integrated aperture coupled patch antennas were not proposed, since a change in the antenna circuit board would necessitate a change in the aperture geometry. Retention of aperture coupled feed lines, as prototyped at 2.5 GHz, allowed the continuation of the philosophy of changing the combination of feed line circuit and antenna array.

4.2.1 Laminates.

In addition to the Roger's RO3000 laminate [4] used at 2.5 GHz, a second, lower cost laminate was procured. This was Taconic TLC30 [5]. The properties of the two laminates are summarised in Table 4.2

Laminate	Rogers RO3000	Taconic TLC30
ε_r	3.0 ± 0.04	3.0 ± 0.05
h (mm)	0.76	0.79
Tan δ (at 10 GHz)	0.0013	0.003
approx. cost UKP per 300 mm square panel	40	10
width of 50 Ω microstrip (mm)	1.96	1.98

Table 4.2 Comparison of laminate properties.

Being mindful of mass production applications, the cheaper laminate was procured, in part, to investigate its performance compared to its costlier counterpart. Also, the Taconic laminate exhibited better mechanical properties and proved to be easier to handle, cut, and was less susceptible to damage. In both cases the laminates were ordered with 18 μm thick electrodeposited copper cladding on both sides. The slight difference in laminate heights yields a very slight difference in the relationship between line impedance, wavelength and width [6]. This effect was not considered sufficient to warrant separate layout design for line interconnects, switches and bias lines, but was expected to yield different patch antenna resonant frequencies for a given mask layout. Therefore, a range of antenna lengths was proposed, while the feed line layout would be common to both substrates.

4.2.2 Antenna Elements.

Linear polarisation was preferred, with the patch antenna's E-plane orientated horizontally to exploit the widest angular response in azimuth (see Figure 3.6). To obviate further complications with parasitic feed line radiation, the feed lines on the antenna circuit were rotated through 90° with respect to the antenna E-plane so that the stub parasitic radiation would be orthogonal to the linear radiating mode of the patch, as illustrated in Figure 4.1.

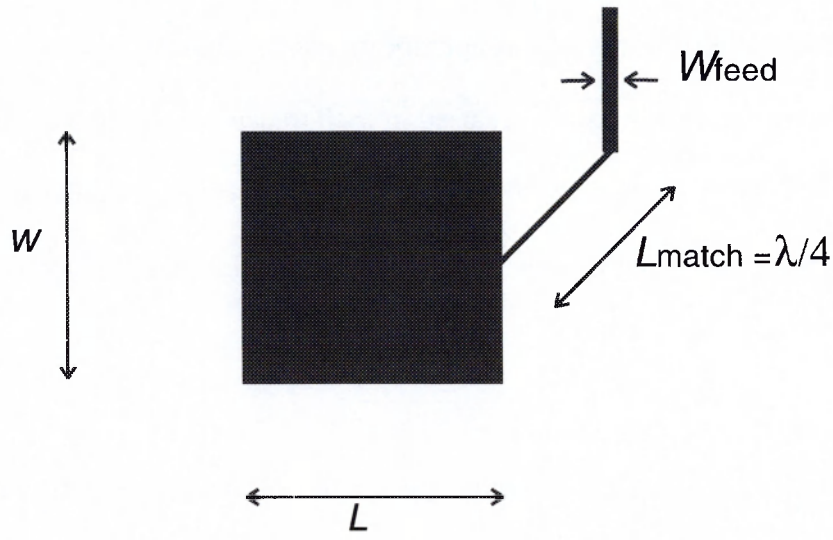

Figure 4.1 patch antenna element with microstrip feed.

As discussed in chapter 3, the feed line should be matched to the input resistance (radiation resistance) of the antenna. For linear polarisation the patch is not required to be square. However, as the patch width *w* is reduced, the radiation resistance increases [7] and becomes more difficult to match to, requiring a matching line of higher impedance and therefore lower width. The minimum track width is a function of the mask and etch resolution, being around 100 μm in this case. Using the methods described in chapter 3 (equations 3.2 - 3.4.) a square patch of length 8.94 mm yielded the target resonant frequency of 9.39 GHz on the Rogers substrate.

Aperture coupling. The method developed at 2.5 GHz was scaled to a 9.39 GHz centre frequency for the Rogers substrate (h=0.76 mm). *Momentum* was used iteratively to minimise the insertion loss of the circuit. Following a manual optimisation of 12 iterations, the slot and stub dimensions (see Figure 3.9) which were derived were: L = 9.0 mm, w = 0.10 mm, s = 4.2 mm, where the line width was 1.0 mm. (The choice of this line width, which does not yield 50 Ω line, is discussed below.) This resulted in a minimum insertion loss 0.18 dB and better than 0.4 dB over the full 500 MHz bandwidth which was simulated. The laminate loss terms were not included in this simulation so as to isolate the inherent, reflective insertion loss of the aperture from the resistive material losses. It is worth adding that, since two apertures are used in each transmission line, the loss term will occur twice in the finished circuit, and also that the non-resonant, broadband response of the aperture justifies use of either substrate, with their slight height difference, with the same layout.

A *Momentum* simulation of the antenna layout shown in Figure 4.1, with aperture coupling, showed that the length needed to be re-scaled to 8.82 mm to achieve the target frequency. This simulation included the substrate loss terms, and predicted a 10 dB bandwidth of 2.1 % or 197 MHz. A further simulation for the Taconic TLC substrate indicated a square patch of length 8.80 mm would be required.

Antenna prototyping: The laminates' dielectric constant are both specified to a tolerance of around 1.3 %, and other factors such as mask accuracy and etch resolution lead to uncertainty in the final resonant frequency achieved. Also, apart from these considerations, the accuracy of the simulation tool was a further unknown, although it had proved invaluable at lower frequency studies. For these reasons a prototyping stage - i.e. fabrication and measurement - was carried out. As long as the achieved resonance is very close to the design figure, the antenna dimensions may be scaled linearly to re-scale the

centre frequency. (A less methodical or accurate theoretical analysis would likely have lead to a bigger error at the first prototyping stage and hence require subsequent stages.)

The 8.80 mm patch was prototyped as a single element using both substrates and the measured resonant frequencies used to derive new patch lengths. In addition, 1.5 % oversize and 1.5 % undersize patches were proposed in anticipation of the final antenna arrays exhibiting further errors in centre frequency due to, albeit weak, mutual coupling between elements in the array [8]. The scaling of the prototype dimensions is summarised in Table 4.3

substrate	Taconic TLC	Rogers RO3000
centre frequency, single patch prototype, L=8.80 mm (fabricated)	9.130 GHz	9.248 GHz
error (%)	2.77	1.51
new required length (mm)	8.56	8.67
+ 1.5 % length (mm)	8.68	8.77
- 1.5 % length (mm)	8.43	8.54

Table 4.3. Patch lengths derived from first prototyping stage for target centre frequency 9.39 GHz

From Table 4.3, four lengths are suggested to "capture" the intended centre frequency in the 16 element retro-reflector. These are: 8.43, 8.55, 8.68 and 8.77 mm. Since the lithography process would handle laminates up to approximately 300 x 300 mm size, 9 circuits could be fabricated in each batch. To maximise the available use of circuit and mask space, a number of antenna matrix variants would be fabricated together. A fifth length of 8.61 mm was used on a spare 16 element matrix. (The remaining 4 domains on the laminate would be used for the feed circuits.) An antenna matrix is shown in Figure 4.2

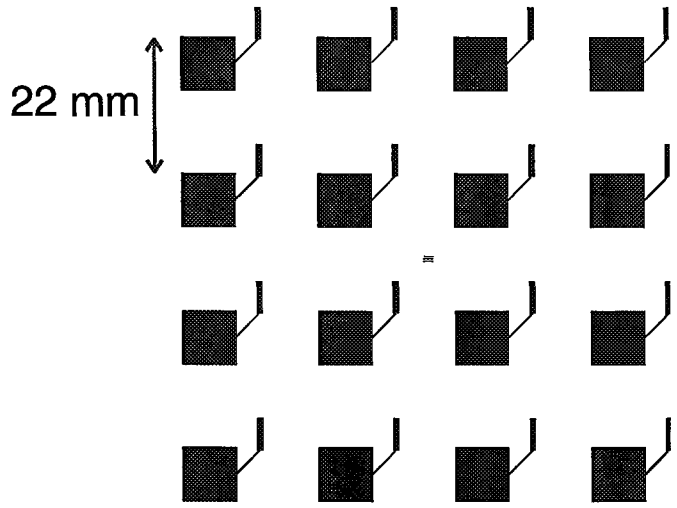

Figure 4.2. X-band retro-array antenna matrix

If the spacing is too close (much less than half a wavelength) coupling between antenna elements may become significant and corrupt radiation patterns [9]. Also, the area for transmission line routing is reduced, which could lead to increased parasitic coupling between lines. If the spacing is increased, the total aperture efficiency is poor and the interconnecting transmission lines are excessively long which leads to excessive loss. The 22 mm antenna spacing was chosen to be similar to the spacing used at 2.5 GHz, and is equivalent to 0.69 wavelengths at 9.4 GHz. This spacing allowed the feed circuit to fit within the target 100 mm square circuit area, so that 9 circuits could be fabricated together, but placed constraints on the routing and line widths of interconnecting lines.

In-situ antenna measurements: Two examples each of the five antenna circuits fabricated for each laminate were tested. The resonant frequency of a single element within each array was measured by connecting a co-axial line to one of the outer antenna feeds. The measured antenna resonant frequencies are summarised in Table 4.4

patch length L (mm)	Taconic TLC		Rogers RO3000	
	predicted centre frequency (GHz)	measured centre frequency (GHz)	predicted centre frequency (GHz)	measured centre frequency (GHz)
8.55	9.40	9.57	9.52	9.59
8.77	9.17	9.29	9.28	9.34

Table 4.4 Measured resonant frequency of *in-situ* patch antenna.

Uncertainties on the validity of the measured frequencies in Table 4.4 includes the mis-match between the 50 Ω co-axial lead and 73.8 Ω microstrip and the proximity of the substrate edge to the outer antenna. For these reasons the measurement of antenna bandwidth, which indicated the order of 150 MHz at 10 dB, is likely to be unreliable and a greater bandwidth would be expected for retro-array operation. The frequency response of the completed transponders is discussed later in the chapter.

Discussion: The extensive antenna prototyping and measurement was carried out partly because of the expected difficulty in achieving the desired centre frequency for an inherently narrowband antenna, with its known sensitivity to manufacturing tolerances and other factors which are difficult to predict such as the effect of neighbouring circuit elements and finite ground plane area. Also, unlike a conventional antenna, it is difficult to establish the frequency response of a modulated retro-reflector with great accuracy, since it has no measurement port for connection to a network analyser. For the latter, the measured (modulation spectra) response is dependent on the RF frequency response of the modulation circuitry in addition to the frequency response of the individual antenna elements. It is also difficult to de-embed the measured frequency response of the device from that of the measurement system, since the measured result includes the frequency response of the transmit and receive antennas in the measurement system although this is ideally flat over the frequency range of interest. In contrast, an antenna may be connected

directly to a network analyser to measure its insertion loss and hence radiation bandwidth. For these reasons, considerable effort was put into a thorough characterisation of the radiating elements in the retro-array and the discrepancies between different stages of simulation and prototyping.

4.2.3 Feed lines

As discussed in chapter 3, the interconnecting feed line width and hence impedance is arbitrary, but limited in practice by the available area on the printed circuit. To a first order, track impedance is determined by width and does not scale with frequency. However, the dimensions of the patch antennas, their spacing, and the switch dimensions do scale with frequency, and the track width of around 2 mm required for 50 Ω line becomes inconvenient as the other circuit dimensions reduce. Conventionally, thinner substrates are used for feedlines at increasing frequencies, but this would yield a lesser antenna operating bandwidth and hence even greater sensitivity to tolerances and so this route was not preferred. A thinner substrate for the feedline and switching circuit compared to the antenna circuit would require aperture coupling between dissimilar substrates and also the procurement of an additional substrate type. While it is suggested that this approach is worth investigating in future work, it was not pursued at this stage due to fabrication constraints (it was preferred to photo-etch groups of antenna circuits and feed circuits from a single sheet of laminate).

For similar reasons a higher dielectric constant for the feed circuit was rejected. Also, while line widths would be reduced in this case, the resulting increase in the *electrical length* of interconnecting lines between antenna pairs, due to the reduced line wavelength, would lead to greater loss.

A narrower feed line was the preferred approach to relax the spacing between congested interconnecting lines. However, excessively narrow microstrip lines exhibit greater loss, which is detrimental. A study of line loss as a function of width was conducted in some

detail and is detailed in the Appendices. A line width of 1 mm was selected as a good compromise to allow for transmission line routing without excessive line loss. For this width, the line impedance is 73.8 Ω and the wavelength 20.9 mm at 9.4 GHz [1].

The principle of unequal feed line lengths discussed in chapter 3 was again used. The line lengths are shown in Table 4.5. for the antenna pairs, which are numbered according to the matrix shown in Figure 4.3. Table 4.5 also includes the difference in length of each line from that of the longest lines, as an integer number of wavelengths. The completed feed line layouts are shown in Figure 4.7

antenna pair	line length (mm)	difference from line 1-16 (λ_{TL})
1-16	221.8	0
2-15	221.8	0
3-14	200.9	1
4-13	180.0	2
5-12	96.4	6
6-11	54.6	8
7-10	159.1	3
8-9	138.2	4

Table 4.5 Lengths of interconnecting transmission lines.

[1] A design frequency of 9.4 GHz is quoted for the switch and transmission line components since these are sufficiently wide band in frequency response that the additional precision used for the antenna centre frequency, i.e. 9.39 GHz, is unnecessary.

1	2	3	4
5	6	7	8
9	10	11	12
13	14	15	16

Figure 4.3 Numbering convention for antenna elements referred to in Table 4.5

4.2.4 Switches.

Phase modulation, being more efficient than amplitude modulation, was the preferred mechanism. To this end, silicon beam lead PIN diodes were used with a similar microstrip switch to that developed at 2.5 GHz. To achieve the required path difference of a half wavelength (10.45 mm in the 1 mm width microstrip), the two path lengths chosen were 5.0 mm and 15.45 mm. Switch bias networks were re-designed for a centre frequency of 9.4 GHz using the conventional approach of using alternate high and low impedance quarter wave lines to achieve a low pass response, with the stop band centred at 9.4 GHz. A *Momentum* simulation of a 3 element bias filter indicated a stop band rejection between 25 dB at 9.0 GHz and 35 dB at 10.0 GHz.

A simplified bias network reduced the number of bias filters by a factor of 2 compared to the method used previously at 2.5 GHz. The new switch microstrip layout is shown in Figure 4.4. A control voltage may be applied to a single terminal and the diodes are biased in series pairs, in contrast to the parallel paired method used for the 2.5 GHz prototypes. In the latter case, the bias current in the individual diodes is not controlled, while series paired bias is preferred since it assures the same bias current in each diode.

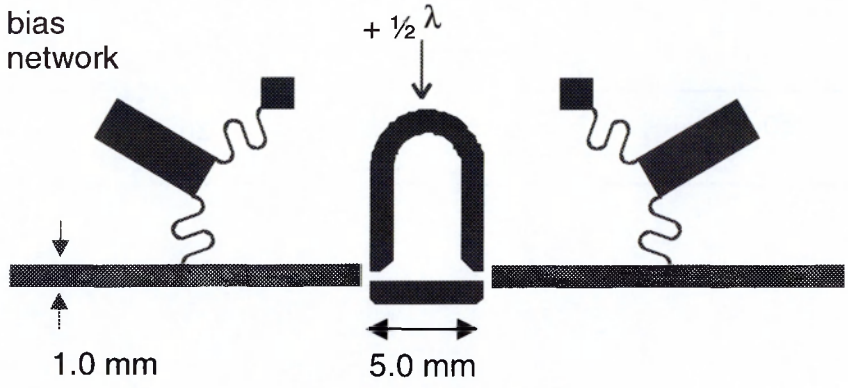

(a) microstrip layout

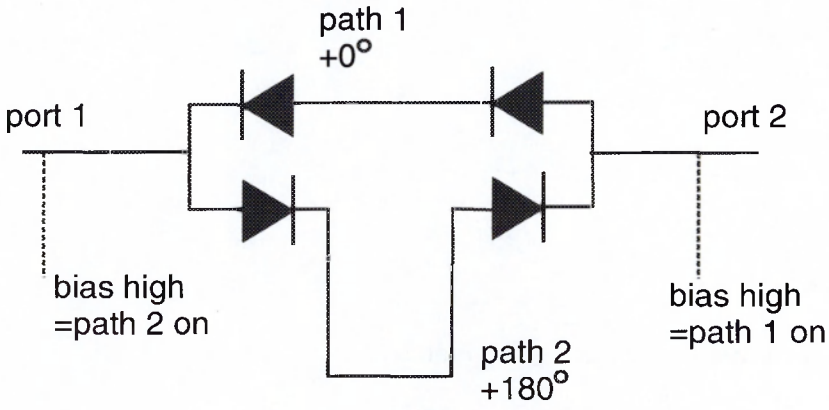

(b)diode configuration

Figure 4.4 9.4 GHz microstrip phase switch

The switch was incorporated with the feed line layout to yield the final mask layout.

Amplitude modulation

A further variant substituted the phase switch for a straight through line, with a single gap in which a single diode could be placed to achieve a crude amplitude modulation. With this arrangement, a modulation index of unity cannot be achieved since the switch can never be totally absorptive. While when "on" the switch is in the low loss state, in other states the switch is reflective. This is because the impedance presented to the transmission line is the series combination of the diode and line impedances, as shown in Figure 4.5

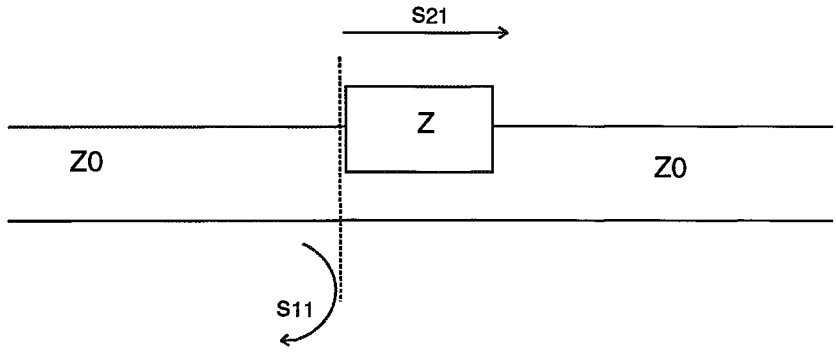

Figure 4.5 Series impedance in transmission line

Where the series impedance z is normalised to the line impedance Z0, the 's' parameters of the switch are given by:

$$S_{11} = \frac{z}{2+z} \tag{4.1}$$

and $$S_{21} = \frac{2}{2+z} \tag{4.2}$$

While the fractional loss in the load z is given by :

$$loss = 1 - S_{11}^2 - S_{21}^2 \tag{4.3}$$

The loss reaches its maximum value of ½ when the normalised impedance z is 2, as shown in Figure 4.6

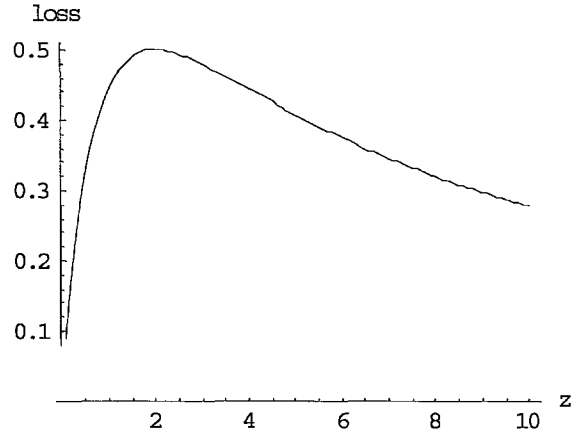

Figure 4.6 Loss in single diode series switch as function of switch impedance

Thus we may expect an amplitude modulation index of up to ½ to be attainable when the diode bias current is switched to a low state and the diode resistance, represented by z, is 2

Z_0 or 148 Ω. This assumes that in the high current "on" state the loss is negligible. However, this neglects the effect of the phase of the reflected energy from the switch. Considering all the switches, the phase of the reflected energy from each switch may add destructively or constructively in the reflected phase front depending on the location of the switch (the mis-match) in the transmission line. Since this location was chosen arbitrarily to suit the physical location of components on the printed circuit, these phase effects should be considered random. For these reasons, the amplitude modulation achieved by this simplistic approach is unlikely to be very efficient, and the phase modulation method is much preferred. However, the single diode amplitude modulation requires one quarter of the number of diodes and hence one quarter of the power consumption, and these advantages should be weighed against the poor modulation index. Mask sets for both cases were printed and the circuits fabricated .

4.2.5 Diodes.

Two batches of diodes were procured. Firstly, a sample of 20 obsolete Alpha DSG 6474-006 silicon beam lead PINs were supplied free of charge by Alpha Industries. These would be insufficient in quantity for a phase modulated device, which would require 32 diodes (4 per switch) and so were used to build up an amplitude modulated transponder.

Secondly, a batch of 50 MA/COM MA4P461 silicon beam lead PINs were procured at a cost of £ 6.90 per diode. These were later built up into a phase modulated transponder. The diode specifications are summarised in Table 4.6.

diode	Alpha DSG 6474-006	MA/COM MA4P461
suggested frequency range (GHz)	1 - 18	1 - 8
insertion loss at 20 mA (dB)	0.5 (at 10 GHz)	0.3 (at unspecified GHz)
isolation	20	12
switching time (ns)	25	15

Table 4.6 Summary of diode specifications.

Specifications for switching PIN diodes generally exhibit trade-offs in terms of isolation and insertion loss. A diode which offers high isolation when unbiased or reverse biased will tend to exhibit poor insertion loss when forward biased. Typically, manufacturers offer variants of a diode family ranging from good isolation with poor insertion loss, to poor isolation with good insertion loss. Also, higher bias currents lead to reduced insertion loss, with the practical limit often not reached until about 50 mA or even 100 mA forward bias current. The DC power consumption associated with these currents leads the designer of a passive transponder to seek the lowest insertion loss possible for the lowest forward bias. Isolation is sought to achieve good depth of modulation in the switching circuits, but beyond a certain value (say 20 dB), further gains in isolation reap no practical benefit. GaAs diodes present an alternative from silicon, and typically offer higher switching speeds due to the increased carrier mobility associated with the former semiconductor material, but with higher bias voltages and power consumption.

It should be stressed that the diodes listed were those which were available from manufacturers at the time (since a number of manufacturers/suppliers proved to be somewhat intractable), and are in no way optimum for the application. In particular, the MA/COM diode would be operated about 1.4 GHz beyond its suggested operating range. In practice, the weakness of this diode when tested proved to be poor isolation (around 6 dB) at 9.4 GHz, although this value would be doubled for the series diode pair in the phase switch.

Reflective loss in imperfect phase switch.

The finite isolation of the switching diodes leads to some leakage of the input signal through the branch of the switch which is ideally infinitely isolated. This "leakage" power adds in anti-phase (due to the 180° path length difference) at the switch output. The reflective loss due to this destructive interference can be estimated as a function of the diode voltage insertion loss I, which is 0 for perfect isolation and 1 for perfect

transmission. A formal circuit analysis is somewhat beyond our scope, as it would require knowledge of the (complex) voltage scattering parameters of the diodes in both forward and reverse biased states. However, an *estimate* can be presented which is valid for small values of I. Here, we assume the "on" diodes are perfect and estimate the voltage attenuation for the "leaky" path as I^2 (i.e. for two diodes). This leads to a relative voltage $\sqrt{1-I^4}$ for the "on" path and a reflected voltage, due to the destructive interference between the two paths, of $1-\sqrt{1-I^4}+I^2$ relative to the input. For a -10 dB diode insertion loss this leads to a reflection coefficient of -19.5 dB, which represents a trivial loss due to reflection at the imperfect switch. However, this reduces to -11 dB (i.e. 8 % reflection) for a diode insertion loss of -6 dB.

In-situ diode performance.

In later measurements of the completed phase-modulated transponder, the diode performance at minimal bias currents proved to be very encouraging - the power in the modulation products could be observed as a function of total diode current, which could be reduced to about 100 μA (through the use of a variable in-line resistor in the bias supply) before the sideband power dropped off significantly. This represents about 12 μA per switch (containing 2 in-series diodes) and from the approximately 1.8 V supply current allows a good estimate of total diode power consumption of 0.18 mW.

Switch assembly.

Being very small (100 micron contacts) and delicate, soldering by hand proved to be impractical with the facilities available. While soldering of components of smaller dimensions, such as chip diodes (i.e. unpackaged and without leads) for sub-millimetre wave devices is routinely performed this requires a dedicated laboratory equipped with microscopes and purpose-built heat jigs. The process usually involves hand application of

flux and finely powdered indium-based solder, followed by a short, pulsed application of heat. The technique is best performed with metal based components such as waveguide, or crystalline substrates such as quartz or alumina, and is not well suited to PTFE based laminates.

As an alternative, a bonding process was developed to secure the diodes to the copper conductor of the microstrip, based on baking silver loaded epoxy. This involved applying the epoxy to the copper conductor by hand whilst viewed through a microscope, and similarly bringing the diode to the contact by hand. The tools used were tweezers and finely cut-down wooden cotton-bud sticks. The heat was applied by placing the circuit in an electric fan oven.

A number of epoxies were tested in an attempt to minimise contact ohmic resistance. Initially, some very poor results were obtained. It was found that some batches of epoxy exhibited surprisingly poor characteristics and were very sensitive to mixing, baking and very probably their history of storage. The best results were obtained with *CircuitWorks* epoxy, samples of which exhibited no measurable ohmic resistance if mixed sufficient rigorously (5 minutes by hand) and baked at 120° C for 30 minutes.

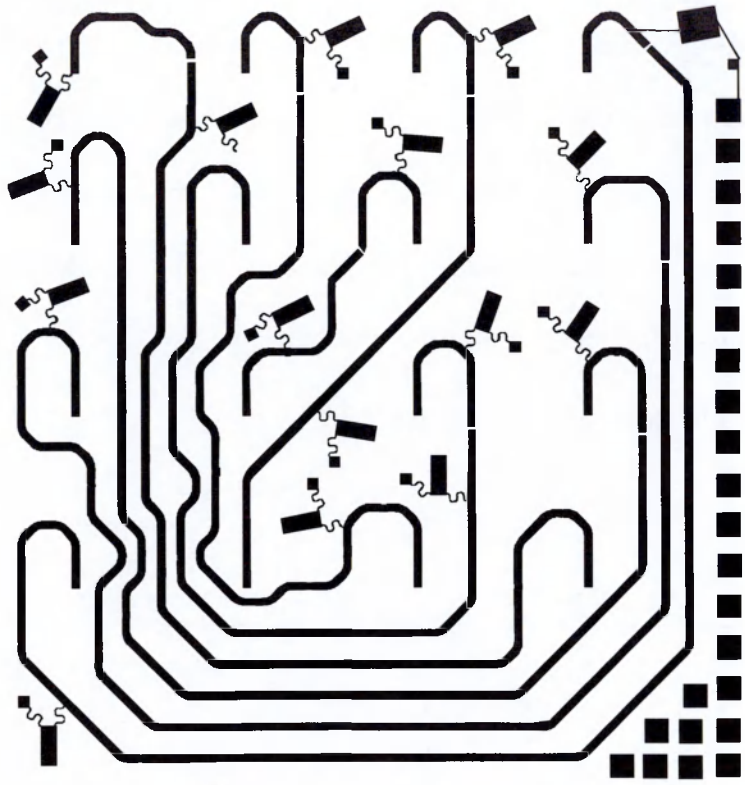

96 mm

(a) amplitude modulation

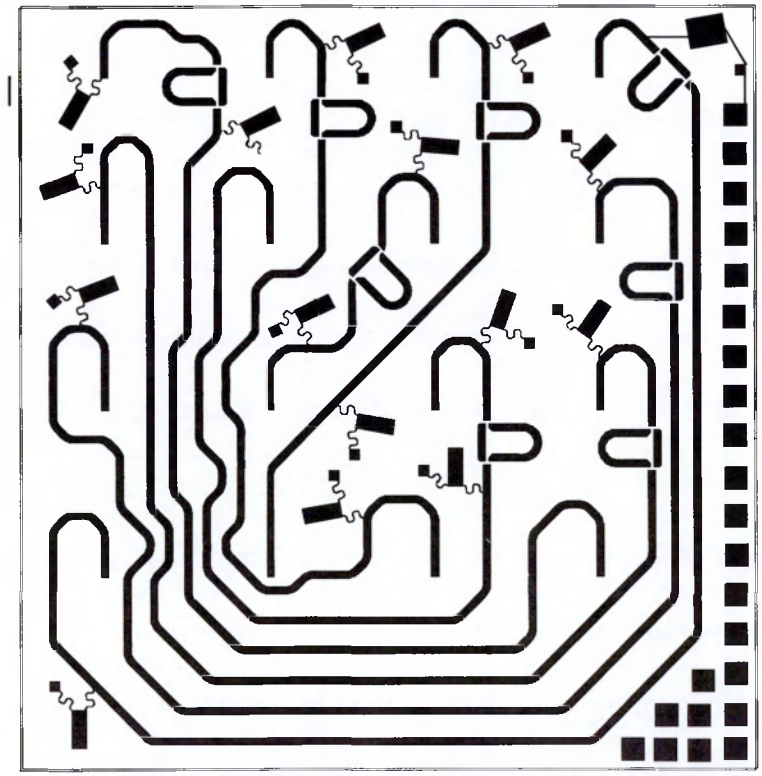

(b) phase modulation

Figure 4.7 X-band retro-array feed networks.

4.2.6 Diode Driver Interface.

The bias network, as described above, requires the bias ports to be alternately high and low voltage with respect to each other, to turn on one of the RF paths. The configuration might well be described as a "push-pull" mechanism. To buffer the diodes to the modulation source, while building in some adjustability to the drive voltage, CMOS inverters were found to be a convenient, clean buffering mechanism. The inverter chosen was the 74HC04. The circuit adopted is shown in Figure 4.8

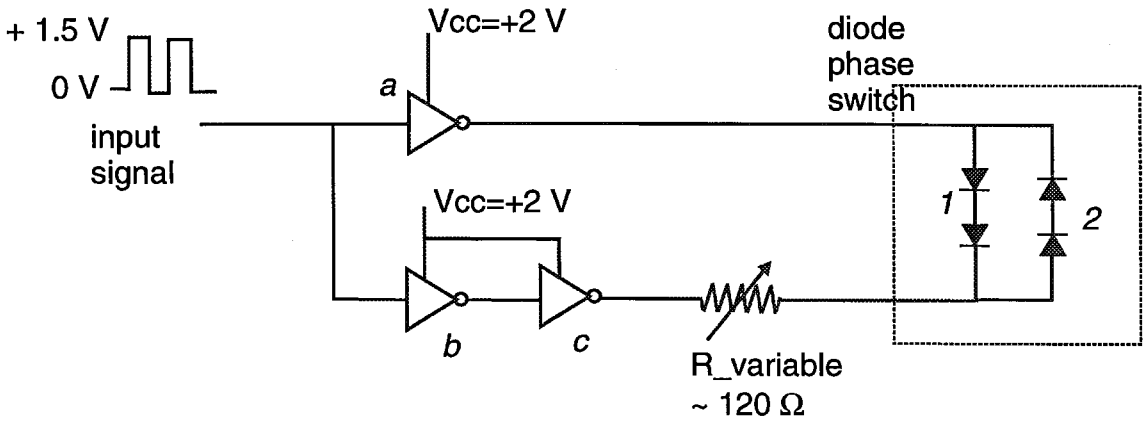

Figure 4.8 CMOS diode interface

CMOS interface principle of operation: When the input signal is low, the output from the inverter *a* is high, while the output from the inverter pair *b,c* is low, and diode pair 1 are forward biased and diode pair 2 are reverse biased. Conversely, when the input signal is high, the situation is reversed. The advantages of this arrangement compared to an op-amp based interface are that the diode currents are fixed by the inverter supply voltage Vcc, and the variable resistor which is in series with the diode pairs, and are not dependent on the input signal voltage. The circuit is insensitive to the input signal voltage as long as it exceeds ½ Vcc in its high state, at which voltage the inverters switch states. The diode pairs require a voltage drop of around 1.8 V to be adequately forward biased, the remainder of the inverter output voltage being dropped across the resistor. The current is most conveniently controlled, or reduced, by varying the resistance value, and the current may be monitored by probing the voltage drop across the resistor.

4.2.7 Final Assembly.

A phase modulated transponder was completed by joining the two aperture coupled circuits boards together. Markers at the circuit edges aided alignment. The transponder antenna array used had 8.77 mm length patch antennas on the Taconic substrate, and the completed feed and modulation circuit using MACOM diodes was also on the Taconic substrate. In addition, an amplitude modulated circuit using Alpha diodes on a Taconic substrate was completed with a Rogers antenna array also having 8.77 mm length patches. In both cases the circuits were initially joined with adhesive tape at the circuit edges to facilitate a non-permanent assembly, so that other circuit combinations could be used. For protection from physical damage aluminium housings were fabricated to contain the transponders, which are illustrated in Figure 4.9

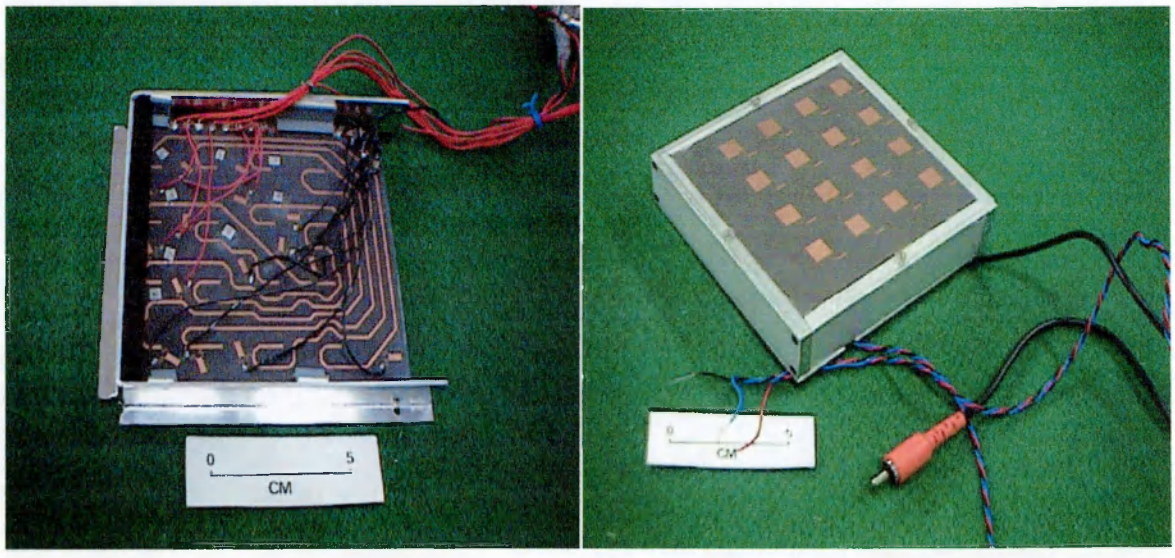

(a) Completed AM feed circuit (b) Housed PM transponder, showing antenna array

Figure 4.9 Completed transponders.

4.3 Transponder Measurements and Testing

In a similar study to that undertaken at 2.5 GHz, the transponder characteristics in terms of modulation rate and angular response were studied. The AM transponder performed adequately and some experimental results for modulation spectra and angular response etc. were recorded. However, the PM transponder tended to exhibit superior performance and the remainder of the chapter will concentrate on measurements with this device.

4.3.1 Phase Modulation Spectra.

Typical modulation spectra for the 16-element X-band phase modulated transponder are presented in Figure 4.10 where the reflected spectrum from the target was captured on a spectrum analyser co-located at the transmitter in the arrangement shown in Figure 2.9. Separate pyramidal horn antennas were used for transmit and receive functions. Since the measurements were performed in an indoor, non-anechoic environment there is always a strong return at the carrier frequency. The carrier frequency here is 9.2 GHz and the modulation signal is a 1 MHz square wave.

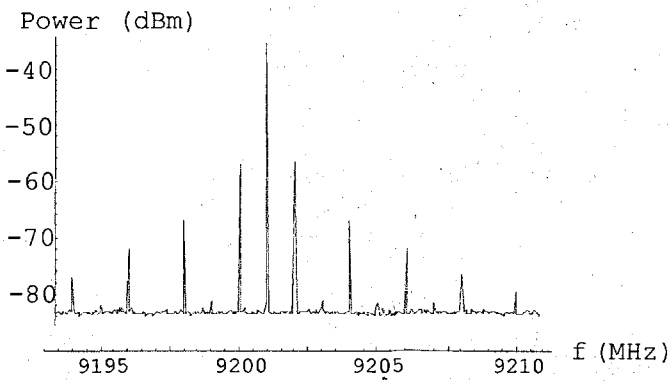

Figure 4.10 Modulation products on boresight.

Figure 4.10 shows the on-boresight response, while Figure 4.11 shows two further cases where the transponder is rotated with respect to the incident RF carrier in the E-plane of the patch antenna elements.

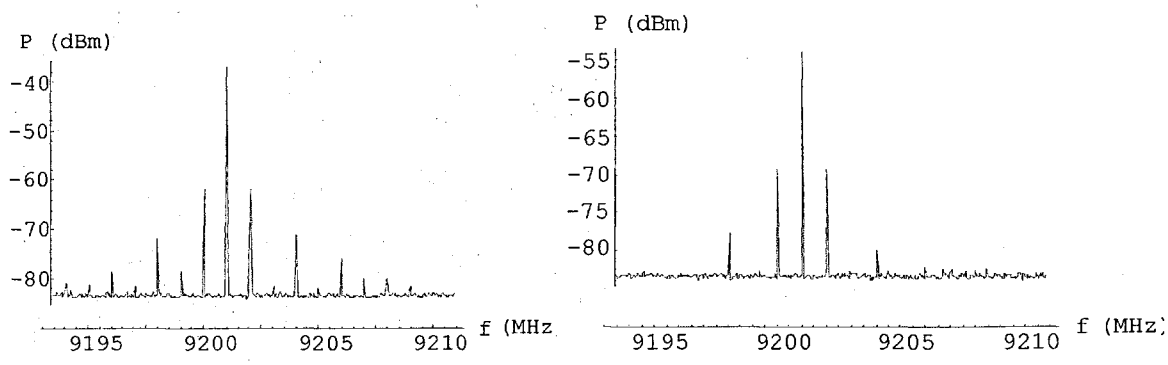

(i) 45° (ii) 80°

Figure 4.11 Modulation spectra for transponder E-plane rotation

Comparing Figure 4.10 and Figure 4.11 we see a drop-off in the power in the modulation products of about 5 dB over a 45° rotation angle and about 13 dB over an 80° rotation angle from boresight. The full E-plane angular response is shown in Figure 4.13. Further modulation spectra are presented in the appendices.

4.3.2 RCS Calibration Method.

To estimate the efficiency of the PM transponder, a conventional 16 element printed array antenna was fabricated to act as a reference. The reference antenna used the same 16 element patch antenna array on the same substrate, while a corporate feed structure was designed along classic quarter-wave impedance matching principles [10]. The layout and completed antenna are pictured in Figure 4.12

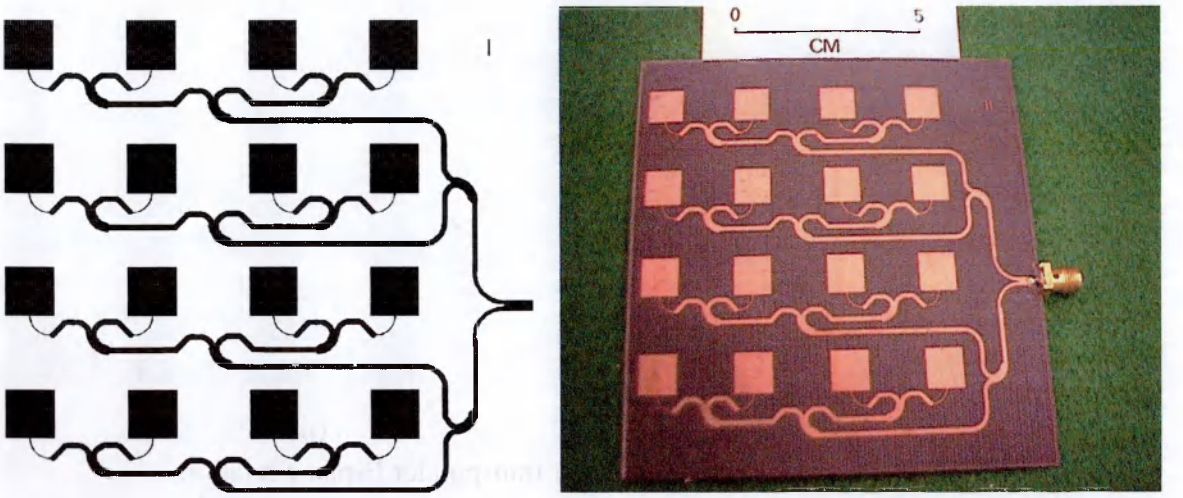

(a) circuit layout (b) photograph of antenna

Figure 4.12 X-band 16 element array antenna

The RCS of the reference antenna was phase modulated by connecting in series with a purpose built phase shifter to which the modulation signal was applied. This phase switch comprised a single diode in series with an open circuit quarter wave length of line. The phase of the reflected signal is hence switched through 180° on switching the diode between conducting and open circuit states. The power of the reflected modulation products was studied for both the transponder and the reference antenna. Figure 4.13 shows the reflected power for the E-plane angular response of both structures at an illuminating RF frequency of 9.2 GHz and a modulation frequency of 1 MHz. The angular response is expected - the retro-array shows strong modulation products over 180° of illumination angle while the reference antenna maintains an equivalent RCS over only 26°. The power in the modulation products is directly proportional to the RCS of both devices. Since the peak modulation power of the modulated retro-array was 1.5 dB lower than the antenna array, this figure represents the additional loss in the former structure, which is chiefly attributable to the additional transmission line lengths and also variations in construction such as the coupling apertures.

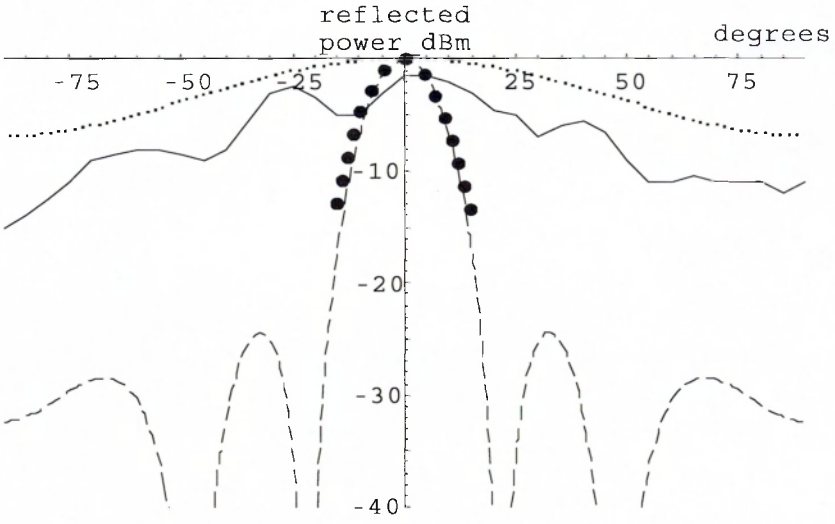

Figure 4.13 RCS calibration results – reflected power in 1st sideband.

Directivity of a two dimensional array.

The gain of the reference antenna may be estimated by calculation. From a consideration of the two dimensional array factor, the theoretical array directivity may be found by integration. The normalised two dimensional array factor [14] is:

$$F(\theta,\phi) = \frac{1}{M}\frac{\mathrm{Sin}\left(\frac{M.u_x}{2}\right)}{\mathrm{Sin}\left(\frac{u_x}{2}\right)}\frac{1}{N}\frac{\mathrm{Sin}\left(\frac{N.u_y}{2}\right)}{\mathrm{Sin}\left(\frac{u_y}{2}\right)} \tag{4.4}$$

where $u_x = k.a_x.\mathrm{Sin}\theta.\mathrm{Cos}\phi + \delta x$ (4.5)

and $u_y = k.a_y.\mathrm{Sin}\theta.\mathrm{Sin}\phi + \delta y$ (4.6)

k is the wave number $\frac{2\pi}{\lambda}$ and a_x and a_y are the element spacings along the x and y axes respectively. Similarly, δ_x and δ_y are the relative phase shifts between elements, but these terms are zero for the uniform array under consideration. M and N are the number of elements along x and y respectively. θ, ϕ are the spherical polar coordinates, referenced to

the array broadside direction which is the antenna boresight in this case. For the square 4 x 4 array, equ.(4.4) becomes

$$F(\theta,\phi)=\frac{1}{16}\frac{\mathrm{Sin}\left(\frac{4.u_x}{2}\right)}{\mathrm{Sin}\left(\frac{u_x}{2}\right)}\frac{\mathrm{Sin}\left(\frac{4.u_y}{2}\right)}{\mathrm{Sin}\left(\frac{u_y}{2}\right)} \tag{4.7}$$

and a_x and a_y are both 22 mm, which is also 0.68 λ at 9.4 GHz. Since directivity is rigorously defined as:

$$D(\theta,\phi)=\frac{4\pi P(\theta,\phi)}{P_{\mathrm{rad}}} \tag{4.8}$$

where P_{rad} is the total power radiated over all space:

$$P_{\mathrm{rad}}=\int_{\theta=0}^{\pi}\int_{\phi=0}^{2\pi}P(\theta,\phi).Sin\theta.d\theta.d\phi \tag{4.9}$$

we can find the directivity of a 16 element array of isotropes by solving equs. (4.8) and (4.9) and substituting the for power:

$$P(\theta,\phi)=M\ N\ F(\theta,\phi)^2 \tag{4.10}$$

(since (4.6) is the *normalised* array factor for electric field, the term $M\ N$ is included to yield the correct scaling for power. Thus F^2 has a maximum of 1, while P^2 has a maximum of $M\ N$ i.e. the total number of elements).

For an array which is delineated by a ground plane, we are concerned with radiation into half space only. Hence we may modify the limits of integration in equ. (4.9)

$$P\mathrm{rad\_half\_space}=4\int_{\theta=0}^{\frac{\pi}{2}}\int_{\phi=0}^{\frac{\pi}{2}}P(\theta,\phi).\mathrm{Sin}\theta.d\theta.d\phi \tag{4.11}$$

In equ.(4.11), the limits of integration define an octant, and we multiply by 4 to find the power radiated into a hemisphere. This abbreviated method is valid because we have symmetry about the θ=0 axis (i.e. antenna boresight).

A numerical solution for equ.(4.11) is 3.12, hence the scaling for directivity in equ. (4.8) is

$$\frac{4\pi}{P_{\text{rad}}} = 4.03 \tag{4.12}$$

Hence the directivity of a 4 x 4 array of half-omni antennas, i.e. radiating into a hemisphere with a spacing of 0.68 λ, is 4.03 x 16 = 64.5 which is 18.1 dB.

Directivity of array of patch antennas.

Thus far we have considered only semi-omni elements, while the directivity of the square patch antenna element will in practice modify the radiation pattern and hence directivity of the array. This pattern has been introduced in chapter 3, and is rather more directive than the theoretical semi-omni pattern. The necessary tools to calculate the patch antenna's directivity have already been introduced: equs. (3.5) and (3.6) define the electric fields in polar co-ordinates, and equs. (4.8) and (4.9) define the relationship between the power pattern and the directivity. It remains only to state that the power is given by:

$$P(\theta,\phi) = E\theta^2 + E\phi^2 \tag{4.13}$$

since the electric field components are orthogonal. We can also substitute for the patch length and width in equs. (3.5) and (3.6):

$$a = b = \frac{1}{2}\frac{\lambda_0}{\sqrt{\varepsilon_r}} \tag{4.14}$$

which is a good approximation for a resonant patch which will yield a function which is independent of a and b and dependent only on substrate height, free space wavelength and dielectric constant. While a further simplification could be applied by fixing height as a small fraction of wavelength, the actual parameters h = 0.79 mm and λ_0 = 0.032 m have been used to evaluate (4.8) for boresight (i.e. θ=0 and ϕ=0) as a function of dielectric constant ε_r. This is shown in Figure 4.14 which shows good agreement with [15].

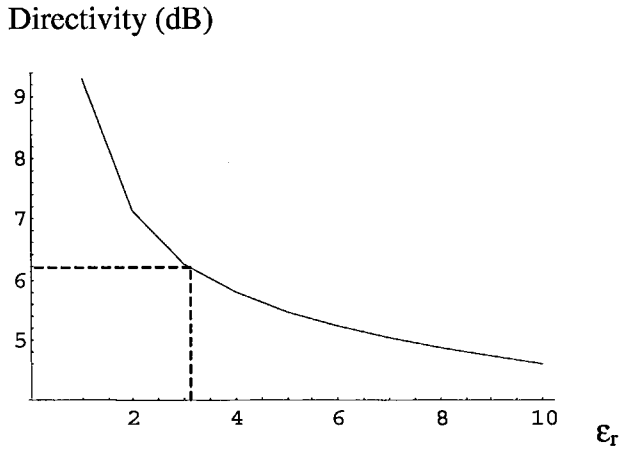

Figure 4.14 Theoretical directivity of resonant square patch antenna as a function of dielectric constant. (h = 0.79 mm, λ_0 = 0.032 m)

We can see from Figure 4.14 that for the laminate of interest (ε_r = 3.0) the theoretical directivity is 6.2 dB. It is also interesting to observe that Figure 4.14 shows that directivity is inversely proportional to dielectric constant, which is consistent with a resonant square patch having a larger length and hence larger aperture as dielectric constant diminishes. For increasing dielectric constant, we would expect the directivity to tend toward 3 dB as the aperture becomes small (recall that the ground plane implies a directivity of at least 3 dB).

We can now combine the theoretical array directivity with that of the patch element, but taking care not to add the 3 dB gain implied by the ground plane twice. Therefore, we take the full-space directivity of the array which is half that derived from (4.12) i.e. 32.25 or 15.1 dB and then add the directivity of the element (which has a ground plane) of 6.2 dB, yielding 21.3 dB.

The measured pattern for RCS for the reference array antenna shown in Figure 4.13 follows the theoretical pattern very closely, from which we can imply that the measurement corroborates the theoretical figure for directivity. This is because directivity

can be in many cases be estimated quite accurately from the half power beamwidths of a radiation pattern [16] by:

$$D\max = \frac{4\pi}{\theta_{3dB}\phi_{3dB}} \tag{4.14}$$

where θ_{3dB} and ϕ_{3dB} are the two orthogonal beamwidths. For the 16 element array antenna these beamwidths are, from symmetry, the same and equal 0.3364 rad. Thus equ.(4.14) gives a figure of 20.5 dB for the directivity using this approximation.

Gain of reference antenna.

Means of deriving a figure for the reference antenna directivity have been explored in some detail, so that an estimate of gain may follow. A direct measurement of gain can often be difficult to achieve with confidence. Measurements using an anechoic chamber (which was not available) and standard antennas derive the gain of an antenna under test directly, but are still subject to calibration procedures. Thus an alternative approach has been developed:

It remains to estimate the losses L in the reference antenna so that gain can be derived since:

$$G(dB) = D(dB) - L(dB) \tag{4.15}$$

Thus D will put an upper bound on G. Measured gain for a single patch antenna is typically the order of 4 dB and commercial specifications typically quote 4 to 7 dB depending on substrate (e.g. "air dielectric" is often used, which implies a higher directivity and reduced loss). We may thus estimate an inherent loss in each patch of 2.2 dB. Additional microstrip feed loss amounts to about 1.1 dB (about 150 mm at 0.008 dB/mm - see Appendices and chapter 5 for discussion of microstrip loss) while a residual uncertainty of about 1 dB would be implied from the combined effects of transmission line discontinuities and

connectors. (This error estimate is manifested as ± 2 dB in the estimate for RCS which is proportional to the square of gain.) The mean of the two above estimates for array directivity are 20.9 dB, from which at least 3.3 dB should be subtracted for loss effects, yielding an estimate for gain of 17.6 dB for the reference antenna. Since the retro-reflector's peak RCS is 1.5 dB below the reference antenna RCS, the former is calculated from equs (2.2) and (2.3) to be 0.19 m^2 or -7.2 ± 2 dB m^2 . (The modulator loss has not been included here, being approximately common to both structures). The figures are summarised in Table 4.7 along with some additional remarks to clarify the method.

	D (dBi) theory	*lossless* RCS (m^2)	Loss (dB)	G (dBi)	RCS (m^2)
retro-array	20.9	1.23	4.1 ***	16.8 **	0.19 *
antenna	20.9	1.23	3.3	17.6	0.27

Table 4.7 Summary of antenna and retro-array aperture gain, directivity, loss and RCS.

* The retro-array RCS is derived from the observation that the modulation products are 1.5 dB below the reference antenna in the measurement of Figure 4.13.

** The retro-array gain cannot be measured directly (it is not an antenna) but can be derived from RCS

*** The retro-array aperture loss is calculated as the difference between the theoretical directivity and the gain derived from the RCS. It differs from the antenna loss by *half* the dB value of the observed difference in RCS (i.e. ½ x 1.5 dB) since RCS ∝ G^2.

4.3.3 Modulation Rates.

An encouraging characteristic of the completed X-band PM transponder was the increase in modulation rates - rates up to 10 MHz were demonstrated with a 3 dB efficiency roll-off compared to 1 MHz. Beyond 10 MHz, the modulation efficiency, measured as the power in the first upper sideband of the BPSK modulation spectrum, dropped off more sharply. The 10 MHz rate represented a significant improvement compared to the earlier work at a 2.5 GHz carrier frequency. The proposed telemetry applications now seemed much more fully demonstrated in view of the data rates which could be achieved, subject to link budget limits.

4.4 Communications Link Demonstrator at 5 M bits /s.

To further explore the potential offered by the available transponder modulation rates, a demonstration of a communications link was sought. This might be representative of a telemetry application or a local area network communications application. The objective was to take a convenient bitstream, apply it to the modulation circuitry of an X-band transponder, and have the bitstream recovered at another location by means of a transceiver with a continuous wave (CW) source illuminating the transponder. A very convenient source was found to be the bitstream output of a domestic audio CD player. This bitstream may be converted to audio by use of a domestic audio DAC, which are often marketed as an "upgrade" to replace the DAC internal to the CD player. The system which was configured is illustrated in Figure 4.15

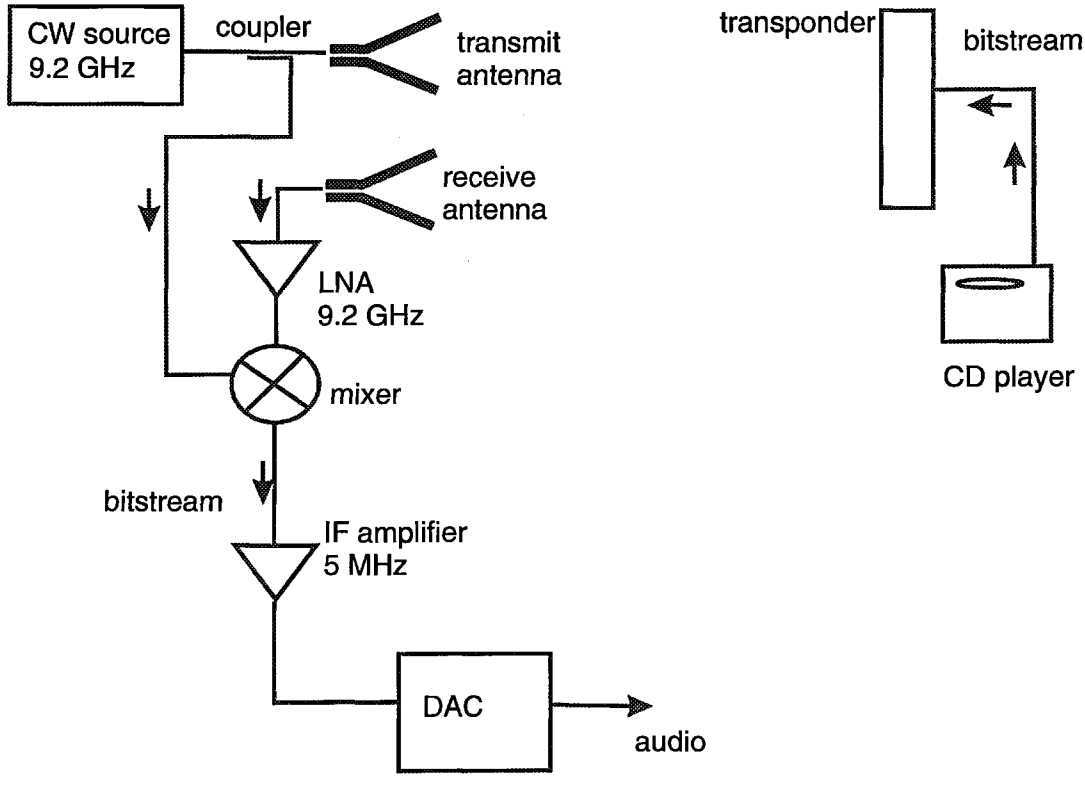

Figure 4.15. Communications link demonstrator using compact disc bitstream.

The bitstream output of the CD player is shown in Figure 4.16. The bitstream is pulse width modulated - the 200 ns minimum pulse width corresponding to a 5 Mbit /s data rate.

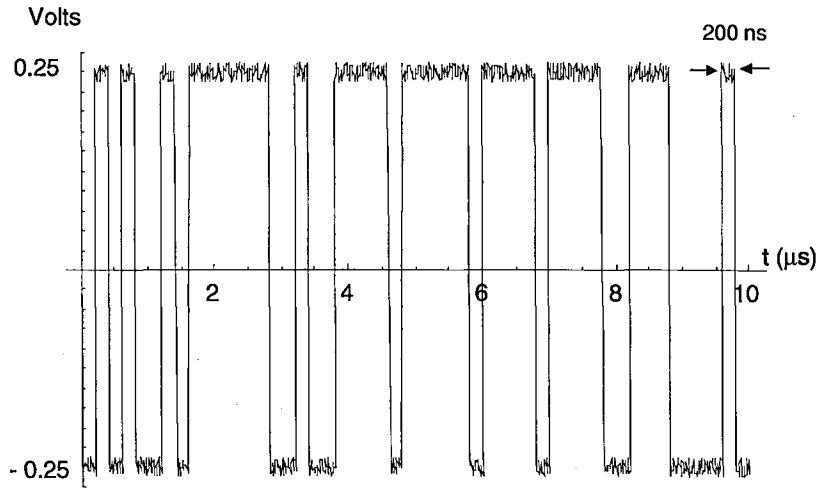

Figure 4.16. CD bitstream

The system, as illustrated in Figure 4.15 is clearly not optimum. An RF bandpass filter is absent, which will tend to contribute to noise and interference, and as the relative phase between the LO and RF signals at the mixer are not controlled they are subject to the path length to the transponder. The received IF signal thus varies between a maximum and a zero as the transponder distance is varied by a quarter free space wavelength or about 8 mm. This characteristic would be unsuitable for most practical applications where some relative movement between the interrogator and transponder is expected - in this case the single mixer architecture would be replaced by a mixer each in I and Q channel in the manner of the coherent transponding system of [13].

The IF amplifier was built using a NE592 video op. amp. (gain-bandwidth product 120 MHz) so as to provide the considerable gain required to yield the 0.5 V peak-to-peak amplitude required at the DAC input.

Available transmit power was approximately 15 dBm. The link functioned satisfactorily over the 4 m. distance available in the laboratory, and also with transponder orientations up to about 70 degrees. Although a measurement of bit error rate was not performed, the audio quality was (at least subjectively) indistinguishable from a hard-wired link. This is to be expected of a digital link with the powerful forward error correction used in CD, and when the link did fail through path length errors or transponder obscuration, it tended to fail suddenly i.e. without graceful degradation.

4.4 Conclusions.

The scaling in frequency from 2.5 GHz to around 9.4 GHz involved a re-appraisal of the microstrip techniques investigated in some detail in chapter 3. For the convenience of fabricating many printed circuits concurrently from a single laminate sheet, the same substrate was used for both antenna and feed line circuits. While the chosen laminate thicknesses (either 0.76 or 0.79 mm) are favourable for printed antenna applications at 9.4 GHz, the congestion of the feed line circuit necessitated a low feed line track width. The effect on impedance and in particular loss was studied in some detail to derive a compromise between inter-line spacing and loss. The unequal-line length approach, previously pioneered at 2.5 GHz, was again adopted with success.

An approximate method for calibrating the radar cross section of the transponder was developed, and indicated that the losses in the device were not excessively severe. The angular response was similar to the theoretical case, and exhibited the characteristic wide-angle response of the retro-reflector, particularly on exploiting the antenna E-plane radiation pattern. The calibration method used a reference antenna array for comparison, whose aperture was the same as that of the retro-directive array, and whose RCS was also phase modulated. The reference antenna gain was not measured directly, since this would require a calibrated anechoic facility, but its directivity was derived from theory and its measured beamwidths corroborated the theoretical result. Estimates for loss in the reference antenna then lead to an estimate for gain in both the antenna and reflector structures. From these methods, RCS has been derived with an uncertainty of around 2 dB. The error is not very significant in the context of the very large dynamic ranges associated with communications links.

One of the most encouraging results from the work was the demonstration of modulation rates beyond 10 MHz. The rates are strongly dependent on the switching speed of the diodes. There was little choice of available switching diodes and it is very likely that better performance could be obtained in this area. Switch fabrication was by hand and involved the use of baked conductive silver epoxy. While phase modulation is preferred, a crude amplitude modulation is more easy to obtain, involving use of a single diode in series with the transmission line. The modulation index in the latter case cannot be optimum, but the number of semi-conductor components and hence power consumption is reduced by a factor of 4.

The efficiency and frequency response of the diode driver interface has not been modelled in detail and the switching circuitry is unlikely to be optimum in this case. It may be improved upon by further work and attention to detail in this area. However, the 10 MHz rate is more than sufficient for a wide range of applications. The establishment of a high data rate link by transmission of only a very narrowband carrier is a fascinating property of the technique in light of the legislative environment and cost of bandwidth, although the legislative implications remain unexplored.

A communications link using the bitstream output of a domestic CD player was constructed. This acted as an interesting demonstration of a 5 M bit/s link over a 4 m. distance using 15 dBm of transmit power. Since any number of interrogators may simultaneously address the transponder, if placed within its range of spatial response, such a link could serve as a point-to-multi-point link for local broadcast type applications.

References.

[1] Radiocommunication Study Group, Document 8/78-E, March 2001, International Telecommunication Union (ITU)

[2] http://www.si-tex.com/koden/MarineRadar

[3] http://www.radio.gov.uk/

[4] http://www.rogers-corp.com/mwu/translations/prod.htm

[5] http://www.4taconic.com/dielctrc/index.html

[6] "Foundations for Microstrip Circuit Design", T. Edwards, *Wiley* ,1991

[7] "Microstrip antenna technology" K. R. Carver and J. W. Mink, *IEEE Trans. Antennas and Propagation.* Vol. AP-29 no.1 Jan 1981. pp.2 - 22.

[8] "Measured mutual coupling between microstrip antennas", R. P. Jedlicka, M. T. Poe, K.R.Carver, *IEEE Trans. Antennas and Propagation.* Vol. AP-29 no.1 Jan 1981. pp.147-149

[9] "Mutual coupling between microstrip antennas", E. Penard, J. P. Daniel, Electronics Letters, vol. 18, 1982, pp. 605-607.

[10] "Antenna Design Using Personal Computers" D. Pozar, *Artech House* 1985

[11] "Antenna Theory, Analysis and Design", C. A. Balanis, *Wiley*, 1997, pp. 309 - 311.

[12] "The Handbook of Antenna Design", Rudge, Milne, Olver, Knight. IEE Electromagnetics Waves Series 15 *Peter Peregrinus Ltd.* 1982. p. 533

[13] "Microwave Homodyne Systems", R. J. King, 1978, *Peter Peregrinus Ltd. on behalf of IEE.* pp 328 - 329.

[14] "Antenna theory analysis and design", C.A.Balanis, *Wiley*, 1997, pp. 309 - 311.

[15] "The Handbook of Antenna Design", Rudge, Milne, Olver, Knight. IEE Electromagnetics Waves Series 15 *Peter Peregrinus Ltd.* 1982. p. 533

[16] Ref [15] p.46

Chapter 5

Modelling the Characteristics of Large Retro-Arrays

In this chapter, general models for the characteristics of larger retro-arrays will be developed. By "large", an increase in size considerably beyond the 16 element prototypes discussed in the preceding chapters is inferred. As more elements are added to the array, the losses in the transmission lines become more significant and, for the unequal-line-length array, an increasing bandwidth limitation is expected. These effects may be estimated by developing general models for transmission line lengths. The implications of choosing different transmission line media will be examined.

5.1 Losses in Antennas and in Retro-arrays.

The properties of some prototype modulated retro-arrays operating at 2.5 GHz and at approximately 9 GHz have been considered. In the latter case the reflectivity of the 16 element, printed (microstrip) retro-reflector compared favourably with that of a conventional uniform antenna array, and it was possible to derive a figure for the efficiency of each. When considering the efficiency of increasingly large arrays, the losses in the interconnecting lines will clearly have an increasingly detrimental effect, which will become much larger than the other (fixed) losses associated with the modulation circuits and antennas. For example, a reasonably efficient modulator might only give rise to 1 dB or so of loss. The loss in the radiating elements should be similarly small, although it has been estimated that about 2 dB is realistic for printed antennas. Where aperture coupled microstrip is used, the modelling discussed in chapter 3 showed that a loss of only 0.15 dB could be expected at 2.5 GHz although alignment errors might lead to a worse figure. The summation of these loss estimates is therefore around 5.3 dB, although the exact value will clearly depend on the type of array geometry and materials chosen. The value represents a

constant term which may be compared with the transmission line loss models which will now be presented.

In this section, models will be developed which present estimates of the severity of the transmission line losses. This is of importance for many applications where a larger array may be required, or where a trade-off between the other parameters of the link budget such as transmit power is to be investigated. Hence an estimate for the required "over design" to accommodate the effects of loss is important when addressing a given application.

Care must be taken to account for the transmission line loss in the correct physical manner. Firstly, consider an antenna of finite efficiency, which may be modelled as a lossless antenna in series with a lossy length of transmission line, as shown in Figure 5.1 (a). To operate the antenna as a reflector, a short (or open) circuit is connected to the other end of the line. The RCS for the system is given by:

$$\sigma = \frac{\lambda^2}{4\pi}(G\eta)^2 \tag{5.1}$$

which is as equation 2.1, with the efficiency η of the antenna included. Here, η may be considered as the efficiency of the transmission line in series with the lossless antenna of gain G. In extending this approach to a retro-reflector, care must be taken over the correct treatment of η. This is because in the case of the shorted antenna, both the incident and reflected wave suffer attenuation (in the transmission line equivalent circuit), whereas for the retro-reflector, the transmission line is routed to another antenna so the incident energy is re-radiated after a single trip through the line. The equivalent circuits are shown in Figure 5.1.

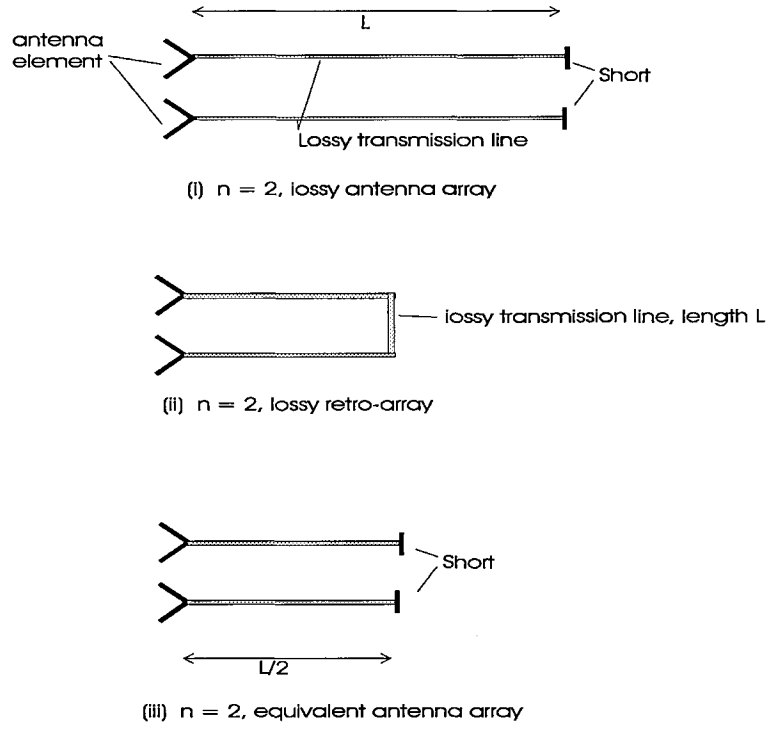

Figure 5.1 Losses in antennas and in retro-arrays.

In Figure 5.1 case (a) an antenna array of 2 elements is shown in series with a lossy transmission line and short circuit. In case (b) the retro-array has the same antenna gain and a single length L of transmission line interconnecting the antenna elements. Thus the reflective loss exhibited is half that of case (a). The true equivalent to the retro-array is the antenna array which has half the line length, as shown in case (c). Thus the RCS of the retro array is given by:

$$\sigma_{retro} = \frac{\lambda^2}{4\pi} G^2 \eta \tag{5.2}$$

where the efficiency is determined by the loss in the interconnecting lines, and occurs once. Thus the gain and efficiency are no longer coupled together in the same composite term, as was the case for the reflective antenna. On re-writing RCS in terms of antenna element effective area we have:

$$\sigma_{retro} = \frac{4\pi}{\lambda^2} \eta (\sum a_{el})^2 \tag{5.3}$$

where a_{el} = effective area of lossless antenna element.

If $\eta = 1$ then we may use $\Sigma a_{el} = N a_{el}$, where N is the total number of elements.

However, in general, the efficiency for each inter-connected antenna pair must be calculated independently, so

$$\sigma retro = \frac{4\pi}{\lambda^2}\left(\sum_i^{N/2} 2a_{el}\sqrt{\eta i}\right)^2 \qquad (5.4)$$

where antenna pairs are considered, and η_i is the efficiency of the interconnecting line of the i^{th} pair. For this reason, the summation is to $\frac{N}{2}$ and a term 2 appears inside the parenthesis to account for the antenna pair2 . The square root of η_i is used as the term has been taken inside the summation, which is squared. In effect, the RCS is here derived from the summation of the antenna element effective areas which are each *weighted* by their corresponding transmission line loss.

5.1.1 Models for Efficiency of n x n Element Square Retro-arrays.

In order to estimate the efficiency, generalised models for the transmission line lengths are presented. A matrix of n x n elements with an inter-element spacing of a - as used in the prototypes discussed in chapters 2, 3 and 4 - will be considered. Two general cases will be explored for different construction methods: transmission lines which are fabricated on a single planar circuit and therefore not allowed to cross, and co-axial lines which occupy the three spatial dimensions and are therefore allowed to cross.

5.1.2 Non-crossing Geometry.

In Figure 5.2 the transmission line routing approximates that which minimises the line lengths. In practice, radii and diagonals could be used in place of 90° corners to minimise the additional line lengths in these regions. Also, electromagnetic coupling effects in microstrip and the requirement to adjust lengths for phase conjugation all have a large influence on the practical routing that is chosen. The essential feature of the diagram is the

relation of the lines to the ports of the antenna matrix, from which a good approximation of the minimum lengths may be derived.

Figure 5.2 shows the innermost two concentric antenna groups within a square array of n x n antenna elements spaced by a. In this case the transmission lines are a planar type such a microstrip, and not allowed to cross. This type of construction is very convenient for integrating with both the modulation circuitry and printed antennas, which has been discussed in chapters 3 and 4.

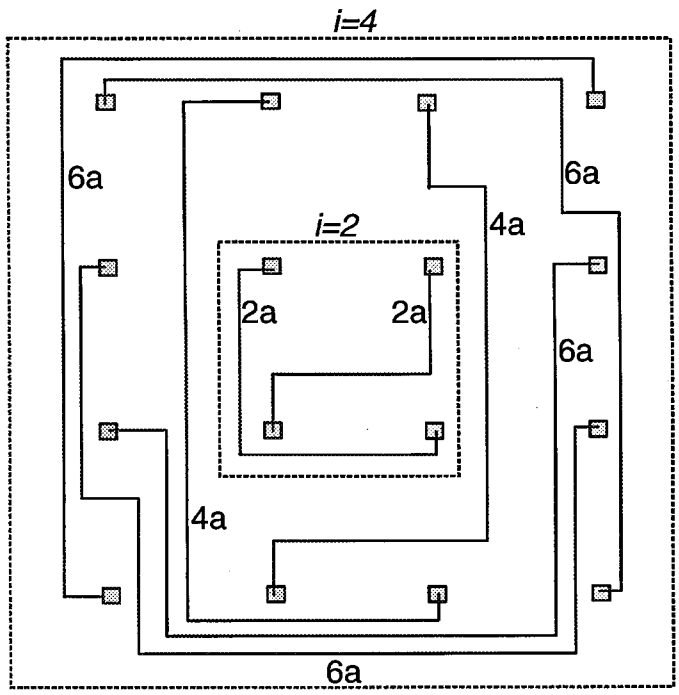

Figure 5.2. Non-crossing lines: model for minimum line lengths.

The interconnecting lines as drawn do not represent a practical circuit, but illustrate a model for deriving *minimum* line lengths. Thus, the inner group i=2 has 2 lines of length $2a$, and the next group i=4 has 4 lines of length $6a$ and 2 lines of length $4a$. Using i as a counter for each concentric group, there are i lines of length $(2i - 2)\ a$ and $(i - 2)$ lines of length $(2i - 4)\ a$ where $i = 2, 4, 6...n$. Modifying (5.4) we have:

$$\sigma = \frac{4\pi}{\lambda^2}\left(\sum_j^{N/2} 2a_{el}\sqrt{\eta j}\right)^2 \tag{5.5}$$

where each antenna *pair* j is considered and hence the summation is to half the total number of elements. We may further extend this argument from an antenna pair to an antenna concentric group i, where the effective area contributed by the group is found by weighting with the appropriate transmission line loss, which is linearly related to the line length. Hence:

$$Ai = 2.a_{el}.i.\sqrt{10^{-\frac{(2i-2)a.lpm}{10}}} + 2.a_{el}.(i-2).\sqrt{10^{-\frac{(2i-4)a.lpm}{10}}} \tag{5.6}$$

is the effective area contributed by the i'th group after losses have been considered, where *lpm* is the loss factor in the transmission line, in dB/m. The RCS for the array may now be calculated by summing over all concentric groups i , hence:

$$\sigma = \frac{4\pi}{\lambda^2}\left(\sum_{\substack{i=2 \\ step2}}^{i=n} Ai\right)^2 \tag{5.7}$$

which may be evaluated by selecting a value for *lpm*, and the array size n. The former is a function of the frequency as well as the transmission line type and material loss, and may often be accurately derived or measured for a range of media such as microstrip or waveguide.

To illustrate the effect of increasing loss, (5.7) has been evaluated as a function of array length L, where $n = L/a$ and $a = 0.5\ \lambda$ at a 2 GHz carrier frequency, as shown in Figure 5.3.

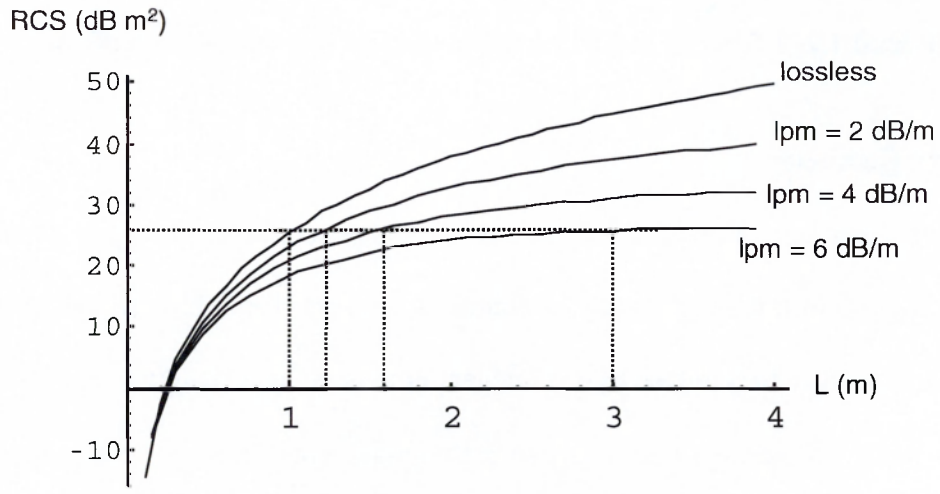

Figure 5.3. Maximum RCS at 2 GHz for a = 0.5 λ, for non-crossing line routing.

[*Aside*: We can test the summation terms of (5.6) and (5.7) by considering the case where the lines are lossless, i.e. *lpm* = 0 dB. In this case the effective areas are summed without any weighting for transmission line loss:

$$Ai = 2.a_{el}.i + 2.a_{el}.(i-2) = 2.a_{el}.(2i-2)$$

For convenience, consider a 6 x 6 element array , which has 3 concentric groups:

the $i = 2$ group has area 4 a_{el}

the $i = 4$ group has area 12 a_{el}

the $i = 6$ group has area 20 a_{el}

and the summation for the 3 groups gives a total effective area of 36 a_{el} which is consistent with the total number of elements $n^2 = 36$]

In Figure 5.3, the effect of increasing transmission line loss is apparent as a slowing of the rate of RCS increase with array length. The results are for the minimum line lengths and hence maximum RCS, and so represent an upper bound on RCS for planar, non-crossing transmission lines. These might typically be microstrip, where loss at 2 GHz might be as low as 2 dB/m. However, where narrower track widths are used to alleviate circuit congestion, losses tend to increase rapidly. The results are useful in showing by how much the dimensions of a lossy retro-directive transponder would need to be increased, compared to the lossless case, to achieve a given link budget. For example, the RCS

highlighted in Figure 5.3 is given by a lossless array of length 1 m, which needs to be increased to at least 1.2, 1.6 or 3.0 m for line losses respectively of 2, 4, or 6 dB/m.

5.1.3 Crossing Geometry.

If transmission lines are allowed to cross, e.g. by using co-axial lines, an alternative derivation of minimum line lengths may be found. It is stressed that the line lengths must still be adjusted so that they differ by an integer number of wavelengths, so that phase conjugation occurs at the design frequency, so these models for minimum lengths represent an optimistic case.

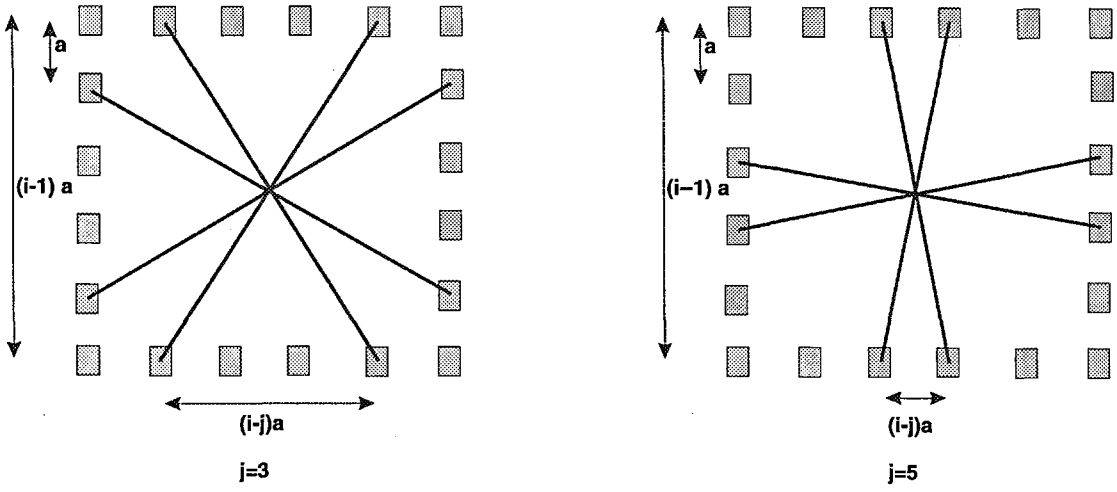

(a) (b)

Figure 5.4 Transmission line lengths: development of general model.

In a similar approach to the above, where each concentric antenna group i is considered, there are 2 lines between the diagonals of length

$$l_{diag} = a\sqrt{2(i-1)^2} \tag{5.8}$$

and from the symmetry of the square matrix, there are groups i,j of 4 lines of length

$$lij = a\sqrt{(i-1)^2 + (i-j)^2} \tag{5.9}$$

where j takes values from 3 to i-1 in steps of 2. Hence the RCS for the co-ax fed array may be expressed as

$$\sigma = \frac{4\pi}{\lambda^2}\left(\sum_{\substack{i=2 \\ step2}}^{n}\left[4.a_{el}.\left(10^{a\sqrt{2(i-1)^2}.\frac{lpm}{10}}\right)^{\frac{1}{2}} + \sum_{\substack{j=3 \\ step2}}^{i-1} 8.a_{el}.\left(10^{a\sqrt{(i-1)^2+(i-j)^2}.\frac{lpm}{10}}\right)^{\frac{1}{2}}\right]\right)^2$$

(5.10)

(5.10) has been evaluated in terms of array length, as shown in Figure 5.5, and compared with the results for the non-crossing geometry. (It is interesting to observe that, in contrast to 5.7, a nested summation is involved in the computation in 5.10 due to the different form of the solutions for line length between the non-crossing and crossing cases for line routing.)

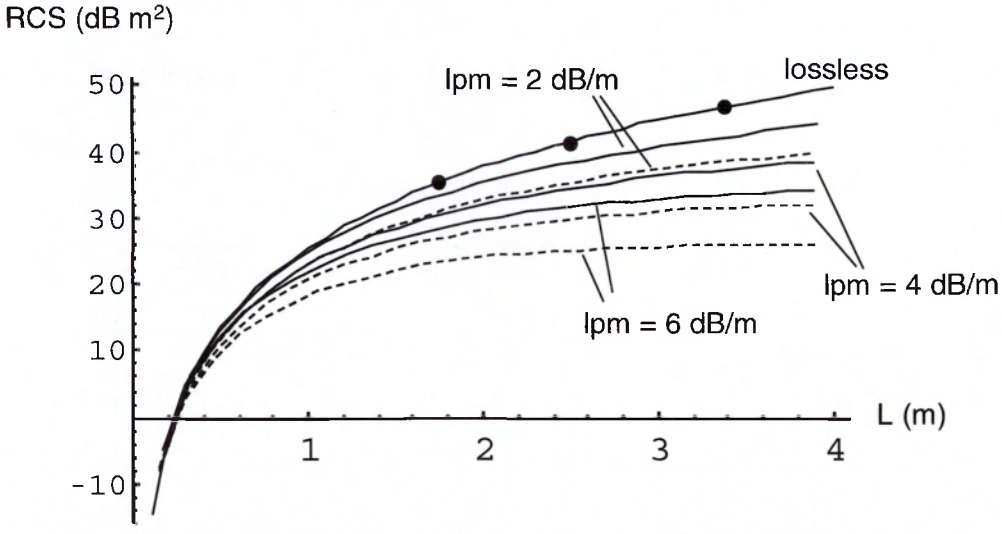

--- non-crossing geometry. — crossing geometry. —●— lossless case

Figure 5.5. Comparison of array RCS for crossing and non-crossing geometries at 2 GHz

In Figure 5.5 the reduced path lengths in the non-crossing geometry lead to a quantifiable increase in array RCS for a given loss factor. In practice, a planar medium such as microstrip tends to exhibit more loss than co-axial transmission line, which would lead to a further advantage in terms of efficiency in the latter case. There are clearly many variable parameters, not least including the RF frequency and the chosen means of construction, but the above results are intended as a first estimate of the severity of transmission line loss where passive transponders of high RCS are sought.

5.1.4 Losses in Practical Transmission Line Media.

In this following sections the transmission line losses applicable at the x-band frequencies used by the transponder prototypes will be applied to the general models for array loss which have been described above. Here, the rationale is to present estimates of efficiency which could be expected on designing and fabricating bigger versions of these prototypes.

5.1.5 Choice of Substrate for Planar Retro-arrays

In the chapter 4 and Appendix 1, a detailed study of loss in microstrip is presented. This comprised a combined consideration of theoretical models from the literature, some measured data and various simulation techniques. These values have been used to evaluate equ.(5.7) for three substrate types (one of which is mythical), where the loss term has been converted to dB per mm. as shown in Table 5.1 below for a 1 mm track width and 0.79 mm substrate height.

Substrate	Loss (dB / mm) at 9.5 GHz
ideal (copper conductor loss only)	0.004
Rogers Duroid	0.005
Taconic TLC	0.008

Table 5.1 Summary of loss terms used to evaluate loss in array from equ.(5.7)

The 22 mm antenna element spacing has been used to evaluate RCS from equ. (5.7) , which is shown in Figure 5.6 for the three substrate types. Here, the RCS is plotted as a linear function of the number of elements along the side of the array.

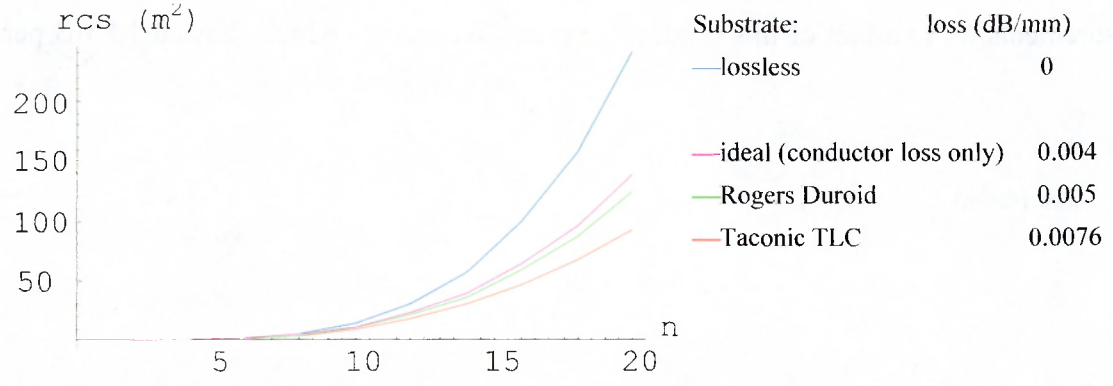

Figure 5.6. Maximum RCS using model for minimum transmission line length, for *n* x *n* array of patch antennas at 9.4 GHz, spaced at 22 mm.

Discussion of model for the n x n array using planar transmission lines.

In the estimate for maximum RCS as shown in Figure 5.6 above, it should be emphasised that the results are optimistic, since the line lengths used in a practical circuit would be expected to be greater than those suggested by the minimum line length model described in section 2 above. Also, semiconductor losses in the modulation circuit and reflective microstrip discontinuities will all add to the loss and further degrade the RCS. For larger square arrays the difficulties of routing lines between elements in the matrix, and the further geometric limitation imposed by coupling apertures, might necessitate a spacing *a* greater than the 22 mm used in the 16 element X-band prototypes, which would lead to additional line lengths and corresponding loss. These effects all suggest that all-planar circuits for retro-arrays are better suited to smaller arrays. Thus applications which require links over short distances and very low mass and low power transponders, such as may be worn by a person or used in a local indoor network, are best addressed using all-planar circuits.

5.1.6 Choice of Coaxial Line.

The loss term *lpm* will now be considered for coaxial transmission line. Figure 5.7 shows typical loss curves for various co-ax types, as a function of frequency. For RG-405 the loss at 9 GHz is about 2.13 dB per m, which compares favourably with the author's

measurements of a variant of this product - Suhner *Sucoform* - which showed 1.8 dB per m.

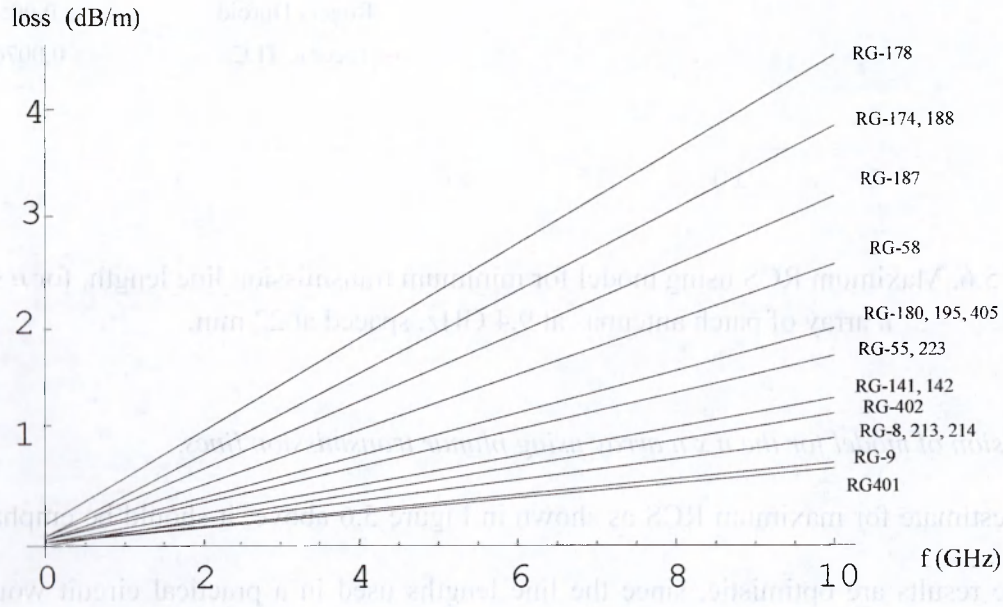

Figure 5.7 Loss in various co-axial lines (After [1])

We may augment this data with theoretical models for loss in co-axial lines. From [1] an expression for the attenuation constant for co-axial line is:

$$\alpha = \frac{1}{2}\left[\frac{R_s}{\eta \ln b/a}\left(\frac{1}{a}+\frac{1}{b}\right)+\omega\eta\varepsilon''\right] \tag{5.11}$$

where the surface resistance of the conductor, R_s, is

$$R_s = \sqrt{\frac{\omega\mu}{2\sigma}} \tag{5.12}$$

ε" is the imaginary part of the dielectric's permittivity. (This term gives rise to loss in the dielectric medium. We recall that this is often specified by the loss tangent: $\tan\delta = \frac{\varepsilon''}{\varepsilon'}$

where ε' is the real part of the permittivity.)

Also, the intrinsic impedance in the dielectric is:

$$\eta = \sqrt{\frac{\mu}{\varepsilon'}} \tag{5.13}$$

and *a* and *b* are the inner and outer conductor diameters as shown in Figure 5.8

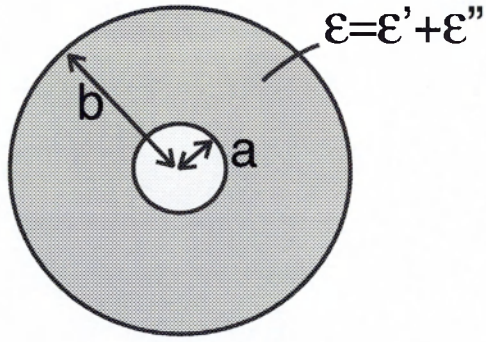

Figure 5.8. Co-ax transmission line cross-section

Values for conductivity σ tend to not vary greatly between commonly used metals, as shown in table 5.2

Material	Conductivity (S/m) at 20° C
Aluminium	3.186×10^7
Chromium	3.846×10^7
Copper	5.813×10^7
Gold	4.098×10^7
Silver	6.173×10^7

Table 5.2. Conductivities for commonly used metals

A further term which accounts for conductor surface roughness should be added, since this tends to increase loss quite significantly. After [2], a quasi-empirical formula for attenuation constant for a co-axial line with rough conducting surfaces is:

$$\alpha' = \alpha\left[1+\frac{2}{\pi}\arctan\left(1.4\left(\frac{\Delta}{\delta s}\right)^2\right)\right] \tag{5.14}$$

where Δ is the r.m.s. surface roughness and δ_s is the skin depth in the conductor:

$$\delta s = \sqrt{\frac{2}{\omega\mu\sigma}} \tag{5.15}$$

We may now evaluate (5.14) for a typical 50 Ω co-axial line with copper conductor. For a PTFE dielectric, we use $\varepsilon_r = 2.1$ and $\tan\delta = 0.0004$. Since the line impedance is

$$Z_0 = \frac{\eta}{2\pi} \ln \frac{b}{a} \qquad (5.16)$$

we may choose a = 0.5 mm and b = 1.68 mm to yield a 50 Ω line (the dimensions are those for RG-405 standard coax.) Figure 5.8 shows the attenuation constant as a function of frequency, here expressed in dB/m *, for various values of surface roughness Δ.

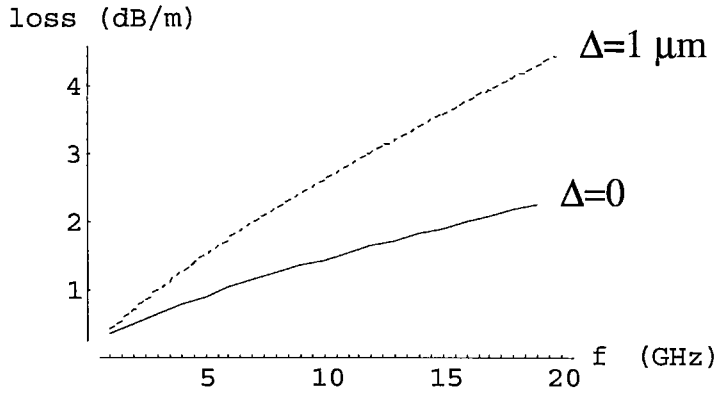

Figure 5.8. Theoretical loss in co-axial line, as a function of frequency

5.2 Bandwidth of Unequal-line-length Retro-arrays.

For the classic Van Atta array, the interconnecting transmission lines have equal length. Phase conjugation occurs at all frequencies, and there is thus no bandwidth limitation implied by the lines themselves (the bandwidth of the radiating elements is the practical limitation). However, in this work we are interested in exploring the properties of the unequal-line-length retro-array. In this case the line lengths differ by an integer number of wavelengths *at the design or centre frequency*. At other frequencies, a phase shift will exist between adjacent radiating elements which is non-zero (strictly, not an integer multiple of 2 π) as shown in Figure 5.9.

* The natural units for attenuation constant - the distance over which a field strength decays to 1/e of its original value - is Neper/m. To convert to dB/m (a power ratio), we multiply by 8.686.

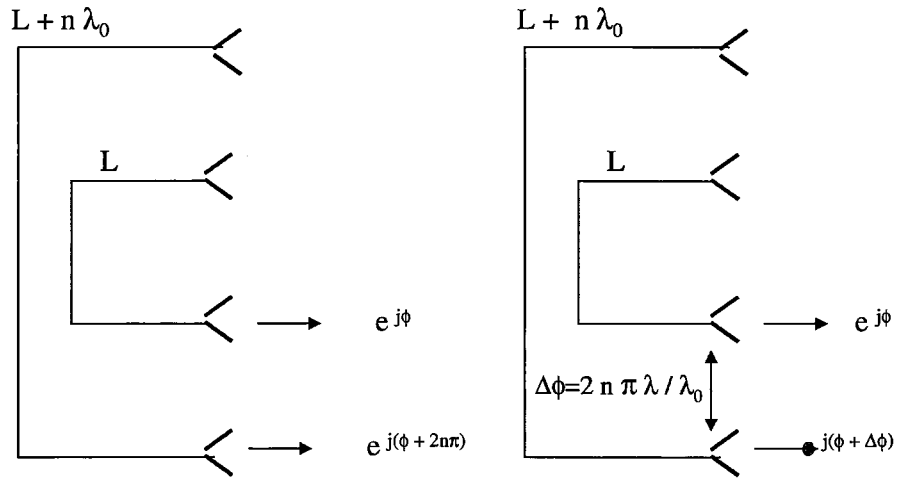

(a) centre frequency: phase conjugation (b) off-centre frequency: interference

Figure 5.9 Phase effects in unequal-line-length retro-array.

Thus, if the array is operated at some other frequency to the centre frequency, interference effects will lead to a modified RCS, which is most likely to be reduced although it is not necessarily reduced. The effect may be quantified by adapting the above models for line length and examining the phase shift produced by each line as a function of wavelength. The field at the aperture may be considered as the summation of the field phase at each element *i*:

$$E = \sum_{i=1}^{N} \exp(J\phi_i) \tag{5.17}$$

For the array with crossing lines, we may re-express the summation in (5.10) in terms of element phase, rather than weighting each element for loss (using upper case *J* for imaginary j, and lower case *j* for the iterator in the summation):

$$\sigma = \frac{4\pi\ a_{el}}{\lambda^2}\left(\sum_{\substack{i=2 \\ step2}}^{n} \left[4.\exp(J\ \phi_i) + \sum_{\substack{j=3 \\ step2}}^{i-1} 8.\exp(J\ \phi_{ij}) \right] \right)^2 \tag{5.18}$$

where ϕ_i is the phase of the field contributed by the elements at the corners of the antenna group *i*. The term is analogous to equ.(5.8) which derives the minimum line length for this group. Similarly, ϕ_{ij} is the phase of the field contributed by each antenna group *ij* and is analogous to equ.(5.9) for length.

We need to modify the lengths in equ.(5.8) and (5.9) to ensure that the only allowed lengths are those which differ from each other by an integer multiple of the transmission line wavelength (the adjustment is trivial when calculating loss, but is important for ensuring correct phase). This is most conveniently achieved by forcing all line lengths to be an integer number of transmission line wavelengths. Thus the modified lengths are the minimum lengths rounded up to the nearest integer wavelength:

$$Ld' = Roundup\left[\frac{Ldiag}{\lambda TL0}\right] \lambda TL0 \tag{5.19}$$

$$Lij' = Roundup\left[\frac{Lij}{\lambda TL0}\right] \lambda TL0 \tag{5.20}$$

Where the function *Roundup* yields an integer. Now:

$$\phi_i = 2\pi \frac{Ld'}{\lambda TL} \tag{5.21}$$

and

$$\phi_{ij} = 2\pi \frac{Lij'}{\lambda TL} \tag{5.22}$$

Also,

$$\lambda TL0 = \frac{\lambda 0}{\sqrt{\varepsilon reff}} \tag{5.23}$$

where λ_0 is the design wavelength, and similarly

$$\lambda TL = \frac{\lambda}{\sqrt{\varepsilon reff}} \tag{5.24}$$

Equ.(5.18) can now be evaluated as a function of *n*, for a fixed spacing *a* and a chosen value of the effective dielectric constant ε_{reff}. Since the solution for crossing lines is being here considered, the implied transmission line type is co-axial so it is appropriate to use $\varepsilon_{reff} = \varepsilon_r = 2.2$ (for PTFE dielectric). Figures 5.10 and 5.11 show the absolute value of RCS from equ.[5.18] for various values of the number of elements along the array side *n* and where the spacing *a* is equal to half a wavelength.

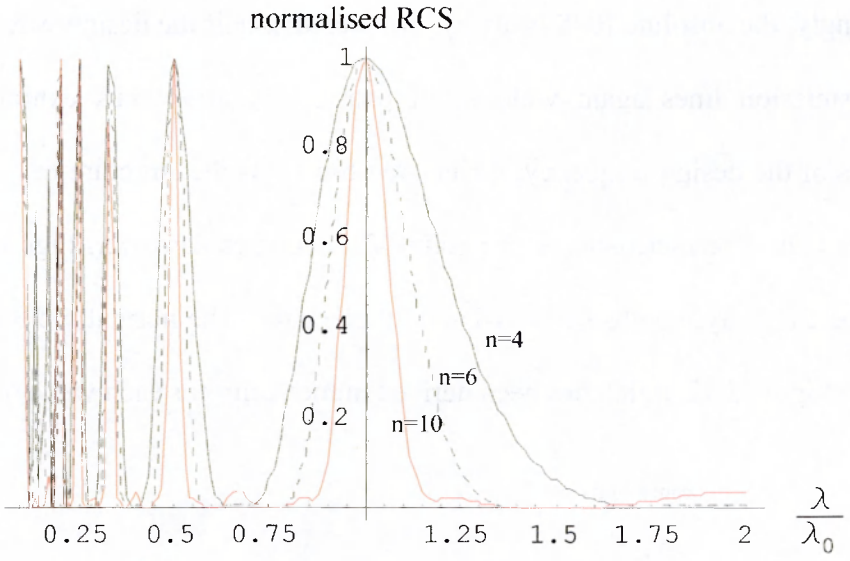

Figure 5.10 normalised RCS as a function of normalised wavelength for n x n element retro-array with crossing lines (n = 4*, 6 and 10)

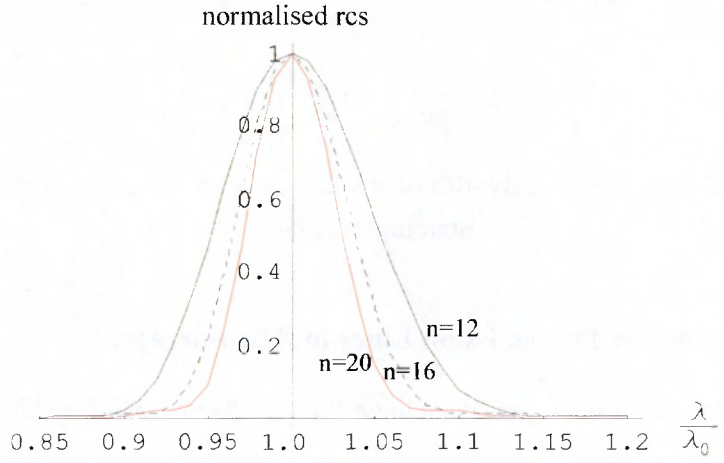

Figure 5.11 normalised RCS as a function of normalised wavelength for n x n element retro-array with crossing lines. (n = 12, 16 and 20)

In Figures 5.10 and 5.11 the wavelength is normalised to the design wavelength. The trend that the bandwidth reduces for increasing n is expected, since a shift in wavelength yields a greater net phase shift as transmission line length increases.

* In this formulation, the n = 2 case is a classic Van Atta array: the two interconnecting lines have equal length and the array exhibits no wavelength dependency. Thus n = 4 is the smallest array of interest.

Interestingly, the absolute RCS is always recovered at half the design wavelength, since all the transmission lines again yield equal phase. The array thus exhibits harmonics at multiples of the design frequency, which we observe as the structure in Figure 5.10 on the left hand side. For increasing *n*, the main lobe becomes narrower. Figure 5.11 shows the main lobe for array lengths of 12, 16 and 20 elements. The normalised 3 dB bandwidth is shown in Figure 5.12 which has been derived numerically for each value of *n*.

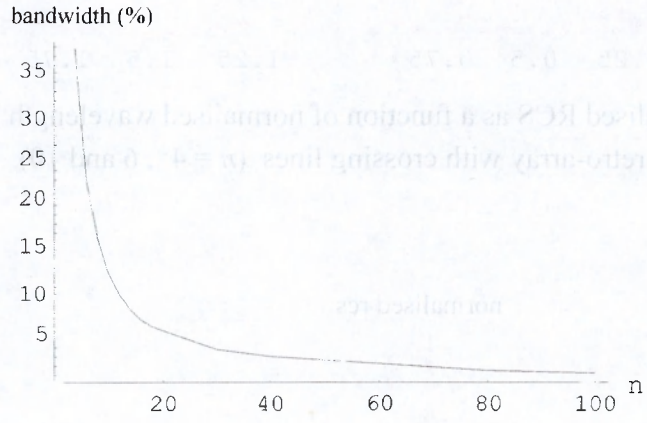

Figure 5.12 Fractional 3 dB bandwidth of *n* x *n* element retro-array with crossing lines, spacing = ½ λ_0.

5.3 Use of Waveguide for Transmission Lines in Retro-arrays.

Two contrasting construction approaches have thus far been considered in detail i.e. planar and coaxial transmission lines. In the former case, microstrip has been assumed to be the transmission line medium and this has been the subject of considerable attention, not least because many of the prototype modulated retro-arrays reported in preceding chapters were fabricated using this medium. However, it is interesting to expand the scope of the work by considering alternative transmission line types which might be used. As discussed in Chapter 3, microstrip is a very convenient medium from a viewpoint of circuit integration, ease of fabrication and cost. However, the loss associated with microstrip presents a disadvantage which for many applications may be prohibitive. For larger array structures use of coaxial lines is clearly advantageous in terms of aperture efficiency, while being less suited to economic production in quantity. Despite these pros and cons, both methods

present problems when addressing carrier frequencies much higher than those used by the prototypes i.e. 2.5 and up to about 9.5 GHz. To successfully exploit higher frequencies, component dimensions need to be reduced. This implies reducing substrate heights (for microstrip) and conductor diameters (for coaxial line) which carries associated requirements of higher manufacturing tolerances such as photo-etching resolution. Additionally, we have seen in section 5.1.6 that thinner coaxial lines exhibit higher loss. Nevertheless, either technique could reasonably be expected to be practicable for frequencies up to around 20 GHz or so, but the effect of dielectric losses would become increasingly detrimental.

These considerations bring us to a third possibility for transmission line type, i.e. waveguide, which presents the advantage of being an air-filled medium which therefore does not exhibit dielectric loss (neglecting the insignificant loss in dry air below about 50 GHz). The properties of waveguide are well documented, but its use in retro-directive arrays has received relatively little attention. The properties of waveguide in the context of a transmission line medium for interconnecting antenna pairs will be presented, with particular emphasis on attenuation in the intrinsic waveguide, integration with modulation and antenna circuits, and fabrication aspects.

In chapter 3 the use of printed circuits for the retro-array fabrication implied an inter-relation of many parameters and properties of the medium. We recall that these included the trade-offs between the physical space available, choice of laminate and the associated effects of inter-component electromagnetic coupling, impedance matching, transmission line loss, antenna properties etc. It is worth approaching a study of waveguide properties in a similar fashion i.e. being mindful that a number of trade-offs and inter-relationships are likely to be encountered. This is well illustrated in the following section which summarises the attenuation mechanisms exhibited by the waveguide medium.

5.3.1 Losses in Waveguide and its Suitability as a Transmission Line in Retro-arrays.

The attenuation properties of waveguide arise from the ohmic losses suffered by currents in the waveguide wall. As is well documented [5], for materials with finite resistivity, these currents exist in a region close to the inner surface of the conductor walls, where the electric and magnetic field intensities decay exponentially with distance. This gives rise to the "skin depth" effect, where the skin depth is the distance at which the fields decay to 1/e of their magnitude at the air/conductor interface. The effect in waveguide is illustrated in Figure 5.13.

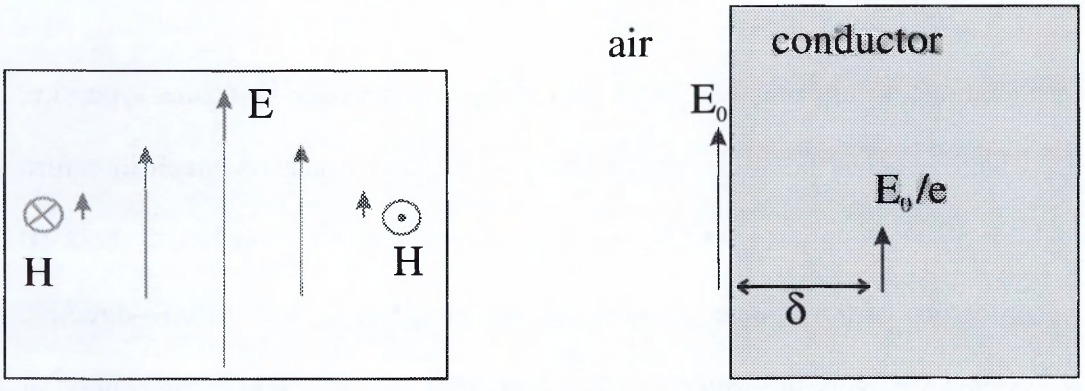

(a) Waveguide cross section, TE_{10} field distribution (b) Skin depth in conductor

Figure 5.13 Waveguide fields and loss mechanism

The attenuation is then also a function of the field and hence current distributions within the waveguide, which are also a function of the waveguide mode. For brevity, the study will be limited to rectangular, metal, air-filled waveguide propagating the dominant TE_{10} mode, since for the purposes of a low-loss transmission line this a commonly used medium which is convenient to fabricate.

A derivation of attenuation may be found in [3], from which we summarise that the loss in Neper per unit length is:

$$\alpha = \frac{\text{power lost per unit distance}}{2\,\text{power transmitted}} \tag{5.25}$$

where the lost power is that absorbed in Ohmic losses in the waveguide walls and found by the loop integral around the guide cross section of the average Poynting vector into the walls. The transmitted power is similarly found by the surface integral of the average Poynting vector in the direction of propagation. While [3] leaves the derivation in these rather general terms, [4] substitutes the actual H-field distributions and evaluates the integrals, which reduces equ. (5.25) to:

$$\alpha = \frac{R_S}{b\,\eta\sqrt{1-\left(\frac{f_c}{f}\right)^2}}\left[1+\frac{2b}{a}\left(\frac{f_c}{f}\right)^2\right] \qquad (5.26)$$

For the fundamental (TE_{10}) mode. (Expressions for attenuation of higher order modes may be found in [5]). Here R_s is the surface resistivity:

$$R_S = \sqrt{\frac{\pi\mu}{\sigma}}\sqrt{f} \qquad (5.27)$$

b and a are the waveguide cross-section dimensions shown in Figure 5.13, f_c is the cut-off frequency of the mode, η is the impedance of free space and μ is the permeability. The waveguide is assumed air or vacuum filled. The conductivity of the waveguide wall, σ, has been discussed in preceding sections and in table 5.2.

Since the attenuation term equ.(5.26) is clearly a function of waveguide cross-section dimensions, the choice of waveguide routing and allowable separation will have a direct influence on the transmission line loss experienced in a waveguide retro-reflector. Figure 5.14 shows the loss term for a 50 mm wide rectangular copper waveguide as a function of frequency, for different waveguide heights.

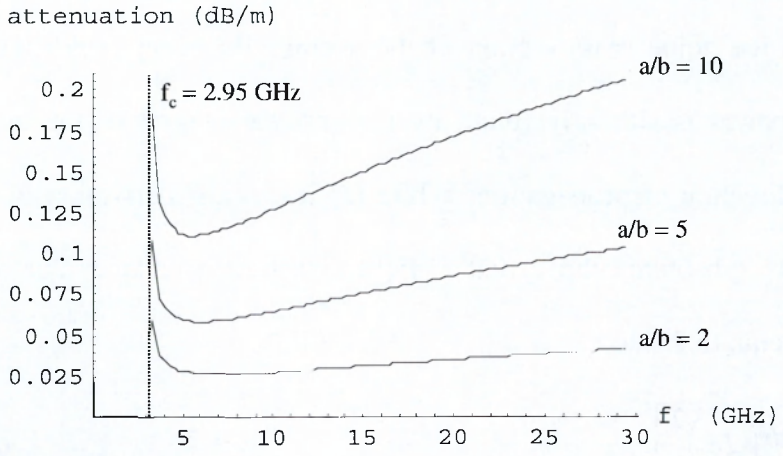

Figure 5.14 attenuation for copper rectangular waveguide, (a = 50 mm)

From Figure 5.14 it can clearly be seen that reduced height waveguide suffers excessive loss compared to standard waveguide (we recall that standard waveguide has a width:height ratio of 2). Thus, changing the width:height ratio from, for example, 2 to 10 leads to an increase in the minimum loss by a factor of about 4.5. This has implications for the type of layout chosen for a waveguide retro-array. A possible layout is illustrated in Figure 5.15 below.

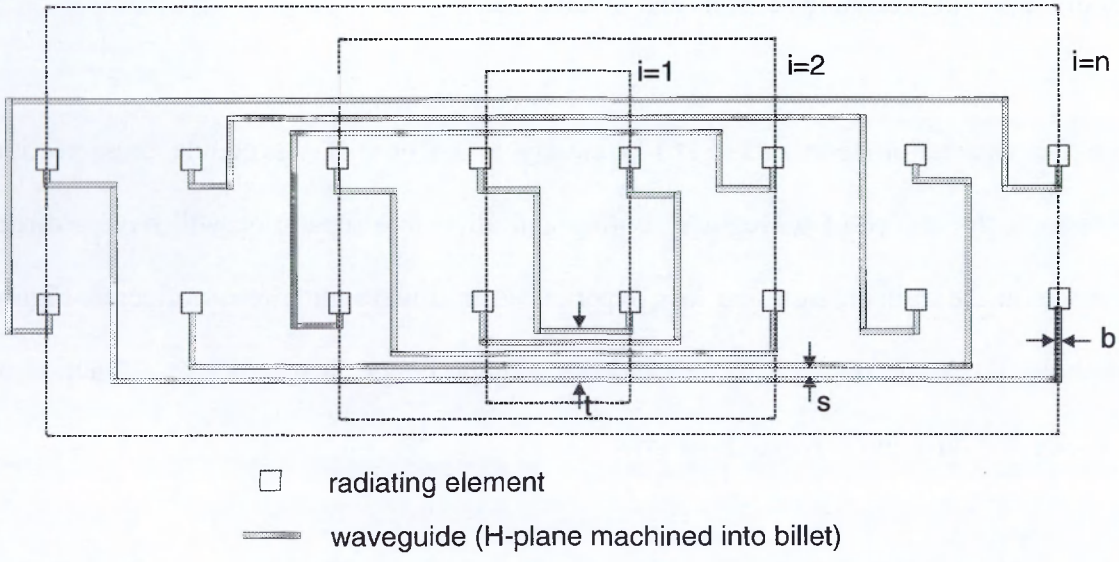

Figure 5.15 Possible configuration for *n* x 2 element waveguide retro-array.

A waveguide fed, square retro-array is likely to be a very cumbersome, indeed impractical proposition for more than a few elements (i.e. radiating elements). This is because the physical volume of the waveguides would lead to large inter-element spacings, which would yield a poor exploitation of the total aperture area.

As an alternative, Figure 5.15 shows a practical configuration for the routing of waveguides which are machined into a metal billet. Thus three of the waveguide walls are contained within the billet, while the 4^{th} would be formed by a lid which would also contain radiating apertures. Here, there are two rows of elements in the array, and n columns leading to a total number of element $2n$. The plane for the machining could be either the E-plane or H-plane, but in the latter case it is the smaller dimension (i.e. waveguide height b) which defines the width of the machined trench, and the larger dimension (i.e. waveguide width a) which defines the depth of the trench. The machined width, b, imposes a limit on the minimum spacing of the waveguides in the congested region (labelled dimension t). Unlike microstrip, waveguide is a shielded transmission line which can be put in very close proximity with a neighbour without cross-coupling of energy. The minimum separation s would in practice be limited by mechanical constraints. If we assume that s is an insignificant dimension, the inter-waveguide separation is limited by b. It can be seen that greater values of waveguide height b lead to a greater waveguide separation hence increased total distance and increased loss. Thus, smaller values of b lead to shorter lines and reduced loss. However, in Figure 5.14 it is clear that smaller values of b lead to increased loss per unit length. A question which thus arises is: *what is the optimum value of waveguide height to minimise loss in a retro-array ?* Since there are a vast number of possible array configurations there will be no single answer to this question, but a trend might be expected. To search for such a trend, an approximate model for the efficiency of the above n x 2 waveguide-fed array will be presented which takes a very similar form to those developed in preceding sections 5.1.2 and 5.1.3 for square (i.e. n x n) arrays. In contrast to the forgoing models, where loss per unit length was assumed

constant for a given transmission line medium, a model for loss in the waveguide-fed array must account for the variation in loss with changes to the waveguide dimensions.

Using similar reasoning as in section 5.1.2 above, an approximation for minimum line lengths for each group *i* in Figure 5.15 is:

$$L1_i = 2\,i\,s + (2\,i - 1)b \tag{5.28}$$

$$L2_i = 2\,i\,s + 2\,i\,b \tag{5.29}$$

Here, each group *i* contains 4 elements, 1 pair of which are joined by a line of minimum length $L1_i$, and the other pair by a line of length $L2_i$. The element separation is *s* (*a* having been used for waveguide height.) The terms in *b* are a consequence of the extra distance imposed by the waveguide's physical volume - thus in the congested region labelled *t* in Figure 5.15 the lines are forced to circumnavigate their neighbours with an extra length of at least 2 *b*. Using the same methodology as before, the RCS may be expressed as a function of the square of the effective area of the aperture, where this area is derived from the sums of the paired elemental effective areas (a_{el}) weighted by the loss term for the interconnecting line:

$$\sigma = \frac{4\pi}{\lambda^2}\left(\sum_{i=1}^{\frac{n}{2}}\left(2\,a_{el}10^{\sqrt{\frac{L1_i\,\alpha}{10}}} + 2\,a_{el}\,10^{\sqrt{\frac{L2_i\,\alpha}{10}}}\right)\right)^2 \tag{5.30}$$

In equ. (5.30), the summation is to $\frac{n}{2}$ since this is the number of groups, and α (the loss per unit length in dB) is taken from equ.(5.26). If (5.30) is normalised by dividing by the RCS for a lossless aperture, the efficiency of the array may be explored as a function of the waveguide dimensions, and waveguide height in particular, as shown in Figure 5.16 below.

relative RCS

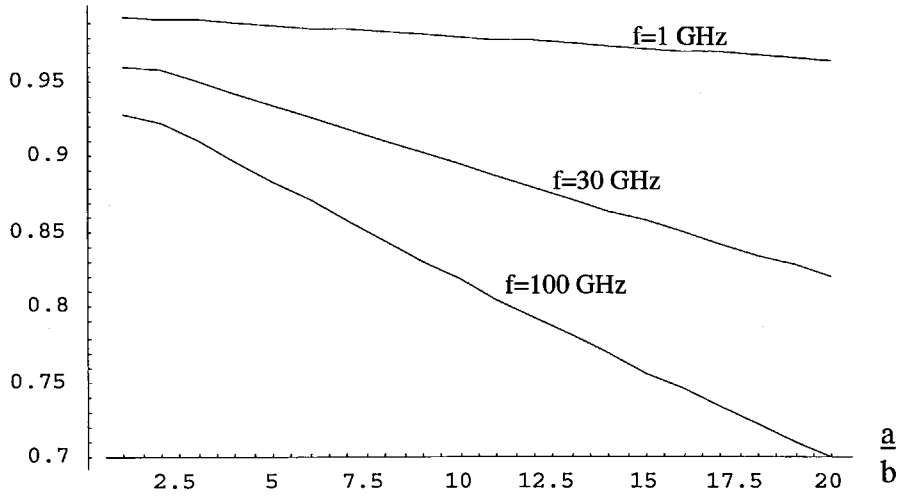

Figure 5.16 Relative efficiency of 2 x 100 element waveguide-fed retro-array as a function of waveguide relative dimensions.

In Figure 5.16 three frequencies have been chosen, and the waveguide width is fixed using the design rule $2a = \lambda_c = 1.7\,\lambda_0$ (A typical design rule for the centre frequency for waveguide is 1.7 times the guide's cut off frequency. Operation at lower frequencies leads to increased loss, as seen in Figure 5.14, while operation above twice the cut-off frequency leads to a likelihood of over-moding which tends to be undesirable.)

Other constants are the number of element pairs n = 100 which is an arbitrary but large figure chosen to examine the effects of waveguide dimension on large arrays, the wall resistivity which is that of copper (see Table 5.2) and the element spacing is half the free space wavelength. Equ.(5.30) was then evaluated as a function of $\frac{a}{b}$ for fixed a.

The trend observed in Figure 5.16 is very clear: it is disadvantageous to use reduced height waveguide for this configuration. While the shorter path length allowed by reduced height waveguide leads to reduced loss, this is more than offset by the increased loss per unit length. This would also lead us to another important conclusion that the configuration studied - H-plane machined into billet - does not offer a significant advantage compared to

using the E-plane. (Recall that the rationale for proposing the H-plane cut was closer waveguide spacing and hence reduced path lengths.)

5.3.2 Integration of Switch Circuits.

A disadvantage of using waveguide for a modulated retro-array is the added complexity of integrating the modulation (switching) circuits Since there are a large number of possible physical configurations for modulating signals in waveguide, this section will be limited to illustrating one variant. Figure 5.17 shows a microstrip insert which would integrate the waveguide probes, switch, diodes and bias circuits on a single circuit board. (For the illustration, a phase switch is shown). This could be placed in a machined cavity so that the probes are coincident with the centre of the waveguide H-plane. The two arms of the waveguide would need to be separated by either a wall (as shown) or a grounded E-plane pin which would have the same effect i.e. terminating the waveguide.

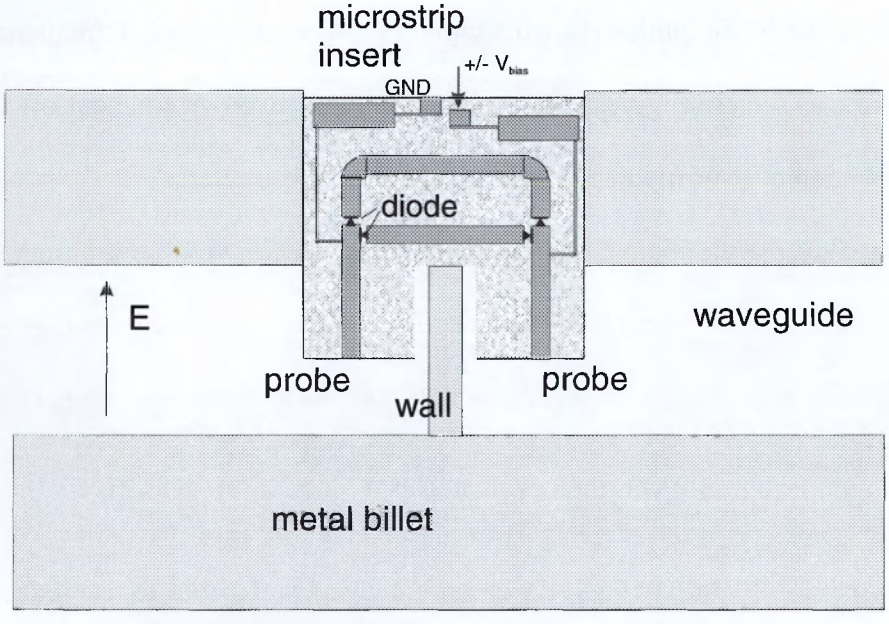

Figure 5.17 Microstrip insert for switch in waveguide

There are clearly many variants of this approach, such as probes orientated in the H-plane, as shown in Figure 5.18.

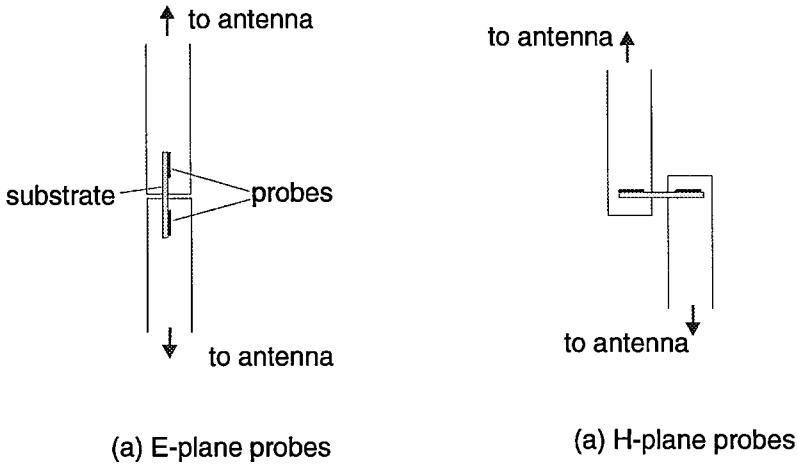

(a) E-plane probes (a) H-plane probes

Figure 5.18 Probes for waveguide switches

The choice of switch orientation would be expected to be influenced by the manufacturing and assembly techniques chosen, which in turn depend on the frequency band of operation.

5.3.3 Antennas for Waveguide Retro-arrays.

A primary objective for the waveguide-fed antenna in retro-arrays is that high directivity is not in general sought, since the retro-array is generally required to have a wide angular response. This implies that the aperture of each antenna is not large, which also allows the antennas to be spaced close together. While a very large number of different configurations are possible (many are described in [6]), a few practical antenna types for the application will be summarised . Figure 5.19 illustrates 4 possible configurations.

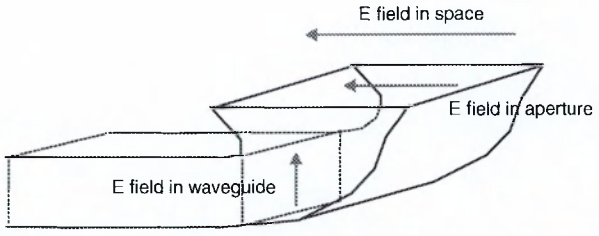

(a) E-plane bend and short horn

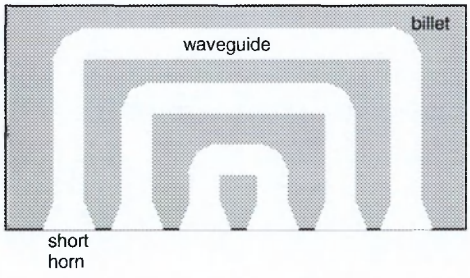

(b) Linear array with short horns

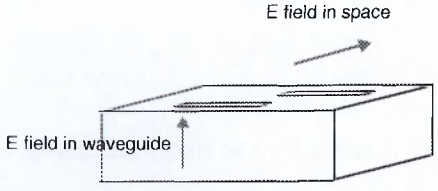

(c) slot or slots in waveguide wall.

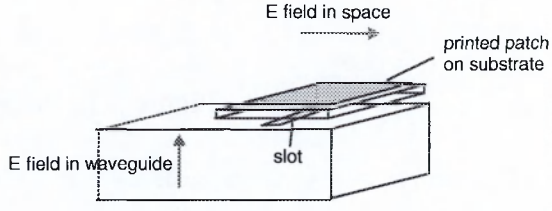

(d) slot fed patch antennal.

Figure 5.19 Antenna and feed variants for waveguide retro-arrays

In Figure 5.19 (a), an antenna suitable for the two dimensional architecture of Figure 5.15 is shown. This comprises a waveguide bend and a short feed horn. The bend is illustrated as an E-plane bend, but the layout would also be applicable to an H-plane bend. The horns may be most conveniently fabricated in a separate billet which would form the lid of the billet containing the machined waveguides. Case (b) shows a simpler variant which is a linear array. Either the broad or short waveguide wall could be machined into the billet and each terminated by short horns. This configuration appears to be among the simplest to fabricate, but leads to a physically bulky structure. Other small aperture antenna variants include the waveguide slot shown in case (c). This may be a single slot, or multiple slots can be used as commonly adopted in waveguide antenna arrays for radar or communications. The orientation of the slot with respect to the waveguide axis dictates the polarisation of the radiated wave. Radiating slots may be placed in either the broad or short wall. The slot in case (d) produces a polarisation with is orthogonal to that of case (c). Case (d) also shows the slot feeding a secondary antenna, which could be a printed antenna as

shown. This is often advantageous in enhancing the antenna bandwidth, improving the impedance match, and/or modifying the radiation pattern.

A disadvantage of horn antennas for retro-arrays is that a short (and hence compact) horn, as illustrated in Figure 5.19 (a) and (b), is less well matched to free space than a longer horn with a larger aperture. Where a larger aperture horn is used the array spacing may need increasing, and the horns become more directional which tends to negate the wide angle spatial response characteristic of the retro-array. However, this may be acceptable depending on the application. Variants of these basic antenna types might include sectoral horns (i.e. with rectangular apertures) to tailor the radiation pattern by increasing the directivity in a selected direction. For example, in the linear array in Figure 5.19 (b), it would be quite straightforward to lengthen the horn to produce a rectangular aperture with an elliptic radiation pattern, or in case (c) increase the number of slots to produce an equivalent effect. Beam shaping is a useful way of increasing RCS in a preferred direction, which will be explored in detail in following chapters.

5.4 Conclusions.

In this chapter the properties of increasingly large retro-arrays have been considered by developing approximate models for the lengths of interconnecting transmission lines. The type of transmission line medium chosen has important implications for the way the array is constructed and the severity of the loss which is to be expected. There is very little (if any) prior literature which explores these issues in detail, and the scope of the work cannot address every possible retro-array configuration. However, three configurations have been considered, each having different transmission line properties and requiring different sets of assumptions in their study. These configurations are crossing transmission lines which have been assumed to be coaxial line, and two variants of planar (non-crossing) lines. The planar variants are microstrip and waveguide.

In each case, approximate models for minimum line length have been derived, and the RCS or efficiency of the array aperture has been found by weighting the effective area contributed by antenna pairs with the associated line loss for the pair. In practice, line lengths must be adjusted so that the only allowed lengths are those which differ from each other by an integer number of wavelengths (strictly, transmission line wavelengths).

For coaxial line the lines may cross and the fabrication of very large arrays would be practicable. In this case, the models for loss and efficiency ought to be very realistic. For large microstrip arrays, the limited circuit area leads to difficulties in transmission line routing and the models for efficiency which have been presented assume that the lines can be kept electrically small by use of thin substrates, but the projected efficiencies for large array sizes should be interpreted as a first order and optimistic approximation. The choice of substrate has been discussed, and an upper bound on efficiency based on conductor loss alone has been presented which suggests that a substrate with zero dielectric loss would allow a large, square retro-array (n x n elements) at X-band frequencies to be at best around 60 % efficient.

For waveguide arrays, while many configurations are possible, a practical approach is to use non-crossing lines machined into a metal billet. Here, the dimensions of the transmission line medium are significant and have been included in the models for the line routing. It was found that minimising the line lengths by using reduced height waveguide (when the H-plane is cut into the billet) was detrimental since the increase in loss per unit length outweighs the line length reduction. Means of integrating waveguide with the switch and antenna components of a modulated array have been briefly discussed and a small number of configurations have been illustrated, while drawing attention to a very wide range of possibilities for further work.

As briefly discussed in section 5.1 there are other constant loss terms totalling about 5 dB for the X-band planar prototypes* and it is worth estimating the array dimensions, in terms of the number of elements, for which the transmission line losses start to dominate. These estimates are presented in Figure 5.20, where lossy RCS relative to lossless RCS is shown for three different combinations of geometry and line loss. The plots are derived from evaluating equ. (5.7) for non-crossing geometry and equ. (5.10) for crossing geometry.

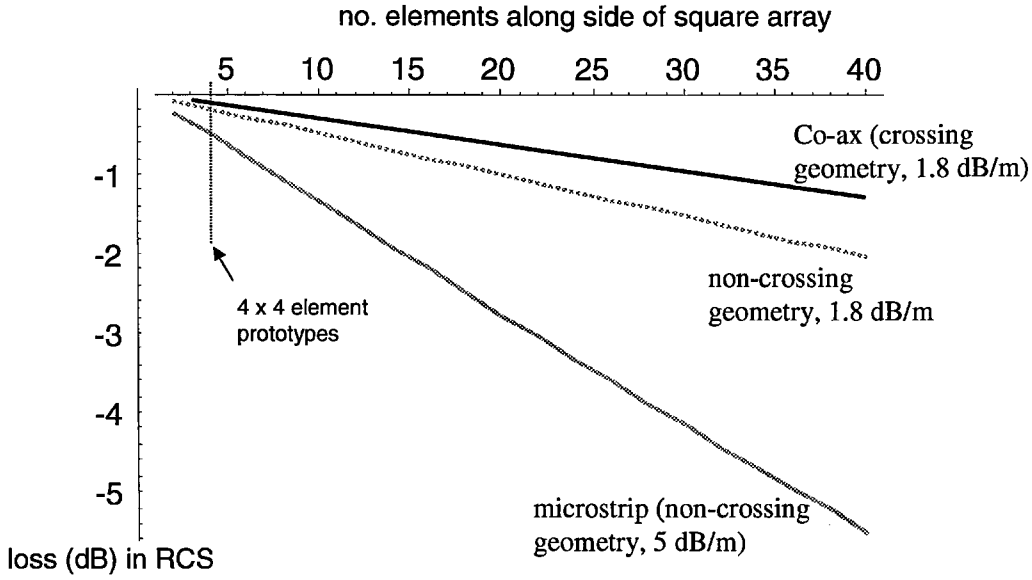

Figure 5.20 Summary of RCS loss due to transmission lines only, as a function of retro-array length.

In Figure 5.20, the line losses are those applicable to co-ax or microstrip at 9.4 GHz. A hybrid case is shown (non-crossing geometry with loss for co-ax) to illustrate how the additional loss associated with microstrip at this frequency presents are more severe disadvantage than the extra line lengths associated with planar construction.

(continued)

* This figure applies to the reduction, due to losses, of RCS, not aperture gain. See chapter 4, Table 4.7. (RCS is proportional to the square of aperture gain.)

Also, the arrowed region shows that for the 16 element retro-array prototypes the loss due to transmission lines, for any construction, is theoretically less than 0.6 dB and thus not the main contributer. For much larger arrays (up to 40 x 40 elements) the transmission line contribution to loss remains less than 2 dB for the less lossy lines (1.8 dB/m) but becomes comparable to the other transponder losses, i.e. around 5 dB, for the microstrip example shown.

References.

[1] "Microwave Engineering", D. Pozar, p.708

[2] "Foundations for Microstrip Circuit Design", T. Edwards, *Wiley* ,1991

[3] "Electromagnetics", J. D. Kraus, 4th ed. *McGraw-Hill Inc.* 1991. pp. 672 - 675

[4] "Fields and waves in Communication Electronics", S. Ramo, J. R. Whinnery, T. Van Duzer, *Wiley* 1965, p. 426

[5] "Foundations for Microwave Engineering" R. E. Collin, *McGraw-Hill Inc.* 1992.

[6] "The Handbook of Antenna Design" Rudge, Milne, Olver, Knight. IEE Electromagnetics Waves Series 15 *Peter Peregrinus Ltd.* 1982.

[7] "Microwave horns and feeds", A. D. Olver, P. J. B. Clarricoats, A. A. Kishk and L. Shafai, *IEE press* 1994

Chapter 6

Range Measurements to Modulated Retro-reflectors.

6.1 Introduction.

In the context of communications applications for modulated retro-reflectors, the important functionality of the system is the recovery of data from the passive target, i.e. the transponder. It is this aspect which has thus far been emphasised: the transponders reported in chapters 2, 3 and 4 have shown modulation spectra in practical measurements. In these measurements, continuous wave (CW) illumination has been used, and a homodyne detection method can conveniently recover the baseband signal applied to the modulation circuits within the transponder. However, the forgoing work has not addressed another important application which is closely related to the original aims of the work. These are radar applications. In contrast to communications applications, it is target location and identification which is here the primary objective. The former objective is primarily the measurement of target range and bearing, and requires a different interrogating waveform to the CW previously reported.

This interrogating waveform requires a periodic structure from which the target range may be derived from measuring the time difference between the transmitted signal and received reflection or "echo". This is traditionally achieved by either transmitting pulses of radiation and timing their return, or sweeping the carrier frequency i.e. using frequency modulation (FM). This chapter will show how the former method has some theoretical promise but has been inconvenient to implement, while the latter method has been implemented very successfully. The FM measurement system will be reported in some detail, as it presents an application which would appear to be of very significant benefit in fields such as vehicle guidance and control, local navigation, collision avoidance and many related areas.

6.1.1 Pulsed Systems.

Historically, pulsed radar has been the predominant mode of radar operation, particularly in the defence, aviation and maritime fields. Therefore, in this section the salient features will be discussed in the context of a pulsed system which might use modulated retro-reflecting transponders. As alluded to in the introductory sections of the first chapter, there is a vast literature on pulsed radar and its development. This was largely driven by requirements for defence applications [1]. While an overview of the field is substantially beyond the scope of this work, the most fundamental concepts will be summarised since they relate directly to the feasibility of using pulsed radar with a modulated transponder.

Broadly speaking, pulsed radar systems may be considered as the transmission of a continuous wave at a fixed frequency multiplied or modulated by a square wave, the product being a pulse train. Most radars only operate for a short period and therefore the truncation of the pulse train can be considered as a further multiplication of a windowing function which in this case is the rectangular pulse envelope. Thus in the frequency domain we have essentially three components : the centre frequency of the sinusoidal carrier, at which the radar operates, the spectrum due to the square wave pulse train forming signal and the window function i.e. the switch on/switch off function of the individual pulse. Thus any transponder modulating the return signal could in theory be identified by a matched filter which was the time inverse of the impulse response of the transmit radar signal modulated by the transponder.

The main parameters of the time domain pulse train are shown in Figure 6.1.

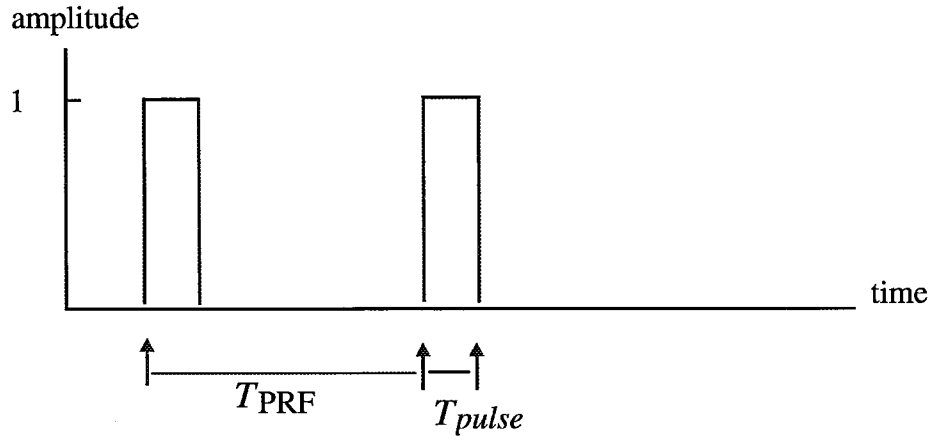

Figure 6.1 Pulse train of pulse radar

PRF and maximum range.

The time interval between pulses is a function of the pulse repetition frequency (PRF). A fundamental trade-off in pulsed radars is the relationship between the PRF and the maximum unambiguous range. Clearly, a target return from a distance greater than that travelled by a previous pulse during the PRF duration T_{PRF} cannot be distinguished from a return by the "current" pulse from a much closer target. This is because the receiver begins its timing function after each pulse has been transmitted, and has no memory of or means of distinguishing each preceding pulse. Thus the PRF tends to be dictated by the maximum range of operation. However, too long a PRF leads to a low power duty cycle and hence low overall signal-to-noise ratio. It is common for different PRF values to be selectable by operators, or for the PRF to be modulated [2] or "dithered" [3] so as to ameliorate the range ambiguity problem.

Range resolution and minimum range.

Since the receiver is switched off during the pulse transmission, a target closer than the distance travelled during the pulse duration T_{pulse} will tend not to be detected. Similarly, the resolution of the measurement is limited by this range. The tendency for pulsed radar to operate at duty cycles of the order of 0.001 and with pulse durations less than 1 μs leads to

considerable difficulty in detecting the modulation waveform of the co-operative transponder, which will be shown in the following section.

6.1.2 Modulated Transponders.

In the case of the modulated retro-reflector transponder the signal is phase or amplitude modulated so that the returned signal can have a well defined and relatively narrow spectral content. The modulated return will have sidebands centred on the original transmit radar frequency, as shown in chapters 2 - 4. Conventional demodulation techniques can be employed to either recover the original transmitted pulse train or the modulating tone. As an illustration, Figure 6.2 shows an experimental measurement in which a pulsed illuminating signal at a carrier frequency of 9.2 GHz is incident on a transponder modulated at 1 MHz. This experimental arrangement is substantially the same as the CW measurements first illustrated in Figure 2.9, and most of the subsequent measurements where the modulated RF spectrum was captured on a spectrum analyser such as shown in appendix A4.2. However, in the pulsed measurements, the CW signal was replaced by what are effectively periodic bursts of the carrier. The required pulse length and PRF were programmed into the synthesised source.

In Figure 6.2 the duration of the pulse is 10 μs and the pulse repetition rate is 100 μs. The received signal was mixed with the outgoing microwave carrier. The received IF signal was Fourier transformed into the frequency domain and reproduced in Figure 6.3

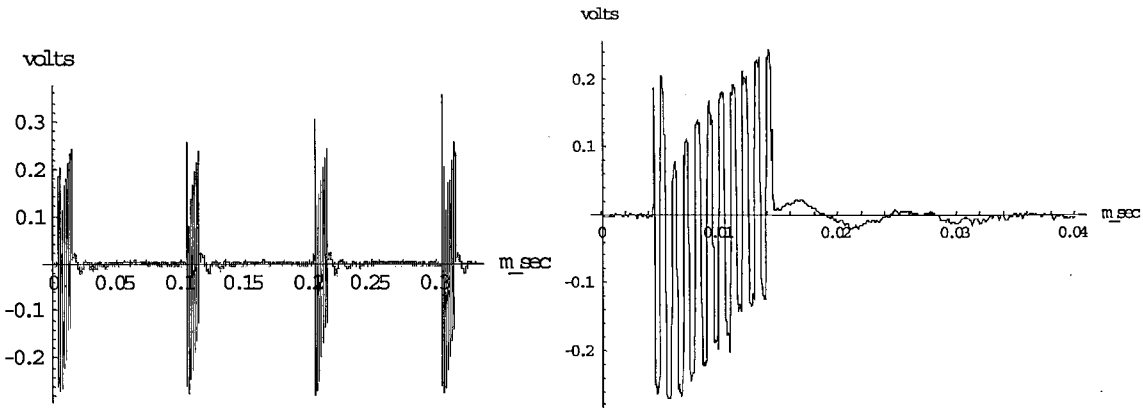

(i) 4 pulses (ii) zoom on single pulse

Figure 6.2. Pulsed radar with modulated transponder : sample time domain measurements of IF. [$T_{pulse} > 1/f_{mod}$ (long pulse with relatively fast modulation), $F_c = 9.20$ GHz, $f_{mod} = 1$ MHz, $T_{pulse} = 10$ μs, $T_{PRF} = 100$ μs]

In Figure 6.2 (ii) the modulation waveform is apparent at 10 cycles of the 1 MHz modulation (square wave) signal. Hence, where CW illumination would yield a continuous 1 MHz monotone at IF following coherent detection, the pulsed illumination yields a corresponding pulse of the 1 MHz modulation signal. Since the pulse is here 10 times longer than the modulation waveform period, we observe 10 cycles of the modulation waveform during the pulsed event. While these phenomena are clear enough, they lead to a number of important implications:

Firstly, attention is drawn to the close proximity of the transponder to the receiver, and the relatively long pulse duration. Hence the leading pulse edge covers, during the 10 μs transmission period, a distance of $c \times 10^{-6} = 3000$ m. This is conventionally taken as the minimum range i.e. in the case where the receiver is switched off during transmission of the pulse. However, in the homodyne detection method used, a target within this range is detected because the receiver LO power is tapped off from the transmit chain. Consequently, a target beyond this range would not be detected by the homodyne receiver, unless its distance is sufficiently large that it is received by mixing with a later pulse than

that which illuminated it (i.e. the target is at the conventional ambiguous range.) The homodyne measurement (receive while transmit) thus yields an inverse situation to the conventional pulsed radar (receive in intervals between short transmit pulses). We may conclude that a homodyne measurement, while convenient for studying the IF waveform in the laboratory, is not a practical approach for deriving range in an operational system. This leads us to a second observation which concerns the tendency for pulsed systems to operate with shorter pulse lengths to yield increased range resolution and accuracy. This in turn leads to a requirement for much faster transponder modulation rates so that each reflected pulse yields a number of modulation cycles. Since the trend for pulsed systems to operate at less than, or very much less than 1 μs pulse length, they would tend to become incompatible with the < 10 MHz transponder modulation rates available. Another inconvenience of the pulsed method in the laboratory compared to CW variants is the severe lowering of the average system energy due to the small duty cycle. While a practical system would use very high pulse power (several kW), this was not feasible for laboratory work.

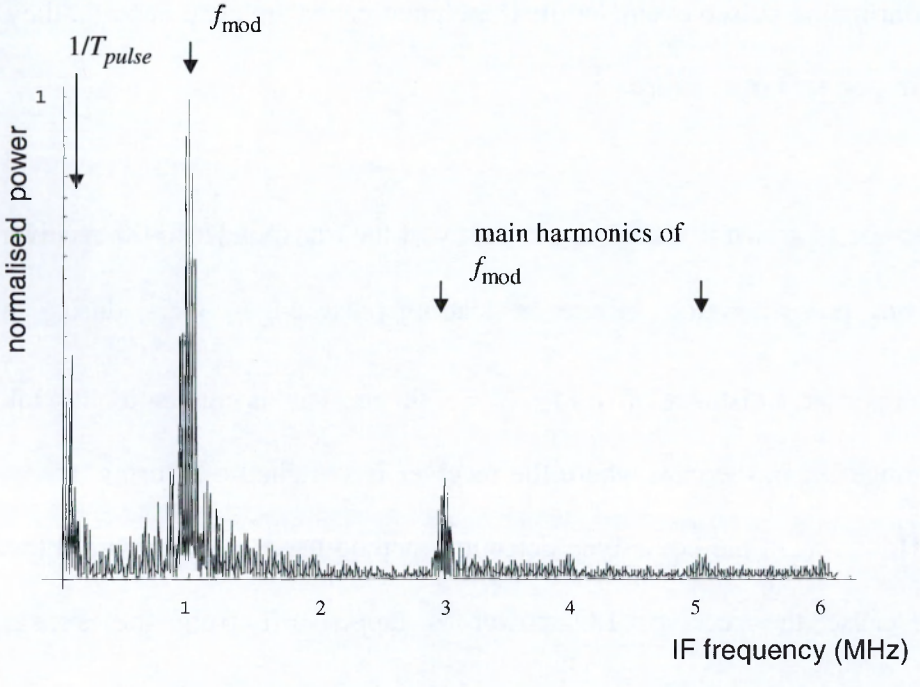

Figure 6.3 The IF spectrum for pulsed illumination.

In the second example (see Figure 6.4) the transponder modulation frequency was lowered, by a factor of 2, to 0.5 MHz. Also, the interrogating pulse train was compressed in the time domain by a factor of 10, to give a shorter pulse length of 1 μs and PRF period of 10 μs. In contrast to the example of Figure 6.1, this yields a short interrogating pulse with a relatively slow modulation waveform. As can be seen in Figure 6.4 the IF frequency spectrum is dominated by the spectrum of the pulse and the modulating spectrum is not clear.

Recovery of the signal would be most tractable as a digital signal processing operation to improve the recovery of the modulating signal within the spectrum of the pulse. It is probable that a process to enhance the signal detection (a matched filter) can be constructed to remove the pulsed signal. Overall clutter rejection performance would then depend on the performance of the matched filter (roll off and pass band) and relative radar cross section of the target relative to the clutter. For more sophisticated transponder modulation schemes we may also consider pseudo random binary sequence modulation. In a simple system a single pulse from the radar incident on an amplitude modulated transponder driven by a pseudo random binary sequence generator, would generate a known sequence of returned pulses. In the receiver a correlator would delay and add the pulses to reconstruct the interrogating pulse. Unmodulated clutter would be decorrelated by this process. In spread spectrum vocabulary [4], the correlator de-spreads the returned spectrum, and in addition spreads the spectrum of the unmodulated or uncorrelated signal. In broad terms for a single interrogating pulse a 1000 bit spreading sequence will spread the power of the one pulse between the 1000 return pulses (assuming no loss or amplification). At the receiver, these 1000 pulses will be shifted (at the known times) and added on a power basis to reform the original pulse. In this operation, random clutter pulses will be shifted but they will not correlate with the known shift periods of the modulated returns and therefore will not add up to form a pulse (they will appear as noise).

While it is worth noting that all the above methods of modulation and demodulation are standard communications techniques - each with advantages and disadvantages in both implementation and performance - they can become less tractable with the very low duty cycles of conventional pulsed radar.

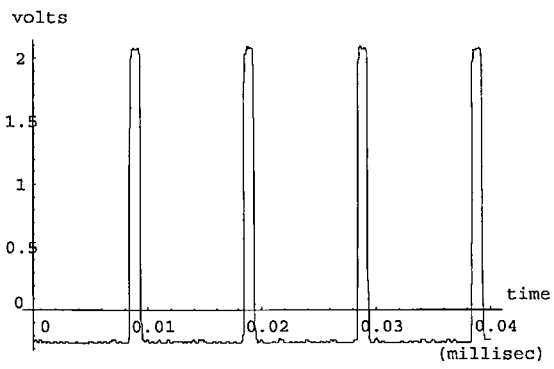

(i) target off, time domain

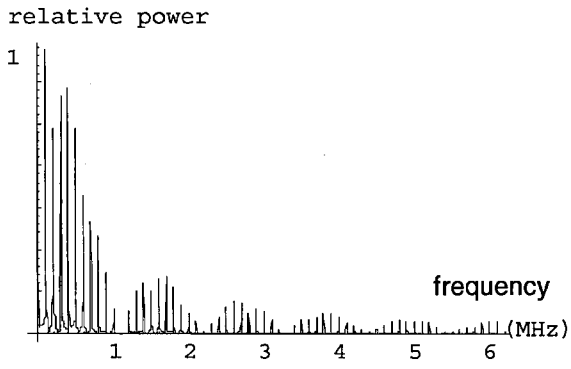

(ii) target off, frequency domain

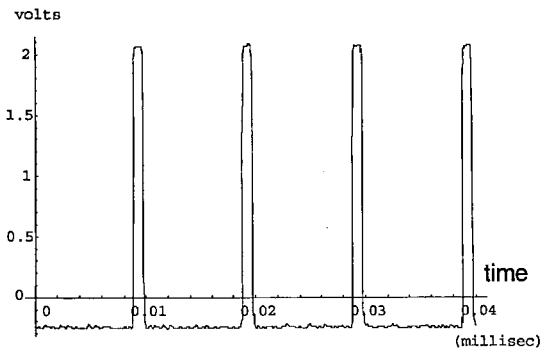

(iii) target on, time domain

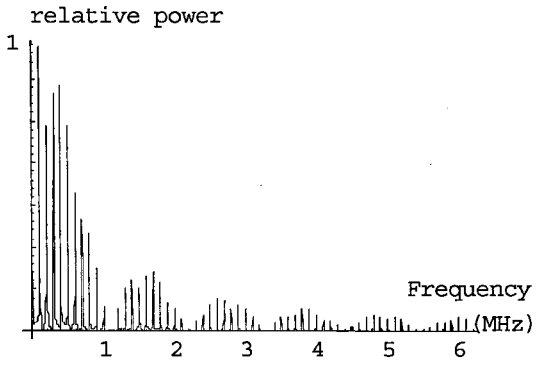

(iv) target on, frequency domain

Figure 6.4 Pulsed Radar: Period of Pulse less than Modulation Period

[T_{pulse} < $1 / f_{mod}$ (short pulse with relatively slow modulation), F_c = 9.20 GHz, f_{mod} = 0.5 MHz, T_{pulse} = 1 μs, T_{PRF} = 10 μs]

6.2 Frequency Modulated Continuous Wave (FMCW) Radar.

6.2.1 Introduction to FM Range Measurement.

In this method, the transmitted waveform frequency varies with time. At any given time, the signal received from a reflection at a given range has a different frequency to that which is currently transmitted. The frequency variation is typically linear, which simplifies signal processing for range. However, where range measurement to multiple targets is not required, such as in a radar altimeter, a sinusoidal modulation can conveniently be used and range determines from the average difference frequency [5]. The case of linear variation of frequency with time is shown below in Figure 6.5 for the transmitted and received signals.

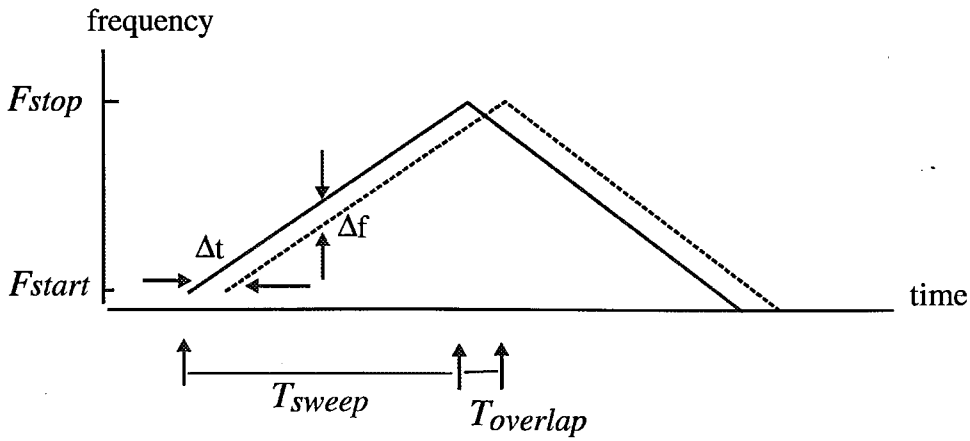

__ transmitted signal .... received signal.

Figure 6.5. FM radar basic principles:

Conventionally, the RF mixer compares the outgoing frequency with the received frequency, the difference Δf being directly proportional to the time interval Δt and hence path length 2 L between the transmitter and target, hence:

$$\Delta f = \frac{F_{stop} - F_{start}}{T_{sweep}} \frac{2L}{c} \tag{6.1}$$

where F_{start} and F_{stop} are the start and stop frequencies in the linear frequency ramp of duration T_{sweep}, and c is the speed of light. As with all radar techniques, it is in general difficult to detect and/or identify specific targets of small RCS particularly in cluttered environments.

Effect of Doppler frequency: for a moving target, the Doppler frequency shift appears as an additional offset, which reverses sign when the ramp gradient reverses. Thus by comparing measurements for the up-ramp and down-ramp, Doppler frequency and range frequency may be resolved unambiguously [6].

6.2.2 Adaptation of Technique for Modulated Reflectors.

In the simplest case of the modulated scatterer technique, the RCS of the target is modulated with, for example, a constant period signal of much higher frequency (f_{mod}) than Δf above. The difference frequency arising from the target's reflection is therefore $\Delta f \pm f_{mod}$ which is decoded by the second mixing stage, i.e. mixing with f_{mod}. This process effectively rejects all other, unmodulated targets (except those at very great range which produce values of Δf close to f_{mod} , which is discussed below). The main frequency components are illustrated in Figure 6.6

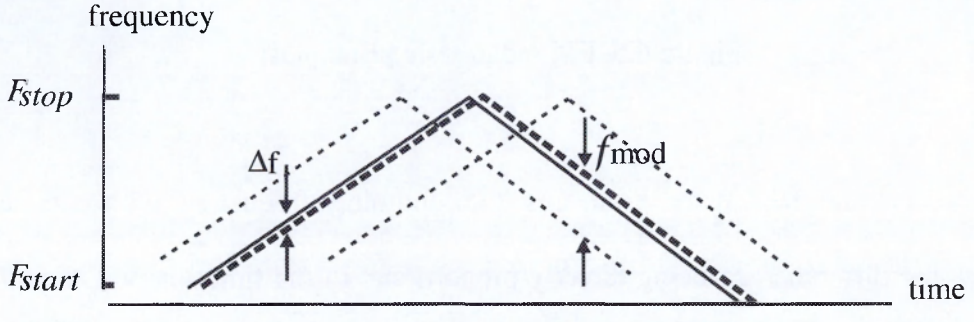

Figure 6.6 Frequency components for FM illumination of modulated transponder.

In Figure 6.6 the product generated by the transponder modulation frequency is shown as two sidebands, one above and one below the reflected carrier. However, where the modulation waveform is a non-sinusoid, harmonics of the fundamental modulation frequency will also be present. This is indeed the case with the square wave modulation used in practice, whose characteristic spectrum (odd harmonics) has been demonstrated in the preceding chapters where a continuous wave, single frequency carrier was used to illuminate the transponders. Also the carrier component shown in Figure 6.6 will be present only from clutter targets, being suppressed in the spectrum of the transponder, when the transponder is phase-modulated. These techniques could be adapted by using multi-tone modulation, or a binary code (for example M-sequence) to effectively modulate with a spread spectrum technique. The pros and cons of various modulation schemes are discussed later.

6.2.3 Detection Techniques.

To aid the study of the output waveforms the measurement of difference frequency, which is directly proportional to the range to the modulated target, was performed using coherent detection as shown in Figure 6.7. This involved using the same reference signal, at the second mixing stage, as that which modulated the target, this technique could not be used in practice without a carrier-recovery stage.

Alternatively, an incoherent detector may be more convenient. For example, a separate signal generator could be used, but this would not be phase locked to the target modulator – hence the measurement would require some averaging as the output magnitude varies randomly between its maximum and zero. Any frequency offset between the two sources results in a measurement error. The simplest incoherent detector is the envelope detector, which may be a convenient solution, and some practical results using this method are presented in section 6.2.8 below.

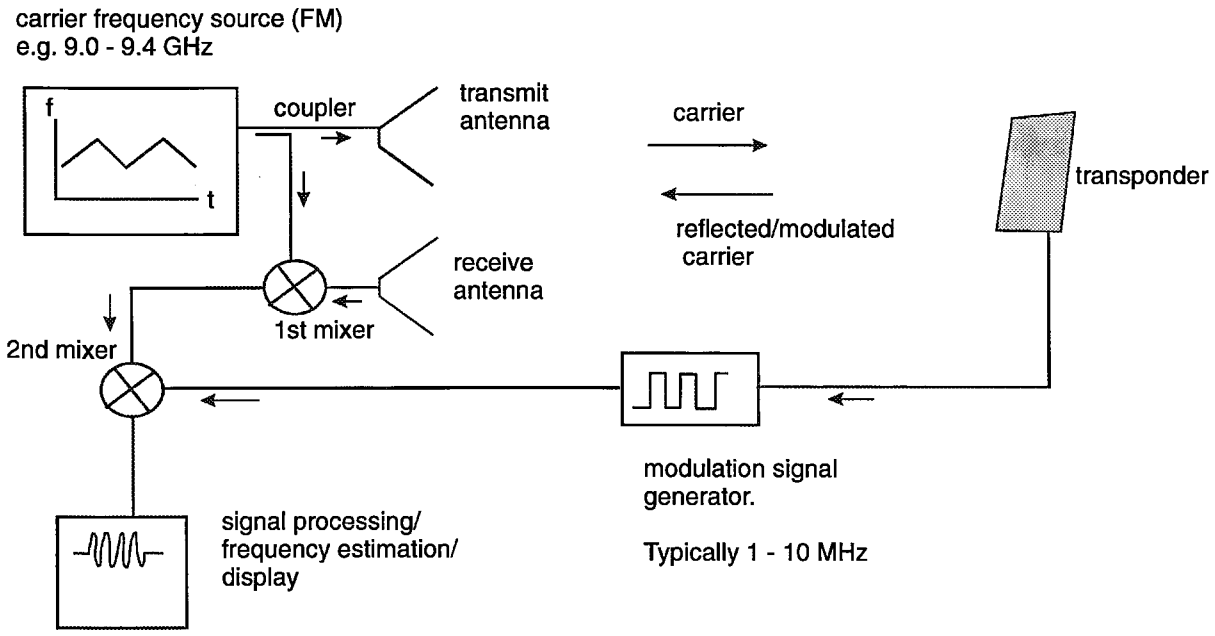

Figure 6.7 FMCW range measurements with coherent detection

6.2.4 Measurement System and Initial Results.

To illustrate typical waveforms, a variety of results are presented which demonstrate the dependence of output waveforms on the sweep parameters.

It is emphasised that the measurements were performed indoors with test equipment that does not represent an optimum system, but was configured to explore the nature and limits of the technique. For example, transmitted power was limited to 20 mW and range was initially limited to 5m. RF and IF filters were not employed. Medium gain printed antennas of the 16-element type discussed in chapter 4 were used as the transmit and receive antennas.

The main system components are listed in Table 6.1 below:

item	manufacturer (model/type)	notes
RF source	Hewlett Packard 83751B 2 - 18 GHz synthesised sweeper.	up or down ramp only, followed by 22 ms idle period. Minimum synthesised sweep time 10 ms.
coupler	10 dB waveguide or microstrip	Microstrip 10 dB coupler designed and fabricated by author.
antennas	pyramidal horns or 16 element printed	printed antennas designed and fabricated by author, typical 10 dB bandwidth approx. 300 MHz. (see Chapter 4)
Transponder	16 element, phase modulated	Developed by author, see chapter 4.
Receiver RF low noise amplifier	Hirotech 1 - 9 GHz, or author's 9 GHz 4-stage GASFET LNA	
1st mixer	Watkins-Johnson MY85C	rated 2-18 GHz, -6 dB nominal conversion loss at 0 dBm LO drive
2nd mixer	MiniCircuits	0.05 - 100 MHz
Modulation signal generator	HP 20 MHz pulse generator or HP synth. with CMOS chopper	CMOS chopper built by author. Provides convenient square wave drive levels from sinusoid input.
Signal processing	Kemo analogue active low pass filter.	Data capture using HP digital oscilloscope.
Frequency estimation	PC/ *Mathematica*	Performed off-line.

Table 6.1 FM range measurement system main components.

The sweep generator could also be driven in un-locked mode using an external ramp generator - faster rates are then possible, but with a reduced sweep bandwidth.

All measured frequencies include a constant offset term for the path lengths of transceiver cables and components, in addition to the free space term. In a completed system, this term would be calibrated out as described below. FFT frequency scaling is shown relative to the length of the data file.

System bandwidth. This is a function of both the transponder RF bandwidth and that of the RF components in the transceiver summarised above. Of these, the most narrow band components were the printed antennas, whose 10 dB bandwidths were measured to be approximately 300 MHz, although they did not share exactly the same centre frequency. Other band-limited components included the printed coupler, and the receiver amplifier, which was being operated on the upper edge of its intended frequency range. A detailed investigation of system bandwidth is rather unnecessary since it can be measured directly by observing IF amplitude as a function of frequency. The 10 dB system bandwidth was thus determined to be centred at 9.2 GHz with a 400 MHz bandwidth.

Example (i): 10 ms synthesised sweep.

Here, the RF sweep has been chosen to cover the most useful 400 MHz bandwidth of the system i.e. from 9.000 GHz to 9.400 GHz . The sweep time here is 10 ms. This yields a frequency ramp rate = 4×10^{10} Hz/s which corresponds to 267 Hz for each metre change in range. The source exhibited a dormant period of 22 ms. The transponder modulation frequency is 2.5 MHz, although this value has little effect on the received waveforms.

The sampling parameters, set on the digital sampling oscilloscope, were chosen to be: 8193 samples at 25 K samples / s . (Hence the data record length = 0.32768 s)

The target range is 3.8 m hence the difference frequency expected is 1013 Hz.

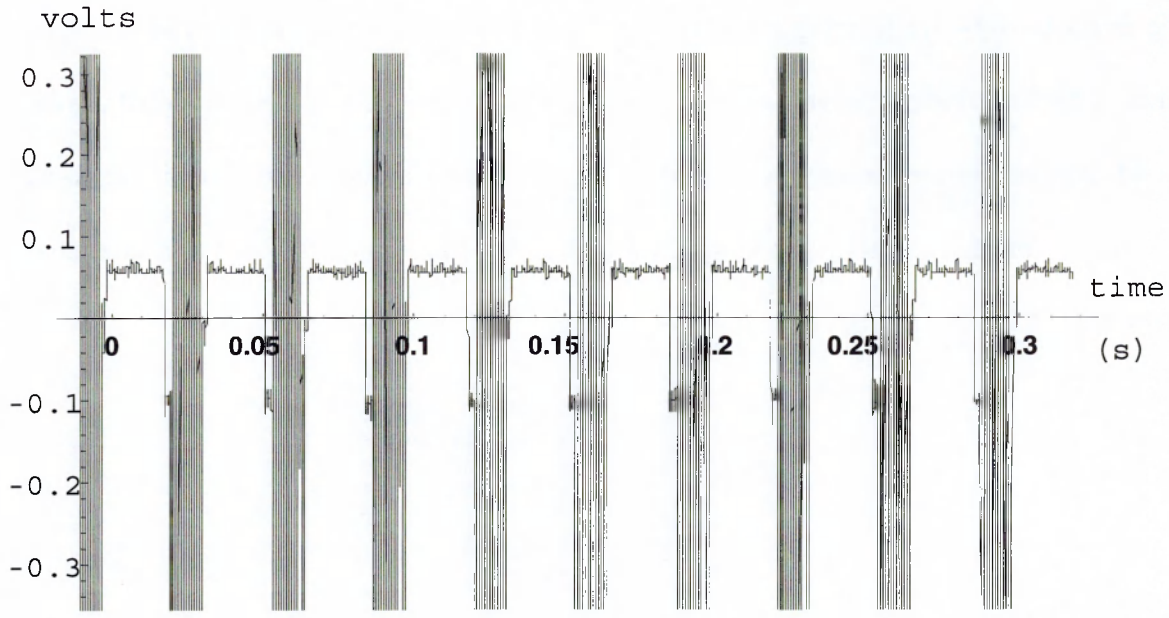

Figure 6.8 Time domain waveform following coherent detection, 10 ms sweep

It is apparent that the measurement of difference frequency is effectively sampled at the repetition rate of the ramp generator. Hence the ramp rate always occurs as a frequency component at the output, but is a known quantity, which may be removed by filtering. Figure 6.9 shows the un-filtered FFT of the time domain waveform shown in Figure 6.8 where the low frequency products at $1 / T_{sweep}$ are apparent as the series of closely spaced spectral lines.

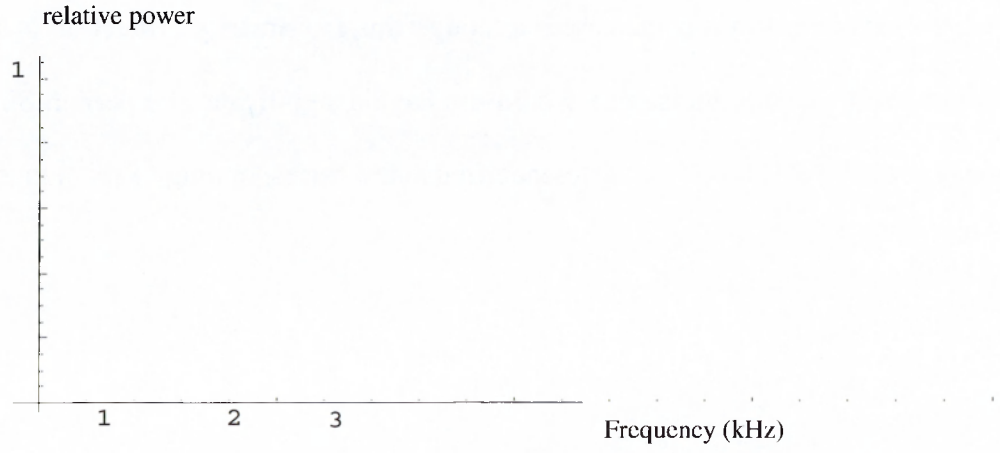

Figure 6.9 FFT of coherently detected difference frequency.

The effect of digitally filtering the ramp repetition frequency is illustrated in Figure 6.10 below. The time domain waveform is a subset of that from Figure 6.8 and selected during the RF transmit period so that the ramp repetition frequency is suppressed; this is observed as removal of the closely spaced spectral lines seen in Figure 6.9 and a consequent smoothing of the spectrum.

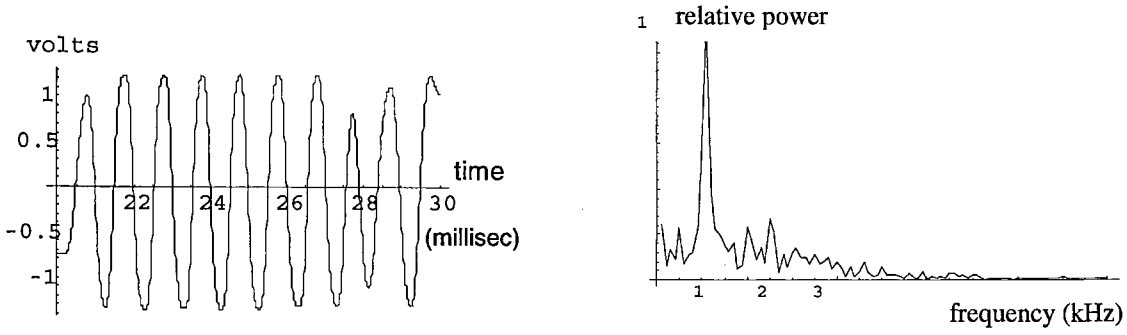

(a) Time domain (b) FFT

Figure 6.10 Effect of digitally filtering out ramp frequency.

Example (ii): 100 ms synthesized sweep.

On decreasing the rate of the frequency sweep, the slower sweep gives rise to a lower value of difference frequency. However, the idle period of the sweeper is less significant, since it yields a frequency term which is now more dissimilar to the sweep rate. Also, the duty cycle of the measurement has increased, although this is primarily a function of the particular source used; ideally the source would not have a significant idle period. Since the target range remains at 3.8 m, the difference frequency corresponding to this range is 101 Hz

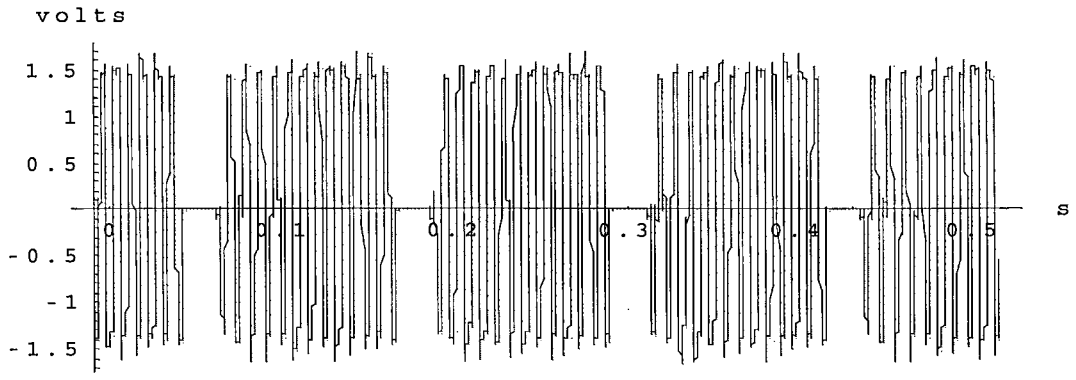

Figure 6.11 Time domain waveform following coherent detection, 100 ms sweep.

The FFT of the time domain waveform which is shown in Figure 6.11 is shown below in Figure 6.12. The (approximately) 101 Hz component is the most prominent term.

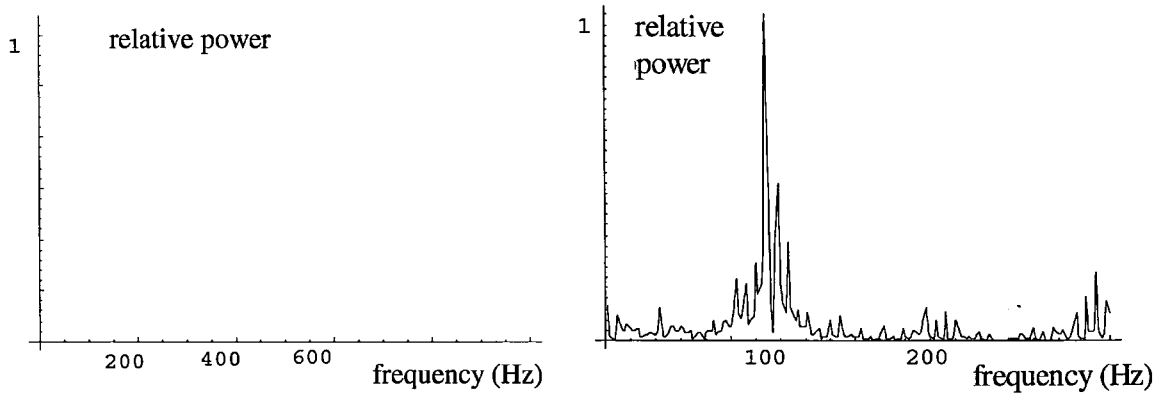

(a) First 1000 points (b) Magnification (first 200 points)

Figure 6.12 FFT for 100 ms sweep

In the above results, while the difference frequency Δf is linearly related to range by equ. (6.1) for the free space path, the relationship is subject to a calibration term which is a function of the path lengths of the transceiver components. Thus the range cannot yet be accurately derived from Δf. The system calibration is described below in section 6.3.3 below

6.2.5 Narrow Band and Wide Band Sweeps.

For any given signal processing method and hardware, minimum range and range resolution are always improved by adopting a wider sweep bandwidth, since this will give rise to a greater difference frequency Δf at any given range. By way of example, a number of experimentally derived time domain waveforms are presented for "narrow band" and "wide band" FM illumination (the terms are relative), while firstly some of the related parameters are discussed.

The measurement of difference frequency is effectively repeated at the repetition rate of the ramp generator. It is advantageous to make the observation during the period t_{sample} during a continuous up or down sweep. The frequency components generated during the overlap period of the outgoing and received ramps ($T_{overlap}$ in Figure 6.5) should be disregarded as they would appear as noise. Clearly

$$T_{sweep} = T_{sample} + T_{overlap} \tag{6.2}$$

and, unless the range is very great:

$$T_{sample} >> T_{overlap} \tag{6.3}$$

Having established that the duration of the observation T_{sample} is very similar to T_{sweep}, we consider the data collected during this period. For a high resolution measurement of Δf, we require many periods of Δf to fall within the period T_{sweep}. This is difficult to achieve at short range unless the sweep bandwidth is large. Figure 6.13 illustrates the captured time domain waveforms in their entirety, for wide and narrow band illumination of the transponder. The range here is 3 m. which we may consider "short" range particularly for the narrow band measurement for reasons which become apparent on studying the IF time domain waveform.

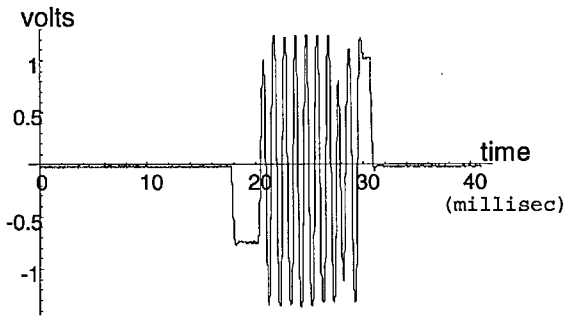

(i) BW = 400 MHz

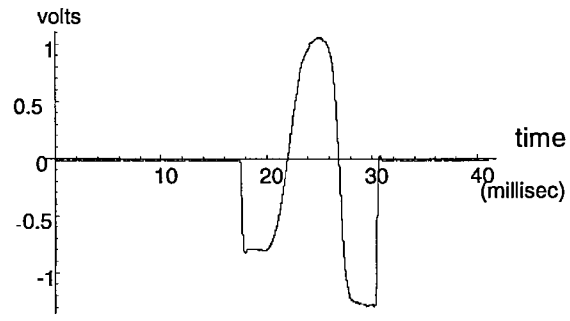

(ii) BW = 40 MHz

Figure 6.13 Wide and narrow band time domain waveforms for Δf at range = 3m. T_{sweep} = 10 ms.

In the narrow band case (Figure 6.13 case (ii)) the ten-fold reduction in bandwidth relative to case (i) gives rise to a factor of ten fewer cycles of the Δf waveform. Figure 6.14 shows the extract of data taken from the 10 ms sweep period, with its associated FFT.

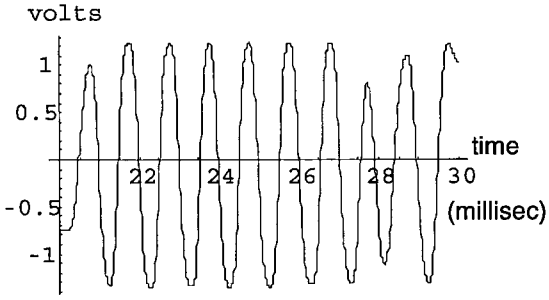

(i) 400 MHz sweep, sampled during T_{sweep}

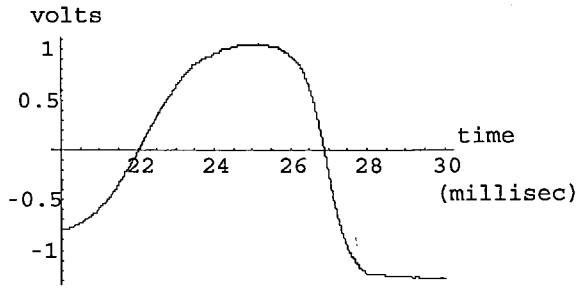

(ii) 40 MHz sweep, sampled during T_{sweep}.

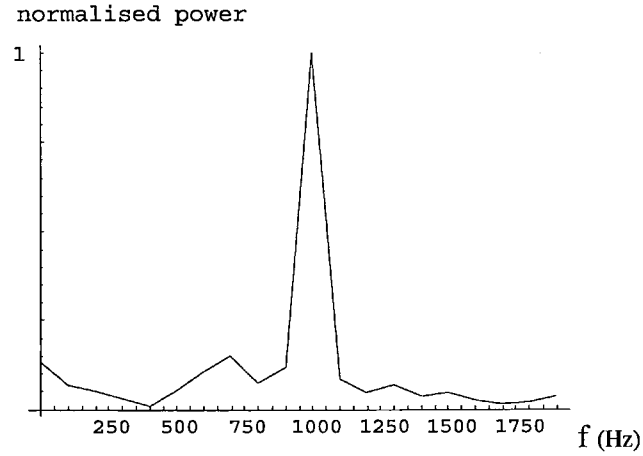

(iii) FFT for 400 MHz sweep
(Δf = 1000 Hz)

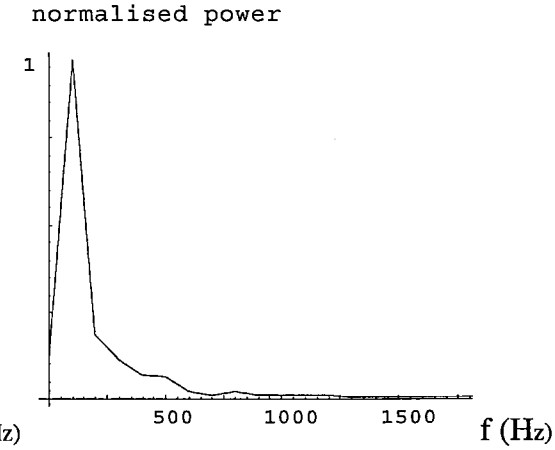

(iv) FFT for 40 MHz sweep
(Δf = 100 Hz)

Figure 6.14 Time and frequency domain plots of waveform sampled during T_{sweep}.

Since the frequency resolution ($f_{res\text{-}FFT}$) of the FFT is the reciprocal of the duration of the time domain file (or, the duration of the observation):

$$f_{res\text{-}FFT} = 1/T_{sweep} \tag{6.4}$$

we have

$$f_{res\text{-}FFT} = 100 \text{ Hz} \tag{6.5}$$

Using this frequency resolution, the corresponding range resolutions - from equ.(6.1) - are shown in Table 6.2 below:

sweep bandwidth (MHz)	Δf (Hz) per m. range	r_{res} (m)
400	267	0.374
40	26.7	3.74

Table 6.2 Frequency and range resolution for wide and narrow band sweeps

Thus, using the basic FFT resolution as the criterion for range resolution, the narrow band range resolution in Table 6.2 is greater than the actual transponder range. While there is a small uncertainty introduced by not including the system calibration term, the situation is consistent with Figure 6.14 (ii) which shows that less than one cycle of Δf occurs during the observation. These results and observations have been included to emphasise that the FFT "resolution" given by the reciprocal of the time domain waveform duration does not lead to an inherent limit on range resolution, since there is information content in the measurement even where less than one cycle of the difference waveform (e.g. Figure 6.14 (ii)) is observed.

Minimum range and frequency resolution.

It has been shown that below a certain range, where Δf and $1/T_{sweep}$ are equal, less than 1 cycle of the difference frequency Δf occurs during the period of the observation. We may define this range as r_{equ}. Since the sweep bandwidth is

$$B = F_{stop} - F_{start} \tag{6.6}$$

and

$$\Delta f = \frac{B}{T_{sweep}} \frac{2 r_{equ}}{c} = \frac{1}{T_{sweep}} \tag{6.7}$$

then

$$r_{equ} = \frac{c}{2B} \tag{6.8}$$

This range is sometimes interpreted as the *minimum* range at which FM radar will operate, or as the quantisation error range when the frequency measurement is performed using a cycle counter [7]. However, since there is still information content in a partial cycle of Δf - as indeed is seen in the narrow band sweep of Figure 6.13 (ii) and Figure 6.14 (ii) and (iv) - a measurement can still be made. For this reason the range r_{equ} is used here to describe the range at which the period of the Δf waveform and the duration of the observation reach *equivalence* but not as an inherent minimum range or error.

6.2.6 Effect of Sweep Period.

Sweep periods of 10 ms to 100 ms have been demonstrated as a matter of convenience for use with the laboratory synthesised source. To maximise the duty cycle of the measurement, the sweep time should be large compared to time-of-flight to the target since this minimises the time $T_{overlap}$ where the mixing product Δf should be ignored. (see Figure 6.5). For the short distances used in the laboratory, (around 5 m.) the time-of-flight is the order of 30 ns and so the sweep period has always been much larger than this value. While this criterion would need re-assessing for measurements at much greater distance, such as a maritime system which is discussed and dimensioned in chapter 7, faster sweep rates may be investigated in the laboratory. The effect of faster sweep rates on the time domain waveforms illustrated in the above results would only result in a re-scaling of the time axis, and would not change the resolution of the measurement.

Increased-sweep rates.

Sweep times below 10 ms could be generated in the laboratory by using the synthesiser with an external sweep generator. This implies driving the source in a mode which is not phase-locked, hence it is behaving more like a frequency modulated VCO than a fully synthesised source, although this has little practical bearing on the measurements beyond an expected increase in phase noise. An important implication of this mode of operation is that the sweep is now sinusoidal rather than linear, since a sinusoidal external source was used. Figure 6.15 shows time domain waveforms for a 1 ms sweep where the range to the transponder is 5.2 m.

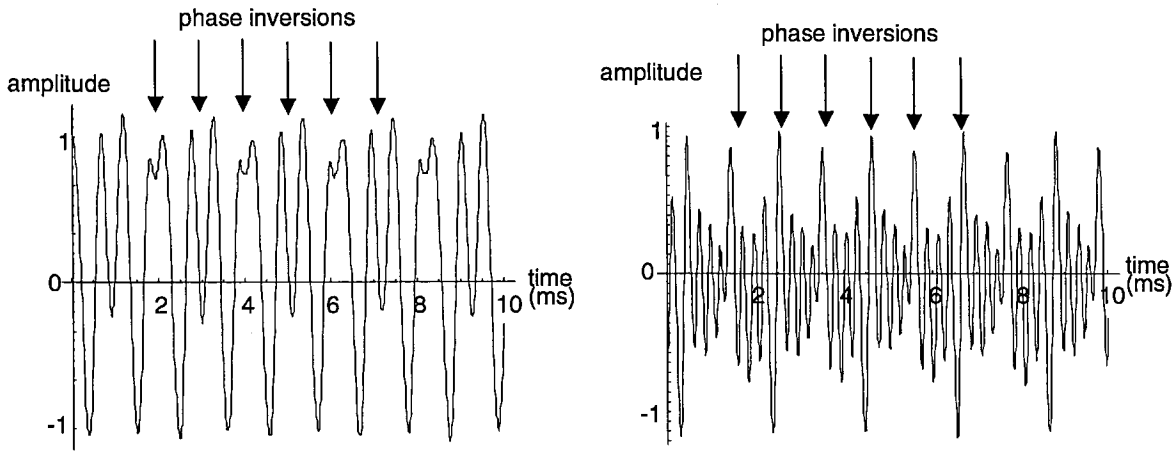

(i) 40 MHz bandwidth

(ii) 100 MHz bandwidth

Figure 6.15 Time domain waveforms, 1 ms external sweep, range = 5.2 m.

In the measurements of Figure 6.15, the phase inversions which occur every cycle of the external generator have been marked. The non-constant amplitude of the Δf waveform, which is expected to be sinusoidal, is particularly apparent in case (ii) since the greater sweep bandwidth gives rise to more cycles of Δf during the sweep. This contrasts with the approximately constant amplitude envelope apparent for the linear sweeps of Figure 6.8, Figure 6.10, Figure 6.11, and Figure 6.14. As discussed in section 6.2.1 and in [5], for the sinusoidal sweep, the frequency component Δf is no longer a single value and would need to be averaged over the sweep to yield the correct term for range.

6.2.8 Incoherent Detection.

While coherent detection is convenient for short range measurements in the laboratory, and facilitates the exploration of a wide range of transponder modulation schemes, the coax link between transponder and transceiver is not suitable for many practical applications. While this may be obviated by a carrier recovery stage at the receiver, an incoherent detection method is a more simple solution. This is basically a bandpass filter centred at the fundamental modulation frequency (which is here a monotone square wave) followed by an envelope detector whose output is the beat frequency between the two sidebands. This system is effectively the "collision avoidance radar" reported by [8], although this reference describes a co-operative target with a single radiating element, which imposes a very minimal radar cross section and hence range of operation.

This beat frequency captured by the detector is thus 2 Δf. This method is less energetically efficient than coherent detection since only the energy of the first (upper and lower) sidebands are captured. The energy in the harmonics of the modulation signal is lost.

Typical waveforms using an incoherent detector are shown in Figure 6.16 below, where a 3.0 MHz modulation frequency was used at the transponder. Here, the RF sweep was from 9.0 to 9.4 GHz with a sweep time of 50 ms. The time domain data is a 5000 data point extract from the 8192 point file recorded from a digital storage oscilloscope.

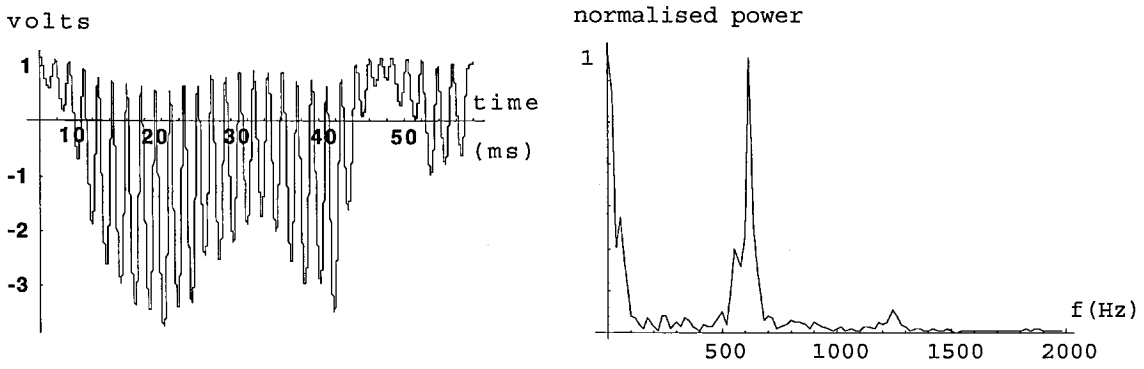

(a) time domain (b) frequency domain

Figure 6.16 Typical beat frequency waveforms using incoherent detector
f_{mod} = 3.0 MHz, r ≈ 5 m.

The envelope of the beat frequency waveform suffers considerable amplitude variations. Some variation is also observed in coherent measurements, particularly at greater distances where multipath effects lead to frequency selective fading during the RF sweep (see following section and *Discussion of results at extended range*). However, most of the amplitude variation in the incoherent measurement is inherent to the particular detector which was used. Additionally, the FFT in Figure 6.16 (b) above indicates a high DC and low frequency content, which demonstrates that the detector was not correctly optimised. Despite the limitations of the incoherent detector which was available, a very clear frequency peak is observed at ~ 600 Hz, which is the expected result of 2 Δf. This is confirmed by results for the coherent case shown in Figure 6.18 below where range was close to 5 m.

6.3. Signal Processing for Increased Measurement Resolution.

Without attempting at this stage a comprehensive review of signal processing techniques for frequency measurement, techniques for increasing frequency and thus range resolution appropriate for this application will be considered.

6.3.1. Data Padding

The above examples of Figure 6.14 illustrate the range resolutions achievable using the inherent FFT resolution. Frequency resolution may be increased for example by padding the sampled data files from Figure 6.14, thus increasing the period of the time domain data file. This process is the equivalent to interpolating between the discrete spectral lines of the FFT of the initial time domain waveform [9]. Figure 6.17 below shows the effect of padding with 3 K samples of zeros before and after the time domain data of Figure 6.14 (i) and (ii)

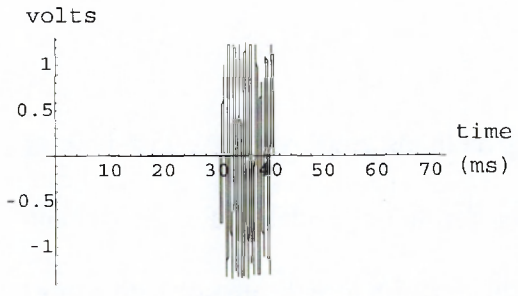

(i) 400 MHz sweep, padded data

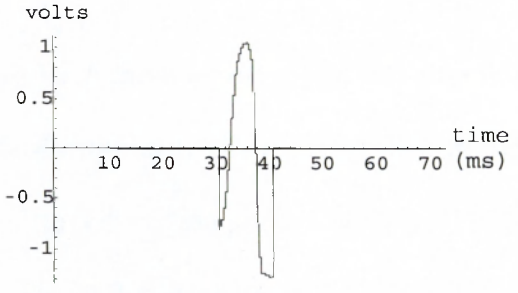

(i) 40 MHz sweep, padded data

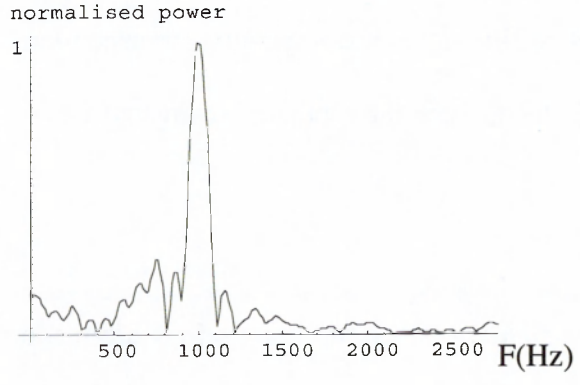

(iii) FFT, 400 MHz sweep

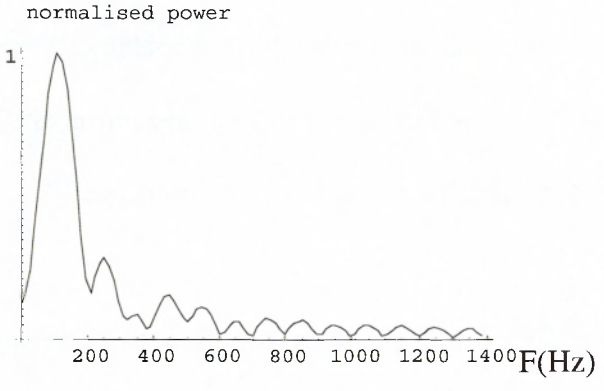

(iv) FFT, 40 MHz sweep

Figure 6.17 Simple signal processing techniques for increased frequency resolution.

The five-fold increase in the length of the time domain data files leads to a corresponding five-fold increase in frequency resolution. Hence the new frequency resolution is 20 Hz and the new range resolutions are as shown in Table 6.3.

sweep bandwidth (MHz)	Δf (Hz) per m. range	r_{res} (m)
400	267	0.075
40	26.7	0.75

Table 6.3 Range resolution following data zero padding (2 x 3 K)

Clearly the increased range resolution is at the cost of an increased processing burden, while for a fixed processing burden, range resolution is always improved by adopting a wider sweep bandwidth.

6.3.2. FFT Versus Parametric Spectrum Analysis.

Power spectrum density is usually determined using methods employing the fast Fourier transform (FFT) which is computationally efficient for a large class of time domain signals. However, the FFT approach suffers inherent performance limitations, the most prominent being frequency resolution, which is limited by the reciprocal of the duration of the time domain sampled data. In this study, we are concerned with exploring the resolution obtainable in the FM method for range finding to a co-operative transponder. Hence a number of alternative spectral analysis techniques have been investigated using experimentally derived time domain data.

The FFT based methods are often termed *nonparametric* since no assumptions are made about how the data were generated. The primary alternative to the FFT methods are hence termed *parametric*. [10] gives a mathematical review of a number of parametric methods, many of which are based on auto regressive (AR) and moving average (MA) techniques and claimed improvements in frequency resolution are demonstrated in this text. [11] gives further background into the parametric techniques.

Since the *Matlab* signal processing toolbox provides a readily accessible implementation of a number of parametric analyses, the experimental time domain data were processed by a number of these available routines, primarily the Burg method [10],[11], in an exploration of the resolution of the frequency measurement. These results were then compared with FFT based methods of the author's devising which involved data padding to obtain extended time domain files followed by FFT. As described below, the frequency domain data thus derived was subject to a frequency peak search, then a curve fit to the peak and maximum search so as to estimate the spectral peak.

Results.

Again using a sweep bandwidth of 400 MHz (9.0 to 9.4 GHz) and a sweep duration of 50 ms., three time domain measurements were recorded using the digital storage oscilloscope. The data length was 8192 samples and the sampling frequency was 100 kHz. The useful time domain data was extracted from the 5000 points which correspond to the 50 ms sweep duration.

Using the DSO as a frequency estimator, the FFT function on the DSO is limited to a frequency resolution given by the reciprocal of the duration of the time domain file, which is in this case $\frac{8192}{100\ 10^3}$ hence the instrument's frequency resolution is = 12.2 Hz. The frequency ramp gives rise to Δf = 53 Hz/m thus the 12.2 Hz frequency resolution corresponds to a range resolution of $\frac{12.2}{53} = 0.23\,\text{m}$

Clearly, to improve on this range resolution, we must adopt a method of spectral analysis which exceeds the frequency resolution of the basic FFT algorithm, as discussed above. Simply increasing the duration of the measurement, beyond T_{sweep} results in many frequency ramp cycles being included in the time domain file, which precludes the

preferred technique of selecting the data from a single sweep only and would also lead to a decrease in the available update rate of the measurement.

The following three measurements used range increments of 10 mm and 100 mm to act as test cases for range resolution below the basic FFT limit of 230 mm.

The first measurement corresponded to a range $r_1 = 5.18$ m, thereafter:

$r_2 = r_1 + 10$ mm hence $\Delta f_2 = \Delta f_1 + 0.53$ Hz , and

$r_3 = r_1 + 100$ mm hence $\Delta f_3 = \Delta f_2 + 5.3$ Hz

The corresponding time domain data are shown in Figure 6.18. The first 30 points of the corresponding FFTs are shown in Figure 6.19, which illustrates the coarse nature of the basic frequency resolution and that the small range increments are thus not resolved.

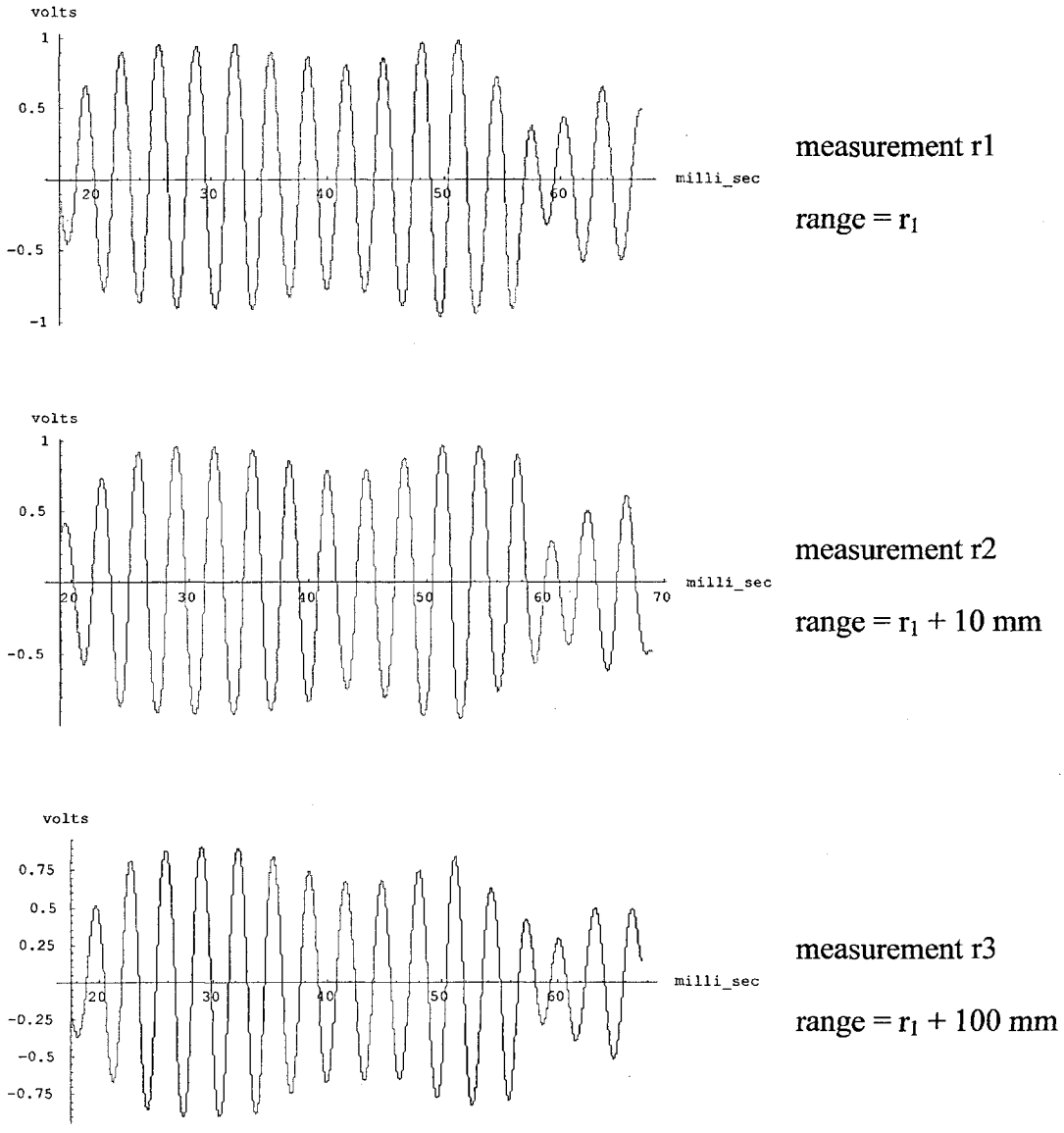

Figure 6.18 Time domain waveforms for difference frequency; small range increments.

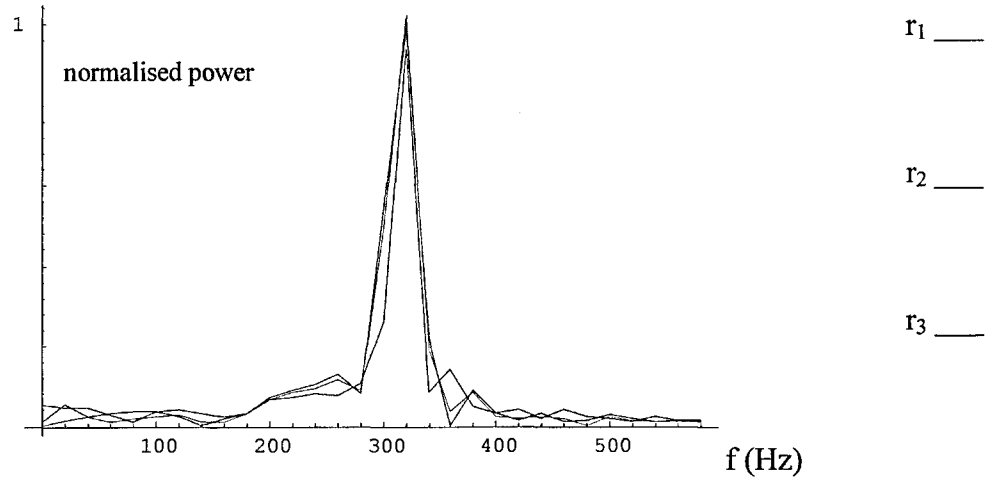

Figure 6.19 FM range measurement using coarse FFT; small range increments

Parametric Spectrum Analysis

The *Matlab* Burg power spectrum analysis routine was employed using the 5000 point time domain sampled data as input. The other parameters required as input are the order p of the AR model and the number of data points n in the output file. The spectral peaks generated by the Burg routine for each of the 3 measurements are listed in Table 6.4 below for various values of p and n.

	Δf (r_1)	Δf (r_2)	Δf (r_3)
$p = 4$, $n = 16$ K	311.28	311.28	311.28
$p = 8$, $n = 16$ K	317.38	317.38	317.38
$p = 2$, $n = 16$ K	317.38	317.38	317.38
$p = 4$, $n = 2$ K	292.97	292.97	292.97

Table 6.4. Results for *Matlab* Burg spectrum analysis.

The above results clearly show that the *Matlab* Burg spectrum routine is failing to resolve differences in the spectral content of the 3 time domain files for measurements r_1, r_2 and r_3. This result necessitated a different approach for fine measurement resolution, which is described in the following section.

Padded FFTs

This approached has been introduced in section 6.3.1 and will be extended so as to investigate the suitability of the technique for resolving the 10 mm and 100 mm range increments. On padding the time domain data files with 48 K of zeros, and recalling that the sample interval is 10^{-5} s, the new frequency resolution derived from the new file duration is:

$$\text{fres} = \frac{1}{(5+48)10^3\ 10^{-5}} = 1.887 \text{ Hz}$$

hence we would expect to resolve r_3 from r_1, being a 5.3 Hz shift, but might not expect to resolve r_2 from r_1, being a 0.5 Hz shift. However, the corresponding FFTs for the padded data, shown in Figure 6.20, reveal that measurement increment of r_2 is just resolvable to the eye, while measurement r_3 is clearly resolved. The measured frequency can be accurately converted to a range following the system calibration which is discussed below.

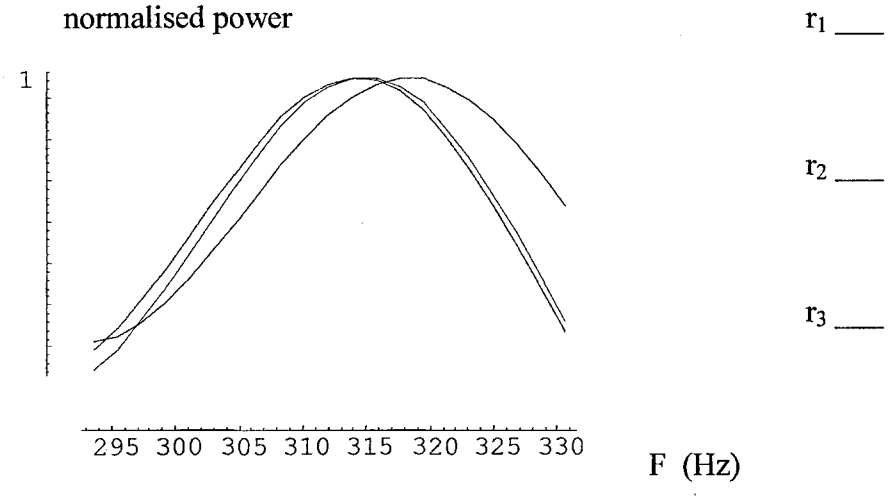

Figure 6.20 Padded data FFTs – Retro-array FM range measurement.

6.3.3 System Calibration.

The path lengths of the transceiver RF components before the RF mixer add a constant offset (or error term) to the measurement of difference frequency. A further term is introduced by the path length (or lengths, as discussed above) in the retro-reflector target. Hence zero metres range does not necessarily give rise to zero Hz difference frequency. Whilst it would be straightforward, if tedious, to add or subtract from cable lengths to remove this term, a better solution is a calibration of the system. This involves comparison with another range sensor – a tape measure in the simplest case. Plotting difference frequency against range yields a straight line, whose gradient is a function of the FM ramp:

$$\frac{\partial f}{\partial r} = \frac{B}{T_{sweep}} \frac{2}{c} \tag{6.9}$$

and whose y-intercept is the constant calibration term i.e. Δf when range is zero. Five measured data points with their linear fit are plotted in Figure 6.21 below.

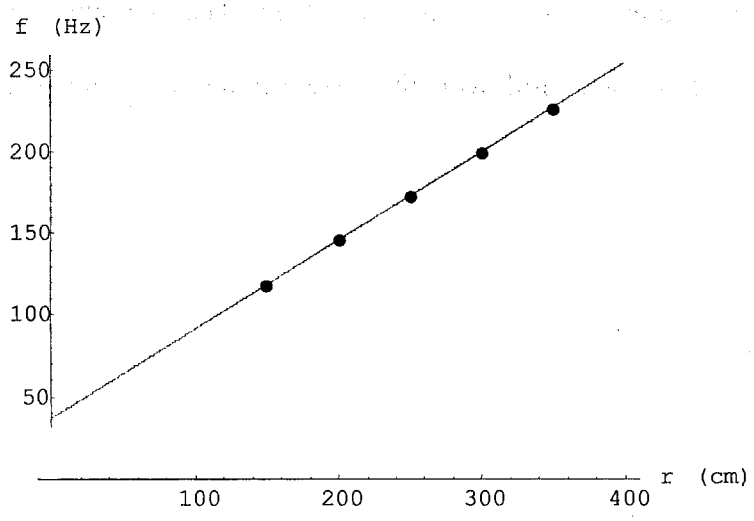

Figure 6.21 Calibration data (•) with linear fit (—).

The linear fit for the above data, derived from a *Mathematica* program, is:

$$\Delta f = 36.96 + 0.54\, r \qquad (6.10)$$

where r is given in cm, and Δf is in Hz.

However, for the 400 MHz sweep of 50 ms duration, the gradient for frequency versus range is known to be 0.5333 Hz / cm. Substituting this value and re-arranging gives:

$$r = \frac{\Delta f - 36.96}{0.5333} \qquad (6.11)$$

applying this result to the difference frequencies listed in the 2nd column of Table 6.5. yielded the ranges in the 3rd column.

A flow chart summarising the stages of the measurement method is shown in Figure 6.22.

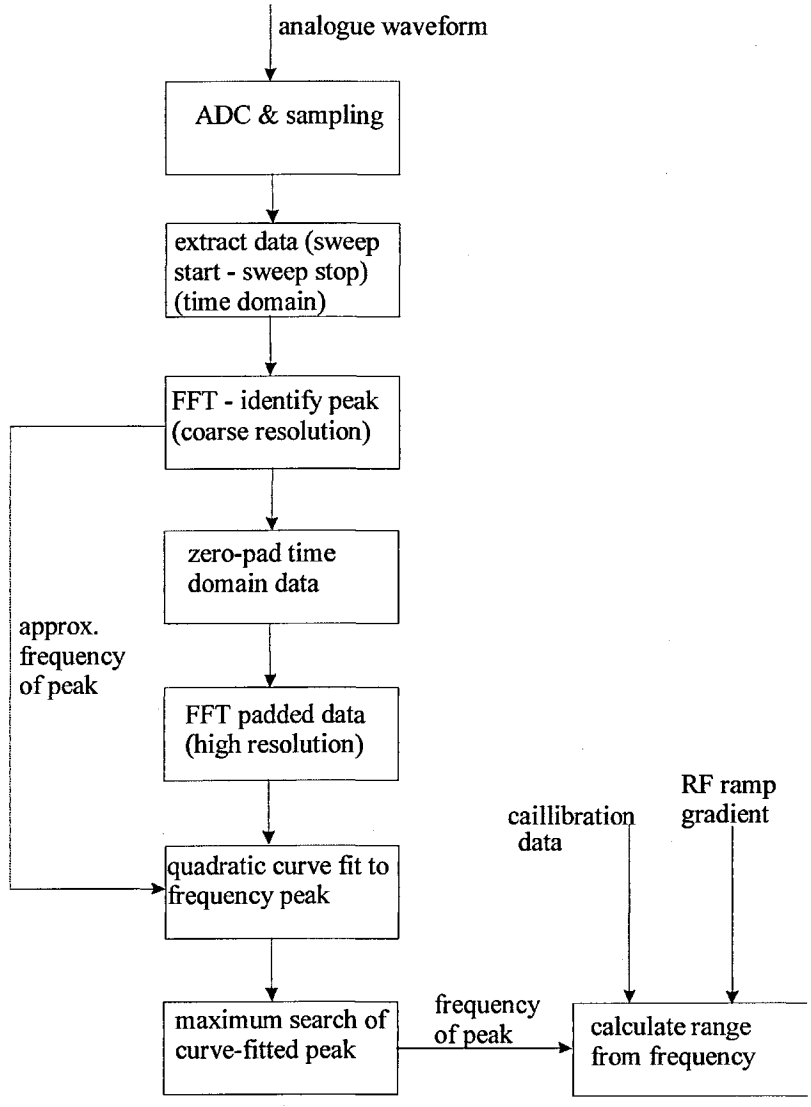

Figure 6.22. FM range measurement and signal processing flow chart

6.3.4 The Unequal-line-length Retro-array in High Resolution FM Range Measurement.

Of particular interest was whether the unequal line length geometry of the retro-array would lead to a splitting of the measured spectrum into discrete frequencies corresponding to the different transmission line lengths, or perhaps as a general broadening of the spectrum. To investigate this effect, FM range measurement to an equal line length retro-array would provide data for comparison, where no line splitting would be expected. As an alternative, a modulated antenna such as that discussed in chapter 4 (see section 4.3.2) could be used, since this structure also would not introduce different path lengths. The

three measurements were repeated for the modulated antenna and the results did not show an effect, the FFT after padding (Figure 6.24) very closely resembling that of the retro-array case. The 3 measurements begin with measurement r_4 at 5.64 m, with r_5 and r_6 being increments of 10 mm and 100 mm respectively.

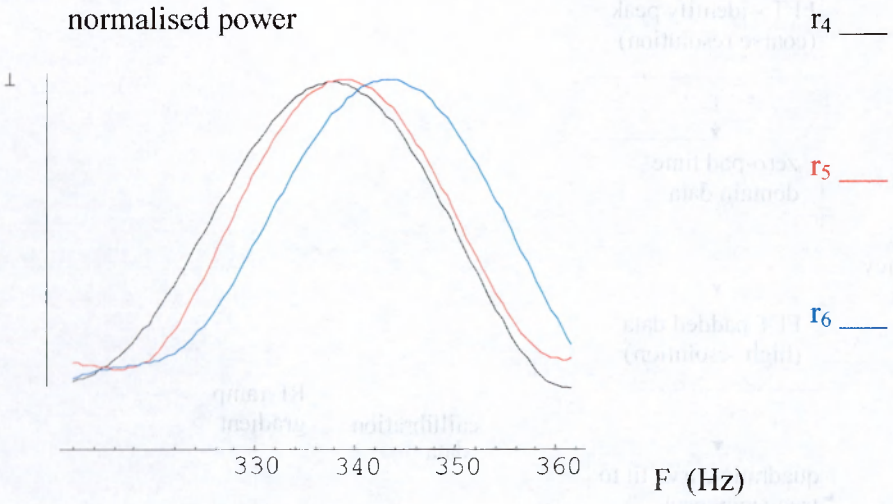

Figure 6.23 Padded data FFTs – modulated antenna FM range measurement.

On attempting to further increase the resolution in both cases (unequal-line-retro-array and antenna) with additional zero-padding, resolution increases were not observed. Hence, the expected line splitting by the unequal-line-retro-array could either (i) not be resolved using the measurement and analysis techniques described or (ii) be masked by the inherent spectral broadening in the measurement system. The latter is the better interpretation of this set of experimental results, since if the information content pertaining to spectral splitting did occur in the time domain data, sufficient padding and hence FFT resolution should make it visible. Since it did not, we may assume that the information content is not present, being lost in the phase noise of the system. It is suggested that contributions to the smearing of the measured spectrum, (which is here being measured to ~ 1 Hz resolution) are chiefly the phase noise of the RF source and the effects of multipath propagation.

Curve fitting routines may be exploited to better identify the peaks in Figure 6.20 and Figure 6.23 . To this end, a *Mathematica* quadratic curve fit routine was exploited for each of the 20 data points in the plots. A maximum search function then identified the corresponding frequency for the centre of each peak, as tabulated in Table 6.5 below.

measurement no.	curve fit maximum search (Hz)	calculated range (cm)
r_1	313.283	518.13
r_2 (r_1 + 10 mm)	313.986	519.46
r_3 (r_1 + 100 mm)	317.718	526.45
r_4	337.536	563.62
r_5 (r_4 + 10 mm)	338.230	566.1
r_6 (r_4 + 100 mm)	342.788	573.46

Table 6.5 Curve fit maxima results.

Following calibration of the system (described above) it was possible to calculate the range between transceiver and transponder as tabulated in the third column of Table 6.5. On inspection of the calculated ranges we observe that the 10 mm increment was measured as 13 mm for both retro-array and antenna targets, while the 100 mm increments were measured as 83 mm (hence 17 mm error) and 98 mm (2 mm error). We may thus observe that while 10 mm increments may be *resolved*, the *accuracy* of the measurement is subject to errors of up to 17 mm over a range of approximately 5 m, which represents a 0.3 % error.

A more thorough, statistical analysis of system error could be performed by making a much greater number of measurements which would form a statistically representative sample. However, it was thought that such a study would not be of great interest at this stage and it was preferred to explore measurements to transponders at increased ranges.

6.4 Accuracy, Resolution and Example Measurements at Extended Range.

In the above examples, digital processing methods for increasing range resolution have been explored. While the absolute accuracy of the measurement has not been demonstrated with a precision beyond a simplistic comparison with the accuracy afforded by a tape measure, *increments* in range may be more easily measured, and have suggested system errors up to 17 mm or 0.3 %.

To explore the accuracy and resolution of the prototype measurement system at extended ranges, a larger laboratory was used which offered ranges up to 16 m. In this case, the measurement accuracy offered by the tape measure, which is unknown, is likely to be worse than the 10 mm resolution offered by the microwave system. For example, a 0.5 % error in the tape measure reading at 16 m. is 80 mm. While the study could be made more comprehensive by adoption of a third sensor (e.g. laser), such a sensor was not available, and a detailed statistical study of the errors incurred by use of the tape measure is not likely to be particularly enlightening in the context of the present work. Also, the high linearity offered by the synthesised sweep generator allows confidence in the linearity of the measurement of range, and further calibration terms ought not to be necessary. It should also be added that part of the motivation for the development of the FM ranging system was as a solution to real engineering applications such as vehicle tracking and control systems. Typical specifications for marine tracking systems, for example, require accuracy and resolution better than 1 m. This sought accuracy is typically an order of magnitude better than that offered by a competing technology such as differential GPS. Therefore, the preferred direction for the work at this stage was the demonstration of measurements at increased ranges of operation. A summary of indoor measurements, including oblique transponder illumination angles, are next presented.

Range measurements at approximately 16 m:

The measurements for the microwave system were derived using the methodology described above, i.e. zero padding (48 K), FFT, identification of major peak, curve fit to major peak and maximum search. Range was then derived from the difference frequency Δf using equation (6.10). The results are summarised in Table 6.6 below. All measurements were made with the phase-modulated retro-reflector transponder on boresight with the exception of the final example, measurement r_{11} where the transponder was rotated to 75 degrees from boresight in the E-plane. Horizontal linear polarisation was used throughout.

measurement no.	approx. range, tape measure (cm)	range, microwave system (cm)
r_7	1600 (accuracy not demonstrated)	1596.6
r_8	r_7 - (10 cm ± 0.2 cm)	1585.8 (10.8 cm increment from r_7)
r_9	r_7 - (100 cm ± 1 cm)	1496.6 (100.0 cm increment from r_7)
r_{10}	1580 (accuracy not demonstrated)	1588.4
r_{11}	as r_{10}, transponder at 75°	1589.6

Table 6.6 Measurements at extended range.

Discussion of results at extended range.

As discussed above, the accuracy of the tape measurement has not been demonstrated. However, small increments between measurements can be made with a better control of the accuracy, as tabulated above. It is apparent in this group of measurements that the microwave system is highlighting errors in the tape system rather than *vice versa*. In particular, the increments of 10 cm and 100 cm are very accurately tracked, having 8 mm error at worst – which compares favourably with the worst error of the previous group of measurements, which was of 17 mm at around 5 m - while the agreement in absolute range is not always good, particularly in case r_{10}. Also, the final measurements shows a

difference of just 12 mm when the 75° rotation is applied at fixed range. The time domain files for these measurements (r_{10} and r_{11}) are shown in Figure 6.24 to illustrate the reduction in the signal level compared to the noise floor. The entire 8192 point data file is included, with arrows marking the start and stop points of the RF sweep.

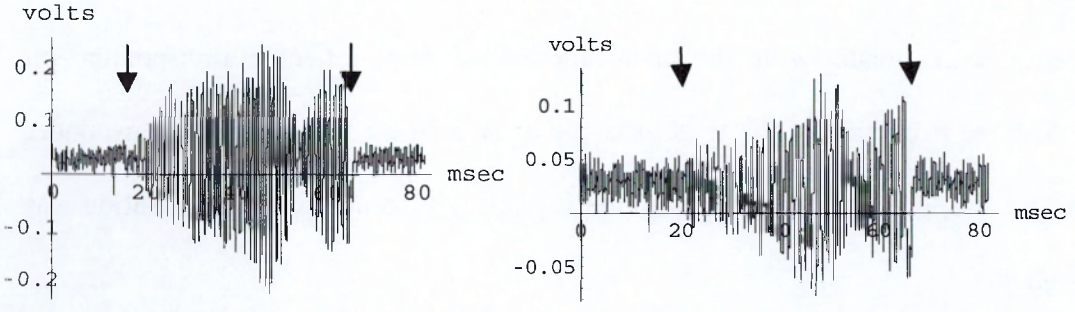

(a) Transponder on boresight (b) Transponder at 75°

Figure 6.24 Time domain data for FM range measurement at 1589 cm ± 0.6 cm

It is also interesting to compare the time domain plots of Figure 6.24 with those of Figure 6.18. Clearly, the period of the waveform is reduced in accordance with the increase in the frequency measured. Also, in both cases, the amplitude of the waveform is subject to much variation. These variations are due to the RF frequency response of the system between 9.0 GHz (first arrow in Figure 6.24) and 9.40 GHz (second arrow in Figure 6.24). Since the 400 MHz sweep corresponds to the 10 dB RF bandwidth of the transponder and approximately to that of the transceiver RF front end, the amplitude variations are caused primarily by the environment. That is, frequency dependent multipath interference results in fading at certain RF frequencies in the sweep. It is apparent that these effects are more pronounced when the range was increased in the larger laboratory, and vary depending on the position of the transponder. To illustrate these variations the time domain files for measurements r_8 and r_9 and presented in Figure 6.25. Interestingly, the positional increment of 90.2 cm results in both a differently shaped voltage amplitude envelope and also a factor of 2 in the maximum magnitude. Since the only change is in the location of the transponder with respect to the transceiver *and environment*, this observation suggests a new possible

application for the measurement system – that of a multipath probing sensor. It is worth noting that retro-directive arrays have previously been mooted as multipath sensors - [14] examines the use of an active (amplified, but not modulated) retro-array as a "probe" in a multipath environment.

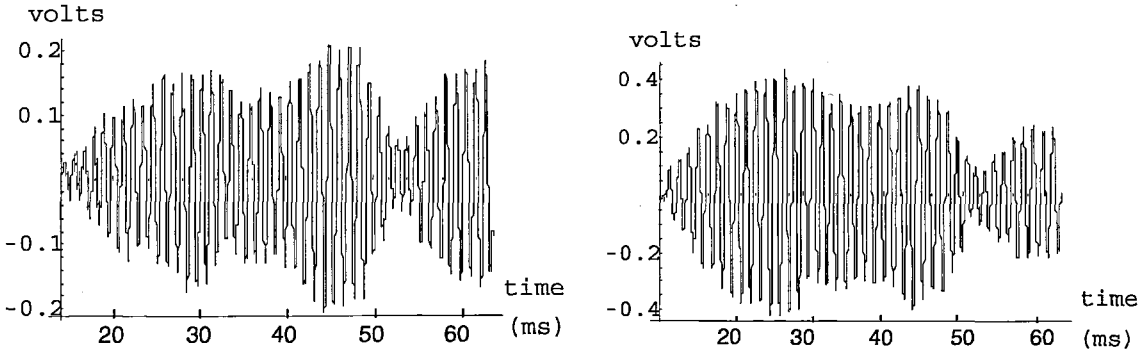

(a) measurement r_8 (b) measurement r_9

Figure 6.25 Time domain waveforms for FM measurement demonstrating differing amplitude envelopes.

6.5 Efficient Frequency Estimation Algorithms.

The signal processing technique, as summarised in Figure 6.22, has been very successful at exploring the limits of range resolution in the laboratory. However, it is not necessarily the best approach for a real-time measurement system, since the computational load, particularly of the zero padding, is excessive compared to other algorithms. The added 48 K of data zeros is almost ten times the length of the original sampled data, whereas a factor of 2 - 4 is considered sufficient [15] for "coarse" frequency estimation i.e. the stage of identifying the spectral peak. "Fine" frequency estimation is often performed using a quadratic fit such as described above, while more computationally efficient methods include a dichotomous search of the spectral peak [16]. This is another means of interpolating between the discrete spectral lines of the FFT, which can be combined with parabolic interpretation to reduce computational load by 88 % [17] compared with parabolic interpolation alone.

6.6 Signal-to-noise-ratio Improvement

The primary advantage of the modulated scatterer method is the ability to perform a radar type measurement while (almost) totally rejecting clutter. Considering thermal noise, the signal to noise ratio is unchanged, but it is more meaningful to consider the ratio of signal to the sum of thermal noise and clutter (SNCR) . In this case, the improvement may be expressed by considering the SNCR for the cluttered measurement is:

$$\mathrm{SNCR} = \frac{P_{signal}}{P_{noise} + P_{clutter}} \tag{6.12}$$

while the SNR for the uncluttered measurement (i.e. with modulation) is:

$$\mathrm{SNR}_{\mathrm{mod}} = \frac{P_{signal}}{P_{noise}} \tag{6.13}$$

hence the ratio of the above is

$$\frac{\mathrm{SNR}_{\mathrm{mod}}}{\mathrm{SNCR}} = 1 + \frac{P_{clutter}}{P_{noise}} \tag{6.14}$$

Considering that the thermal (bandwidth limited) noise P_{noise} is fixed for a given measurement, (6.14) is dependent on the severity of the clutter term and can take any value from 1 upwards.

6.7 Range Measurement Conclusions.

The FM range method here considered differs from most conventional radar techniques in that a modulated scatterer is employed, thus effectively rejecting clutter from the measurement. In itself a known technique [8], it has not found wide application since the scatterer, i.e. the transponder, has previously not been realised as a multi-element target such as a retro-directive array. Thus the severe limitation to link budgets has limited the range of useful applications. This work extends the technique to include retro-reflector transponders and therefore opens up the possibility of high resolution range measurement to co-operative targets over greatly increased distances compared to the single element scatterer configuration. Indeed, a practical demonstration of the maximum range of useful operation for the prototype transponders would have required a larger measurement range than was available.

A cyclic experimental approach has successfully demonstrated that 10 mm range increments may be resolved using modest signal processing techniques. While conventional high resolution parametric spectral analysis was found lacking in this application, tailored variants of FFT based analysis, combined with curve fitting, enabled range resolution below the inherent FFT limit (the reciprocal of the duration of the sampled data). The signal processing method demonstrated that range resolutions of 10 mm were achievable using a 400 MHz sweep, at ranges of about 5 m where the signal-to-noise-ratio was very high. Incremental measurements demonstrated an accuracy of 1.7 cm in this case.

On increasing the range to around 16 m. incremental range measurements were shown to continue to be accurate to within this 10 mm tolerance (i.e. 8 mm.) while overall range accuracy exceeded that of the alternative method available i.e. the tape measure. On

rotating the transponder to 75° at the 16 m. range, the measurement was consistent to 12 mm despite the reduction of signal to noise ratio, which from Figure 4.5 (RCS versus angle) would be estimated at 8 dB. A more thorough statistical approach to parameterising resolution and accuracy would require a much larger number of experimental observations. The results described should therefore be regarded as qualitatively representative of the measurement system in its indoor environment.

The use of modulated microwave retro-reflectors as transponders in a range measuring system would appear to represent an excellent application for their useful properties. Many applications could be envisaged, and some of those which have been mooted are: automotive collision avoidance, aircraft landing aids including ad-hoc airfield and covert landing system, airport localisation and decision aids, maritime docking sensors, and precise vehicle guidance in general.

References.

[1] "Introduction to Radar Systems", (2nd. ed.) M. I. Skolnik, *McGraw-Hill Inc.* 1980.

[2] Ref [1] pp. 53 - 54

[3] "An algorithm for calculation of range in a multiple PRF radar", S. A. Hovanessian, *IEEE Trans* Vol. AES-12, pp. 287 - 290, March 1976.

[4] "Spread Spectrum Systems with Commercial Applications", R. C. Dixon, *Wiley*, 1994, pp. 3 - 15.

[5] "Frequency Modulated Radar", D. G. C. Luck, *McGraw Hill*, 1949

[6] Ref [1] p. 83

[7] Ref [1] pp. 86 - 87.

[8] "Microwave Homodyne Systems", R. J. King, 1978, *Peter Peregrinus Ltd. on behalf of IEE.* pp 344 - 346

[9] "Handbook for Signal Processing, S. K. Mitra, J. F. Kaiser, *Wiley*, 1993. pp.1146 - 1150.

[10] "Introduction to Digital Signal Processing." J. G. Proakis, D. G. Manolakis, *Macmillan Publishing* 1989. Chapter 11.

[11] "Spectrum Analysis – A Modern Perspective", S. M. Kay, S. L. Marple, *Proceedings of the IEEE* Vol.69, No.11, November 1981

[12] "Array Signal Processing", edited by S. Haykin, *Prentice-Hall* 1985

[13] "Digital Signal Analysis", Bruel and Kjaer Technical Review August 1981, pp. 121 – 152

[14] "Use of an active retrodirective antenna array as a multipath sensor", S. L. Karode and V. F. Fusco, *IEEE Microwave and Guided Wave Letters*, Vol.7, No. 12. December 1997.

[15] "Further results in the fast estimation of a single frequency", M. P. Fitz, *IEEE Transactions on Communications*, vol 42, 1994, pp. 862 - 864.

[16] "Frequency estimator with dichotomous search of periodogram peak", Y. V. Zakharov and T. C. Tozer, *Electronics Letters* 16th Sept. 1999, Vol 35. No. 19, pp 1608 - 1609.

[17] "DFT-based frequency estimators with narrow acquisition range", Y. V. Zakharov, V. M. Baronkin and T. C. Tozer, *IEE Proceedings on Communications*, Vol. 148, No. 1, Feb 2001

Chapter 7.

Case Studies for Dimensioning Retro-reflector System Applications.

The work reported in the preceding chapters has introduced the rationale for developing modulated microwave retro-reflectors and described in some detail methods for their design and fabrication. A quantity of measured data for modulation spectra have been reported, as have general models for predicting their aperture efficiencies. The evolution of a range finding measurement has been reported in some detail. Throughout the preceding chapters a wide variety of possible applications have been alluded to - these might be classified, somewhat arbitrarily, into communications applications and radar applications, while it is hoped that a particularly important feature would be a combining of both these characteristics. Thus while communications applications may include point-to-point links (for example telemetry to a robotic or an autonomous vehicle), and radar applications may include vehicle guidance and collision avoidance, it should not be overlooked that these applications can be combined through a suitable choice of a sufficiently agile interrogating waveform.

In this chapter two of the more promising possible future applications will be discussed and the outline of the required system parameters will be presented. These will include a vehicle guidance system (a radar application) , and a link to a stratospheric platform (a communications application). While a very comprehensive analysis of each system is beyond the intended scope, it is the system dimensions - i.e. estimates of power budgets as a function of transponder size - which will be discussed along with the important and interesting features of each system.

7.1 A Maritime Range Finding System.

In chapter 6 a range finding system was discussed and a number of indoor experimental results were presented. The dimensions and link budget for a practical system will now be explored, with the emphasis on a maritime system where a transceiver is located on a vehicle and a transponder on some other target. It is likely that, for example, the vehicle is a ship and the target is some point of interest, such as a harbour entrance, jetty, or another ship. It will be important to consider the maximum range of operation from estimates of power and noise levels.

Another important feature of the system will include a multi-access scheme, whereby a number of transponders may be simultaneously interrogated. Also, the required spatial response of the transponder will present interesting implications for the means of its construction.

7.1.1 Link Budget.

The link budget encapsulates the received power and signal to noise ratio (SNR) as a function of many variables. These include the carrier frequency, transmitted power, antenna properties such as gain and the receiver noise figure. The link budget may be summarised by equation 7.1 for received power P_r, which is here expressed in dBm for a transmit power P_t in dBm.

$$P_r = 10\,\mathrm{Log}_{10}\left(m^2 0.66^2 \sigma \frac{\lambda^2}{(4\pi)^3 r^4} \right) + 2G + P_t \qquad (7.1)$$

In equation 7.1 the term m^2 accounts for the effect of a non-ideal modulation index, which is a ratio of voltages. The term 0.66^2 similarly accounts for the power associated with the first harmonic of the square wave which modulates the transponder RCS, since we assume that only the first harmonic is detected. Using these assumptions, the theoretical link

budget for the 16 element X-band retro-array of RCS 0.1 m^2 (see chapter 4) is compared with measured data in Figure 7.1. Here, the power in the first upper sideband was measured using a spectrum analyser connected to a dedicated receive antenna, as shown in Figure 2.9. The transmit and receive antennas gains were both 16 dBi, and an additional 2 dB system loss has been included as a very good estimate for combined transmission line, connector and pointing losses. Transmit power was 14 dBm and the carrier frequency 9.2 GHz.

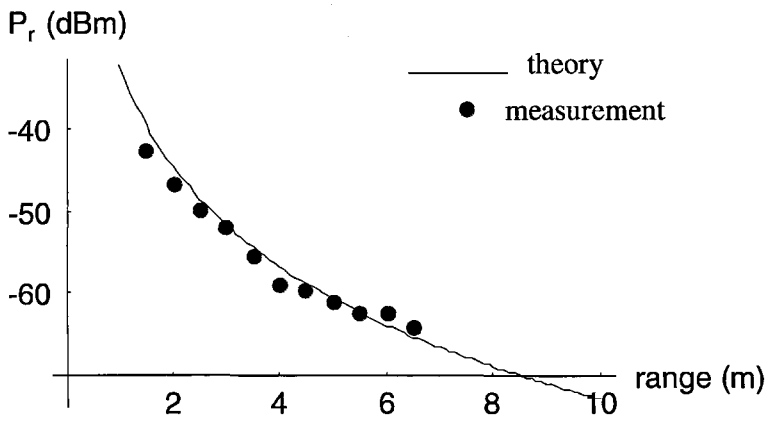

Figure 7.1. Measured and theoretical received power for 16-element X-band retro-array.

In Figure 7.1 the measured received power is very close to the theoretical case, although some data tend to deviate from the theoretical $\frac{1}{r^4}$ trend of the radar equation for free space. This effect is most likely due to the indoor measurement environment where the actual power incident on the transponder aperture tends to be perturbed by reflections and multi-path. These effects have also been discussed in chapter 6 (see section 6.4) where they were manifested as an amplitude envelope (of the difference frequency measurement in the FM sweep) which varied with the position of the transponder within the laboratory.

Returning to a link budget model for a maritime range finding system, reasonable estimates for parameters can be used, and predicted SNR may be plotted as a function of distance or

transponder dimensions. A centre frequency of 9.2 GHz will again be used. The proposed link budget parameters are listed in Table 7.1

parameter	**symbol**	**value**	**remarks**
centre frequency	f	9.2 GHz	common maritime usage. Prototype system reported.
transmit power	P_t	20 dBm	reasonable estimate (100 mW)
transceiver antenna gain	G	30 dBi	common, modest radar antenna
transponder radar cross section	σ	variable m^2	function of transponder size
transponder modulation index	m	0.9	ideally 1, allows for non-ideal phase modulators.
receiver noise figure	NF	6 dB	reasonable estimate
range	r	to be studied, e.g. up to 10 km	

Table 7.1. Link budget parameters for maritime system

Received power from equ. 7.1 is plotted in Figure 7.2 below, where the transponder RCS has been evaluated using equations 1.6 and 2.1, which relate RCS to the aperture gain. In this evaluation, the aperture gain is the sum of the gain of the antenna elements in the retro-array, and a gain of 4 dBi has been used. Estimates for transponder loss have not at this stage been included. In Figure 7.2 three cases for the number of antenna elements n have been included. When n =1, the transponder is a simple reflective tag rather than a retro-array. The other cases are n=16, chosen to be representative of the 16 element prototypes reported, and n=96 , which while to some extent an arbitrary value has been chosen to be a good compromise between transponder size and manufacturing complexity. Means of fabricating a 96 element transponder for maritime applications are discussed in section 7.1.2.

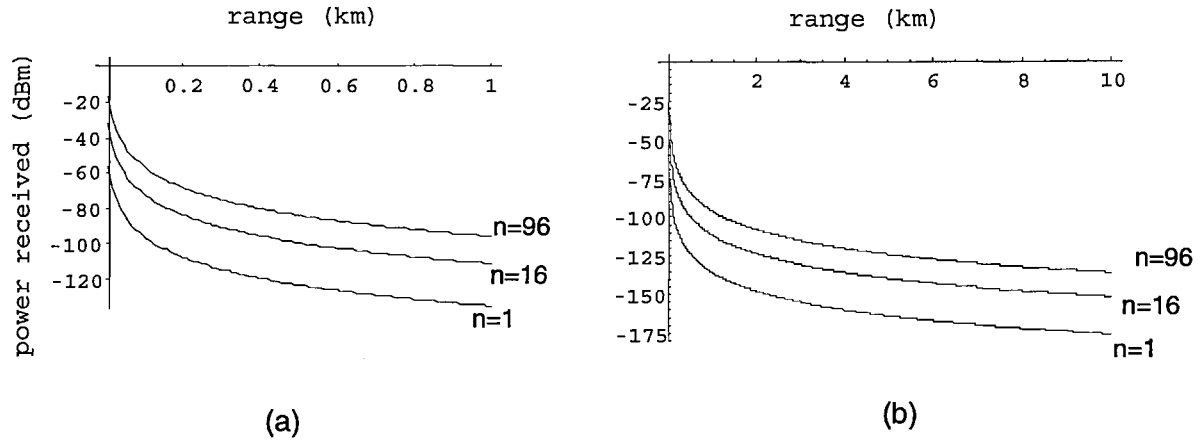

Figure 7.2 Basic link budgets for different numbers of transponder radiating elements. (a) up to 1 km range, and (b) up to 10 km range.

The results shown in Figure 7.2 have also been separated into a "short range" case (a) and a "long range" case (b), so as to help illustrate the very wide dynamic range which is a consequence of the $\frac{1}{r^4}$ free space loss term of the radar equation. The improvement in received power on increasing the transponder size is evident, and represents the primary advantage of the retro-reflector technique compared to the more simplistic approach of the single-element modulated scatterer such as described by the homodyne ranging system of [1]. The signal to noise ratio (SNR) should now be considered, and is given by :

$$\mathrm{SNR} = 10\,\mathrm{Log}_{10}\left(\frac{P_r}{k\,T\,B}\right) - \mathrm{NF} \qquad (7.2)$$

where k is the Boltzman constant ($1.38\ 10^{-23}$ J K^{-1}), T the system temperature (300 Kelvin will be used), and B is the noise bandwidth.

Choice of noise bandwidth.

Since the measurement in this case is that of an estimation of the frequency of a single tone, the noise bandwidth is the reciprocal of the duration of the observation. This term will clearly have a large influence on the SNR, and an estimate is not immediately obvious. However, many fast and noisy measurements may be averaged to yield an equivalent SNR

to a measurement of longer duration. The other time variables in the system should also be considered. The first of these is the FM sweep duration. This might for example be between 1 ms and 100 ms, as discussed in chapter 6; a value of 50 ms will be used. Where a directive and rotating antenna is used, another timing parameter is the sweep rate of the antenna, which is assumed to rotate with constant angular velocity. This combines with the antenna's horizontal plane radiation pattern to provide a narrow timing window of illumination of the target. A typical marine radar antenna might have a half power beam width (HPBW) of 2° in the horizontal plane and a 1 Hz sweep rate. The dwell period of the HPBW on a point target is therefore the order of 5 ms. The disadvantage of attempting to minimise noise bandwidth by maximising the duration of the observation is the likely relative velocity of the interrogating vehicle to the transponder. At 20 knotts (about 10 m/s), this equates to 10 mm of displacement per ms which is the order of the range resolution expected and demonstrated in chapter 6.

From these considerations, it would be reasonable to propose an observation window the order of 1 ms in duration, from which 5 measurements could be made during the sweep of the antenna HPBW. Using this 1 ms period to derive noise bandwidth, the received SNRs applicable to the link budgets presented in Figure 7.2 are shown in Figure 7. 3.

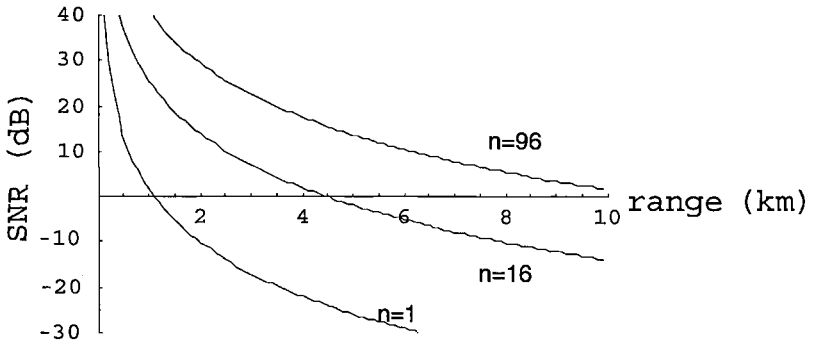

Figure 7. 3 Received SNR for different numbers of transponder radiating elements.

The estimate SNRs of Figure 7. 3 show that on adopting multi-element transponders, an approximately 4-fold increase in range (for positive received SNR) is given by the 16-element case, and more than ten-fold for the 96 element transponder. The expected range of operation in this latter case would thus be the order of ten kilometres.

7.1.2 Array Geometries for a Maritime Transponder.

The square retro-array, fabricated on either microstrip or using coaxial lines (which may cross) has been considered in some detail, and successful prototypes have been built. It is now important to observe that this is not necessarily the best layout to choose for a given practical application. For large arrays, the transmission line routing becomes more problematic. It is also worth noting that a rectangular array has the same monostatic RCS as a square array with the same number of elements – the spatial response is still the same as that of the radiating element chosen. For a rectangular array the transmission line routing can be less difficult, and the physical dimensions of the circuit may be either more or less convenient and specially efficient for a given application.

Consideration should also be given to the geometry of the theatre of operation for a proposed retro-reflector system. Little work appears to have been reported in this area previously. [2] (1994) makes brief reference to an aircraft carrier landing system which might use a millimetre wave retro-directive array. A 4 element array is reported, but the work does not appear to be very advanced. In particular, the region of required spatial coverage has a direct influence on the radiation pattern chosen. For example, a landing system for fixed wing aircraft may require a coverage area over a relatively narrow conical beam through which aircraft approach a runway. In such a case, the angular coverage could be tightened by the use of higher gain antennas (for example sub-arrays of patch antennas), which would increase RCS without increasing the number of transmission lines and hence the practical complexity of their routing. The sub-array radiation pattern could be tailored

to yield asymmetrical beam widths in azimuth and elevation if this was an operational requirement. A contrasting example is that of a system for vertically landing aircraft which may approach from any direction within a hemisphere. In this case, the coverage area would need to be as broad as possible, and the use of half-omni-directional antenna elements would be preferable to directional sub-arrays.

Returning to the maritime environment, where a ship-to-ship or ship-to-shore link is required, it is apparent that a wide spatial coverage is likely to be required in azimuth whereas the coverage in elevation may be narrow - perhaps only a few degrees. One scenario is illustrated in Figure 7. 4.

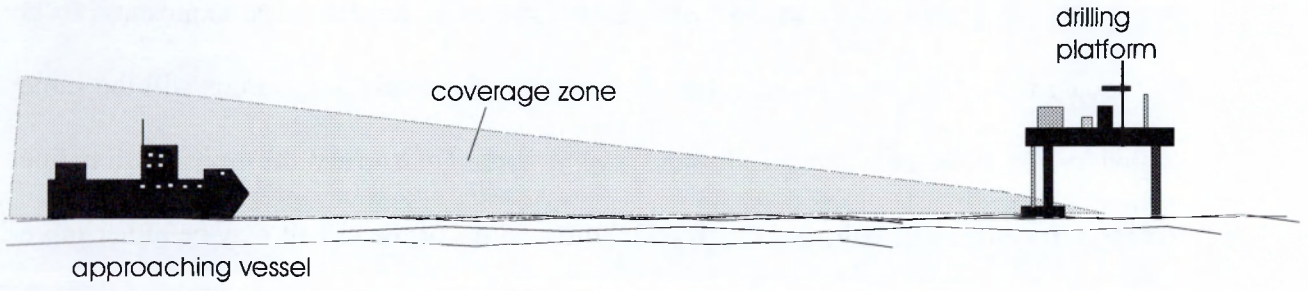

Figure 7. 4 Likely coverage zone for a typical maritime range sensor.

In this example, the retro-reflector transponder is placed on the fixed maritime installation, and the approaching vessel illuminates the environment. To help achieve a large radar cross section for the reflector, sub-arrays could be employed which are directional in elevation but retain a wide beam pattern in azimuth. A convenient method would be a vertically stacked sub-array of horizontally polarised patch antennas. The azimuthal pattern is broad, being that of the E-plane radiation pattern for the antenna as investigated in chapter 3, whilst the vertical stacking increases the gain of the sub-array, at the "expense" of the loss of the unrequired vertical coverage. Figure 7.5 shows a geometry which might be adopted for such a purpose.

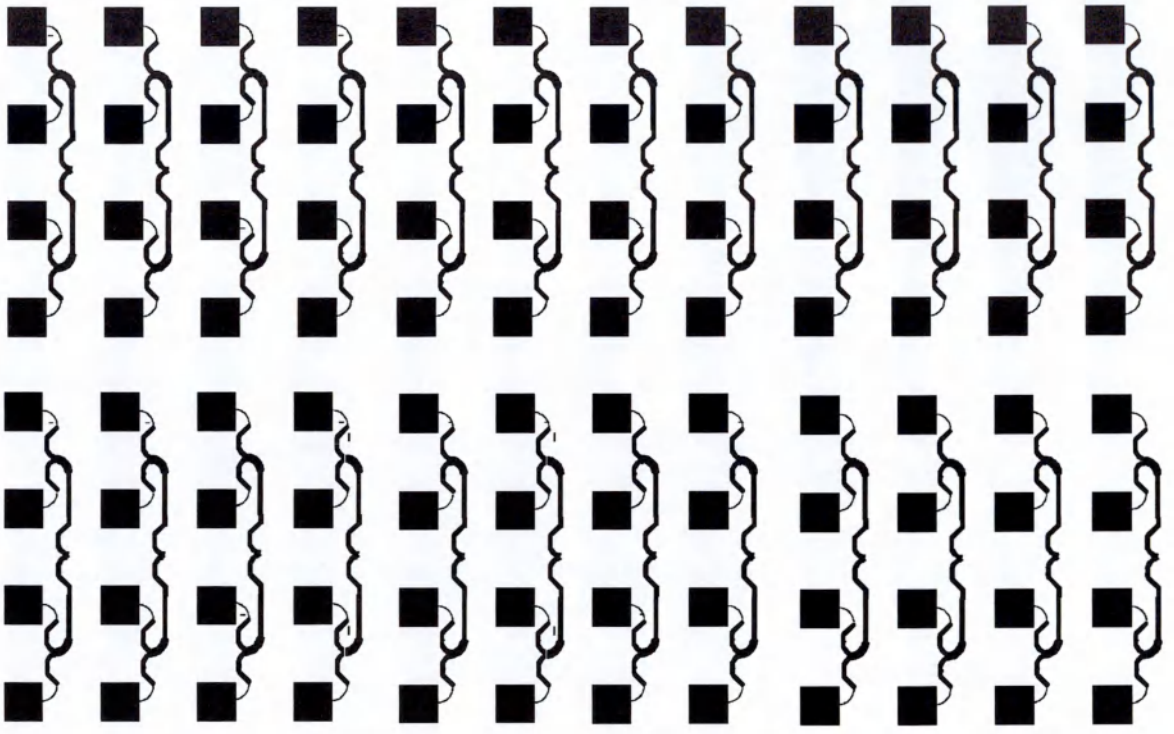

Figure 7.5 12 x 2 array of 4-element sub-arrays, tailored to narrow vertical coverage.

In Figure 7.5, 24 sub-arrays are arranged in a 12 x 2 grid. Thus there are 96 radiating elements, but only 12 interconnecting transmission lines are required. The maximum RCS, from equ. 2.1 is 12.5 m^2 (before losses are accounted for). The effect of the 4-element sub-arrays is a 4-fold increase in effective area without the associated additional transmission line and switching complexity. The vertical (elevational) coverage is defined by the square of the radiation pattern of the sub-array, which may be calculated from the product of the 4-element array factor and the H-plane radiation pattern of the patch antenna. These patterns are presented in Figure 7.6 - in case (ii) it can more easily be seen that the 3 dB beamwidth is about 15 degrees.

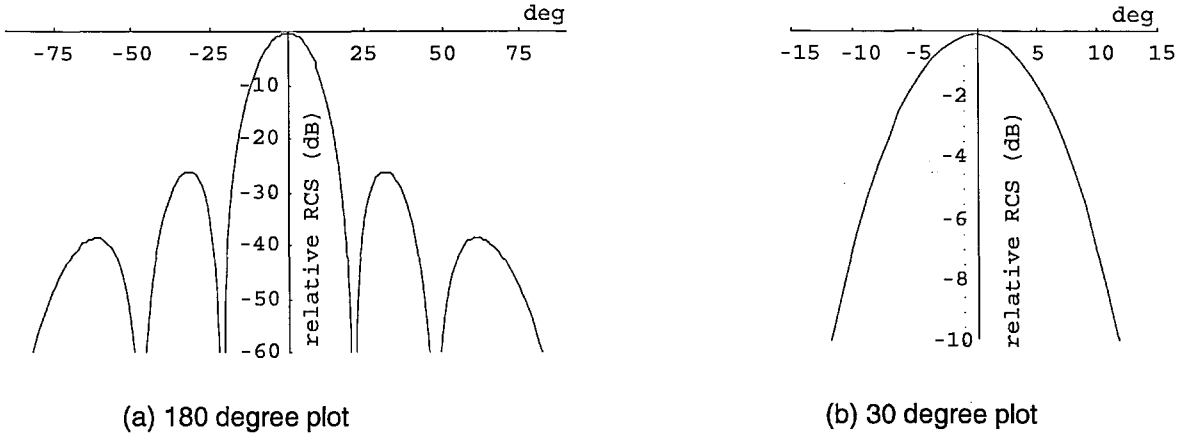

(a) 180 degree plot

(b) 30 degree plot

Figure 7.6 H-plane radar cross section for 4 element sub-array of patch antennas at 22 mm spacing and 9.2 GHz.

Besides the reduction in transmission lines required to yield a given RCS magnitude, another fortunate consequence is a similar reduction in the number of RF modulators (switches). This yields a significant saving in fabrication costs and the power consumption of the transponder. This saving is in a direct relationship to the number of antennas in the sub-array.

The extent to which sub-arrays can be exploited is dependent on the expected relative angular movement between the vehicles in the system. For example, if the platform illustrated in Figure 7. 4 was subject to significant pitch and roll movements, the extent of these would need to be considered. Similarly, changes of relative height due to ocean tide levels might place a constraint on the extent to which elevational coverage could be sacrificed.

There are clearly an infinite number of possible configurations for retro-arrays, and the example of Figure 7.5 has been chosen as a natural extension of the 16 (single) element prototypes reported in chapter 4. The sub-arrays would be fabricated using the same photo-lithographic techniques, and the circuit dimensions would be approximately 300 mm by

200 mm. Such a circuit could be fabricated on a single laminate, with either aperture coupling to microstrip transmission lines, or coaxial feeds. In either case the sub-array feed point is mid-way between to two antenna pairs. (The curved lines are the quarter-wave impedance transformers inherent to the microstrip corporate array feed.) It is also easy to envisage a modular approach where sub-arrays are added to the ends of the n x 2 row and connected to a bank of modulators numbering $\frac{n}{2}$.

Another interesting possibility for applications where DC power is limited (perhaps for a solar-powered transponder) is that of an idle mode for a large transponder. In this case, a sub-section of the array's modulators could be powered when the range is relatively small, thus saving DC power when a large RCS is not required

7.1.3 FM System for Multi-target Detection.

The range measurement system reported in chapter 6 was configured to detect a single transponder only. Estimates for transponder bearing (i.e. angular direction from the interrogating transceiver) were not available. In practice, and particularly for the maritime system which is here being considered, estimates for bearing are very likely to be required. Two methods for deriving this additional information may be immediately suggested. The first method would use a scanning antenna of narrow azimuthal beamwidth, typical in most marine applications. The scanning is most conveniently achieved by mechanical rotation (also discussed above in section 7.1.1 under *choice of noise bandwidth.*) The bearing estimate would thus be derived from a knowledge of the antenna pointing angle during the observation of the transponder modulation products and the associated range measurement. A second method for estimating bearing would be the observation of multiple transponders, whose relative locations are known. For example, transponders could be placed at opposite ends of a vehicle, or other structure of interest such as a harbour entrance. The relative transponder locations may be known from a database, or "downloaded" from the transponders themselves via a separate communications link which

would employ a CW burst from the interrogating transceiver. Measurement of bearing would therefore involve triangulation on the multiple transponder range measurements. This method could use a much wider beamwidth antenna than the 2° suggested above, or could be used as a means of augmenting the bearing estimates where a narrow beamwidth scan is employed.

Since a system for multiple and simultaneous transponder detection is advantageous, a suitable multi-access scheme will be discussed.

7.1.4 Modulation Schemes and Jamming.

Thus far monotone modulation of the transponder has been considered. While this is straightforward to achieve and detect, certain disadvantages should be considered. If we consider the IF spectrum at the first RF mixer, frequency components from all targets (modulated and un-modulated) are included, as illustrated in Figure 7.7.

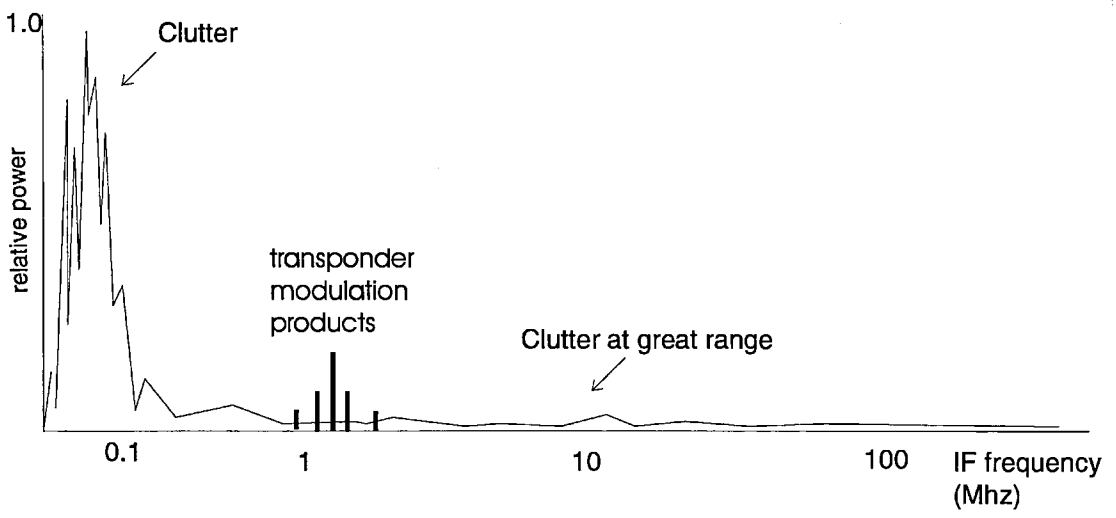

Figure 7.7 Frequency components at IF

In the illustration of Figure 7.7 strong reflections from nearby clutter produce relatively low frequencies. The modulation frequency is contrived to be well above this region, so that detection of the modulation spectrum, which employs a bandpass filter, is essentially

free of clutter. However, if a clutter target produces a difference frequency which is sufficiently close to the transponder modulation frequency that it falls within the filter passband, a spurious frequency component will give rise to a false reading. This effect could be referred to as jamming, and occurs when:

$$\Delta f \text{ (clutter)} \approx f_{\text{mod}} \text{ (transponder)} \tag{7.3}$$

which using equ. (6.1) gives

$$\frac{2 r_{\text{jam}} B}{c T_{sweep}} \approx f_{\text{mod}} \tag{7.4}$$

therefore the range to the clutter target is:

$$r_{\text{jam}} = \frac{f_{\text{mod}} \; c T_{sweep}}{2 B} \tag{7.5}$$

The magnitude of the spurious component is proportional to the RCS of the clutter target. The greater the value of the range at which jamming can occur, the less likely it is to occur since the clutter target would need to be of rapidly increasing RCS, as range increases, to yield a reflection of significant magnitude. To produce a reflection of equivalent magnitude to that of the transponder (whose RCS is σ_{tran} at range r), the RCS of the equivalent clutter target may be derived from the radar equation as:

$$\sigma_{\text{clutter}} = \sigma_{\text{tran}} \left(\frac{r_{\text{jam}}}{r} \right)^4 \tag{7.6}$$

A few typical values for r_{jam} based on the parameters of the FM sweep are tabulated in Table 7.2 below, where the transponder modulation frequency has been fixed at 1 MHz.

sweep bandwidth B (MHz)	T_{sweep} (ms)	r_{jam} (m)
400	10	3,750
400	50	18,750
400	100	37,500
40	50	187,500

Table 7.2 Values of jamming range as a function of FM sweep parameters.

Choosing a transponder RCS of 12 m^2 at a range of 10 km, and a jamming range of 20 km, it can be seen from equ (7.6) that the clutter RCS would have to have a RCS of 12 x 2^4 = 192 m^2 to yield a frequency term comparable to the wanted term from the transponder, whereas for r_{jam} = 200 km the clutter RCS would have to be a huge 1.9 x 10^6 m^2.

Apparent from equ. (7.5) is the advantage of low sweep bandwidth, slow sweep rate and high modulation frequency to maximise the jamming range and hence minimise the likelihood of its occurrence. This is in conflict with the high bandwidths required to maximise range resolution. Fortunately, a multi-mode system may be envisaged where the sweep bandwidth is reduced for long range operation where high resolution is less likely to be required, and increased at short range where resolution is more likely to be required, and SNR values are high.

7.1.5 Modulation Schemes for Multiple Transponders.

The maximum difference frequency Δf_{max} and hence maximum range of interest corresponds to the maximum deviation of the upper and lower sidebands of the first harmonic of Δf. Hence additional transponders must utilise modulation frequencies separated by at least 2 Δf_{max}. Consideration of the harmonic frequencies of each transponder's modulation spectrum, which are generated by the digital modulation, place a further constraint on the use of spectrum. The available spectrum for multi-target detection, in this case, is the maximum modulation frequency at which the transponder will operate. The prototype transponders reported in chapter 4 achieved modulation rates of 10 MHz and this figure will be used as an upper limit to illustrate how a multi-target system would operate based on frequency division multiple access (FDMA), as illustrated in Figure 7. 8

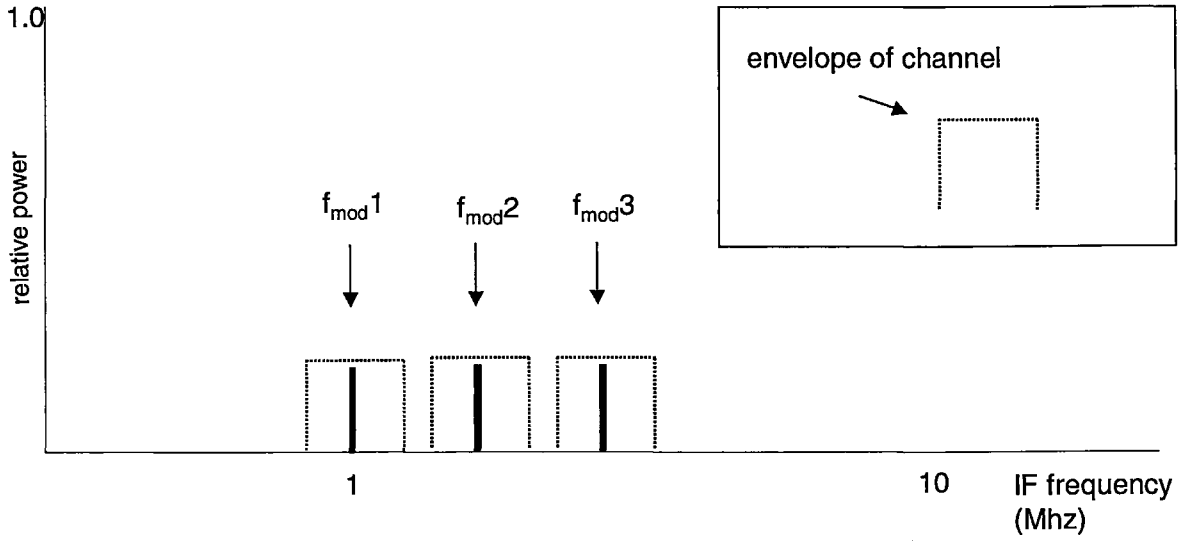

Figure 7. 8 IF spectrum for FDMA, monotone transponder modulation.

In this case, the targets are located uniquely by multiplexing and each transponder occupies a separate piece of spectrum. For a given maximum modulation rate, the widths of each channel's bandpass filter and hence maximum range (or maximum sweep rate) are increasingly constrained when the number of transponders is increased. Each term f_{mod} must be chosen carefully to avoid harmonic interference, for example, the third harmonic of $f_{mod}1$ breaking into the channels for targets 2 and 3. These limitations may be mitigated by a changing the sweep parameters according to the range of operation, such as reducing the sweep bandwidth when the range is large.

To overcome the spectral inefficiencies of the rather simplistic monotone FDMA scheme, more advanced schemes such as multi-tone modulation may be advantageous, and also reduce the effect of spectral contamination from distant targets. The extension of this idea is to use a pseudo random binary sequence as the modulation signal. If orthogonal codes are used, the targets may share spectrum with minimal co-channel interference. Both two-tone and PRBS modulation have been demonstrated for short ranges, (see measured modulation spectra of appendix A4.2) where an M-sequence generator [3] based on a TTL

shift register [4] replaced the monotone generator. However, in this laboratory configuration (Figure 6.7), coherent detection is automatically achieved and the measurements for difference frequency have essentially the same form as the results for monotone modulation. For a practical system, the detection of difference frequency on (suppressed) multi-tone carriers would involve considerable further work, as would a sliding correlator detector for the PRBS case. A time division multiple access (TDMA) scheme could also be envisaged. An advantage of this scheme would be the possibility of each transponder using a simple modulation waveform, such as a monotone, at the maximum modulation rate possible, such as the 10 MHz rate achieved by the X-band prototypes. This would minimise the likelihood of a clutter target giving rise to a jamming signal.

7.2 A High Altitude Communications Platform Downlink.

Introduction.

High Altitude Platforms (HAPs) - craft located in the stratosphere at altitudes above about 17 km - are increasingly being cited as playing an important role in future communications systems and applications [5], [6]. Proponents claim they have the potential to exploit many of the best aspects of terrestrial and satellite based systems, while offering advantageous propagation characteristics. Platforms based on airships [5], solar powered un-piloted aircraft [7], and conventional piloted aircraft [8] have all been mooted and are at various stages of development. While the latter approach would seem the least technologically challenging, being essentially a conventional aircraft flown in shifts of a few hours duration, the solar powered solutions would appear most attractive from considerations of endurance and hence running costs, and of environmental impact. Such platforms are unlikely to be fully developed for several years, but their potential for supporting high capacity wireless services does appear to be attractive.

A disadvantage of the solar powered HAP is the reliance on batteries or fuel cells which would be charged during daylight hours to power the platform and its payload by night. The power budget afforded by this cycle of charge and discharge using current solar cell and fuel cell technology may be marginal, and particularly so at increasing latitudes during the winter months. While advances in technology are anticipated to improve matters, a HAP communications payload will always be allocated only the electrical power which is remaining after that consumed by the motors and control systems which keep the platform aloft (for aircraft) or on-station (for airships). The majority of the available power is likely to be consumed by these propulsion and stability systems. The prime power consumer in the communications payload would be the RF power amplifiers (PAs), which, along with the antennas, are among the most critical components. In circumstances where the supply

of power is marginal, the PAs may have to be run at reduced power or shut down completely, with implication for reduced quality or complete loss of service. The backhaul down link - a high data rate link connecting all the down link data into a terrestrial network via a hub, (a ground-station) - has been identified as the most susceptible to marginal link budgets such as would be encountered during severe rain events [9]. To some extent, this can be obviated with spatial ground-station diversity [6], but cannot mitigate against a loss of DC power on the HAP. In this section the feasibility of using a retro-directive transponder on a HAP is explored, since this has the potential to circumventing the problem of link loss where RF power is lacking and remove the need for a steered high gain antenna on the HAP

7.2.1. Historical Background.

A link via a reflector was suggested by the pioneers of satellite communications as a means of facilitating over-horizon communications, where the reflector might be passive or include amplifiers [10], [11]. Other references to reflective links via satellite from the 1960s are discussed in the introductory sections of chapter 1. The very much reduced path length to a HAP compared to a satellite leads to new possibilities for a link via a reflector, which may now be examined in a fresh light.

7.2.2 A Passive Transponder for a HAP Link.

The geometry is illustrated in Figure 7.9. Since the link suffers $\frac{1}{r^4}$ free space loss, means of increasing the link budget are sought which include maximising the following parameters within practicable limits:

- transmit antenna gain
- receive antenna gain
- transmit power
- transponder RCS.

The first three of these parameters are functions of the ground station and ought not present severe restrictions beyond those of cost. (It is interesting to observe that a similar philosophy has been proposed, albeit in a more extreme form, to provide *all* of a platform's power needs, including propulsion, via multiple microwave links from the ground [12] .)

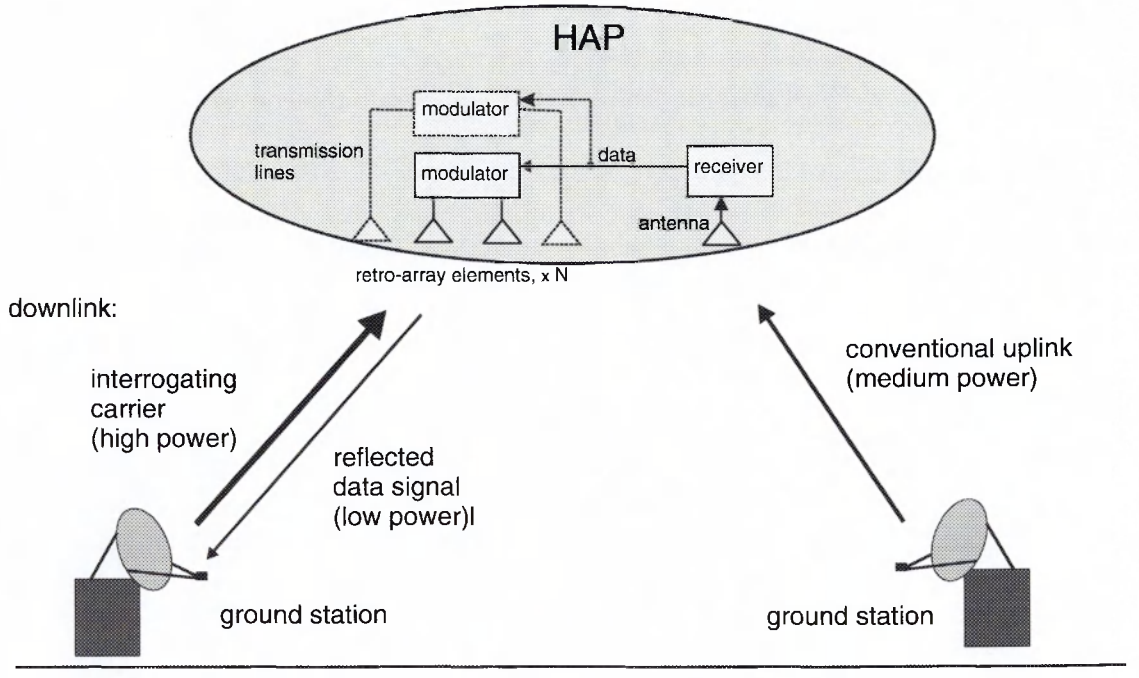

Figure 7.9. HAP communications link via a passive transponder.

Since the transponder would be placed on the HAP, its size and weight would be expected to be limiting factors, and the expected RF efficiency of the transponder as a function of its size increases may be estimated from the models developed in chapter 5. At this stage the frequency of operation should be discussed. Proposed HAP carrier frequencies include the bands close to 2 GHz allocated to 3rd generation mobile services and the Local Media Distribution Service type bands around 28 GHz and 38 GHz discussed in [6]. An additional band specifically for HAPs is close to 48 GHz, where 600 MHz of bandwidth is allocated. The choice of carrier frequency would dictate the type of technology adopted for the transponder. While microstrip has been used with success at 2.5 GHz and 9.5 GHz, and would be very suitable for the maritime transponder proposed in the first part of this

chapter, it is likely to be less suitable at millimetric bands where waveguide might be a better solution, which has also be explored in chapter 5.

A further complication in choosing the carrier frequency arises from the apparent fluidity of the international regulations - a platform below a height of 20 km may be treated as part of a terrestrial system, and may be allowed a greater choice of bands. In addition, the link under discussion has no RF transmitter on the HAP and would appear to fall outside the conventional classifications. For these reasons, the choice of carrier frequency will be deferred and a link budget will be presented as a function of aperture area only.

7.2.3 Link Budget.

The HAP downlink backhaul groundstation might be similar in specification to a typical satellite earth station, but with some important differences. The reduced path length allows for a lesser antenna gain and transmit power - their product commonly being referred to as equivalent isotropic radiated power (EIRP). It is interesting to observe that the transmitted bandwidth is that of the carrier only, since no data is present in the outgoing signal. This bandwidth is that of the RF source alone, which is governed by its phase noise. Also, the RF power amplifier(s) may be driven fully into saturation without the usual corollary of intermodulation distortion, which is again due to the absence of modulation (i.e. data) in the transmitted carrier.

To present an elementary link budget which is frequency independent, we may plot received power or signal-to-noise-ratio at the ground as a function of the reflector aperture length L. For a square array with uniform element spacing, the total number of elements is given by :

$$n = \left(\frac{L}{a}\right)^2 \tag{7.7}$$

where a is the element separation. Since the total aperture gain is the product of the number of elements and the gain of each element ($n\,g$), the RCS for the aperture is:

$$\sigma = \frac{L^4 g^2}{4\pi\ s^4 \lambda^2} \tag{7.8}$$

where $a = s\,\lambda$. Substituting equ. (7.8) into equ. (1.9) yields a term for received power P_r which is independent of wavelength λ hence:

$$P_r = 10\,\mathrm{Log}_{10}\left(\frac{L}{4\,\pi rs}\right)^4 g^2 + 2Gtr + P_t \tag{7.9}$$

Where powers P_r and P_t are here expressed in dBW, and the transmit/receive antenna gain G_{tr} in dBi. The ratio of received signal power to noise may be shown by subtracting from (7.9) the thermal noise power (in dBW). Hence signal-to-noise ratio is shown as a function of reflector length in Figure 7.10, where noise temperature of 290 K and noise bandwidths of 1, 10 and 100 MHz have been used by way of illustration. Element separation a is 0.5 λ and the element directivity is 3 dBi, which is typical of a single printed antenna.

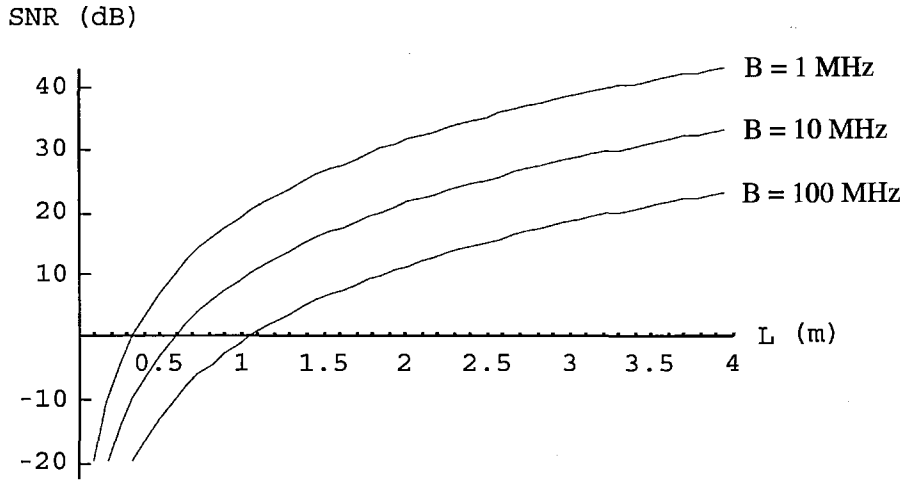

Figure 7.10 Received SNR from square, lossless reflect-array of side length L, at distance of 30 km, for ground EIRP = 45 dBW.

In Figure 7.10, the quantities G_{tr} = 35 dBi and P_t = 10 W have been used. To some extent the figures are arbitrary, but they have been chosen to be significantly less than for a typical satellite earth hub where we may have an antenna gain of 45 dBi and P_t = 50 W

[13]. The distance to the reflect-array is 30 km (equating to a ground distance of 22 km and a platform height of 20 km). The derivation in Figure 7.10 is straightforward and intended only to initiate a first order estimate of the required reflector dimensions - loss terms have not yet been included. The actual efficiency of the modulated reflect-array would be rather less than unity, and dependent on the carrier frequency and means of construction, as discussed below. The dimensions will also be constrained by the payload capability of the platform. For example, the European *HeliNet* [7] solar powered HAP proposes an aperture area between 1 and 2 m^2 for its broadband payload, while it is anticipated that future airship based platforms would support several square metres of aperture.

7.2.4 Link Budget for Lossy Reflectors.

The models for reflector efficiency developed in chapter 5 may be directly applied to estimating the effect of reduction of the predicted SNR values. Unlike the derivation of Figure 7.10, a carrier wavelength must be chosen, since this scales the lengths of the lines which give rise to the loss. The SNR value will be reduced by the difference between the lossless aperture and the lossy reflector as illustrated in Figures 5.3 and 5.5, for a given line loss *lpm*. Choosing again a frequency of 2 GHz, the modified SNR values for a 10 MHz signal bandwidth are plotted in Figure 7.11 for nominal *lpm* values of 2 dB/m and 4 dB/m for both the crossing and non-crossing geometries (from chapter 5, section 5.1).

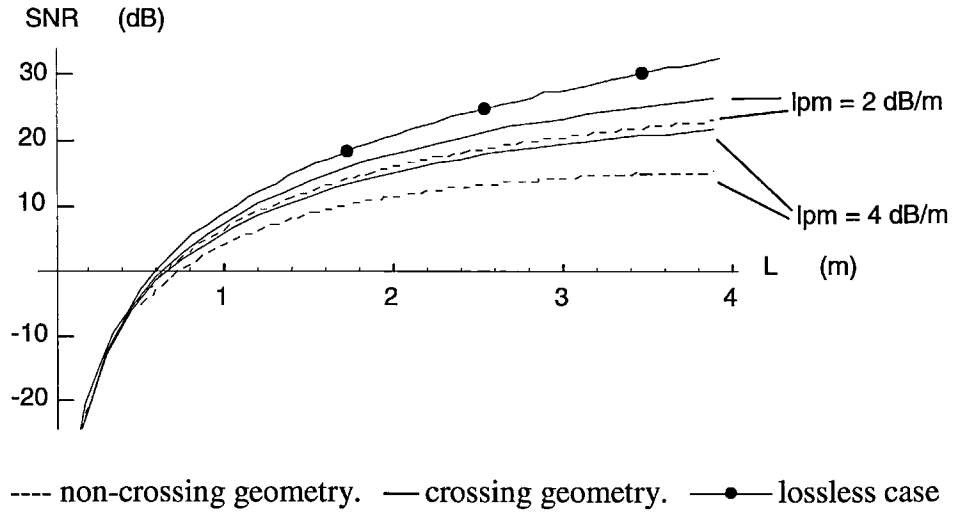

Figure 7.11. Received SNR from square, lossy reflect-arrays of side length L, at distance of 30 km, for ground EIRP = 45 dBW and 10 MHz noise bandwidth at 2 GHz carrier.

The results in Figure 7.11 will of course scale linearly on changing the EIRP or bandwidth etc. It is interesting to observe that where line loss is severe, the link budget improves very slowly above a certain aperture length (e.g. 3m. in Figure 7.11) to the extent that the increase in fabrication complexity may be considered pointless. It is hence very important to choose materials which minimise transmission line loss.

7.2.5 Communications Link to HAP: Conclusions.

The novel type of link described is different from the traditional view of a High Altitude Platform downlink implementation: the conventional requirement for antenna alignment and power amplification is removed by using a retro-directive array of sufficiently large aperture, which acts as a passive transponder. The emphasis on communications infrastructure is placed on the ground station, where power and weight constraints are much more relaxed than on the platform. We may summarise the properties of the link as follows:

Advantages:

- The HAP transponder requires no RF power amplifiers.
- The HAP transponder need not be steered or stabilised.

- The majority of the RF infrastructure is placed at the ground station.
- The RF power can be increased during adverse weather
- The ground station power amplifiers can be driven into saturation without intermodulation distortion occurring.

Disadvantages:

- The ground station requires higher RF power compared to a conventional point-to-point link, hence it is relatively expensive.
- The transponder is difficult to make efficient and large at higher frequencies.
- The atmospheric loss is squared compared to a one-way link.

The economic viability of the HAP concept for delivery of telecommunications remains to be proven. Limitations of solar power sources and uncertainties over stability and station keeping present obstacles to communications systems designers. The technique discussed could substantially mitigate these limitations, at least in securing a downlink to dedicated ground stations for critical data such as command and control, or a backhaul for services such as news gathering.

References

[1] "Microwave Homodyne Systems", R. J. King, 1978, *Peter Peregrinus Ltd. on behalf of IEE.* pp 344 - 346

[2] "The evolution of radar technology into commercial systems", B. S. Hewitt, IEEE MTT-S Int. Microwave Symposium Digest, 1994, pp. 1271-1274.

[3] "Spread Spectrum Systems with Commercial Applications", R. C. Dixon, *Wiley*, 1994, pp. 60 - 64. / Chapter 3.

[4] "Spread Spectrum Techniques for Multiplexing and Ranging Applications", A. M. Street, Doctoral Thesis, 1994, Department of Engineering Science, University of Oxford, UK. section 3.3 and Appendix A2.1.

[5] "Establishing Wireless Communications Services via High-Altitude Aeronautical Platforms: A Concept Whose Time Has Come?", G. M. Djuknic, J. Freidenfelds and Y. Okunev, *IEEE Communications Magazine*, pp. 128-35, September 1997.

[6] "High-altitude platforms for wireless communications", T. C. Tozer and D. Grace, *IEE Electronics and Communications Engineering Journal*, June 2001. pp. 127-137

[7] "Broadband communications from a high altitude platform - The European *HeliNet* programme", J. Thornton, D. Grace, C. Spillard, T. Konefal, T. Tozer, *IEE Electronics and Communications Engineering Journal*, June 2001.

[8] "The HALO Network", N. J. Colella, J. N. Martin, and I. F. Akyildiz, *IEEE Communications Magazine,* June 2000, pp. 142-8.

[9] "Prediction of monthly and annual availabilities on 10-50 GHz satellite-Earth and aircraft-to-aircraft links", T. Konefal, P.A. Watson, A.K. Shukla and A. Akram, *IEE Proceedings, Microwaves Antennas and Propagation,* Vol.147, No.2, April 2000, pp122-127.

[10] "Microwave Scanning Antennas Vol 3 - Self-Phased Arrays", R. C. Hansen, Academic Press, 1966, pp.371-372.

[11] "Quasi-Passive Satellite Relay Communications System", E.L.Gruenberg, C.M.Johnson, *IEEE Trans. Ant. Prop.* Vol. 12, 1964, pp. 215 - 223.

[12] "A microwave powered high altitude platform", J. J. Schlesak, A. Alden, T. Ohno, *IEEE MTT-S Int. Microwave Symp.* New York, May 1988.

[13] "Earthstation Technology Handbook", 5th revision June 1999, ITELSAT Application Support and Training, 3400 International Drive, NW, Washington, DC, USA.

This page intentionally blank

Chapter 8

Thesis Conclusions and Suggestions for Further Work.

8.1 Conclusions

The original premise of this work, and thesis, was that a structure which can combine the properties of retro-directivity and modulation of radar cross section would act as a microwave transponder whose power requirements are minimal, and yet support a directive and potentially high bandwidth link (in the communications context) and clutter immunity (in the radar context). The opening chapter sets out the background for this concept, and reviews the literature which is closely related to its aims.

Whilst "optical" reflectors i.e. trihedral reflectors were briefly examined, a modulated variant of the Van Atta retro-array was quickly identified as the most promising structure to fulfil the above aims. A very limited amount of prior literature on this structure was identified. This being the case, a further premise of the work was that means of constructing modulated retro-arrays should be explored so as to:

- achieve a manufacturable structure.
- perform measurements to compare with theoretical models of behaviour.
- identify the limits of performance, and seek to expand them.
- identify applications and markets.
- explore and pursue such related discoveries that may occur.

All the above aims have been explored to some extent, and the findings have been reported in the body of the thesis. The first fabrication techniques involved the use of dipoles as the radiating elements. A carrier frequency of 2.5 GHz was used, and co-axial cables were used to inter-connect the antenna pairs. Amplitude (and later phase) digital switches were incorporated into these lines to act as modulators. When illuminated with a continuous wave source, a spectrum analyser co-located at the site of the transmitter acted

conveniently to capture the modulation spectrum reflected from the retro-array. As reported in chapter 2, a number of indoor measurements were performed, which demonstrated the wide angular response characteristic of the retro-array, and also modulation rates up to 250 kHz.

With an aim of making a more manufacturable structure, printed circuits were then designed and constructed to combine the functions of antenna, transmission line and modulator switch. Initially, the 2.5 GHz design frequency was retained. This part of the work involved a very intensive review of microstrip design techniques, and their application to developing integrated circuits for retro-arrays. In particular, the layout of the printed circuit components on the finite area of the boards required a deep investigation of the trade-offs which were identified during the design stages. These are discussed in chapter 3. A creative outcome of this work was the development of a further variant of the retro-array, which used unequal-length transmission lines. In this case, the wavelength in the transmission line medium must be accurately modelled, and line lengths allowed to differ by an integer number of wavelengths. Since phase-conjugation then occurs at the design wavelength, the structure is a narrow-band variant of the retro-array. Estimates for bandwidth were developed in chapter 5, along with models for loss in the array as a general case.

The novelty of this approach, which allows for a much less congested printed circuit and reduced transmission line loss, formed the pivotal content of an application for intellectual property (i.e. a patent application).

An underlying objective, or application, had been the development of a structure to enhance target detectability to radar, particularly in the maritime context. This prompted a survey of RF frequencies which might be used to scale the foregoing techniques with an aim to demonstrating some marketable applications. To this end, x-band was adopted for

the next phase of the investigation, and specifically the range 9.0 - 9.5 GHz. A further design and fabrication stage produced successful prototype 16-element PIN diode modulated retro-arrays (both amplitude and phase modulated), whose useful RF bandwidth was between about 9.0 and 9.4 GHz and which yielded modulation rates up to 10 MHz (for 3 dB roll-off in sideband power). These circuits measured about 100 mm square. The inherent power consumption of the modulators was modest at around 0.2 mW. (Although the CMOS based diode interface consumed considerably more power than this, little attention has been paid to this aspect, being a feature of the low frequency electronics components.)

The X-band prototypes proved to be a very successful laboratory workhorse and lead to a number of experimental results for modulation spectra, received power, DC power consumption, angular response, etc. A means of measuring the absolute RCS of the phase modulated transponder was developed. In the absence of an anechoic chamber and the associated calibration standards, the method compared the power in the spectra of the transponder with that of a conventional array antenna of the same aperture, i.e. the same antenna element size and spacing. This RCS of this antenna was also phase modulated by series connection to a phase switch. The theoretical directivity of the reference antenna was derived, and thence its gain by estimating the losses in the printed circuit.

Demonstration of applications were pursued, and these included a communications link which utilised a CD bitstream at 5 M bits/s which could be representative of a local-area-network or telemetry type application. A further application was a range finding technique which used frequency modulated illumination of the transponder. This proved to be a very promising application, and signal processing techniques to complement the FM measurement were developed which allowed transponder displacements of as little as 10 mm to be resolved. This accuracy is very good for a radar system, and is possible because

the transponder acts as a co-operative target to yield an essentially clutter-free measurement. The development of this technique is reported in chapter 6.

To close the thesis, two of the more promising applications for passive transponders were chosen for discussion in chapter 7, where the dimensioning of the retro-array and the corresponding link budget were developed. These applications were (i) a maritime range sensor, and (ii) a passive downlink for an aerial platform.

Having presented the conclusions, it remains to close with a short section suggesting some of the areas for future work which have occurred to the author.

8.2 Suggestions for Further Work.

8.1.1 Improvements to the X-band Transponders.

The design of the X-band transponders is covered in detail in chapter 4, where certain limitations were identified. These included constraints imposed by the performance of the available materials and components, particularly the microwave laminates (substrates) and the diodes. Future work could address improvements in this area such as:

- use of dissimilar substrates for the antenna circuit and feed/modulator circuit, i.e. thinner substrates for the latter.
- use of better switching diodes, rated to at least 9.5 GHz.
- increasing the number of elements beyond 16

It would also be very interesting to explore the limits of the printed circuits and diodes in terms of operating at higher carrier frequencies, where diode selection and handling/contacting would be expected to be a critical issue.

8.1.2 Multi-layer Planar Retro-arrays.

A most promising method which might be explored is the use of multi-layer planar feed networks for retro-arrays. In chapter 3, the constraints of limited circuit area were discussed in some detail, and it is apparent that if the number of array elements is increased it would become increasingly difficult to route the interconnecting transmission lines on a single planar circuit. However, many of these restrictions could be considerable eased by adopting further layers of planar circuit, which might be "stacked". This would require more apertures or else apertures which allow for electromagnetic coupling between substrates of increased separation. Alternatively, soldered pins might be used to interconnect the various circuit layers. From the point of view of the general models for transmission line length and the associated attenuation which were developed in chapter 5, such an approach would be a hybrid case in between the "crossing" and "non-crossing"

geometries, since the lines on a given circuit board could not cross, but those on different boards would be free to cross. It should be added that a planar transmission line bounded by two ground planes is stripline rather than microstrip, and this medium is also well characterised. A disadvantage would be the added complexity of the mechanical housing and bias supply routing for the diodes. An advantage would be the reduction in circuit board congestion. This might allow for more sophisticated modulators to be accommodated.

8.2.3 Modulators

The modulators used throughout the work tended to be among the simplest possible, each having only 2 switched states. The modulation waveform was therefore inherently digital amplitude or phase modulation, with 1 bit per symbol. In a future extension of this work, it would be worth considering higher-order modulators so as to allow, for example, quadrature phase shift keying, also called 4-PSK, or indeed higher order PSK or combined amplitude and phase shift digital modulation. Since such modulation would be done at the RF frequency of operation, this would require additional transmission line states (or track lengths), each switched by a PIN diode at each end. This would require additional circuit space and diodes, but ought not lead to greater power consumption, since only one state per switch is powered at any one time. The additional space might be found by adopting a multi-layer structure as described above. Data rates would be increased by the associated increase in the number of bits per symbol, but of course become more sensitive to noise since the energy states in the modulation constellation become closer together.

8.2.4 Applications using superconductivity.

There are an abundance of microwave applications for materials exhibiting superconductivity, and related research in these areas. In particular, the materials exhibiting "high temperature superconductivity" (HTS) show the most promise for

marketable applications, although these materials require cooling to around 80 K (for Yttrium based compounds) or as high as 125 K (for Thallium based compounds), which requires that the HTS device is placed in a cryocooler. For retro-directive arrays, the effect of resistive loss in interconnecting transmission lines, (studied and quantified in chapter 5) degrades the efficiency of the array and the power budget in the associate communications link. If HTS materials could be exploited as the transmission line material, this loss could be very substantially reduced. However, the requirement for the cryocooler severely limits the applicability of future work in this field: there would be obvious economic disadvantages, and the idea of using a retro-directive array as a cheap and lightweight transponder would be more-or-less rejected. It might still be worth studying possible retro-directive HTS applications for fixed installations (satellite tracking stations, space applications etc.) and also operating at higher frequencies e.g. millimetric bands, where a multi-element array would be expected to fit within the confines of a cryocooler. (Obviously, the latter would need a transparent cover coincident with the array aperture.) Even so, it is likely that a more practical solution to the problem of loss is simply to scale up the aperture size to achieve the required RCS, and it is hard to imagine that the cost and complexity of a cryocooled HTS solution would compete with this approach.

However, if this discussion is extended to the more general field of active self-phasing circuits, which are briefly summarised in Appendix 2, an intriguing possibility is suggested by the method shown in Section A 2.3. Here, an antenna array achieves self-phasing by use of a pilot carrier, and the pilot and signal channels are diplexed by means of filters. For good operation, the pilot and signal need to be very close in frequency, but the finite isolation and roll-off of conventional filters place a limitation in this respect. If HTS filters could be exploited in this area, then a self-phasing antenna could be realised. This would have no phase shifters, processor, or moving parts. Possible applications might include ground station antennas for Ka band satellites in low earth orbits (LEOs), or indeed

stratospheric platforms as discussed in chapter 7. As an example, an antenna with a gain of 30 dB at 30 GHz requires a diameter the order of 100 mm. One could envisage this dimension as manageable for a circuit placed in a cryocooler. An alternative approach to the filtering requirement in this self-phasing architecture is down-conversion of the RF pilot and signal channels to an IF frequency tractable for digital signal processing techniques. Thus, HTS and DSP represent quite different solutions to achieving very tight filter specifications, the former operating at RF and in the analogue domain, the latter at IF and in the digital domain. Their pros and cons, and also the extent to which they can be complementary techniques, are discussed in [1] in the context of filtering and frequency transposition for digital terrestrial broadcasting.

[1] "Transposer systems for digital terrestrial television", P. B. Kenington, K. Hayler, P. N. Moss, D. J. Edwards, A. P. Jenkins and M. Johnstone, IEE Electronics and Communication Engineering Journal, February 2001, pp.17 - 32.

Appendices

A 1. Microstrip Losses.

At the earliest stages of the design of the microstrip circuits, the trade-offs between practical layout and performance, in terms of losses, impedance matching and parasitic coupling, were always carefully considered. These issues have been explored in some detail in chapters 3 and 4. Of particular interest are the inter-relationships between transmission line characteristic impedance and attenuation as a function of line width. Characteristic impedance may be estimated by the equations given in chapter 2, and the CAD tool *Linecalc* (HP EESOF/Libra) was also extensively used in practice. In this appendix, three methods are used to derive the microstrip transmission line loss term, since its magnitude is of such direct consequence to the efficiency of the passive transponder. Firstly, empirical models from the literature are summarised. Secondly, the CAD simulation tools are compared, and the implications of modelling non-50 Ω transmission lines explored. Thirdly, some of the lines on a spare feed line circuit were measured.

A 1.1 Empirical Models.

(i) Conductor loss.

To estimate conductor losses, the relationship [A.1]:

$$\alpha_c = \frac{Rs}{wZo} \quad \text{Np/m} \quad \text{where } Rs = \sqrt{\frac{\omega\mu_0}{2\sigma}}$$

which for copper may be written [A.2]:

$$\alpha_c = 0.072\frac{\sqrt{f}}{wZo}\lambda_{TL} \qquad \text{dB per microstrip wavelength}$$

where f is the frequency in GHz, λ_{TL} is the wavelength in the line, w is the line width and Zo is the characteristic impedance. An addition multiplication factor of 1.6 may be applied to account for a 1 μm r.m.s surface roughness which is typical of commercially available copper cladded laminates.

To calculate α_c , values of *Zo* as a function of *w* were first derived from EESOF *Linecalc*. The laminate used here is Taconic TLC with h = 0.79 mm and ε_r = 3.0. A *Mathematica* program was written to derive an estimate of λ_{TL} for each value of *w*, using equations 2.3 and 2.4 (see chapter 2) and hence derive α_c , - the results are presented in Figure A.1.1 below.

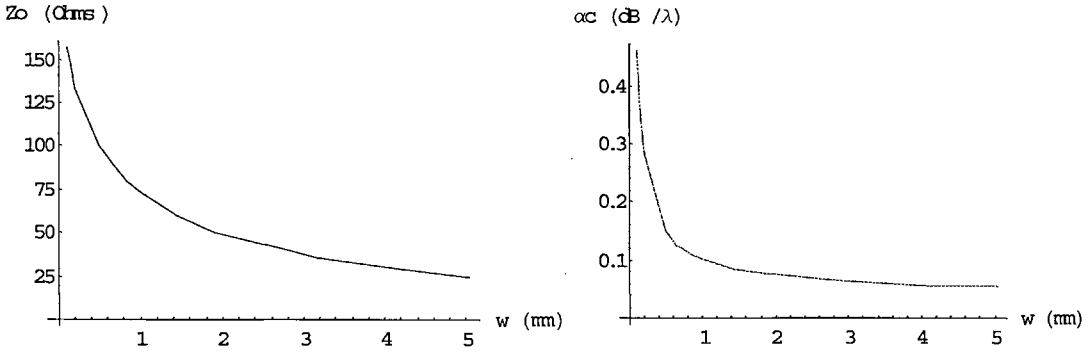

(a) Zo versus w. (b) α_c versus w

Figure. A.1.1: Characteristic impedance and conductor loss (including 1.6 factor for roughness) as a function of microstrip line width in Taconic TLC microwave laminate. (h = 0.79 mm and εr = 3.0)

(ii)Dielectric loss.

Although conductor loss dominates the dielectric loss for low-loss microwave laminates such as alumina and sapphire [A.2], for the PTFE based laminates used the dielectric loss becomes significant. The approximation:

$$\alpha_d = 27.3\frac{\varepsilon_r(\varepsilon_{reff}-1)\tan\delta}{\varepsilon_{reff}(\varepsilon_r-1)} \quad \text{dB per microstrip wavelength}$$

was used. Figure A.1.2 below shows this parameter as a function of line width *w* for the Taconic substrate.

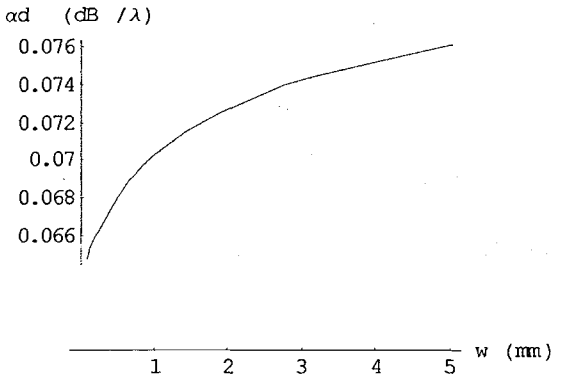

Figure A.1.2. Dielectric loss in microstrip for Taconic TLC microwave laminate. ($h = 0.79$ mm and $\varepsilon_r = 3.0$)

(iii) Total loss.

The sum of the conductive and dielectric losses from the above derivations, in dB per microstrip wavelength, is shown in figure A.1.3

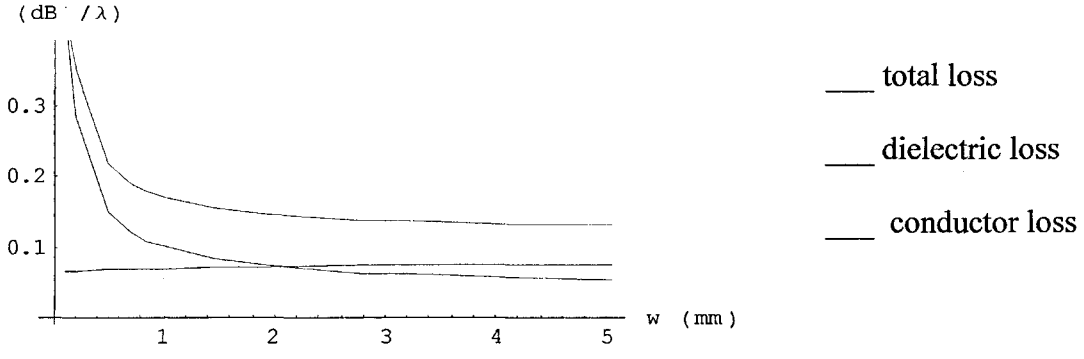

Figure A.1.3: Estimated total microstrip loss and its components, in Taconic TLC microwave laminate. ($h = 0.79$ mm and $\varepsilon_r = 3.0$)

The essential conclusion from the above results is that narrower microstrip lines rapidly become more lossy when the width is reduced below a certain value – about 1 mm in this case. This work justified the use of 1 mm wide lines in the x-band retro-array prototypes (recall that a reduction in line width was sought to increase the spacing between the antenna feed lines).

A 1.2. Simulation.

To model loss effects in lines of various widths, re-course to the CAD simulators was not entirely straightforward. The simulators available were the *Libra* transmission line model, and the *Momentum* method-of-moments simulator. In each case, conductor loss and dielectric loss factor are used as input parameters in addition to the usual microstrip geometry. For the main substrate of interest (Taconic TLC), the material specifications were:

$h = 0.79$ mm, Tan $\delta = 0.003$, $\varepsilon_r = 3.0$

while the value for copper resistance used was 0.022 Ω per square.

When transmission lines of other than 50 Ω characteristic impedance were analysed, it was necessary to avoid a mis-match at the port by either:

(i) Editing the port impedance to match the line impedance, possible in *Libra* only (not *Momentum*)

(ii) Add additional quarter wave impedance matching lines between the ports and the line of interest.

In case (i), an uncertainty arose from a possible mismatch at the port, i.e., the line impedance derived from *Linecalc* may not have been exactly the same as the line impedance used by the *Libra* simulator. Therefore, any reflection at the port, however small, corrupts the simulated measurement of loss. For this reason, a line length of 100 wavelengths was used so that the result would be dominated by the resistive loss, not reflections. The results thus obtained are shown in figure A.1.4 below.

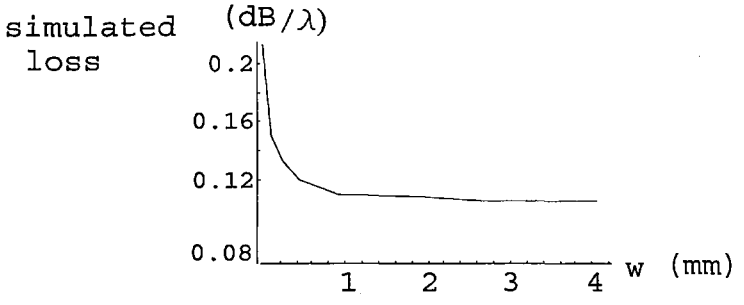

Figure A.1.4: EESOF *Libra* Simulated microstrip loss, in Taconic TLC microwave laminate. (h = 0.79 mm and ε_r = 3.0)

In case (ii), the addition of matching sections imposes a bandwidth limitation on the study, although this is of little consequence. It also implies that the loss in the matching sections is included in the overall result. This method is unnecessary for the *Libra* simulator, where the port impedance can be edited as described, but is vital for the *Momentum* simulator. In the latter case, the physical accuracy of the simulator models the reflections at the step discontinuities – hence a reflective effect corrupts the measurement of resistive loss. However, by arranging for a line length of one quarter wavelength, the step reflections approximately cancel. The "approximately" caveat applies because the quarter wavelength dimension derived from *Linecalc* is not necessarily in agreement with the more "physical" *Momentum* simulator. To minimise both effects (reflection and matching section line loss) a second simulation utilised an additional half wavelength of line in the microstrip line of interest. The geometries are shown in figure A.1.5 below, where the reflective plane is represented by Γ.

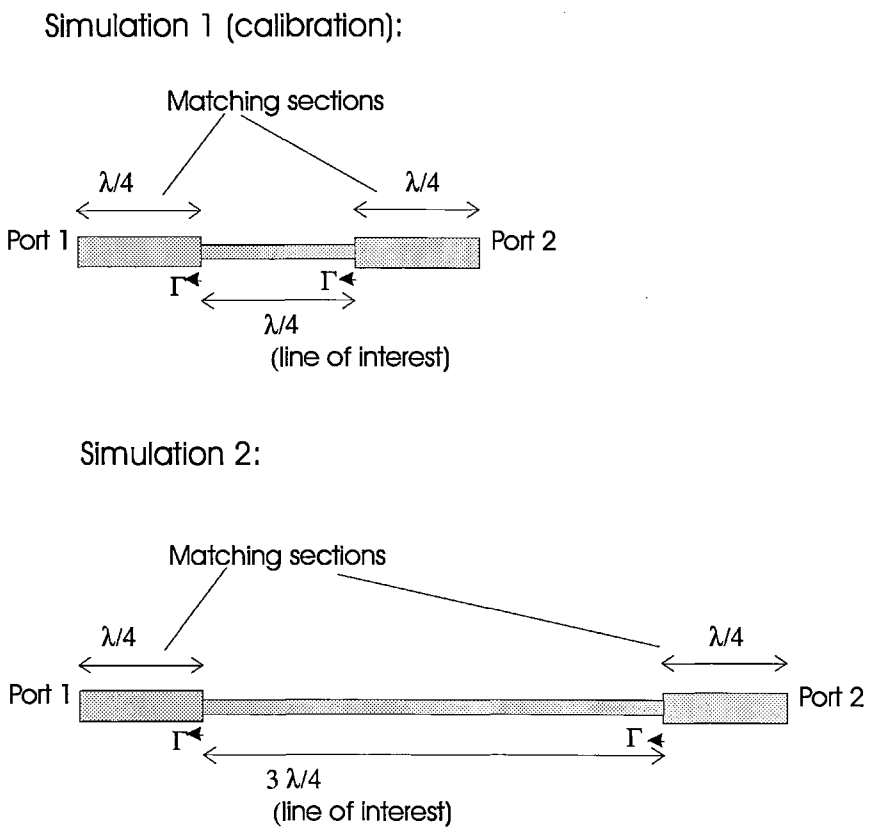

Figure A.1.5 Microstrip loss simulation in EESOF *Momentum*.

Hence the first simulation acts as a calibration standard for the second simulation. The difference between the second and first simulations gives the loss for a half wavelength of the line of interest, where the first simulation has acted as a calibration standard to minimise the effects of resistive and reflective loss in/at the matching sections.

Results derived using *Momentum*, for the TLC substrate at 9.5 GHz, are as follows:

(For the 50 Ω case, the matching sections were not required)

w = 1.9 mm, Zo = 50 Ω, loss = 0.04 dB /λ

w = 1.0 mm, Zo = 73 Ω, loss = 0.078 dB / λ

w = 0.5 mm, Zo = 100 Ω, loss = 0.080 dB / λ

The 1 mm width line was that used in the X-band retro-reflector prototypes. The results from the simulations suggest that the empirical approximations in Figure A.1.3 above are slightly pessimistic, since the *Libra* simulated result is lower by a factor of about 1.5. Too few *Momentum* simulations were performed to demonstrate the rapid rise in loss below 1 mm line width.

A 1.3 Measured loss in a retro-reflector feed circuit

Measurements of loss in an X-band feed circuit were performed. Coaxial probes were used to couple a spare circuit to a vector network analyser, via drillings through the laminate. The antenna circuit was not required, so the apertures in the ground plane were covered with copper tape. The gaps in the feedlines intended for the PIN diodes were bridged with solder.

Since the microstrip characteristic impedance of 73 Ω involves a match of -14 dB at the interface with the 50 Ω coax measurement system, the measurement of loss is slightly corrupted by this reflective component. However, a 14 dB match is sufficient that the resistive loss dominates the measurement. Also, the loss in the co-axial probes (of about 25 mm length each) could not be calibrated out of the measurement. These effects are removed by taking a number of measurements of different line lengths – the difference in loss for a given change in line length allows computation of loss in the microstrip alone.

The results are summarised in figure A.1.6 below, where total measured loss is plotted against microstrip line length. The slope of the linear fit gives the loss per unit length, and the intercept on the y-axis gives the loss in the co-axial probes and connections.

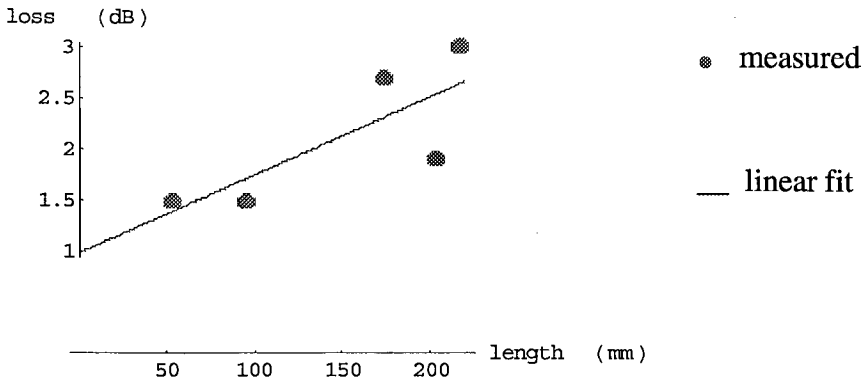

Figure A.1.6 measured microstrip loss at 9.5 GHz, and linear fit, in a retro-array feed circuit on Taconic TLC microwave laminate. (h = 0.79 mm and ε_r = 3.0)

Measured results.

The linear fit for measured microstrip loss is :

$$\text{Loss (dB)} = 0.986 + 0.0076\,L$$

where L is the line length in mm. Hence the un-calibrated loss in the measurement (y-axis intercept) is 0.986 dB and the inherent microstrip loss is 0.0076 dB per mm, or 0.16 dB per microstrip wavelength at 9.5 GHz.

A 1.4 Summary of loss study.

Table A.1 below summarises the results for loss in the 1mm wide microstrip on the Taconic TLC microwave laminate.

empirical model	*Libra* simulation	*Momentum* simulation	measured & linear fit
0.180	0.115	0.078	0.160

Table A.1 Loss in dB per microstrip wavelength at 9.5 GHz.

Economic Considerations.

The loss may be minimised by selection of the lowest loss laminates commercially available. While detailed results for the Taconic TLC laminate have been presented, it has not been feasible to repeat the study for every laminate available. However, a reasonable estimate of a minimum figure for loss may be obtained by consideration of the loss tangent specified by manufacturers. For example, the laminate RT/duroid 6002 manufactured by Rogers has a specified loss tangent of 0.001. Although this appears to be much better than the Taconic TLC figure of 0.003, it should be kept in mind that the conductor loss tends to dominate the dielectric loss, as seen in Figure A.1.3 above. Recalling that the empirical model was pessimistic compared to the measured result by the order of 0.2 dB per microstrip wavelength, and considering an ideal laminate with zero dielectric loss, we would still expect a conductor loss of about 0.09 dB per microstrip wavelength in this ideal case. For RT/Duroid 6002, a figure of 0.11 dB per microstrip wavelength is estimated, representing an improvement of 0.05 dB per microstrip wavelength at an estimated five-fold increase in cost. Clearly the effect of loss is an important factor in the performance of a microwave retro-reflector, especially when fabricated on microstrip. Reflector loss has a direct effect on the link budget for a communications system employing a retro-reflector. If an increase in reflector RCS is sought by designing and fabricating a larger array, the circuit loss increases rapidly for the lines connecting the outer elements of the antenna array, as explored in some detail in chapter 5.

A 2. Active Self-phasing Architectures.

The retro-directive array, which has been the central theme of the thesis, is one sub-class of a more general class of structures which achieve approximate self-phasing through phase conjugation. As alluded to in the first chapter, while a retro-directive array without significant sources of microwave power can be called "passive", a structure which either amplifies the retro-directed signal, and/or achieves phase conjugation through the use of mixers and their associated local oscillators is better described as an "active" circuit. (In practice, phase conjugator circuits would be implemented as arrays - i.e. a multiplicity of circuits - for the term to be meaningful.) Since the active phase conjugator differs from the "passive" in terms of circuit complexity and power consumption, it represents a quite different type of solution for self-phasing communications applications. However, for the sake of completeness, and with the intention of both setting this work in a wider context and stimulating ideas for further related research, this section will review some of the active phase conjugator methods which have appeared in the literature.

A 2.1 Active Van Atta Array.

The Van Atta array achieves phase conjugation through use of equal length transmission lines. The modulated variant has been the subject of this work, and a novel variant using unequal-length transmission lines has been demonstrated and discussed at length in the thesis. It has been called a passive array, or transponder. Thus it is a repeater, rather than a transmitter or receiver. It operates at any frequency, within the bandwidth of the radiating elements. It does not add energy to the system. Thus, to be particularly useful, it needs to be electrically large and have many elements and thus exhibit a radar cross section which is much larger than that of a single scattering element.

The unmodulated variant has zero power requirement, while the modulated variant has fairly minimal power requirements.

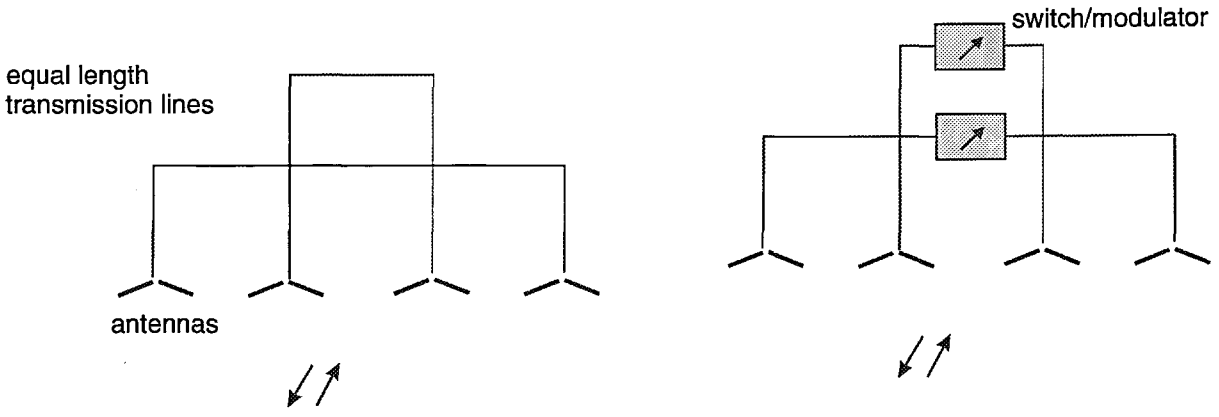

(a) Van Atta Array (b) Modulated Van Atta Array

Figure A.2.1 "Passive" Van Atta Array

In the active case, amplifiers are used to add power to the retro-directed signal [A.5], [A.6]. This requires the use of circulators, the finite isolation of which limit the magnitude of amplification which can be practically used, since the circuit would tend to oscillate. A second configuration does not use circulators, and increases the isolation between the elements by adding a (small) frequency offset and also using the orthogonal antenna polarisation for the retro-directed signal. The use of a frequency offset leads to a phase conjugation error, or pointing error $\Delta\theta$ given by

$$\Delta\theta = -\frac{\Delta f}{f}\tan\theta_0$$

where θ_0 is the scan angle i.e. the angle of arrival from boresight.

(Approximate) phase conjugation is still produced by the equal transmission line lengths.

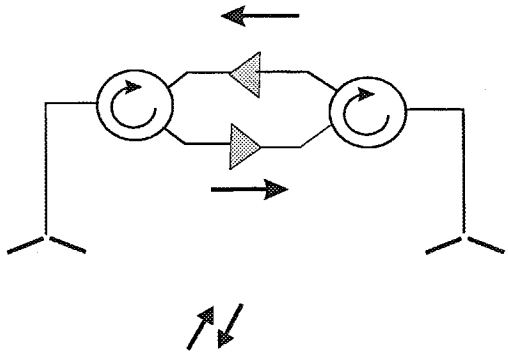

(a) Active Van Atta Array

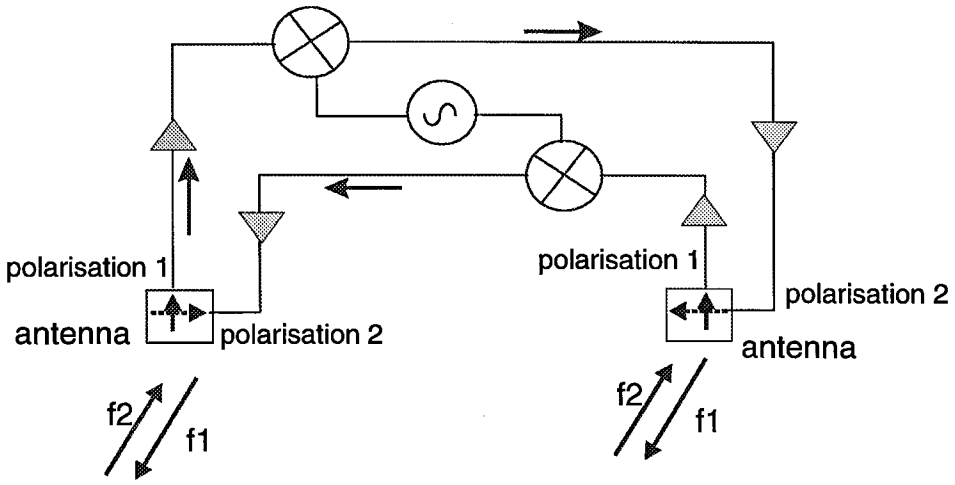

(b) Frequency Offset Active Van Atta Array

Figure A.2.2 "Active" Van Atta Array

A 2.2 Heterodyne phase conjugation.

(i) simple phase conjugator.

Here, the incident signal $V_{RF}\exp(j\omega_0 t+\varphi)$ has a phase ϕ, while the local oscillator $V_{LO}\exp(j2\omega_0 t+\alpha)$, running at twice the incident signal frequency and with an arbitrary phase α, have a mixing product $V_{prod}\exp(j\omega_0 t-\alpha+\varphi)$. Thus the phase front of the outgoing signal has phase - ϕ at every element, plus the arbitrary term α. While only a single element has been shown, array gain is sought in practice and many elements would be used. In this case, the elements are not inter-connected in the manner of the Van Atta array, and phase conjugation will occur for arbitrary element positioning. However, all the local oscillators must be phase locked so that the term α is indeed constant at every

element. Thus the LO distribution is a significant practical problem. The finite circulator isolation means that the above circuit is not generally accepted as a practical one.

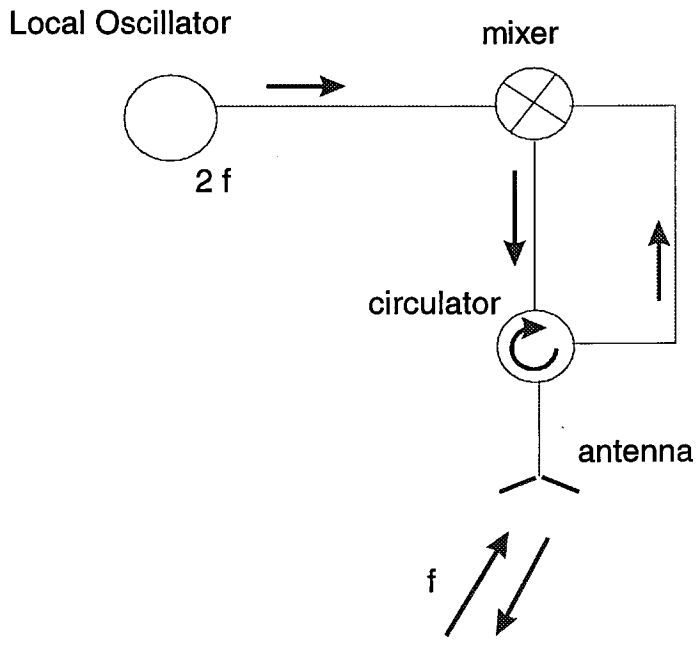

Figure A.2.3 Simple phase conjugator circuit

(ii) Heterodyne conjugator

This is basically the simple conjugator with a frequency offset. As shown above, use of a frequency offset improves the isolation between the incident and outgoing signal, but leads to a pointing error. Refs [A.7],[A.8],[A.9] provide useful material. In a large array, the need to distribute a coherent LO signal to each element can be problematic [A.10].

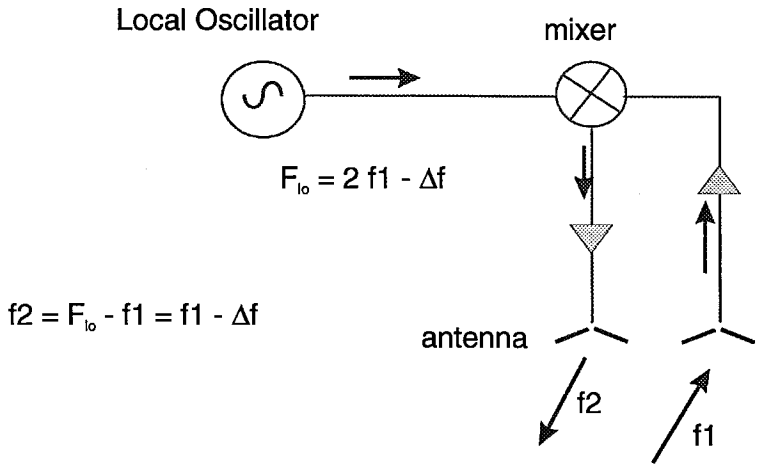

(a) Heterodyne phase conjugator (after Pon)

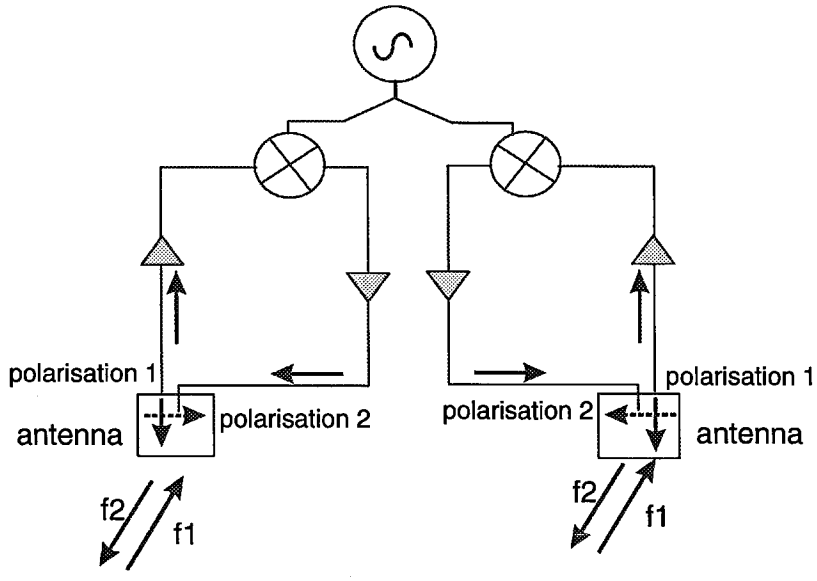

(b) Pon retro-directive array

Figure A.2.4 Heterodyne phase conjugator circuit

A 2.3. Pilot signal as local oscillator.

Here, a pilot signal which is very similar in frequency to the message signal, is transmitted [A.11], [A.12]. In Figure A 2.5 one receiver element is shown, where the pilot and message frequencies are separated by filtering, and then mixed so as to produce approximately coherent down-conversion. In an array, the output of many such elements may be summed. Variants for combining transmit and receive functions are described in [A.11].

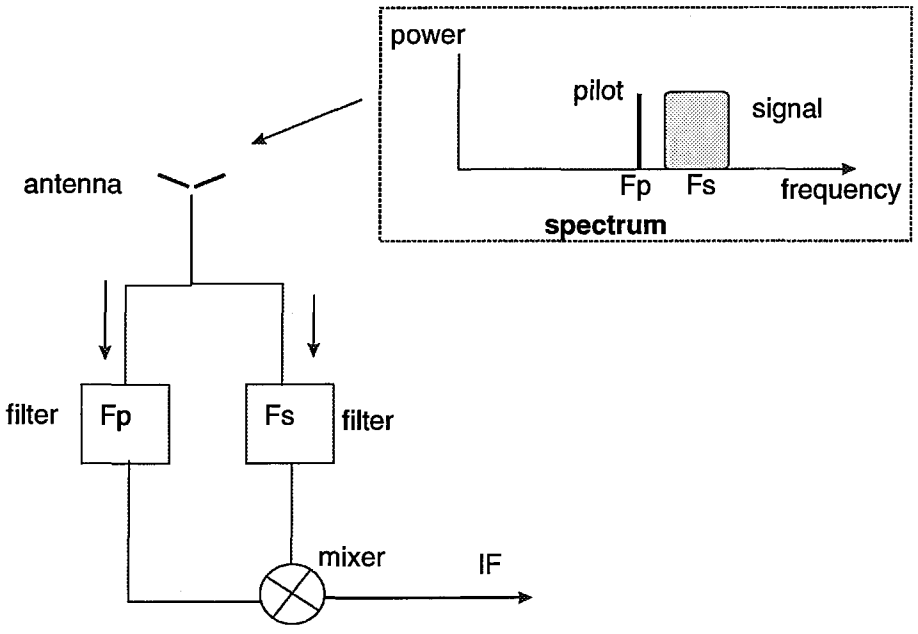

Figure A 2.5 Receiver with Signal and Pilot.

A 3. Multi-tone modulation.

Further to chapter 4, section 4.3.1, modulation spectra for non-monotonic modulation waveforms are here presented. The carrier is again a continuous wave at 9.2 GHz and the transponder orientation is on boresight.

A 3.1 Dual tone modulation.

Dual tone modulation represents a progression from monotone modulation whereby the transponder is assigned a unique signature or code. In this case, identification of the transponder requires de-modulation to obtain the two modulation frequencies only. By way of example, Figure A.3.1 shows spectra for dual tone modulation

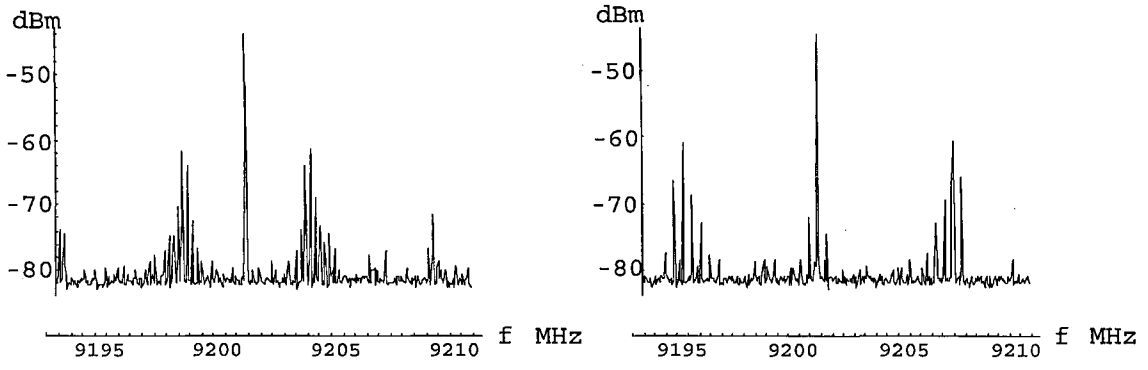

(i) 2.5 MHz and 2.9 MHz (ii) 6.1 MHz and 6.5 MHz

Figure A.3.1 Dual tone modulation spectra

A 3.2 Direct sequence spread spectrum modulation.

Figure A.3.2 shows example spectra where the modulation waveform is a pseudo random binary sequence, or code, obtained from the output of a sequence generator [A.3]. The code is a 127 bit M-sequence [A.4] where the clock (or "chipping") rate may be varied. As the clock rate is increased, the modulation products are evidently more widely spread, to the extent that the spectrum starts to appear noise-like, as seen in case (iii).

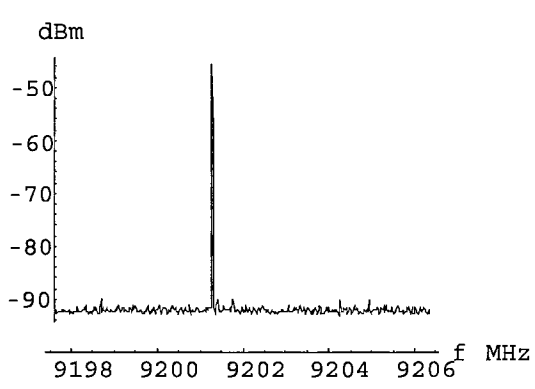

(i) no modulation:

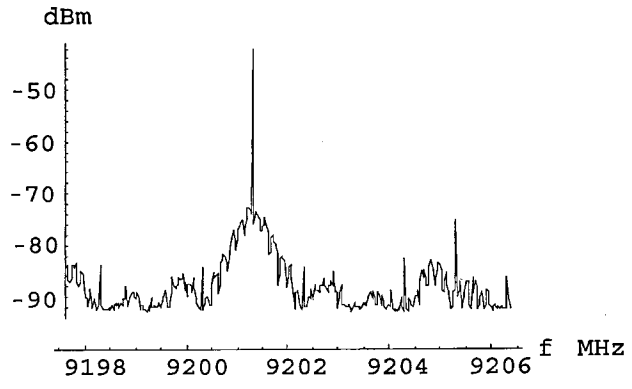

(ii) clocked at 1 MHz

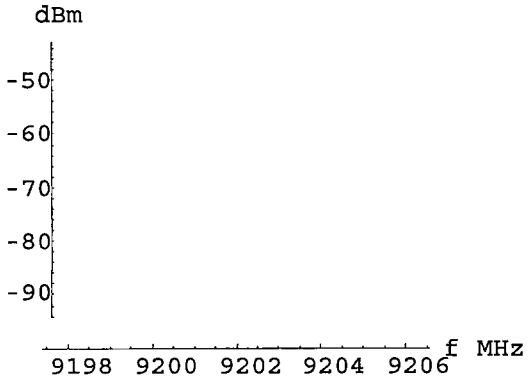

(iii) clocked at 5 MHz

Figure A.3.2 Direct sequence spread spectrum: modulation spectra

References.

[A.1] "Microwave Engineering". David M. Pozar. *Addison Wesley* 1993, p.163

[A.2] Ref [6] of chapter 4

[A.3] Ref [4] of chapter 7

[A.4] "Spread Spectrum Systems with Commercial Applications", R. C. Dixon, *Wiley* 1994, pp. 64-70

[A.5] "Microwave Scanning Antennas Vol 3 - Self-Phased Arrays", R. C. Hansen, Academic Press, 1966, pp.370-372

[A.6] Refs [5] and [6] of Chapter 1

[A.7] "Self-phasing antenna array techniques for mobile communications applications", V. F. Fusco, S. L. Karode, *IEE Electronics and Communications Engineering Journal* Vol 11 No. 6, December 1999

[A.8] "Retrodirective array using the heterodyne technique", C. Y. Pon, *IEEE Trans. Ant.Prop.* March 1964, pp. 176-180

[A.9] "A Conformal Retrodirective Array for Radar Applications Using a Heterodyne Phased Scattering Element", C. W. Pobanz, T. Itoh, IEEE MTT-S Digest 1995 pp. 905 - 908.

[A.10] "Large Active Retrodirective Arrays for Space Applications", R. C. Chernoff, *IEEE Trans Ant Prop.* Vol Ap-27 No.4 July 1979

[A.11] "An Experimental and Theoretical Study of Self-Phased Arrays in Mobile Satellite Communications". P. V. Brennan, *IEEE Trans Ant Prop.* Vol 37 No.11 Nov 1989

[A.12] "A Self-Steering Planar Array Antenna for Satellite Broadcast Reception." T. Murata, M. Fujita, *IEEE Trans. Broadcasting* Vol.40, No.1, March 1994